



# Component Characterization of T-plug Bending Around Weak Axis

**Experiment design and numerical study of a new type plug-and-play joint**

M.M.H. (Milco) Hahury





# Component Characterization of T-plug Bending Around Weak Axis

## Experiment design and numerical study of a new type plug-and-play joint

by

M.M.H. (Milco) Hahury

in partial fulfilment of the requirements for the degree of

**Master of Science**  
in Civil Engineering

**Track**  
Structural Engineering

**Specialization**  
Steel, Hybrid and Composit Structures

at the Delft University of Technology  
to be defended publicly on Friday July 17th 2020 at 14:00.

Student number: 4371399  
Project duration: July 15, 2019 – July 10, 2020  
Thesis committee: Prof. dr. M. Veljkovic, TU Delft, chairman  
R. Yan (MSc), TU Delft, daily supervisor  
Dr. ir. M.A.N. Hendriks, TU Delft, committee member

An electronic version of this master thesis report is available at  
<http://repository.tudelft.nl/>.

*Cover: set of test specimens in the Stevin II laboratory at the Delft Univeristy of Technology*





# Acknowledgement

As a child going to the primary school, I already developed, by then still innocently, a great passion for buildings and structures. What started back then with wooden blocks, quickly escalated into an enormous collection of LEGO. It was just a matter of time until I applied for the Bachelor in Civil Engineering at Delft University of Technology in the summer of 2014. This MSc thesis is my final assignment in obtaining the Degree of Master of Science in Civil Engineering for the track 'Structural Engineering' at the Delft University of Technology.

I want to express my gratitude to Prof. dr. Milan Veljkovic for given me the opportunity to graduate on the subject "Component Characterization of T-plug Bending Around Weak Axis" and contribute to the INNO3DJOINTS project. This even resulted in my first business trip to Caxarias, Portugal in January 2020, which was a great experience to present my research to the complete team of professionals. Also, I sincerely want to thank Rui Yan for his incredible time and support during the week, weekend and even holidays and Dr. ir. Max Hendriks for complementing my thesis committee. Without their knowledge and feedback I was not able to deliver this MSc thesis. In short, I want to thank Peter de Vries, Louis den Breejen for their cooperation in the design of the experiment, Shuang Qui for his help in the component derivation, Helder Craviero for sharing knowledge of the University of Coimbra.

Last but not least, I would like to thank my family, Lisan and all friends, who surrounded me during my incredible joyful time as a student in Delft. I am grateful for their support and laughter, which made it possible for me to the finish this thesis.

*M.M.H. Hahury (SE)*  
*Delft, July 10, 2020*





# Abstract

Explicit rules for safety verification of open cold-formed lightweight beam-to-tubular column joints are missing in the current EC3-1-8. By developing economical detailing, with design guidance based on Eurocodes, the market share for new buildings, renovation and for additional storeys on existing buildings will increase. Within the INNO3DJOINTS project an innovative plug-and-play joint is developed, allowing for modularity and industrialization for low to mid-rise buildings. This solution will increase the competitiveness and sustainability of steel construction. The goal of this MSc thesis is to characterize the behaviour of the plug-and-play joint using the component test; T-plug bending around weak axis. The strength, stiffness and deformation capacity following the EC3-1-8 component method approach are investigated.

An experiment is designed for testing in the Stevin-II laboratory at Delft University of Technology. This work includes both the design of the set of test specimens and laboratory set-up. Secondly, a numerical study is performed to predict the experimental results and an extending parametric study is performed to derive new components, using the finite element software of ABAQUS. The influence of geometrical properties; thickness ratio (reverse channel vs. T-plug web), use of stiffeners, use of tubular sections and length of the T-plug web, is studied for a steel grade S355. The numerical study is validated for three configurations using the component test; T-plug in tension, provided by the INNO3DJOINTS project. As the parametric study is based on an elasto-plastic material model, these numerical results are directly used to derive new analytical expressions/models and characterize new components and component interactions for design verification.

The numerical study resulted in the identification of seven active components for the plug-and-play joint, consisting of basic EC3-1-8 components and tubular components from the CIDECT report 16F: *Component method for tubular joints*. In addition, two new components are introduced namely, the reverse channel in bending and T-plug in bending. Based on a total of 127 unique joint configurations, new analytical expressions are derived to characterize the behaviour of the new components for resistance and stiffness. The component interaction is established by proposing a physical spring model and a component model suitable for Eurocode implementation. This results in the characterization of the joint behaviour for the experimental configuration C-SHS200 with a 7.5% deviation on the resistance and a 20.5% deviation on the stiffness compared to the numerical result.

The accuracy of the joint stiffness can be improved if the component stiffness derivation also includes non-governing configurations and a wider range of parameters is studied, such as the position of the bolt holes along the net-section and the use of tubular section. The results, derivations and the physical spring model contribute to the INNO3DJOINTS project and could be used for implementation in the software tool, to be developed by the French Institute CTICM. Besides, the Eurocode aligned component model is recommended for practical use in design standards, but further research should be performed on the verification of the rotational stiffness on the joint level.





# Contents

<b>Acknowledgement</b>	<b>i</b>
<b>Abstract</b>	<b>iii</b>
<b>List of Figures</b>	<b>ix</b>
<b>List of Tables</b>	<b>xiii</b>
<b>1 Introduction</b>	<b>1</b>
1.1 Research context . . . . .	1
1.2 Problem definition . . . . .	2
1.3 Research question . . . . .	2
1.4 Scope . . . . .	3
1.5 Methodology . . . . .	3
1.6 Document structure . . . . .	4
<b>2 Literature research</b>	<b>5</b>
2.1 State of art: design of joints . . . . .	5
2.2 Plug-and-play joints . . . . .	7
2.3 Classification of joints . . . . .	8
2.3.1 Classification by stiffness . . . . .	9
2.3.2 Classification by strength. . . . .	9
2.4 Introduction to the component method . . . . .	10
2.4.1 Design resistance . . . . .	11
2.4.2 Rotational stiffness . . . . .	11
2.4.3 Rotation capacity . . . . .	12
2.5 3D behaviour of joints . . . . .	12
2.6 Previous research . . . . .	13
2.6.1 Component test. . . . .	13
2.6.2 Numerical modelling . . . . .	14
2.6.3 Research methodology. . . . .	15
<b>3 Experiment design</b>	<b>17</b>
3.1 Experimental objectives . . . . .	17
3.2 Test specimens . . . . .	18
3.3 Material characterization . . . . .	23
3.4 Laboratory set-up. . . . .	23
3.4.1 Frame resistance . . . . .	24
3.4.2 Frame design . . . . .	24
3.4.3 Frame detailing . . . . .	25
3.4.4 Instrumentation . . . . .	27
<b>4 Numerical study on plug-and-play joints</b>	<b>31</b>
4.1 Numerical model . . . . .	31
4.1.1 Geometry . . . . .	32
4.1.2 Material properties . . . . .	33
4.1.3 Finite element and mesh type . . . . .	34
4.1.4 Assembly conditions . . . . .	37
4.1.5 Computational solver. . . . .	39

4.2	Numerical results . . . . .	41
4.3	Parametric study . . . . .	45
4.3.1	Thickness ratio (reverse channel vs. T-plug web) . . . . .	45
4.3.2	Use of stiffeners . . . . .	46
4.3.3	Use of tubular sections . . . . .	47
4.3.4	Length T-plug web . . . . .	48
<b>5</b>	<b>Component method application</b>	<b>49</b>
5.1	Active components . . . . .	49
5.2	Evaluation. . . . .	50
5.2.1	Chord side wall in transverse compression . . . . .	50
5.2.2	Chord side wall in transverse tension . . . . .	52
5.2.3	Chord face in bending . . . . .	53
5.2.4	Welds . . . . .	54
5.2.5	Reverse channel in bending . . . . .	54
5.2.6	Bolts in tension . . . . .	57
5.2.7	T-plug in bending . . . . .	57
5.3	Joint assembly . . . . .	61
5.3.1	Design resistance . . . . .	61
5.3.2	Rotational stiffness . . . . .	61
5.3.3	Rotation capacity . . . . .	63
5.4	Component results . . . . .	63
5.4.1	Component level . . . . .	63
5.4.2	Joint level . . . . .	65
<b>6</b>	<b>Conclusion</b>	<b>67</b>
<b>7</b>	<b>Recommendations</b>	<b>69</b>
	<b>Bibliography</b>	<b>71</b>
<b>A</b>	<b>Validation numerical tension model</b>	<b>73</b>
A.1	Numerical tension model. . . . .	73
A.1.1	Geometry . . . . .	73
A.1.2	Material properties . . . . .	75
A.1.3	Finite element and mesh type . . . . .	75
A.1.4	Assembly conditions . . . . .	76
A.1.5	Computational solver. . . . .	76
A.2	Analysis of results . . . . .	77
A.2.1	Specimen: A-RP . . . . .	77
A.2.2	Specimen: B-RP . . . . .	78
A.2.3	Specimen: B-U-RP . . . . .	79
A.3	Conclusion . . . . .	80
<b>B</b>	<b>Preliminary numerical study</b>	<b>81</b>
B.1	Loading conditions . . . . .	82
B.2	Modelling simplification. . . . .	83
B.3	Prediction of experimental results . . . . .	84
B.3.1	Thickness ratio (reverse channel vs. T-plug web) . . . . .	84
B.3.2	Use of stiffeners . . . . .	85
B.3.3	Use of tubular sections . . . . .	86
<b>C</b>	<b>Component derivation: reverse channel in bending</b>	<b>89</b>
C.1	Design resistance . . . . .	90
C.2	Stiffness coefficient. . . . .	95

---

<b>D</b>	<b>Component derivation: T-plug in bending</b>	<b>103</b>
D.1	Design resistance . . . . .	103
D.1.1	Partial T-stub model analogy. . . . .	104
D.1.2	Derivation parameter: "m" . . . . .	105
D.1.3	Derivation parameter: " $b_{eff}$ " . . . . .	110
D.2	Stiffness coefficient. . . . .	116



# List of Figures

1.1	T-plug bending around weak axis . . . . .	3
2.1	$CO_2$ emissions of the ISI and CMI during 1992-2012. Note: pie charts show the proportion of the ISI and CMI in China's $CO_2$ emissions structure; the size of pies indicates China's total $CO_2$ emission size in studied years. (Liu et al., 2018)	5
2.2	Schematic representation of the plug-and-play joint (Da Silva et al., 2019) . . .	7
2.3	Schematic representation of the assembled plug-and-play joint (Da Silva et al., 2019) . . . . .	7
2.4	Classification of joints according to stiffness (EN 1993-1-8, 2005) . . . . .	9
2.5	Full-strength joints design criteria (EN 1993-1-8, 2005) . . . . .	10
2.6	Equivalent spring model for steel connections (Da Silva and Coelho, 2001) . . .	11
2.7	Comparison between all tested configurations of component T-plug in tension (Da Silva et al., 2019) . . . . .	14
3.1	Geometric configuration of specimens A-RP . . . . .	19
3.2	Geometric configuration of specimens B-RP . . . . .	19
3.3	Geometric configuration of specimens B-U-RP . . . . .	20
3.4	Geometric configuration of specimens B-UU-RP . . . . .	21
3.5	Geometric configuration of specimens C-RP . . . . .	21
3.6	Geometric configuration of specimens C-SHS200 . . . . .	22
3.7	Geometric configuration of specimens C-SHS260 . . . . .	22
3.8	Design of the coupon specimen (F10) . . . . .	23
3.9	Laboratory set-up for rigid plate specimen (left) and tubular specimen (right) .	25
3.10	Set-up boundary conditions HEA100 load beam . . . . .	25
3.11	HEA100 load beam (red) to specimen (blue) detail . . . . .	26
3.12	Rigid plate specimen (blue) to corner profile (orange) detail . . . . .	26
3.13	Tubular specimen (blue) to corner profile (orange) detail . . . . .	27
3.14	Instrumentation arrangement A-RP specimen: T-plug (thickness 6 mm) and reverse channel (10 mm) in bending, with stiffeners. . . . .	28
3.15	Instrumentation arrangement B-RP specimen: T-plug (10 mm) and reverse channel (6 mm) in bending, with stiffeners. . . . .	28
3.16	Instrumentation arrangement B-U-RP/B-UU-RP specimen: T-plug (10 mm) and reverse channel (6 mm) in bending, with respectively unstiffened reverse channel/double unstiffened reverse channel and T-plug. . . . .	28
3.17	Instrumentation arrangement C-RP specimen. Complete assembly in bending with the same thickness for both elements (T-plug and reverse channel with 10 mm) with stiffeners, acting as benchmark configuration for tubular influence. .	29
3.18	Instrumentation arrangement C-SHS200 specimen. Complete assembly in bending with the same thickness for both elements (T-plug and reverse channel with 10 mm) with stiffeners, considering the influence of the tubular profile (SHS 200x200x10). . . . .	29
3.19	Instrumentation arrangement C-SHS260 specimen. Complete assembly in bending with the same thickness for both elements (T-plug and reverse channel with 10 mm) with stiffeners, considering the influence of the tubular profile (SHS 260x260x6). . . . .	29
4.1	Bolt geometry and 3D representation of the finite element model . . . . .	31
4.2	Stresses on the throat section of a fillet weld (EN 1993-1-8, 2005) . . . . .	32
4.3	Weld geometry finite element model . . . . .	33

4.4	Plastic material models with true stress-strain conversion . . . . .	33
4.5	Presentation of the finite element type: Hexahedral "C3D8R" . . . . .	35
4.6	Interpolation vs. integration . . . . .	35
4.7	Hourglassing . . . . .	36
4.8	Finite element mesh of the numerical model . . . . .	36
4.9	Surface-to-surface discretization . . . . .	37
4.10	Boundary condition schematization . . . . .	38
4.11	Reference point location in the numerical model . . . . .	38
4.12	Force-displacement curves of specimen model: A-RP (X at 5% and 25% PEEQ limit) . . . . .	41
4.13	Numerical results of specimen model: A-RP . . . . .	42
4.14	Force-displacement curves of specimen models: B-RP, B-U-RP and B-UU-RP (X at 5% and 25% PEEQ limit) . . . . .	43
4.15	Final deformed shape of specimen models B . . . . .	43
4.16	Force-displacement curves of specimen models: C-RP, C-SHS200 and C-SHS260 (X at 5% and 25% PEEQ limit) . . . . .	44
4.17	Final deformed shape of specimen models C . . . . .	44
4.18	Results of the parametric study: thickness ratio . . . . .	45
4.19	Results of the parametric study: use of stiffeners . . . . .	46
4.20	Results of the parametric study: length T-plug web (X at 5% PEEQ limit) . . . . .	48
5.1	Active components for the plug-and-play joint to tubular column section . . . . .	50
5.2	Chord side wall in transverse compression (Weynand et al., 2015) . . . . .	50
5.3	$\beta = b_1/b_0$ ratio, where $b_1$ is the leg between both legs of the reverse channel (Garifullin et al., 2019) . . . . .	51
5.4	Chord side wall in transverse tension (Weynand et al., 2015) . . . . .	52
5.5	Chord face in bending (Weynand et al., 2015) . . . . .	53
5.6	Simplified reverse channel model . . . . .	56
5.7	Simplified mechanical model . . . . .	59
5.8	Comparison between the physical (INNO3DJOINTS) vs. component (Eurocode) model . . . . .	62
5.9	Force-displacement verification on component level . . . . .	64
5.10	Force-displacement verification on joint level . . . . .	65
6.1	Characterization of the joint behaviour . . . . .	68
A.1	Geometry of test specimen A-RP (Da Silva et al., 2019) . . . . .	74
A.2	Geometry of test specimen B-RP (Da Silva et al., 2019) . . . . .	74
A.3	Geometry of test specimen B-U-RP (Da Silva et al., 2019) . . . . .	74
A.4	Force-displacement tension validation of test specimen: A-RP . . . . .	77
A.5	Final deformed shape tension validation for test specimen: A-RP . . . . .	77
A.6	Final deformed shape tension validation for test specimen: B-RP . . . . .	78
A.7	Force-displacement tension validation of test specimen: B-RP . . . . .	78
A.8	Final deformed shape tension validation for test specimen: B-RP . . . . .	79
A.9	Force-displacement tension validation of test specimen: B-U-RP . . . . .	79
B.1	Pure bending loading conditions . . . . .	81
B.2	Results of the shear load condition . . . . .	82
B.3	Load beam model vs. simplified model comparison . . . . .	83
B.4	Load beam model vs. simplified model force-displacement comparison . . . . .	83
B.5	Comparison of final deformed shapes . . . . .	84
B.6	Failure mode: B-RP (Von Mises) . . . . .	85
B.7	Force-displacement graph on varying thickness ratio (X at 5% and 25% PEEQ limit) . . . . .	85
B.8	Final deformed shape of specimen models B . . . . .	86
B.9	Force-displacement graph on the use of stiffener (X at 5% and 25% PEEQ limit) . . . . .	86
B.10	Final deformed shape of specimen models C . . . . .	87

B.11 Force-displacement graph on the use of tubular sections (X at 5% and 25% PEEQ limit) . . . . .	87
C.1 Component simplification: RC in bending . . . . .	89
C.2 Regression plots for the derivation of $\alpha_b$ . . . . .	90
C.3 Regression plot for the derivation of $\alpha_{st}$ . . . . .	91
C.4 Regression plots for the derivation of $\alpha_\omega$ . . . . .	92
C.5 Regression plots for the derivation of $\alpha_t$ . . . . .	92
C.6 Regression plots for the derivation of $\alpha_b$ . . . . .	96
C.7 Regression plot for the derivation of $\alpha_{st}$ . . . . .	96
C.8 Regression plot for the derivation of $\alpha_{rc}$ . . . . .	97
C.9 Regression plots for the derivation of $\alpha_\omega$ . . . . .	98
C.10 Regression plots for the derivation of $\alpha_t$ . . . . .	98
D.1 Component simplification: T-plug in bending . . . . .	103
D.2 Axial stress (S33) distribution in the T-plug of numerical model: A-RP . . . . .	104
D.3 T-stub model: yielding of the flange (failure mode 1) . . . . .	104
D.4 definition of various lengths of the T-plug . . . . .	105
D.5 Regression plot for the derivation of factor $\alpha_t$ . . . . .	106
D.6 Regression plot for the derivation of factor $\alpha_\omega$ . . . . .	107
D.7 Regression plot for the derivation of factor $\alpha_{bm}$ . . . . .	107
D.8 Yield pattern 1: (A-U1-RP) . . . . .	109
D.9 Yield pattern 2: (A-RP) . . . . .	109
D.10 Yield pattern 3: (A-U2-RP) . . . . .	110
D.11 Regression plot for the derivation of $\alpha_b$ . . . . .	111
D.12 Regression plots for the derivation of $\alpha_\omega$ . . . . .	111
D.13 Regression plot for the derivation of $\alpha_{st}$ . . . . .	112
D.14 Regression plots for the derivation of $\alpha_t$ . . . . .	113
D.15 Regression plot for the derivation of $\alpha_l$ . . . . .	114
D.16 Regression plot for the derivation of $c_b$ . . . . .	118
D.17 Regression plots for the derivation of $c_\omega$ . . . . .	119
D.18 Regression plot for the derivation of $c_{st}$ . . . . .	120
D.19 Regression plot for the derivation of $c_l$ . . . . .	121
D.20 Regression plot for the derivation of $c_t$ . . . . .	122





# List of Tables

2.1	Traditional (bolted and welded) joints versus plug-and-play joints . . . . .	6
2.2	Type of joint model (EN 1993-1-8, 2005) . . . . .	9
2.3	Characteristic dimensions of the studied specimen (Da Silva et al., 2019) . . . . .	13
3.1	Test matrix for the component test; T-plug bending around weak axis . . . . .	18
3.2	Coupons for steel characterization . . . . .	23
3.3	Reaction forces per bolt of the rigid plate specimens . . . . .	24
3.4	Reaction forces per bolt of the tubular specimens . . . . .	24
4.1	Plastic material input parameters in ABAQUS . . . . .	34
4.2	Characteristics summary of the finite element type . . . . .	37
4.3	Summary of the boundary conditions . . . . .	39
4.4	Computational settings: Static, General (Implicit) . . . . .	40
4.5	Computational settings: Dynamic, Explicit . . . . .	40
4.6	Joint model characteristics . . . . .	42
4.7	Joint characteristics: thickness ratio (1) . . . . .	45
4.8	Joint characteristics: thickness ratio (2) . . . . .	46
4.9	Joint characteristics: use of stiffeners . . . . .	47
4.10	Joint characteristics: use of tubular sections . . . . .	47
4.11	Joint characteristics: length T-plug web . . . . .	48
5.1	Values of $\alpha_\omega$ . . . . .	55
5.2	Values of $\alpha_t$ . . . . .	55
5.3	Values of $\alpha_\omega$ . . . . .	57
5.4	Values of $\alpha_t$ . . . . .	57
5.5	Values of m . . . . .	58
5.6	Values of $\alpha_\omega$ . . . . .	59
5.7	Values of $\alpha_t$ . . . . .	59
5.8	Values of $c_\omega$ . . . . .	60
5.9	Values of $c_t$ . . . . .	60
5.10	Overview of stiffness coefficients part of the assembly . . . . .	61
5.11	Results on the component level . . . . .	64
5.12	Overview of design resistance per component: model C-SHS200 . . . . .	65
5.13	Results on the joint level . . . . .	66
A.1	Plastic material input parameters . . . . .	75
A.2	Finite element characteristics tension models . . . . .	75
A.3	Assembly conditions tension model . . . . .	76
A.4	Computational settings tension model . . . . .	76
A.5	Ultimate strength comparison . . . . .	80
C.1	Results $F_{rc,Rd}$ : $\alpha_b$ contribution . . . . .	91
C.2	Results $F_{rc,Rd}$ : $\alpha_{st}$ contribution . . . . .	91
C.3	Values of $\alpha_\omega$ . . . . .	92
C.4	Values of $\alpha_t$ . . . . .	93
C.5	Results definition $F_{rc,Rd}$ : 1. Double stiffened (A-RP) . . . . .	93
C.6	Results definition $b_{eff}$ : 1. Double stiffened (B-RP) . . . . .	93
C.7	Results definition $F_{rc,Rd}$ : 2. Stiffened T-plug / unstiffened RC (A-U1-RP) . . . . .	94
C.8	Results definition $F_{rc,Rd}$ : 3. Unstiffened T-plug / stiffened RC (A-U2-RP) . . . . .	94

C.9 Results definition $F_{rc,Rd}$ : 4. Double unstiffened (A-UU-RP) . . . . .	94
C.10 Results $k_5$ : $\alpha_b$ contribution . . . . .	96
C.11 Results $k_5$ : $\alpha_{st}$ contribution . . . . .	97
C.12 Values of $\alpha_\omega$ . . . . .	97
C.13 Values of $\alpha_t$ . . . . .	99
C.14 Results $k_5$ : 1. Double stiffened (A-RP) . . . . .	99
C.15 Results $k_5$ : 1. Double stiffened (B-RP) . . . . .	99
C.16 Results $k_5$ : 2. Stiffened T-plug / unstiffened RC (A-U1-RP) . . . . .	100
C.17 Results $k_5$ : 3. Unstiffened T-plug / stiffened RC (A-U2-RP) . . . . .	100
C.18 Results $k_5$ : 4. Double unstiffened (A-UU-RP) . . . . .	100
D.1 Results $m$ : $\alpha_{bm}$ contribution . . . . .	108
D.2 Results $m$ : $b = 100 \text{ mm}$ . . . . .	108
D.3 Results $m$ : $b = 150 \text{ mm}$ . . . . .	108
D.4 Values of $m$ . . . . .	110
D.5 Results $F_{tp,Rd}$ : $\alpha_b$ contribution . . . . .	111
D.6 Values of $\alpha_\omega$ . . . . .	112
D.7 Results $F_{tp,Rd}$ : $\alpha_{st}$ contribution . . . . .	112
D.8 Values of $\alpha_t$ . . . . .	113
D.9 Results $F_{tp,Rd}$ : $\alpha_l$ contribution . . . . .	114
D.10 Results $F_{tp,Rd}$ : 1. Double stiffened (-RP) ( $b = 100 \text{ mm}$ ) . . . . .	114
D.11 Results $F_{tp,Rd}$ : 1. Double stiffened (-RP) ( $b = 150 \text{ mm}$ ) . . . . .	115
D.12 Results $F_{tp,Rd}$ : 2. Stiffened T-plug / unstiffened RC (-U1-RP) . . . . .	115
D.13 Results $F_{tp,Rd}$ : 3. Unstiffened T-plug / stiffened RC (-U2-RP) . . . . .	116
D.14 Results $F_{tp,Rd}$ : 4. Double unstiffened (-UU-RP) . . . . .	116
D.15 Individual bending and shear contributions . . . . .	117
D.16 Results $k_7$ : $c_b$ contribution . . . . .	119
D.17 Values of $c_\omega$ . . . . .	119
D.18 Results $k_7$ : $c_{st}$ contribution . . . . .	120
D.19 Results $k_7$ : $c_l$ contribution . . . . .	121
D.20 Values of $c_t$ . . . . .	121
D.21 Results $k_7$ : 1. Double stiffened (-RP) ( $b = 100 \text{ mm}$ ) . . . . .	122
D.22 Results $k_7$ : 1. Double stiffened (-RP) ( $b = 150 \text{ mm}$ ) . . . . .	123
D.23 Results $k_7$ : 2. Stiffened T-plug / unstiffened RC (-U1-RP) . . . . .	123
D.24 Results $k_7$ : 3. Unstiffened T-plug / stiffened RC (-U2-RP) . . . . .	124
D.25 Results $k_7$ : 4. Double unstiffened (-UU-RP) . . . . .	124

# Introduction

In this chapter a general introduction of this MSc thesis, part of the INNO3DJOINTS project, is given. In Section 1.1 some background information is given on the project. Next, in Section 1.2 the problem definition is stated, followed by the research question in Section 1.3, the scope in Section 1.4 and the methodology in Section 1.5. At last, the document structure for the remaining part of the report is given in Section 1.6.

## 1.1. Research context

This MSc thesis is commissioned by the Delft University of Technology participating in the INNO3DJOINTS project, working on innovative 3D plug-and-play joints for robust and economic hybrid tubular construction. INNO3DJOINTS is a European cooperation between universities, companies and a research institute. The three universities; University of Coimbra (Portugal), University of Naples (Italy) and Delft University of Technology (Netherlands), are responsible for the research. The three companies; CONDENSA (Spain), FAMETAL (Portugal) and FERPINTA (Portugal), are responsible for the supply of materials and the fabrication of the test specimens. Furthermore, the research institute; CTICM (France), is responsible for the application of the results in a software tool, for implementation in design standards.

The main goal of INNO3DJOINTS is to develop innovative plug-and-play joints for hybrid tubular construction, whereby tubular steel columns (CHS, SHS or RHS) are combined with cold-formed lightweight steel profiles to provide a highly efficient structural system. As the project is co-financed by the Research Fund for Coal and Steel (RFCS) of the European Union, the following objectives have to be fulfilled:

- Development of a design procedure in the framework of the component method for innovative plug-and-play joints, currently not addressed in the structural Eurocode. This is accomplished by carrying out extensive experimental and numerical studies. These are carried out both at the joint level and the component level;
- Codifying the design procedures for cold-formed connections (EC3-1-3) in a consistent format with the component method and EC3-1-8;
- Characterization of particular aspects of joints involving cold-formed tubular sections, influences of manufacturing procedures in the behaviour of the profile and influence of the corner welded region on the welding of the plug-and-play connection;
- Implementation of a general procedure for tackling the 3D behaviour of these particular steel joints, essential to deal with robustness issues. A generalized finite element that includes all studied components of the design model for joints with 3D behaviour is developed and further implemented in a software tool – firstly for analysis of the connection itself and secondly for the overall structural building analysis. Although this

aspect may be further extendable to other types of cross-sections and fabrication procedures, in this project focus is only given to the hybrid connections. (INNO3DJOINTS, 2015)

These objectives are subdivided into several work packages, of which one is *the characterization of components* (work package 3) and can be summarized as follows:

*Newly developed components require their behavioural characterization which is accomplished by means of the experimental investigation on these components (components tests). Then, from the experimental and numerical results, new analytical expressions/models are derived to characterize new components and components interaction – not only for hybrid joints but also for other joints sharing similar components/interactions. This work generates input for the joint model and the generalized joint element application.* (INNO3DJOINTS, 2015)

The contribution of this MSc thesis to the INNO3DJOINTS project is established within the work package 3, as the component test; T-plug bending around weak axis, is the subject of this MSc thesis. By performing both an experimental and numerical study, the behaviour of the plug-and-play joint is studied, in terms of strength, stiffness and deformation capacity. Besides, general formulae are derived to characterize new components and component interactions, within the framework of the EC3-1-8 component method. These findings are shared with INNO3DJOINTS and incorporated in their report.

## 1.2. Problem definition

This MSc thesis addresses a connection between tubular cold-formed steel columns and cold-formed lightweight steel profiles to provide a highly efficient structural system. By developing an innovative plug-and-play joint, modularity and industrialization are allowed for low to mid-rise buildings, increasing the competitiveness (fast-track construction and increasing the quality of the finished product) and sustainability (reduction of raw materials and waste) of steel constructions.

However, explicit rules for safety verification of open cold-formed lightweight beam-to-tubular columns joints are missing in the current EC3-1-8. These plug-and-play joints imply the need to efficiently connect beams to columns in the arbitrary directions taking account of the 3D behaviour in the nodal zone. Therefore the aim is to develop a consistent design approach for the prediction of the 3D behaviour of steel connections under arbitrary loading, to be incorporated in the Eurocode 3 following the component method approach. To achieve this, new components and component interactions have to be characterized. In this MSc thesis, the behaviour of the component test; T-plug bending around weak axis, is characterized, by performing both an experimental and numerical study on a new type plug-and-play joint.

## 1.3. Research question

The main goal of this research is to characterize the behaviour of the component test; T-plug bending around weak axis, of a new type plug-and-play joint in terms of strength, stiffness and deformation capacity, as required by the EC3-1-8 component method. This is accomplished by means of experimental and numerical study on the component, which leads to the following definition of the main research question:

***How does the component test; T-plug bending around weak axis, perform in terms of strength, stiffness and deformation capacity, and can its behaviour be characterized following the component method approach?***

In order to gather an answer to the main research question, an experiment is designed and a numerical study is performed. Additionally, an extending parametric study on the geometry of the joint is performed, to describe the behaviour on the component level for the complete spectrum of possible failure modes. This leads to the following definition of the sub-questions:

- *What is the influence of the thickness ratio (reverse channel vs. T-plug web), in terms of strength, stiffness and deformation capacity on the joint behaviour?*
- *What is the influence of the use of stiffeners on the reverse channel and/or T-plug in terms of strength, stiffness and deformation capacity on the joint behaviour?*
- *What is the influence of the use of tubular sections in terms of strength, stiffness and deformation capacity on the joint behaviour?*
- *What is the influence of the length of the T-plug web in terms of strength, stiffness and deformation capacity on the joint behaviour?*
- *Given the parametric study defined by the previous sub-questions, what new components have to be defined?*

## 1.4. Scope

The scope of this MSc thesis is limited to the following:

- Performance of a preliminary numerical study on the component test; T-plug bending around weak axis, to predict the experimental results, using the finite element software of ABAQUS (ABAQUS/CAE, 2014).
- Design of the experiment, consisting of a set of test specimens and a laboratory set-up for testing in the Stevin-II laboratory at the Delft University of Technology. In addition, coupon specimens are designed for the characterization of the material used in the experiment.
- Numerical modelling to extend the range of studied parameters. The parametric study is devoted to the influence of geometrical properties; thickness ratio (reverse channel vs. T-plug web), use of stiffeners, use of tubular sections and length of the T-plug web, for a steel grade S355. The numerical study is again performed with the finite element software of ABAQUS.
- Derivation of new analytical expressions/models to characterize new components, for resistance and stiffness, and components interaction, following the EC3-1-8 component method approach.

## 1.5. Methodology

In this MSc thesis the component test; T-plug bending around weak axis, of a new type plug-and-play joint is studied, as shown in Figure 1.1. In order to provide an answer to the research question stated in Section 1.3, the following steps are taken in the methodology.

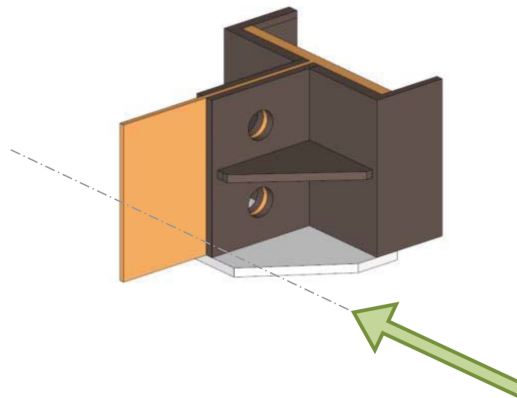


Figure 1.1: T-plug bending around weak axis

As the first step, the findings by previously performed research are closely analysed. Already some very useful research has been performed on this specific plug-and-play joint within the INNO3DJOINTS project. The research on the component test; T-plug in tension, is an adequate starting point for building a numerical model. The numerical model is built using the finite element software of ABAQUS. Next, the numerical model is validated under the same circumstances in term of geometry, material properties and failure modes, with the provided results of the component test; T-plug in tension.

Hereafter, the validated numerical models are used to predict the behaviour of the component test; T-plug bending around weak axis, in the experiment. A preliminary numerical study is performed, by varying a number of geometrical dimensions, based on the sub-questions stated in Section 1.3. Hereby the complete behaviour within the range of interest is covered for the joint under weak axis bending.

Based on the preliminary numerical study an experiment is designed for testing in the Stevin-II laboratory at the Delft University of Technology. The experimental study includes the design of the set of test specimens and laboratory set-up. Also, specimens are designed for coupon testing, in order to obtain the actual material properties of the set of test specimens.

Besides, a parametric study is performed, using an elasto-plastic material model, to characterize the behaviour of the component test; T-plug bending around weak axis, in terms of strength, stiffness and deformation capacity, following the EC3-1-8 component method approach. This results in the derivation of new components and component interactions. Finally, results and recommendations are shared with the INNO3DJOINTS project and the French institute CTICM, for the implementation in the report and software tool.

## **1.6. Document structure**

The main content of this report is divided into four chapters, namely literature research, experimental study, numerical study and component method application. In Chapter 2 the literature research is presented, among other things the state of art: design of joints, plug-and-play joints and an introduction to the component method. Chapter 3 presents the design of the experiment, including the set of test specimens and laboratory set-up. Next, Chapter 4 addresses the numerical model, the numerical results on the prediction of the experiment and the parametric study on the component derivation. Chapter 5 presents the component method application of the plug-and-play joint, in terms of identification, evaluation and assembly, following the EC3-1-8 component method approach. Finally, conclusions and recommendations are given in respectively Chapters 6 and 7.



# 2

## Literature research

This chapter presents the required background information for a better understanding of this MSc thesis. Section 2.1 provides the state of art: design of joint, followed by the concept of plug-and-play joints in Section 2.2 and the classification of joints in Section 2.3. Next, in Section 2.4 the component method is introduced, in terms of design resistance, rotational stiffness and rotation capacity. Hereafter, the 3D behaviour of joints is elaborated in Section 2.5 and finally in Section 2.6 previous research is discussed on performing component tests, numerical modelling and research methodology.

### 2.1. State of art: design of joints

In the modern construction material industry, subjects as sustainability and circular economy are becoming increasingly important, as a consequence of the finite resources of raw materials and the serious concern regarding the global warming potential. This is illustrated in Figure 2.1 for currently the leading country in steel and iron ore production; China (Liu et al., 2018). For the steel construction industry, cost optimisation is one of the most important aspects to remain competitive in the construction market, where one of the biggest opportunities lies in the design of joints, as up to 40% of the total costs of a steel structure are determined by those joints (Bijlaard and Brekelmans, 2007).

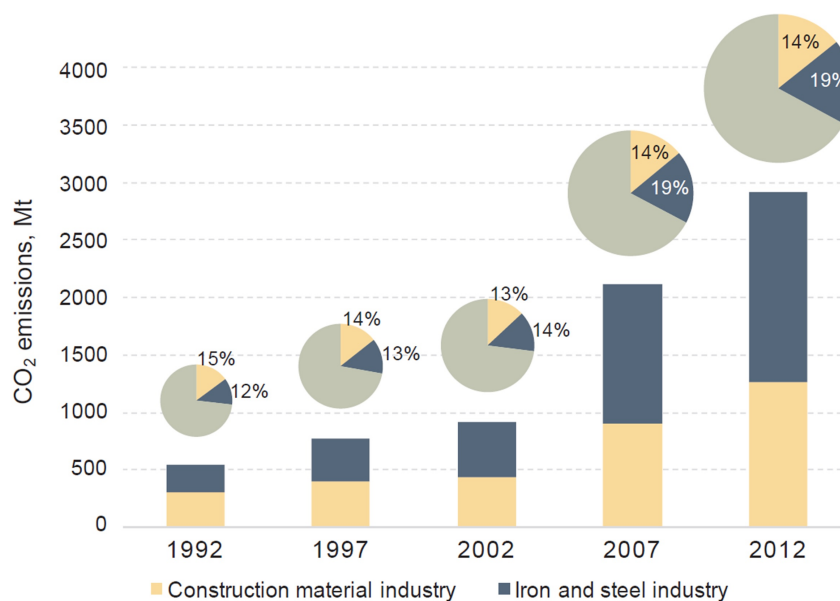


Figure 2.1:  $CO_2$  emissions of the ISI and CMI during 1992-2012. Note: pie charts show the proportion of the ISI and CMI in China's  $CO_2$  emissions structure; the size of pies indicates China's total  $CO_2$  emission size in studied years. (Liu et al., 2018)

Since last century, huge progress has been made on the cost optimisation of joints, as the analysis method on semi-rigid joints has considerably evolved to obtain the true structural response. This already started in 1917, when Wilson and Moore carried out the first studies on semi-rigid joints, which eventually led to the publication of the Eurocode 3 in May 2005 (Díaz et al., 2011). The biggest achievement is the introduction of a new design philosophy, named "modern" design, besides the present "traditional" design. In the traditional design joints are either pinned or rigid, but generally assumed as rigid, along with the linear-elastic theory to determine force and moment distributions. This assumption needs to be checked, which is in practice commonly neglected. The strength of the joint is usually adjusted to the required level, resulting in low deformation or rotation capacity. As a consequence, unnecessary additional stiffeners between the flanges are used, leading to the over-dimensioning of joints and unnecessary high fabrication costs. Furthermore, the joint design is often performed at later stages by either other personnel or even another company, which adds up to costs of the joint. However, most joints have an actual behaviour (finite stiffness) somewhere in between pinned and rigid, known as semi-rigid. The Eurocode 3 accounts for this behaviour by the modern design approach, where joints are considered as structural components with properties as stiffness, strength and deformation capacity, which is further elaborated in Section 2.4. For this reason, modern design potentially leads to a better and more economical design of joints compared to traditional design, of which the joint layout is only influenced in favor of fabrication and assembling considerations. (Bijlaard, 2006) (Veljkovic et al., 2015)

Currently, the most important challenge for the steel construction industry, besides cost optimisation, is the increase in the safety of labour during erection and onsite work while decreasing fabrication and erection time. Onsite labour costs are rapidly increasing, due to the limited availability of skilled workers and more strict safety measures imposed by governments. In modern building construction, a steel framework with hot-rolled members is a commonly used structural system, where beam-to-column joints transfer loads from beam to column. These moment-resisting joints are often welded connections, bolted end plate connections and bolted connections with angle cleats, which assembly process involves skilled labour, in fabrication and fieldwork, under varying and dangerous working conditions.

Table 2.1: Traditional (bolted and welded) joints versus plug-and-play joints

Criteria	Traditional joints	
Sustainability	Not reusable within the same lifetime, only after demolition	-
Fabrication	Standard hot-rolled or cold-formed profiles	+
Assembly	Onsite bolted or welded at every stage, requiring skilled work	-
Safety	Varying, difficult and dangerous working conditions	-
Erection time	Slow, due to a lot of onsite assembling	-
Design standard	Component method EC3-1-8	+
Total costs	Longer erection time and more onsite assembling leads to higher costs	-
Criteria	Plug-and-play joints	
Sustainability	Potentially reusable within the same lifetime	+
Fabrication	Modularity of elements	+
Assembly	Fastening of bolts after stability and bearing capacity of the structure is established	+
Safety	Less onsite work in safe working conditions	+
Erection time	Fast, due to modularity and less assembling	+
Design standard	No design standard available yet, but component method is applicable if components are comparable	-
Total costs	Fabrication may be slightly more expensive, given that the total costs of fabrication and construction decrease	+

In Table 2.1 a comparison is given between traditional joints and plug-and-play joints on several criteria. This raises the question of whether the use of plug-and-play joints becomes a more favourable market target for future steel constructions, as the joint concept moves from a local production technology towards an industrialised or automatic production. The use of plug-and-play joints is generally characterised by modularity and fast erection methods, due to the modernisation of fabrication processes. This has led to an enormous decrease in fabrication costs and a significant decrease in onsite work. For this reason, the costs of these plug-and-play joints can eventually turn out to be lower than the costs of traditional bolted and welded connections. The only serious disadvantage for plug-and-play joints remains that

no explicit rules for safety verification exist in the current EC3-1-8. Therefore experiments have to be performed to characterize the behaviour of components, in order to be implemented in future design standards. (Bijlaard et al., 2009) (Bijlaard and Brekelmans, 2007)

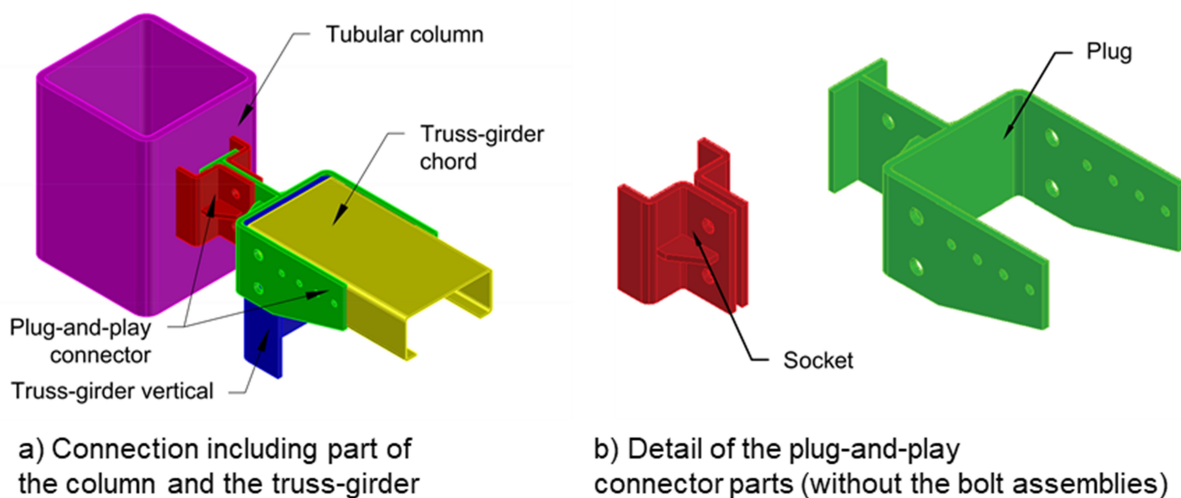


Figure 2.2: Schematic representation of the plug-and-play joint (Da Silva et al., 2019)

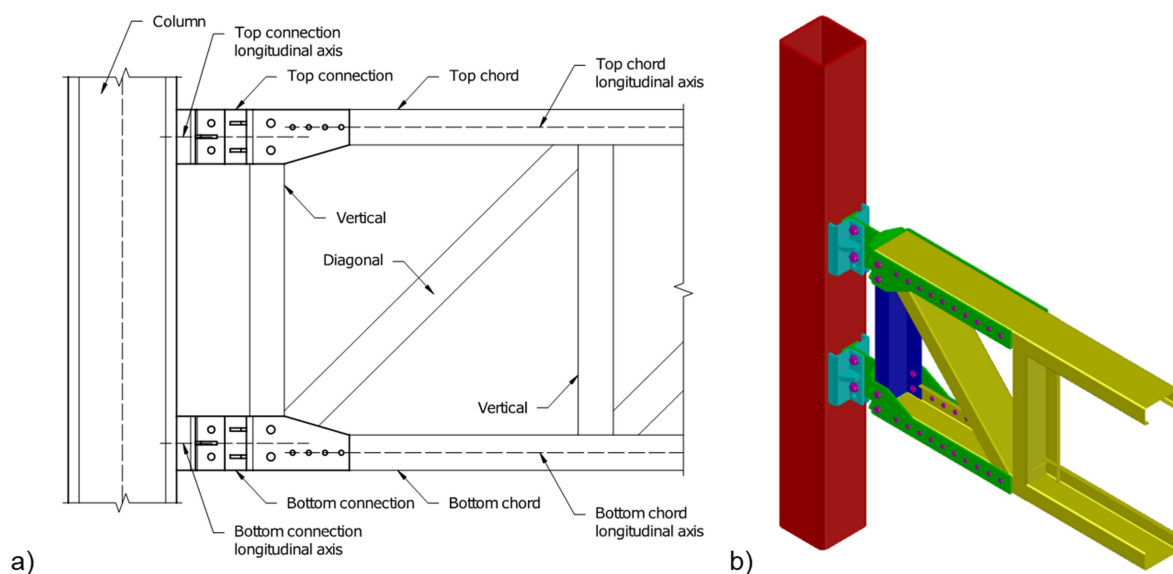


Figure 2.3: Schematic representation of the assembled plug-and-play joint (Da Silva et al., 2019)

## 2.2. Plug-and-play joints

Recently, INNO3DJOINTS has developed a new hybrid plug-and-play joint for tubular cold-formed steel columns (CHS, SHS or RHS) connected to cold-formed lightweight steel profiles to provide a highly efficient structural system. This new hybrid plug-and-play joint has several advantages compared to the traditional bolted and welded joints, in addition to the advantages already mentioned in Section 2.1, such as the use of light steel floors, modularity emphasizing simplicity in transport and erection and improved performance to seismic action. (INNO3DJOINTS, 2015)

The plug-and-play joint consists of two parts; a steel socket and a plug connector, as shown in Figure 2.2b. In Figure 2.2a, also the connecting elements are included, such as a tubular cold-formed steel column and a cold-formed lightweight steel truss-girder. The steel socket is made of a reverse channel profile, which is welded connected to the tubular cold-formed steel column. Additionally, the reverse channel is reinforced with a stiffener, but as explained in Chapter 1.3, specimens both with and without stiffener are considered for the component test; T-plug bending around weak axis. Accounting for all these elements, the assembly of the plug-and-play joint is as follows:

1. The tubular column is welded into the socket in which the plug is slid and bolted into position;
2. The socket is fastened to the plug using two bolts;
3. The plug is connected to the truss girder by several bolts, the larger bolts distribute forces between the plug and the truss girder chords. (Da Silva et al., 2019)

The assembly of the plug-and-play joint, see Figure 2.3, brings along some additional aspects to be considered in the design and fabrication process. The main joint characteristics to consider in the automated construction of the plug-and-play joints are mentioned below:

- **Tolerances:** the connection must have tolerances regarding self-alignment, to be able to guide the beam towards the proper location once contact is made between connection elements located on the beam and column, and adjustment, as it is unlikely that the connection will be precisely in its correct position after erection;
- **Strength, stiffness and stability:** the connection must be strong enough to carry design loads while possessing a suitable amount of stiffness to control deflections. Furthermore, the connection must be stable enough to allow erection of the structure to continue until the final fastening;
- **Modularity:** the connection should be able to be mass-produced with a standard shop fitting operation and with quick, automatic erection capabilities. (Lytle et al., 2003)

### 2.3. Classification of joints

When it comes to joint modelling, EC3-1-1: General rules and rules for buildings, states that in general the effects of the behaviour of the joints on the distribution of internal forces and moments within a structure and on the overall deformations of the structure may be neglected. However, when those effects are significant they should be accounted for and to identify whether this is the case, there is referred to EC3-1-8: Design of joints, where a distinction is made out of three simplified joint models, namely:

- Simple joint model, in which the joint may be assumed not to transmit bending moments;
- Continuous joint model, in which the behaviour of the joint may be assumed to not affect the global analysis;
- Semi-continuous joint model, in which the behaviour of the joint needs to be taken into account in the global analysis. (EN 1993-1-1, 2005) (EN 1993-1-8, 2005)

Following the Eurocode approach, all joints are classified by either stiffness or strength to fit in one of these joint models, as shown in Table 2.2. In the following paragraphs, each of those approaches is discussed.

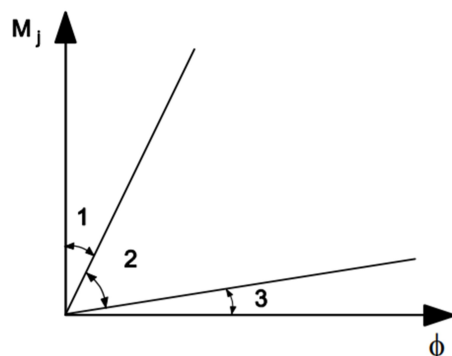
Table 2.2: Type of joint model (EN 1993-1-8, 2005)

Method of global analysis	Classification of joints		
Elastic	Nominally pinned	Rigid	Semi-rigid
Rigid-plastic	Nominally pinned	Full-strength	Partial-strength
Elastic-Plastic	Nominally pinned	Rigid and Full-strength	Semi-rigid and partial-strength Semi-rigid and full-strength Rigid and partial-strength
Type of joint model	Simple	Continuous	Semi-continuous

### 2.3.1. Classification by stiffness

When a joint is classified by stiffness, its rotational stiffness is compared to its initial rotational stiffness with the boundaries given in Figure 2.4. The joint can be placed in three categories, namely nominally pinned, rigid or semi-rigid:

- *Nominally pinned joints*: the joint is capable of transmitting the internal forces, without developing significant moments. Besides, the joint can withstand the resulting deformations of the design loads.
- *Rigid joints*: the joint has sufficient rotational stiffness to be analysed on full continuity. Generally these type of joints require additional material, such as stiffeners, which makes the joint more expensive (Bijlaard, 2006).
- *Semi-rigid joints*: all joints not meeting the requirements of the two other categories are classified as semi-rigid, resulting in both moments and deformations due to the design loads. (EN 1993-1-8, 2005)



Zone 1: rigid, if  $S_{j,ini} \geq k_b EI_b / L_b$

where:

$k_b = 8$  for frames where the bracing system reduces the horizontal displacement by at least 80 %

$k_b = 25$  for other frames, provided that in every storey  $K_b/K_c \geq 0,1$  <sup>\*)</sup>

Zone 2: semi-rigid

All joints in zone 2 should be classified as semi-rigid. Joints in zones 1 or 3 may optionally also be treated as semi-rigid.

Zone 3: nominally pinned, if  $S_{j,ini} \leq 0,5 EI_b / L_b$

<sup>\*)</sup> For frames where  $K_b/K_c < 0,1$  the joints should be classified as semi-rigid.

Key:

$K_b$  is the mean value of  $I_b/L_b$  for all the beams at the top of that storey;

$K_c$  is the mean value of  $I_c/L_c$  for all the columns in that storey;

$I_b$  is the second moment of area of a beam;

$I_c$  is the second moment of area of a column;

$L_b$  is the span of a beam (centre-to-centre of columns);



$L_c$  is the storey height of a column.

Figure 2.4: Classification of joints according to stiffness (EN 1993-1-8, 2005)

### 2.3.2. Classification by strength

When a joint is classified by strength, its design moment resistance ( $M_{j,Rd}$ ) is compared to design moment resistances of the connecting members. The joint can be placed in three categories, namely nominally pinned, full-strength or partial-strength:

- *Nominally pinned joints*: the joint is capable of transmitting the internal forces, without developing significant moments. Besides, the joint can withstand the resulting deformations of the design loads. This is satisfied if its design moment resistance is not greater than 25% of the design moment resistance required for a full-strength joint.
- *Full-strength joints*: the design moment resistance is not less than the connecting members, column and beam, following the criteria in Figure 2.5.
- *Partial-strength joints*: all joints not meeting the requirements of the two other categories are classified as partial-strength. (EN 1993-1-8, 2005)

a) Top of column		Either	$M_{j,Rd} \geq M_{b,pt,Rd}$
		or	$M_{j,Rd} \geq M_{c,pt,Rd}$
b) Within column height		Either	$M_{j,Rd} \geq M_{b,pt,Rd}$
		or	$M_{j,Rd} \geq 2 M_{c,pt,Rd}$

Key:

$M_{b,pt,Rd}$  is the design plastic moment resistance of a beam;

$M_{c,pt,Rd}$  is the design plastic moment resistance of a column.

Figure 2.5: Full-strength joints design criteria (EN 1993-1-8, 2005)

## 2.4. Introduction to the component method

The complete spectrum of moment-rotation curves can be estimated by several methods (Diaz et al., 2011), whereby the Eurocode 3 makes use of the component method. The component method is most commonly accepted and used approach, because of its simplicity in use and its sufficient accuracy to reproduce reality. This type of structural analysis simplifies an actual structure into a set of basic components, which can be easily hand calculated for practical use. The application of the component method can be summarized in the following three steps:

1. *Identification* of all the active components in the joint, selected from the list of basic joint components in the EC3-1-8.
2. *Evaluation* of the stiffness and resistance characteristics for individual basic components chosen in the previous step.
3. *Assembly* of all the individual components, as parallel or series springs, see Figure 2.6, to describe the behaviour of the joint, and evaluation of the stiffness and resistance characteristics of the whole joint.

A more detailed description on the EC3-1-8 component method approach, regarding the main structural properties of the joint; the design resistance, the rotational stiffness and the rotation capacity is given in the following paragraphs.

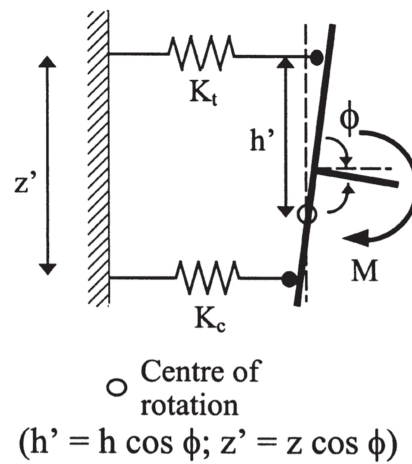


Figure 2.6: Equivalent spring model for steel connections (Da Silva and Coelho, 2001)

### 2.4.1. Design resistance

For determining the design resistance of the whole joint, the joint is divided into several basic components depending on the type of joint. The first step is to determine the design resistance of the active components of the joint. The design resistance consists of three forces, namely normal forces, shear forces and bending moments. In general the stresses due to these forces in a member may be assumed not to affect the design resistance of the basic components. For the few exceptions that exist, the normal and shear forces are already accounted for within the determination of the resistance of the basic component itself. When determining the individual resistance of the basic components, for some specific components an equivalent T-stub model is used. Therefore, it is required to determine if prying forces occur, besides the effective yield lines for individual bolt rows and groups of bolt rows if present.

When the design resistance of all individual basic components is determined, the resistance of the joint is determined, whereby the joint is modelled as an assembly of springs (basic components) and rigid links. All joint models are composed of a tension zone, concentrating all components in tension, a compression zone and a shear zone. Therefore each zone is replaced by an equivalent spring, retaining all the original relevant characteristics. Based on the lever arm between the equivalent tension and compression spring the design moment resistance of the joint is determined. (Da Silva and Coelho, 2001)

### 2.4.2. Rotational stiffness

The procedure for determining the rotational stiffness is very similar to the design resistance described above. Again, the stiffness of the individual basic components are determined first, before assembling the joint model with the same equivalent spring configuration. If the stiffness of an individual basic component can be assumed to be infinite, this stiffness can be neglected in the joint model. The stiffness of the whole joint is subsequently determined with the following equation:

$$S_j = \frac{Ez^2}{\mu \sum_i \frac{1}{k_i}} \quad (\text{Eq. 2.1})$$

With,

- $k_i$  is the stiffness coefficient for basic joint component  $i$ ;
- $z$  is the lever arm;
- $\mu$  is the stiffness ratio  $S_{j,ini}/S_j$ .



### 2.4.3. Rotation capacity

For the rotation capacity the Eurocode provides a simple general rule, if the design moment resistance ( $M_{j,Rd}$ ) of the joint is at least 1.2 times the design plastic moment resistance ( $M_{pl,Rd}$ ), the rotation capacity of the joint does not need to be checked and may be assumed to be sufficient. However, the rotation capacity for bolted and welded connections can also be determined using the provisions of the EC3-1-8, under the condition that the design axial force ( $N_{Ed}$ ) does not exceed 5% of the design plastic resistance ( $N_{pl,Rd}$ ). (EN 1993-1-8, 2005)

As explained, in the current Eurocode the subject of rotation capacity for joints is only addressed by provisions securing the joint has sufficient rotation capacity without actually determining its maximum rotational capacity. Da Silva et al. have tried to develop a ductility model for steel connections incorporating all required connection properties (resistance, stiffness and ductility) into one single consistent model. (Da Silva and Coelho, 2001)

## 2.5. 3D behaviour of joints

To incorporate 3D effects in the analysis of joint behaviour, computational FE models are currently the only tool available. This type of analysis has various advantages, as it can perform more complex calculations and accounts for the effect of joint stiffness. Besides, it optimizes the maximum capacity of the structure, due to the redistribution of moments. The downside of these FE models is that these are still very time consuming and required advanced knowledge in use. (INNO3DJOINTS, 2015)

In theory, a steel connection can also be modelled as a six degrees-of-freedom non-linear spring, accounting for the 3D behaviour of the joint. Each of the six degrees-of-freedom (three rotations and three translations) can be uncoupled in an independent degree-of-freedom, representing two bending moments (strong and weak axis), a torsional moment, an axial force and two shear forces. Generally this complexity is not required, as the bending around strong axis usually mostly influences the results of structural analysis. Therefore the remaining degrees-of-freedom are allowed to be simplified with either infinite or zero stiffness.

As previously mentioned in Paragraph 2.4.2, in comparison with the derivation of the joint resistance and stiffness, few knowledge is still available on the determination the rotation capacity. Regarding the recent concern on the robustness of structures, a slight overstrength of a ductile component can shift the failure mode to the second weakest, and possibly brittle, component, changing the rotation capacity of the joint drastically. (Da Silva et al., 2003) Therefore designers now face a strong need to predict the 3D behaviour of steel joints in a consistent design framework under generalised 3D loading following the component method approach. To establish the design framework accounting for generalised 3D loading the standard six degrees-of-freedom is not sufficient anymore, as several beam members connect to different parts of the same column cross-section. Therefore the joint has to be composed of multiple generalised connections, resulting in much more than six degrees-of-freedom and for each stiffness coefficient a corresponding component in the EC3-1-8. (Da Silva, 2008)

This is a major adjustment compared to the current design of joints following the EC3-1-8: component method, where the 3D spatial behaviour of the joint is fully neglected. Generally, traditional bolted and welded joints are very suitable for this design simplification, where the basis of forces results solely from plane frame analysis. This is because traditional joints have by themselves sufficient resistance against the spatial behaviour, which is usually caused by a wind load creating tensile forces in the joint and/or eccentric loading producing torsion moments in the joint. To which extend plug-and-play joints can be checked using the component method, depends on the willingness to accept this simplification and the ingenuity to recognise components of the plug-and-play joints to be comparable to the basic components listed in the EC3-1-8. However, in designing new types of plug-and-play joints the designer needs to be explicitly aware of this spatial behaviour, which can be neglected in designing traditional joints. (Bijlaard and Brekelmans, 2007)

For a future increasing market share the need for a design procedure in the framework of the component method, incorporating the 3D spatial behaviour of the joint, is growing. Therefore it is necessary to perform experiments and evaluate the results to obtain reliable values for the determination of the mechanical properties; strength, stiffness and deformation capacity, of the plug-and-play joint. As mentioned in Section 1.1, INNO3DJOINTS aims to develop a framework for a consistent design approach for a new steel type plug-and-play joint under 3D generalized loading. For the completeness characterization of new components and components interaction is required. The component test; T-plug bending around weak axis, is investigated in this MSc thesis. (INNO3DJOINTS, 2015)

## 2.6. Previous research

For any research project, previous research forms a good starting point. In this section is specifically looked at previous research regarding the component test and parametric study procedure, numerical modelling of the specimens and the general research method.

### 2.6.1. Component test

Currently, a lot of research has already been performed by INNO3DJOINTS on the new plug-and-play joint, shown in Figure 2.2. In particular, the research on the component test; T-plug in tension, can be interpreted as useful as it treats the exact same joint configuration. For this reason, the methodology and the parametric study, regarding the component test; T-plug in tension, have to be studied closely.

Table 2.3: Characteristic dimensions of the studied specimen (Da Silva et al., 2019)

Name of the specimen	T-plug thickness [mm]	Socket thickness [mm]	Remarks
A-RP	6	10	-
A-SH-RP	6	10	Slotted bolts
B-RP	10	6	-
B-U-RP	10	6	Unstiffened socket
Q3-RP	10	10	-
Q3-SHS	10	10	-
Q3-CHS	10	10	-

The main goal of a component test is to identify as many as possible failure modes for the plug-and-play joint under a specific load application, in order to analytically describe the complete behaviour of the joint, in terms of strength, stiffness and deformation capacity. In the research on the component test; T-plug in tension, the influence of the following parameters on the overall performance of the component have been investigated: the plate thickness of the socket (reverse channel) and T-plug, the use of stiffeners, the influence of bolts and of the tubular sections. These parameters are tested as a number of specimens, shown in Table 2.3, with a rigid plate (RP), square hollow section (SHS) and circular hollow section (CHS).

A summary of the obtained results is given in Figure 2.7. Based on a performance-based analysis can be concluded that configurations with similar thickness for T-plug and reverse channel or with a larger T-plug thickness have the highest load-bearing capacity in tension. By analysing the failure modes, the first two specimens, A-RP and A-SH-RP, both failed in the net-section of the T-plug. However, the failure for the A-SH-RP specimen occurred at a larger deformation, since the bolts in shear only start contributing to the overall resistance at a later stage, due to the slotted holes. Comparing the B-RP and B-U-RP specimens, in general, similar behaviour is shown in the graph, except the elastic resistance is slightly lower for the B-U-RP specimen (unstiffened reverse channel). When looking at the specific failure modes, the B-RP specimen failed when the stiffener loses contact with the reverse channel and the B-U-RP specimen has a shear-out failure of the bolts. Looking at the final three specimens, again, no major differences are found in terms of resistance between the tubular

configurations and the rigid plate. However, the Q3-RP specimen failed due to fracture of one of the bolts in shear, the CHS specimen failed in the yield line of the reverse channel and the SHS specimen failed due to extensive deformations in all elements. (Da Silva et al., 2019)

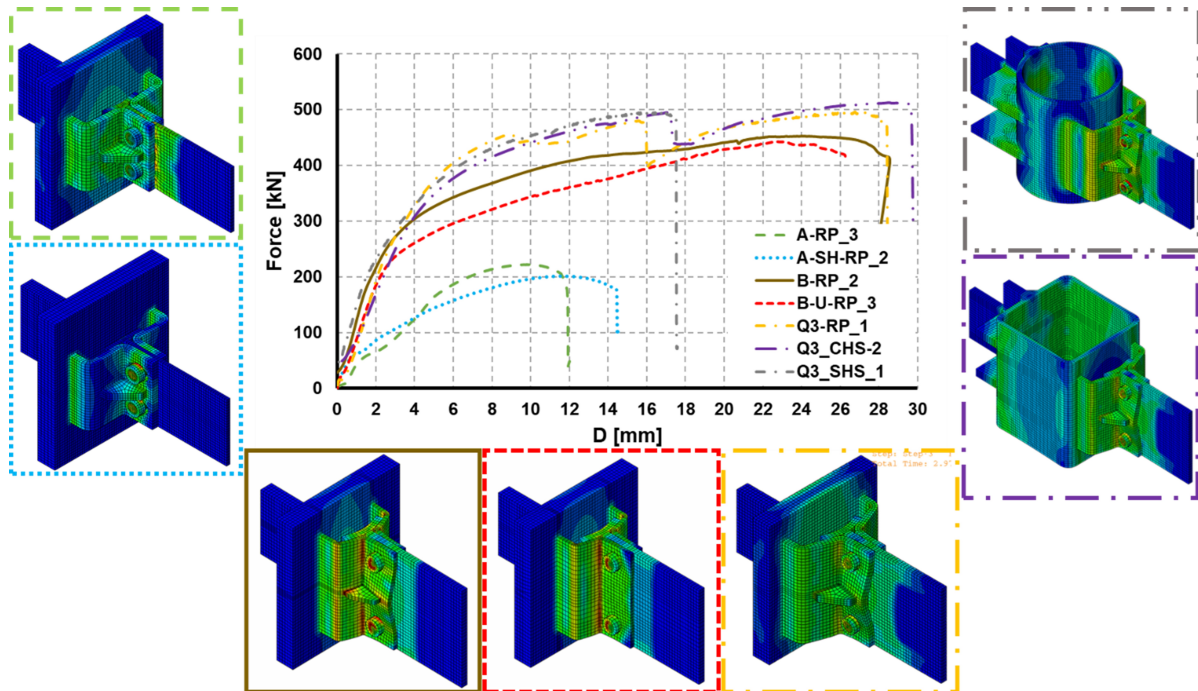


Figure 2.7: Comparison between all tested configurations of component T-plug in tension (Da Silva et al., 2019)

These findings form a basis for a first version of the numerical model on the component test; T-plug bending around weak axis. The same configuration can be modelled and tested under tension to validate the numerical model. Hereby important design aspects, such as the maximum load-bearing capacity, initial stiffness, total deformation and failure mode, form the basis of validating. This process is explained in further detail in Appendix A.

### 2.6.2. Numerical modelling

After analysing the procedure of the component test and the corresponding parametric study, a numerical model is built to predict the component behaviour under an applied load. First, the model is validated under a tension load, before applying bending around weak axis and eventually building a numerical model for the experimental configurations. All the specimens are chosen to be modelled by means of finite elements using the software ABAQUS. It is important to validate the numerical models after the experiments have been performed, both in terms of geometrical dimensions and material properties, in order to compare the experimental and numerical retrieved results, to perform an extending parametric study to broaden and expand the geometric range of properties and being able to analytically characterize the behaviour of the joint.

Besides the geometry, numerous other aspects have to be defined accurately to be able to reproduce valid test results. The materials used in the FE models have to be the same as in the experiments. This is achieved by the true stress-strain curves retrieved from coupon tests of the test specimen. In this way, the FE models are calibrated to reproduce the behaviour of the test specimens, regarding strength, stiffness and deformation capacity. The remaining aspects include the finite element type, interactions and boundary conditions, type of analysis and time functions. The research on T-stub behaviour under out-of-plane bending by Gil et al. shows similarities to this research on the component: T-plug bending around weak axis, both in research method, explained in Paragraph 2.6.3, and numerical modelling. Here is chosen to model with the ABAQUS 8-node solid elements with reduced

integration, element type C3D8R. For interactions between surfaces, contact properties are defined for both normal, by means of "hard contact" allowing surfaces to be separated after contact, and tangential direction, with a defined friction coefficient. Also, the boundary conditions have to be defined similarly as in the experiments. Special attention is given at the boundary condition of load application, as only deformations in the direction of the applied load are present. For an extra check to confirm the model is valid, two types of analysis are performed, namely an explicit and implicit solver, which should give similar results. At last, the time function has an important share in the reliability of the numerical results and therefore often is chosen to apply the load displacement-based, as no turning points in the graph have to be overcome. (Gil and Goñi, 2015)

### 2.6.3. Research methodology

As mentioned above, the research on T-stub behaviour under out-of-plane bending by Gil et al. is a good indication of a research method to be used in this research on the plug-and-play component test; T-plug bending around weak axis. In the research on the T-stub behaviour under out-of-plane bending also numerical models and experiment results are compared to analytically characterize new components in the concept of the component method. Therefore, an important aspect in the research method is to perform coupon tests on the test specimens, beside the tests on bending around weak axis, to retrieve true stress-strain curves for validation of the numerical models. Similarly, this method is also applied in the component test; T-plug in tension, by INNO3DJOINTS (Da Silva et al., 2019).

Another useful aspect for this research is the procedure of classification of joints, in terms of strength and stiffness, in order to determine real boundary conditions to try to optimise structural elements. This is because 3D behaviour of steel joints and the behaviour of the weak axis bending have not been fully investigated and therefore not included in the design codes, like the Eurocode. In order to extrapolate the component method to 3D cases, additional components need to be characterized based on the component method. Therefore new effective lengths and analytical expressions have to be established and these components are compared with the experimental results and finite element models. This can only be done, by testing the specific components on full-scale in experiments. This procedure of characterization of components can be very useful in characterizing the behaviour of the component test; T-plug bending around weak axis. (Gil and Goñi, 2015) (Gil et al., 2015)



# 3

## Experiment design

In this chapter the complete design of the experiment is elaborated, starting with the experimental objectives in Section 3.1. Next, in Section 3.2 the configurations of the set of test specimens are discussed, followed by the material characterization of the coupon tests, in Section 3.3. Finally, in Section 3.4 the design of the laboratory set-up is discussed, including the frame resistance, frame design, frame detailing and instrumentation.

### 3.1. Experimental objectives

In the experiment, a plug-and-play connection between a tubular cold-formed steel column and a cold-formed lightweight steel frame is studied. In detail, the focus is given on the interaction between the steel socket, consisting of a reverse channel profile, and the T-plug connector, connected by a pair of M16 bolts. The test specimens are fabricated by Fametal S.A. and the experiments are performed in the Stevin-II laboratory at the Delft University of Technology. The main aim of the experiment is to capture the behaviour for various configurations of the plug-and-play joint under an applied load, developed by a bending moment around the T-plug weak axis. The experimental results can be used to validate the corresponding numerical models in ABAQUS. The numerical results are used to characterize the behaviour of the component test; T-plug bending around weak axis, in terms of strength, stiffness and deformation capacity.

However, following the EC3-1-8 component method approach for the design of joints, no explicit rules for safety verification exist for plug-and-play joints. In order to derive general analytical formulae to describe the joint behaviour experiments are required at first, which includes the component tests; T-plug bending around weak axis. Given the aim of this experiment, various geometrical dimensions are taken as a variable parameter to broaden the spectrum of analysis, as the steel grade is kept constant at S355. This leads to the definition of the following objectives for the experiments:

- (a) To study the behaviour of the component test; T-plug bending around weak axis, considering both bending and shear deformation, by restraining all rotations, both translations in the horizontal plane and allowing only for a vertical translation in the direction of load application.
- (b) To compare and validate the results of the numerical study, in order for the numerical models. The validation is performed in terms of material properties (initial stiffness, strength and stress-strain relation), boundary conditions and geometrical dimensions.
- (c) To study the influence the use of stiffeners on the T-plug web, using two groups of specimens, one according to the original plan (B-UU-RP) and one according to the improved plan (B-U-RP) of the project. See Appendix B for more details/motivations concerning the plan adjustment.

- (d) To study the influence of the thickness ratio (reverse channel vs. T-plug web), using three groups of specimens with ratios of  $>1$  (A-RP),  $<1$  (B-RP) and  $1$  (C-RP).
- (e) To study the influence of the use of stiffeners on the reverse channel, using two groups of specimens an identical configuration, one with (B-RP) and one without (B-U-RP) stiffener.
- (f) To study the influence of the use of tubular sections, using three groups of specimens with identical configurations, but connected to a rigid plate (C-RP) and two tubular sections instead. The group consists of a stiff configuration, with the legs of the reverse channel close to the chord side walls in combination with the largest available thickness (C-SHS200), and a flexible configuration, with a considerable distance in between the leg and the chord side wall in combination with a smallest available thickness (C-SHS260).
- (g) To retrieve the actual material properties from the coupons with corresponding thickness, either flat or bent, of reverse channel and T-plug. These actual material properties can be used for the validation of the numerical models, as explained above.

### 3.2. Test specimens

For the experimental study a total of seven groups of specimens are designed, based on the findings of the preliminary numerical study elaborated in Appendix B. Following the objectives of the experiment, explained in Section 3.1, the influence of the following geometrical parameters is studied in the experiment: the thickness ratio (reverse channel vs. T-plug web), the use of stiffeners and the use of tubular sections.

Specimens A-RP, B-RP and C-RP are part of the study on the influence of the thickness ratio, with varying ratios from 10:6 to 6:10 and 10:10, including two types of design for the reverse channel. Specimens A-RP and C-RP have a similar reverse channel configuration, where specimen B-RP has slightly different dimensions in height, length and width. Next, specimens B-RP and B-U-RP represent the study on the use of stiffeners on the reverse channel since the influence of the stiffener is most dominantly expressed in combination with the smallest thickness ratio reverse channel vs. T-plug. For similar reasons, specimens B-U-RP and B-UU-RP represent the study on the use of stiffeners on the T-plug web. At last, the specimens C-RP, C-SHS200 and C-SHS260 are used to study the influence of the use of tubular sections. Since the influence on the tubular section is the largest in combination with the strongest thickness ratio, being 10:10. For the study on this parameter both the distance between the chord side wall and leg of the reverse channel as well as the thickness of the tubular section are taken into account, by testing a very stiff (profile SHS200x12.5) and very flexible configurations (profile SHS260x6). Given these parameters, 7 different configurations are designed resulting in a total of 14 experiments for the characterization of the component test; T-plug bending around weak axis. Table 3.1 provides the test matrix for the component test; T-plug bending around weak axis.

Table 3.1: Test matrix for the component test; T-plug bending around weak axis

Specimen	Reverse channel			T-plug			Column section	Number of test
	Quality	Thickness	Stiffener	Quality	Thickness	Stiffener		
A-RP	S355	10	Yes	S355	6	Yes	Rigid plate	2
B-RP	S355	6	Yes	S355	10	Yes	Rigid plate	2
B-U-RP	S355	6	No	S355	10	Yes	Rigid plate	2
B-UU-RP	S355	6	No	S355	10	No	Rigid plate	2
C-RP	S355	10	Yes	S355	10	Yes	Rigid plate	2
C-SHS200	S355	10	Yes	S355	10	Yes	SHS 200x12.5	2
C-SHS260	S355	10	Yes	S355	10	Yes	SHS 260x6	2

In the following figures, the geometric configurations of each test specimen are defined. Figure 3.1 depicts the geometric configuration of the specimen A-RP, which includes basic features as a stiffened reverse channel/T-plug and a rigid plate connection. The objective of this



specimen is to study the influence of the thickness ratio  $>1$  (reverse channel vs. T-plug web) on the overall behaviour of the joint. Hence, this configuration has a 10 mm reverse channel compared to the 6 mm T-plug.

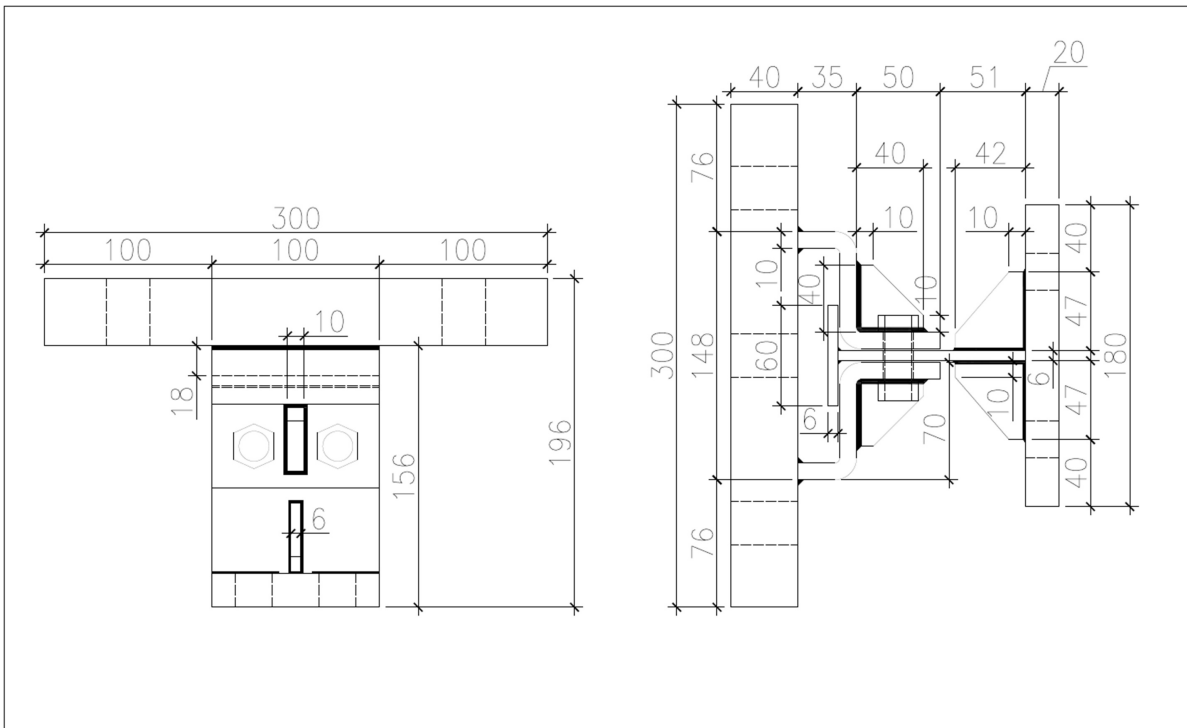


Figure 3.1: Geometric configuration of specimens A-RP

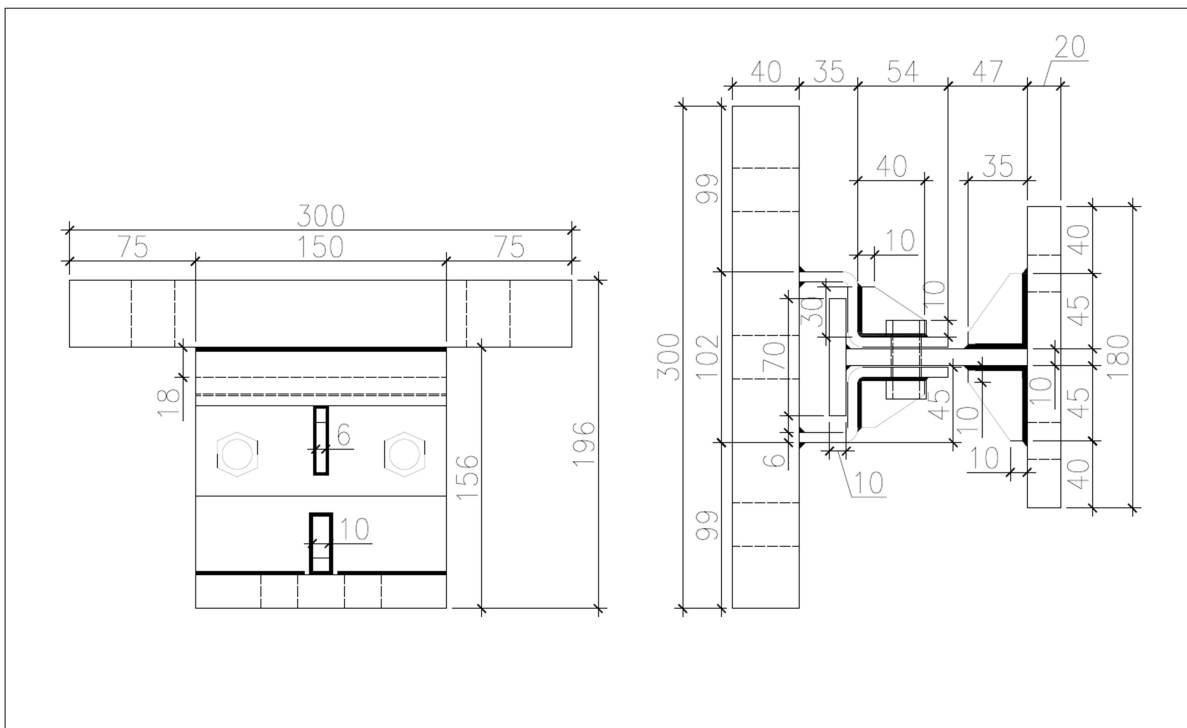


Figure 3.2: Geometric configuration of specimens B-RP

In Figure 3.2 the geometric configuration of the specimen B-RP is depicted. The specimen contains the same features and objective as specimen A-RP, but then for a thickness ratio  $< 1$  and a slightly different configuration of the reverse channel. Hence, this configuration has a  $6\text{ mm}$  reverse channel compared to the  $10\text{ mm}$  T-plug. Besides, this specimen is also involved in the investigation on the use of stiffeners, representing the double stiffened configuration for both reverse channel and T-plug.

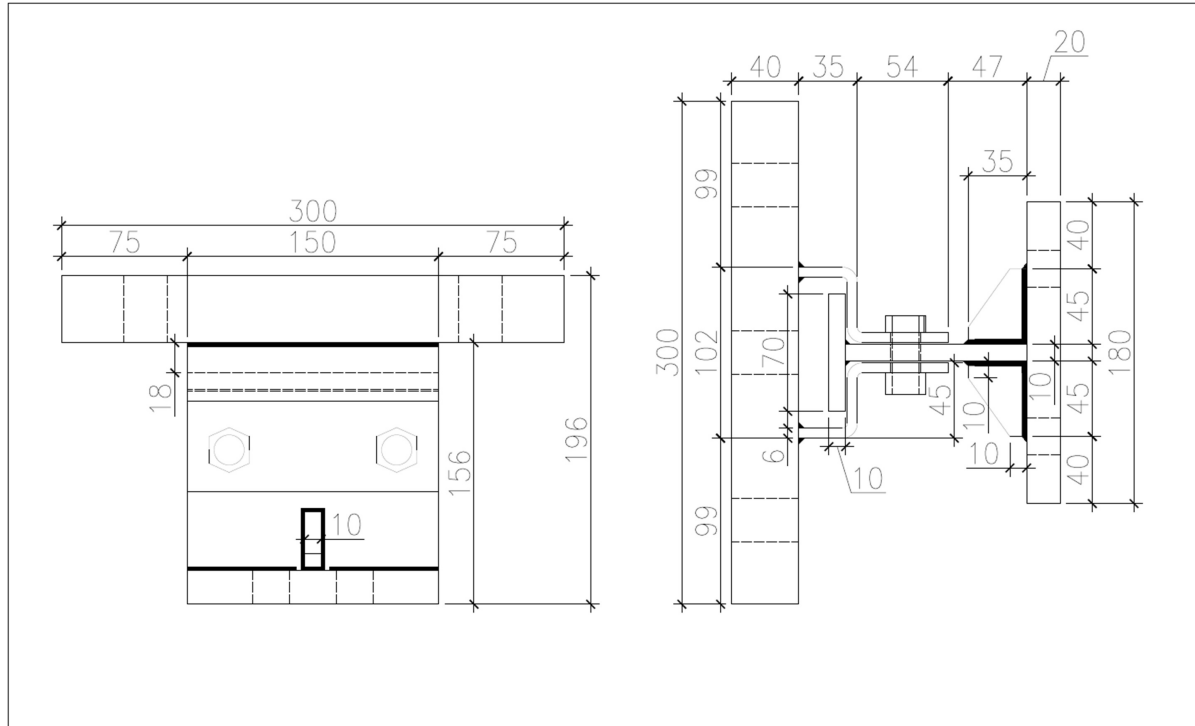


Figure 3.3: Geometric configuration of specimens B-U-RP

In Figure 3.3 the geometric configuration of the specimen B-U-RP is depicted. Compared to the previous specimen B-RP, the same configuration is defined, except for the use of stiffeners on the reverse channel. The objective of this specimen is to study the influence of the use of stiffener on the overall behaviour of the joint.

In Figure 3.4 the geometric configuration of the specimen B-UU-RP is depicted. Compared to the previous specimen B-U-RP, the same configuration is defined, except for the use of stiffeners for the T-plug web. The objective of this specimen is to study the influence of the use of stiffener on the overall behaviour of the joint.

In Figure 3.5 the geometric configuration of the specimen C-RP is depicted. In this specimen the basic features as stiffened reverse channel/T-plug and a rigid plate connection are again used. The objective of this specimen is to study the influence of the thickness ratio equal to 1 on the overall behaviour of the joint. Hence, this configuration has a  $10\text{ mm}$  reverse channel and a  $10\text{ mm}$  T-plug, following the same configuration for reverse channel as specimen A-RP. Besides, this specimen is involved in the investigation on the use of tubular section, representing the configuration connected to a rigid plate.

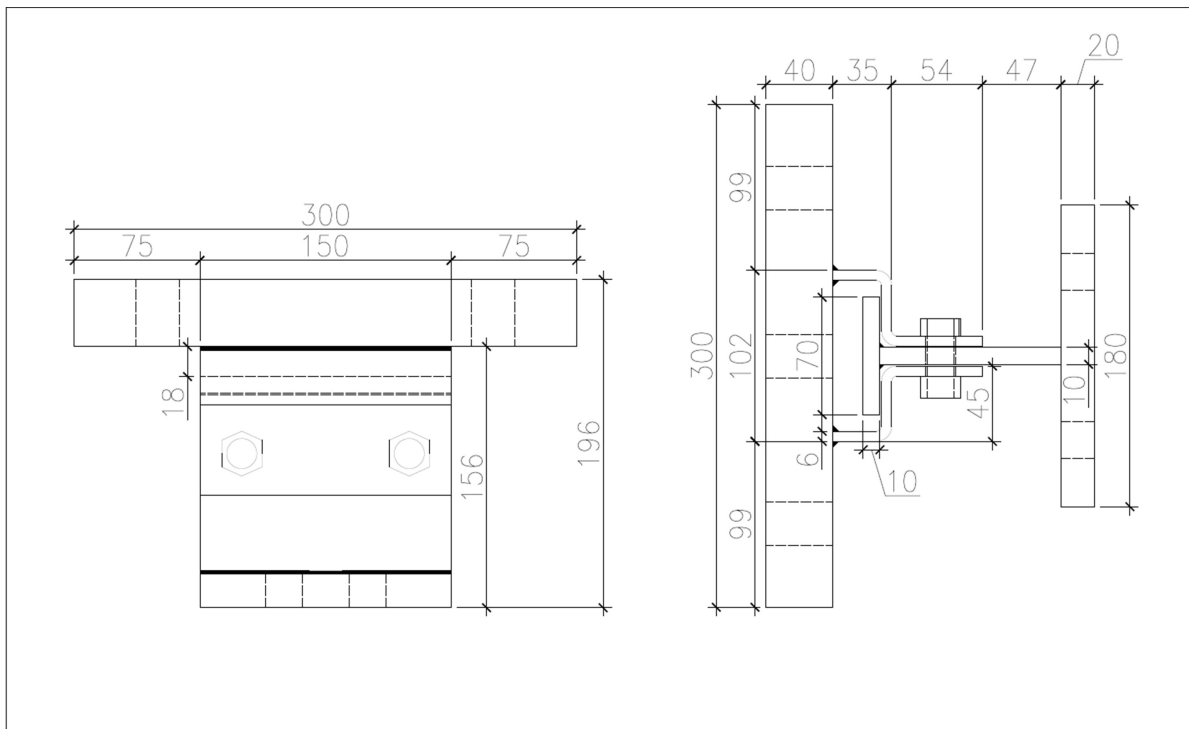


Figure 3.4: Geometric configuration of specimens B-UU-RP

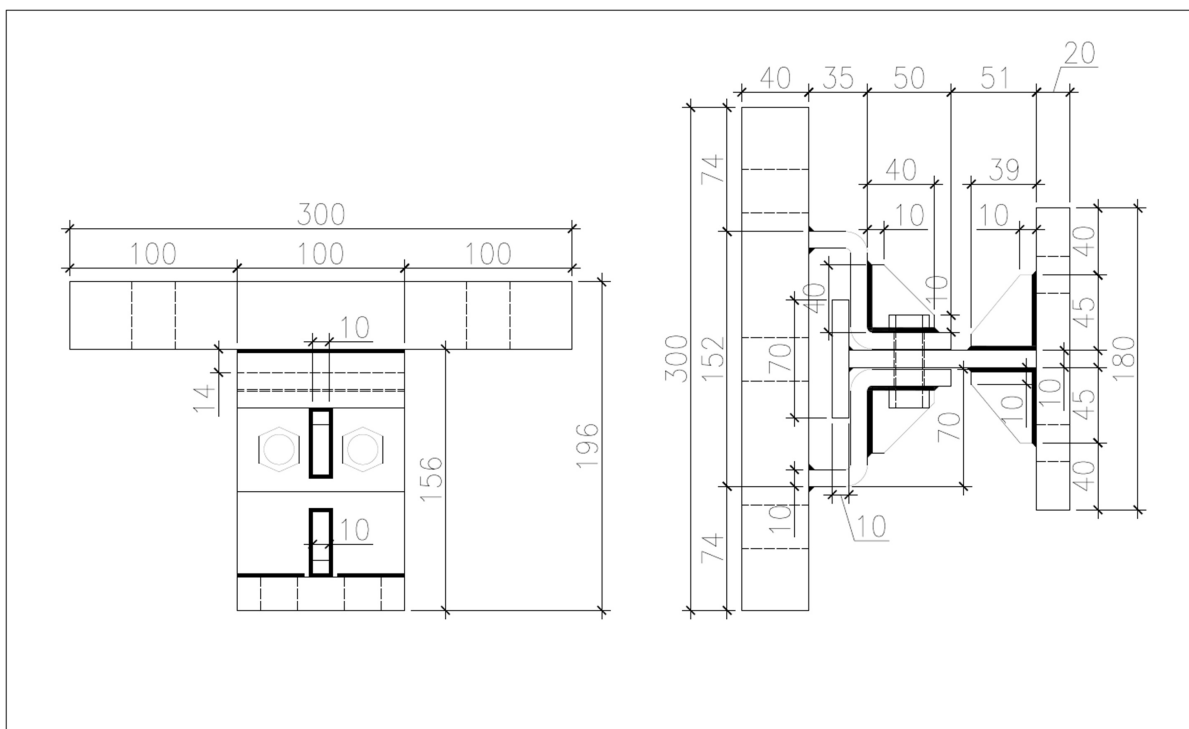


Figure 3.5: Geometric configuration of specimens C-RP

In Figure 3.6 the geometric configuration of the specimen C-SHS200 is depicted. Compared to the C-RP specimen the same configuration is defined, in which the rigid plate connection is replaced by a tubular section connection of a square hollow section (SHS) with the following dimensions:  $200 \times 200 \times 12.5 \text{ mm}$ . The objective of this specimen is to study the influence of the



At last, in Figure 3.7 the geometric configuration of the specimen C-SHS260 is depicted. Similar to the previous two specimens, this specimen is used in the study on the use of tubular sections. Therefore the same configuration is used for reverse channel and T-plug but connected to a square hollow section (SHS) of  $260 \times 260 \times 6 \text{ mm}$ . The objective of this final specimen is to study the influence of the use of tubular section on the overall behaviour of the joint considering a relatively flexible tubular section, with a substantial distance between the legs of the reverse channel and chord side wall, in combination with the smallest available thickness ( $6 \text{ mm}$ ) for size SHS260x260, again provided by the cooperating steel company FERPINTA.

### 3.3. Material characterization

In order to compare both experimental and numerical study the actual material properties of the steel plates, used to fabricate the test specimens, are required. Therefore coupons are designed to characterize the steel material properties under uniaxial tensile tests. In Table 3.2 an overview of the coupons is given. Coupons are extracted for 6 and 10 mm plate thickness, representing the T-plug and reverse channel in all test specimens. Since the corner sections of the reverse channel are under plastic deformation, caused by residual stresses due to cold-formed bending, the hardened steel properties are valuable information for the validation of the numerical models. Therefore bent coupons are extracted for 6 and 10 mm plate thickness, representing the corner regions of the reverse channel. Although no standard exists for bent coupons the similar geometry and test procedure are used as the flat coupons.

Table 3.2: Coupons for steel characterization

Coupon	Thickness [mm]	Steel class	Quantity	Plate
F6	6	S355	7	Flat
F10	10	S355	7	Flat
B6	6	S355	6	Bent
B10	10	S355	6	Bent

The geometry of the coupons is determined, according to the design standard EN10002-1, resulting in an original gauge length ( $L_o = 50 \text{ mm}$ ) and parallel length ( $L_c = 65 \text{ mm}$ ), see Figure 3.8. The width is varied between 13 mm for 6 mm plate thickness and 8 mm for the 10 mm plate thickness. In the coupon tests all relevant mechanical properties of the specimen are addressed; Young's modulus, yield strength, ultimate strength, ultimate plastic strain and the elongation at fracture.(EN 10002-1, 2001)

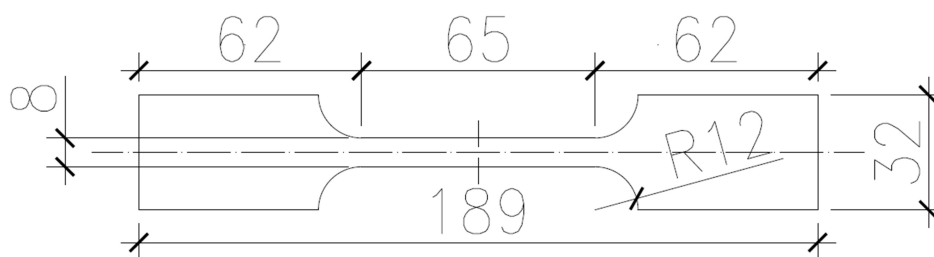


Figure 3.8: Design of the coupon specimen (F10)

### 3.4. Laboratory set-up

For the preparation of the experiments, a laboratory set-up is designed to fit within the Stevin-II laboratory at the Delft University of Technology. As explained in Section 3.2, the experimental study includes both rigid plate and tubular specimens, which have to be connected to a supporting frame. Therefore two configurations for the laboratory set-up are designed, see Figure 3.9 for the set-up for the rigid plate specimens (left) and tubular section specimens

(right). In the following paragraphs, the frame resistance, frame design, frame detailing and instrumentation are elaborated.

### 3.4.1. Frame resistance

Based on the preliminary numerical study performed in Appendix B, a maximum load of 364.4 kN is predicted at a maximum displacement of 40 mm. This displacement is chosen as an upper limit to ensure the failure mode is recognized in the joint even though such a displacement is undesired in real structures. To minimize deformation in the supporting frame and account for a possible over-strength of the actual material properties, the hydraulic jack and the load cell in the set-up are designed for a maximum load of 400 kN. The load is applied in a displacement-controlled manner with a rate of 0.01 mm/s.

Furthermore, to design a sufficiently strong supporting frame, the governing reaction forces are calculated for each specimen. This includes the resistance of the bolted connection to the corner profiles for both situations; rigid plate specimens, see Table 3.3, and tubular specimens, see Table 3.4.

Table 3.3: Reaction forces per bolt of the rigid plate specimens

Specimen	Maximum applied load [kN]	Reaction forces	
		Tension [kN]	Shear [kN]
A-RP	254.6	135.1	48.8
B-RP	232.5	140.9	44.6
B-U-RP	215.5	130.6	41.3
B-UU-RP	157.9	95.7	0.3
C-RP	358.8	186.0	68.7

Table 3.4: Reaction forces per bolt of the tubular specimens

Specimen	Maximum applied load [kN]	Reaction forces	
		Tension [kN]	Shear [kN]
C-SHS200	364.4	46.7	74.5
C-SHS260	323.0	36.5	66.0

### 3.4.2. Frame design

Given the information above, a design for the laboratory set-up is made using the software of Autodesk Inventor 2018 (Autodesk, 2018). The design includes the specimen, additional supporting elements and available laboratory elements with the corresponding dimensions, such as the hydraulic jack, load cell, corner profile and beams from all sorts of lengths. As illustrated in Figure 3.9, two configurations for the laboratory set-up are designed; a set-up for the rigid plate specimen (left) and for the tubular specimen (right).

Breaking down the set-up bottom-up, the basis of both set-up configurations is a floor structure, consisting of four beams with a length of 2100 mm, interconnected between themselves by two crossbeams of 1200 mm. In the tubular set-up, two special corner profiles (orange) are designed to connect the tubular specimens: C-SHS200 and C-SHS260 (blue) to the crossbeams. An end-plate is welded at both ends of the tubular section and bolted connected by a total of twelve M24 bolts at each end to the corner profile. In the rigid plate set-up an additional beam of length 900 mm is mounted in between the crossbeams to allow for a connection between the rigid plate specimens: A-RP, B-RP, B-U-RP, B-UU-RP and C-RP (blue) and the supporting frame by only one corner profile (orange). The rigid plate specimens are connected to the corner profile by six M24 bolts. The supporting frame for the hydraulic jack consists of two horizontal (1500 mm) and two vertical beams (2100 mm) mounted onto the floor structure. The hydraulic jack is mounted underneath the horizontal beams by a cylinder plate. The applied load is transferred from the hydraulic jack through a load cell

and load beam to the specimen in both set-ups. These details are elaborated in full detail in the next paragraph.

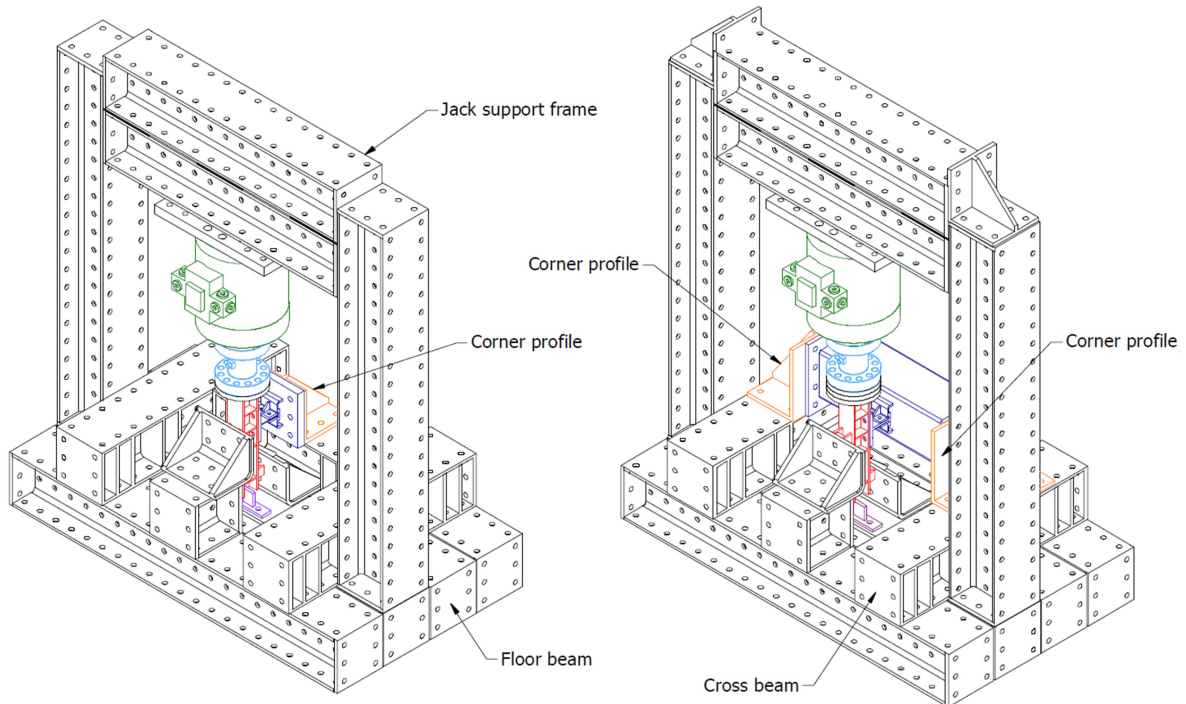


Figure 3.9: Laboratory set-up for rigid plate specimen (left) and tubular specimen (right)

### 3.4.3. Frame detailing

Part of the frame detailing is dependent on the set-up boundary conditions. Besides, as mentioned in Paragraph 3.4.1, the design of various details are verified on the shear and/or tension resistance of the bolts, bearing resistance and block tearing resistance. This leads to the design of the following frame details: load beam to specimen, rigid plate specimen to frame and tubular specimen to frame.

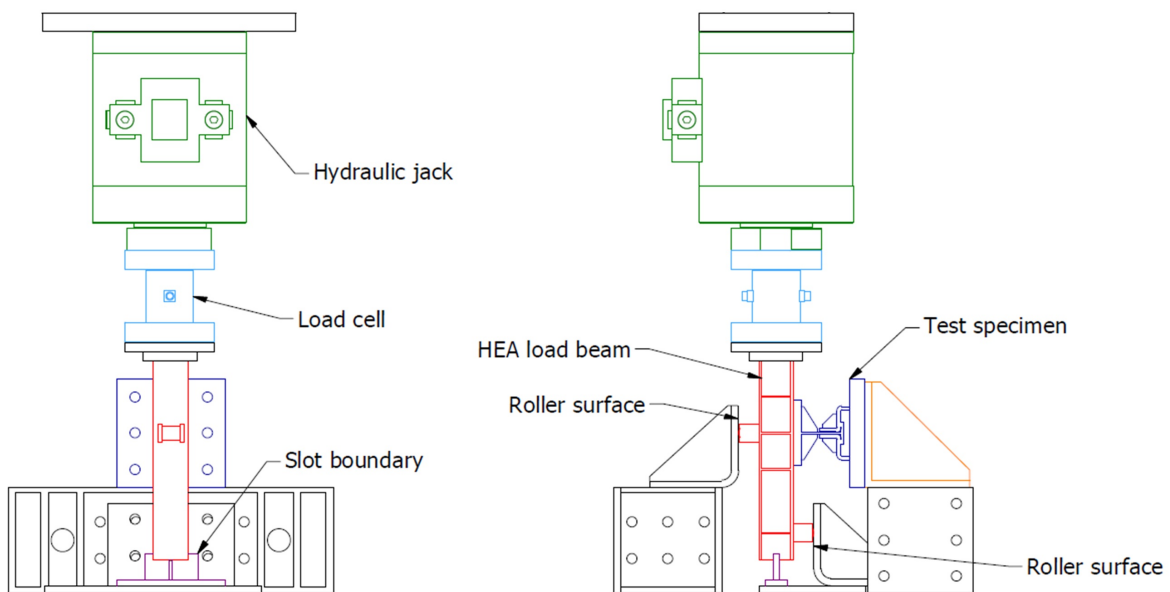


Figure 3.10: Set-up boundary conditions HEA100 load beam

### Set-up boundary conditions

The boundary conditions for the experiment allow only for a vertical translation since the objective of the experiment account for both bending and shear deformation. This situation is established by restraining all translations in the horizontal plane, by two roller supports in the strong axis and by a steel slot in the weak axis, see Figure 3.10. The two rollers are pinned connected to two plates welded onto the load beam, see Figure 3.11. Since the load is applied in the centre, the displacement in the weak axis can be simply restrained by creating a slot through which the web of the load beam is guided. This is established by two plates welded vertically on a base plate, which is connected with threaded bolt holes onto the floor structure.

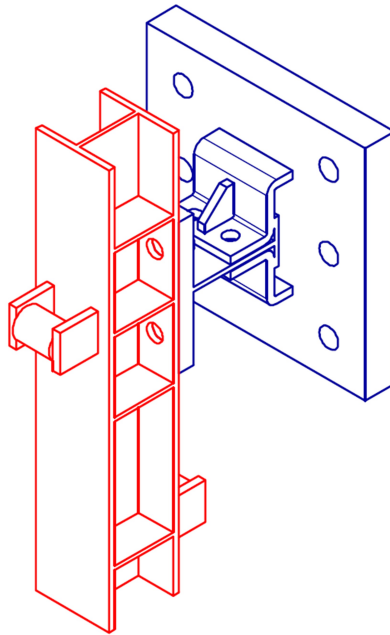


Figure 3.11: HEA100 load beam (red) to specimen (blue) detail

### Load beam to specimen

The T-plug of the specimen is connected by four M20 bolt to the load beam flange through a 20 mm thick stiffened support plate. The load beam is made of the profile HEA100 and has a locally stiffened web around the bolt holes. This connection is verified on the shear resistance of the bolts, bearing resistance and block tearing resistance, resulting in the design shown in Figure 3.11.

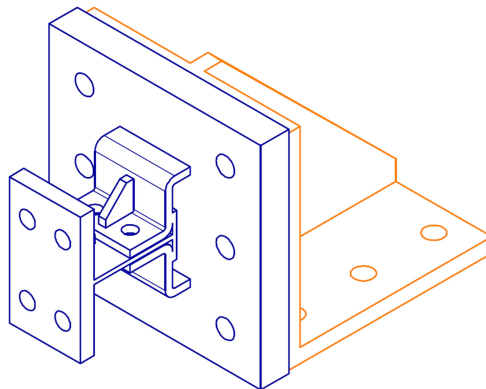


Figure 3.12: Rigid plate specimen (blue) to corner profile (orange) detail



### Rigid plate specimen to frame

As the plug-and-play joint is connected to a rigid plate, this same rigid plate is used to connect the specimen by six M24 bolts to the corner profile. This connection is verified on both tension and shear resistance of the bolts, bearing resistance and block tearing resistance. This gives the design of the connection, shown in Figure 3.12.

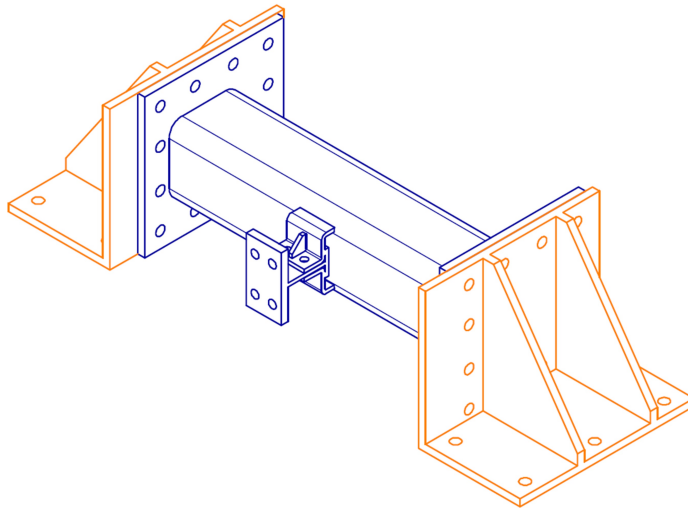


Figure 3.13: Tubular specimen (blue) to corner profile (orange) detail

### Tubular specimen to frame

At both ends of the tubular section an end-plate is welded to provide the connection to the corner profiles. The tubular specimens are connected by six M24 bolts on each end-plate to two corner profiles. The connection is verified on the tension and shear resistance of the bolts, bearing resistance and block tearing resistance. Besides, the end-plate to tubular section connection is verified on the weld resistance. This leads to the design of the connection, see Figure 3.13.

### 3.4.4. Instrumentation

The experiment aims to analyse the behaviour of the connection, in terms of strength stiffness and deformation capacity, and derive individual components following the EC3-1-8 component method approach. To validate the numerical models, data is gathered from the experiment using LVDTs and inclinometers. A data acquisition is connected to all instrumentation, in a way that the main sources of deformation are monitored. The LVDTs are used to measure vertical displacement between two points and inclinometers are used to measure the partial joint rotation for various components.

The displacement in the net-section of the joint is used in the derivation of components; reverse channel in bending and T-plug in bending. Therefore LVDT's are placed on the reverse channel with equal distance to the centre of the reverse channel. For the unstiffened test specimens; B-U-RP and B-UU-RP, only one LVDT per reverse channel is placed in the centre of the net-section. Since the component; reverse channel is bending, is derived using the relative displacement between the net-section and the connection to the rigid plat/tubular section, an extra LVDT is place there. Next, each test specimen contains an inclinometer in the net-section of the top reverse channel to measure the partial rotation. At last, since the load is applied in a displacement-controlled manner, the reacting force at the location of load application is measured.

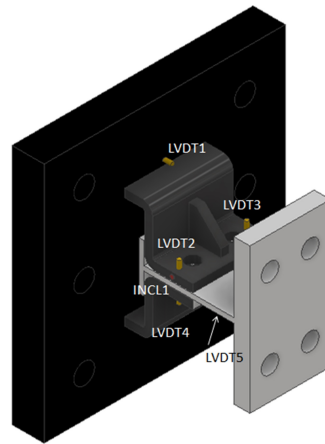


Figure 3.14: Instrumentation arrangement A-RP specimen: T-plug (thickness 6 mm) and reverse channel (10 mm) in bending, with stiffeners.

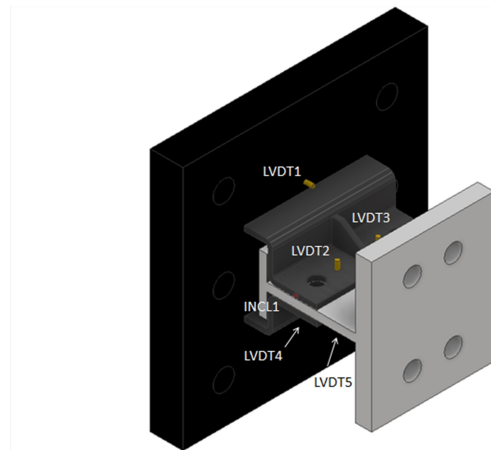


Figure 3.15: Instrumentation arrangement B-RP specimen: T-plug (10 mm) and reverse channel (6 mm) in bending, with stiffeners.

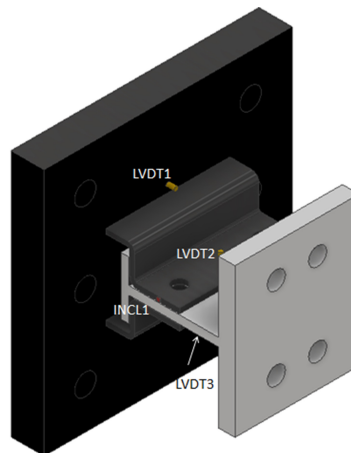


Figure 3.16: Instrumentation arrangement B-U-RP/B-UU-RP specimen: T-plug (10 mm) and reverse channel (6 mm) in bending, with respectively unstiffened reverse channel/double unstiffened reverse channel and T-plug.

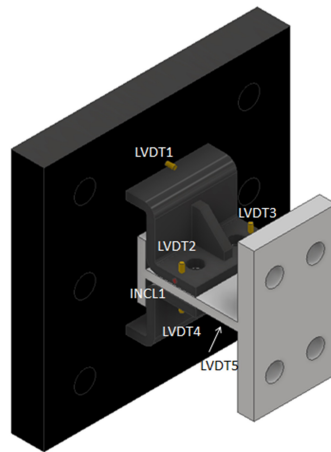


Figure 3.17: Instrumentation arrangement C-RP specimen. Complete assembly in bending with the same thickness for both elements (T-plug and reverse channel with 10 mm) with stiffeners, acting as benchmark configuration for tubular influence.

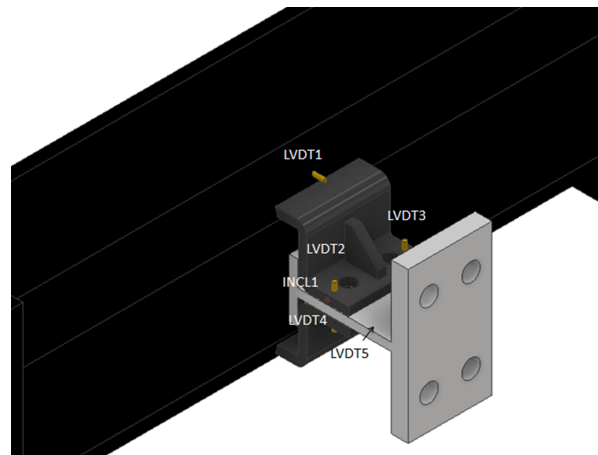


Figure 3.18: Instrumentation arrangement C-SHS200 specimen. Complete assembly in bending with the same thickness for both elements (T-plug and reverse channel with 10 mm) with stiffeners, considering the influence of the tubular profile (SHS 200x200x10).

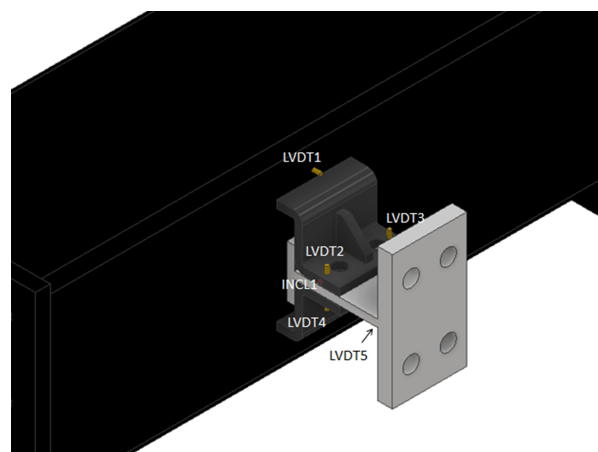


Figure 3.19: Instrumentation arrangement C-SHS260 specimen. Complete assembly in bending with the same thickness for both elements (T-plug and reverse channel with 10 mm) with stiffeners, considering the influence of the tubular profile (SHS 260x260x6).



# Numerical study on plug-and-play joints

The numerical study forms an important part in the research on the behaviour of the new type of plug-and-play joint. At first, Section 4.1 describes the numerical model in detail, in term of geometry, material properties, finite element and mesh type, assembly conditions and computational solver. Hereafter, the numerical results of the specimen models are analysed in Section 4.2, before an extending parametric is performed and analysed in Section 4.3.

## 4.1. Numerical model

Experiments are an important asset in the research on the behaviour of the component; T-plug bending around weak axis. However, a limited amount of specimens are available, since the experiments are expensive and time-consuming. For the completeness of the research Finite Element Analysis (FEA) is included to address the broader spectrum in a parametric study. An essential step for the use of the numerical model is the validation based on the experimental study. After establishing a valid numerical model, new models can be designed to complement the research in a parametric study.

In this section all required information is given to accurately rebuild the finite element model of this MSc thesis for future researches. The finite element is built using the finite element software of ABAQUS, version 6.14 (ABAQUS/CAE, 2014).

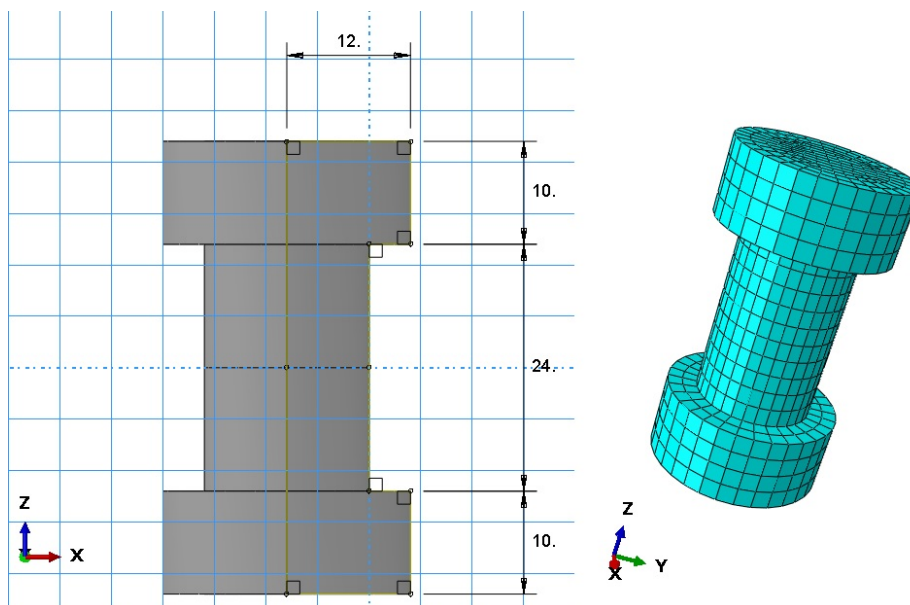


Figure 4.1: Bolt geometry and 3D representation of the finite element model

### 4.1.1. Geometry

Regarding the geometry of the finite element model, no symmetry simplifications are applicable and therefore the whole joint is modelled. The parts are modelled with three-dimensional deformable solid elements according to the nominal dimensions of the configurations defined in Section 3.2, except for the bolts/nuts and welds.

The bolt model is simplified by neglecting the threaded shank/nut contact surface and the hexagonal shape of the bolt head and nut. Instead, the bolts are modelled assuming a tubular shape with extended circular end sections representing head and nut. By neglecting the complicated contact surface interaction between the threaded shank and nut, a considerable amount of computational time is saved. Besides, from previous studies can be concluded that the solid bolt model among all simplifications most accurately represents the actual behaviour of the joint (Kim et al., 2007). Since the bolt is not the critical element in failure, it does not significantly affect the results and therefore this simplification is justified. For the joint a pair of M16 bolts are designed with the following dimensions; 16 mm shank diameter, 24 mm head/nut diameter and 10 mm head/nut height, see Figure 4.1. Depending on the configuration of the joint, the shank height varies between 24 – 34 mm for the test specimens.

The fillet welds are modelled as an isosceles triangular cross-section with a specific throat thickness satisfying the requirement of the weld resistance > base material. The weld resistance is determined according to the EC3-1-8 directional method for design resistance of fillet welds (EN 1993-1-8, 2005). The throat thickness is determined by trial-and-error, since the throat thickness is dependent on the design load obtained from the numerical analysis, in which a first estimation of the weld is included. The design resistance of the fillet weld may be assumed sufficient if the following criteria are both satisfied:

$$\sqrt{\sigma_{\perp}^2 + 3(\tau_{\perp}^2 + \tau_{\parallel}^2)} \leq \frac{f_u}{\beta_w \gamma_{M2}} \quad (\text{Eq. 4.1})$$

$$\sigma_{\perp} \leq \frac{0.9 f_u}{\gamma_{M2}} \quad (\text{Eq. 4.2})$$

With,

- $\sigma_{\perp}$  is the normal stress perpendicular to the throat, see Figure 4.2;
- $\tau_{\perp}$  is the shear stress (in the plane of the throat) perpendicular to the axis of the weld, see Figure 4.2;
- $\tau_{\parallel}$  is the shear stress (in the plane of the throat) parallel to the axis of the weld, see Figure 4.2;
- $f_u = 490 \text{ N/mm}^2$ ;
- $\beta_w = 0.9$ ;
- $\gamma_{M2} = 1.25$ .

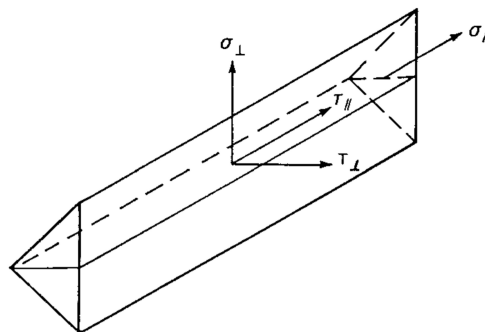


Figure 4.2: Stresses on the throat section of a fillet weld (EN 1993-1-8, 2005)

Since the weld stresses are dependent on both ultimate load and the lever arm between the legs of the reverse channel, the throat thickness is determined individually per specimen. For this reason, the throat thickness ( $a$ ) varies between 3 – 7 mm depending on its location and configuration, see Figure 4.3.

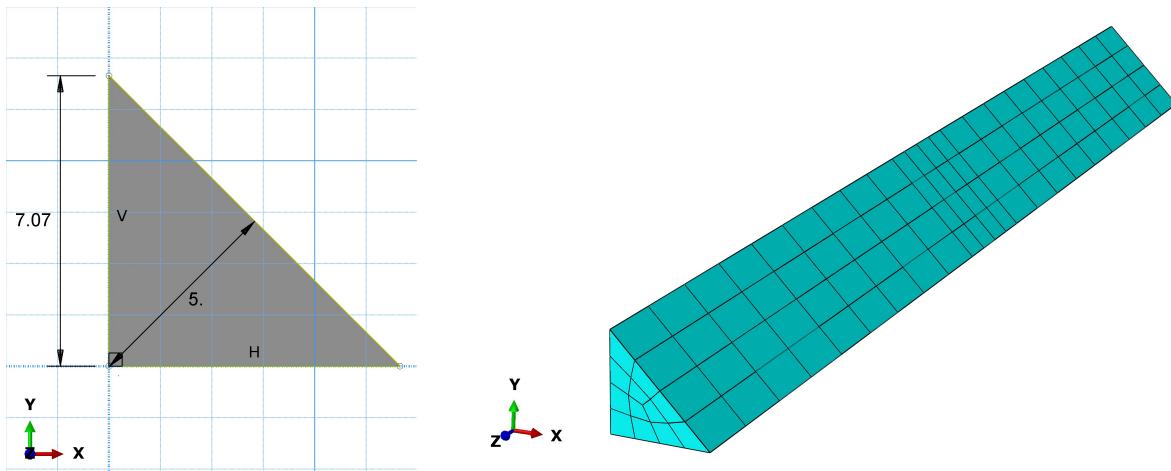


Figure 4.3: Weld geometry finite element model

### 4.1.2. Material properties

In the numerical model a total of three materials are defined, named "Bolt 10.9", "Steel S355" and "Steel S355 hardened" to describe the material behaviour of specific elements/parts of the model. The "Bolt 10.9" material is used for elements representing bolt and nut of the strength class 10.9. For all remaining elements, which includes the reserve channel, stiffeners, T-plug and the set-up supporting elements, the "Steel S355" material is used. Special attention is given to the reverse channel element, which is defined by both "Steel S355", for the straight sections, and "Steel S355 hardened", for the corner sections, which are under considerable plastic deformation due to the cold-formed bending.

In the numerical study a distinction is made in the plastic material model for prediction of the experimental results, using an isotropic hardening model, and the parametric study on the component derivation using an elasto-plastic model. Figure 4.4b presents the different material models of steel grade S355 with corresponding true stress-strain relation, which is the required input data for ABAQUS.

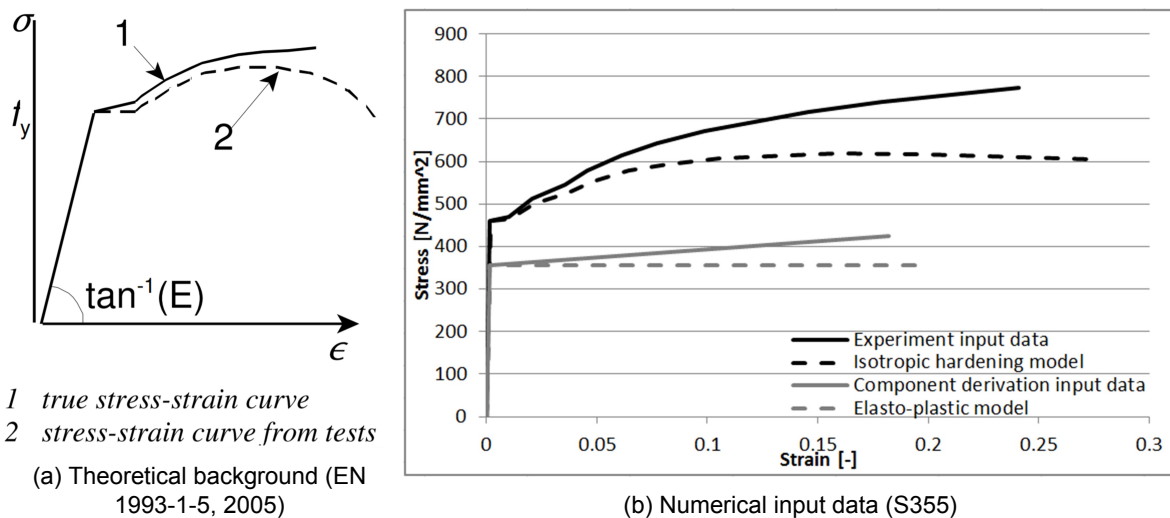


Figure 4.4: Plastic material models with true stress-strain conversion

The elastic material properties are defined by a linear elastic material model with isotropic and homogeneous behaviour. The elastic properties are similar for all three defined materials, with a specified density of  $7850 \text{ kg/m}^3$ , Young's modulus of  $210000 \text{ N/mm}^2$  and a Poisson's ratio of 0.3.

The plastic material properties of the experiment model are defined by an isotropic hardening model with homogeneous behaviour. The finite element software of ABAQUS requires the true stress-strain relation, correlating the current deformed condition with the history of previously conditions, instead of the engineering stress-strain relation, correlating with initial cross-section and length (Mavrodontis, 2017). Therefore, the results obtained from the coupon tests, see Section 3.3, have to be converted until ultimate strength, as shown in Figure 4.4a, using the following analytical equations:

$$\sigma_{true} = \sigma(1 + \epsilon) \quad (\text{Eq. 4.3})$$

$$\epsilon_{true} = \ln(1 + \epsilon) \quad (\text{Eq. 4.4})$$

The final step towards the plastic material input parameters in ABAQUS is converting the true strain past yielding to a logarithmic plastic strain with the following equation:

$$\epsilon_{pl} = \epsilon_{true} - \frac{\sigma_{true}}{E} \quad (\text{Eq. 4.5})$$

Given the converting formulae, the plastic material input parameters in ABAQUS for each material are shown in Table 4.1.

Table 4.1: Plastic material input parameters in ABAQUS

<b>Bolt 10.9</b>		<b>Steel S355</b>		<b>Steel S355 hardened</b>	
Yield stress [N/mm2]	Plastic strain [-]	Yield stress [N/mm2]	Plastic strain [-]	Yield stress [N/mm2]	Plastic strain [-]
903.857143	0	460.59	0	716.447	0
914.4	0.01151906	470.403	0.00851912	739.264	0.033549336
1090	0.08098722	511.609	0.019115766	773.015	0.095404643
0.1	0.18232156	546.569	0.034014879		
		580.075	0.044016885		
		615.22	0.059588791		
		641.974	0.075663904		
		670.547	0.097126711		
		716.447	0.143927169		
		739.264	0.177476505		
		773.015	0.239331812		

### 4.1.3. Finite element and mesh type

The choice for the appropriate finite element type largely depends on the type of simulation performed, which regards a stress/displacement simulation in this numerical study. A wide range of elements is available in the ABAQUS element library, characterized in terms of family, degrees of freedom, the number of nodes/order of integration, formulation and integration. In the numerical model is made use of the hexahedral "C3D8R" element, as is shown in Figure 4.5. In the this paragraph, the choice for this finite element type is elaborated.

In the numerical model the finite element is chosen from the family; continuum (solid) elements, also known as "3D Stress" family in the ABAQUS interface. The family is indicated by the first index of the element's name "C". The continuum elements are applicable for both linear and non-linear stress analyses, involving contact, plasticity and large deformations, which are in line with the analysis performed in this numerical study.



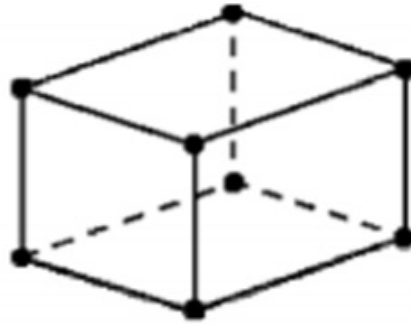


Figure 4.5: Presentation of the finite element type: Hexahedral "C3D8R"

Since dealing with a stress/displacement simulation the degrees of freedom are only three translations, which are indicated by the second index of the element's name "3".

Next, the first-order interpolation is applied, which gives only nodes at the corners of the element. This results in an 8-node linear brick element, indicated by the third and fourth indices "D8", see Figure 4.5. Although quadratic elements possibly give more accurate results, this comes at a much higher computational cost. Besides, first-order elements are less sensitive for distortion and perform better in contact problems, which is applicable in this numerical model.

Furthermore, a Lagrangian formulation is applied, in which the element deforms with the material. In other words, each element consists of 100% out of a single material, as the material boundary is equivalent to the element boundary.

	Full integration	Reduced integration
First-order interpolation		
Second-order interpolation		

Figure 4.6: Interpolation vs. integration

At last, reduced integration is applied on all elements, indicated by the fifth index "R". ABAQUS uses the Gaussian quadrature method to numerically approximate the material response at each integration point. The reduced integration is slightly less accurate for the bending stress in comparison with the full integration, but on the other hand, it eliminates the effect of shear locking at a smaller computational cost.

Given the combination of first-order interpolation and reduced integration, see Figure 4.6, in combination with only one continuum element over the thickness, this leads to the phenomenon called hourglassing, see Figure 4.7. A single element through the thickness does not detect strain in bending, which results in deformation without strain. To obtain reliable results at least four elements over the thickness are required, where each element captures either compressive or tensile axial strains instead of both, resulting in correctly measured axial strains. (ABAQUS, 2014)

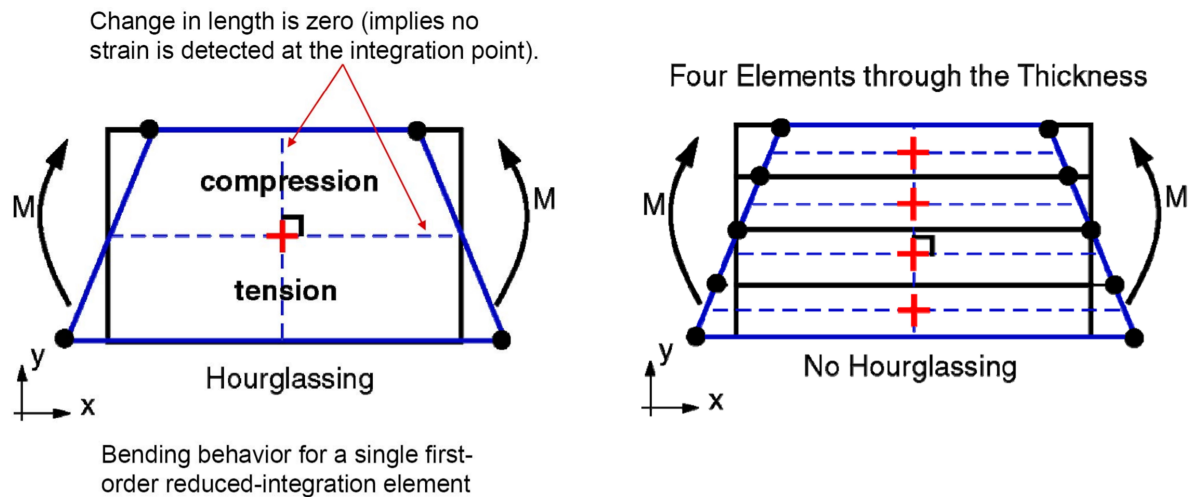


Figure 4.7: Hourglassing

Finally, for the best and most cost-effective result, hexahedral elements are preferred over tetrahedral elements for the mesh generation, as equivalent accuracy is achieved at a lesser cost. However, when modelling complex geometries tetrahedral elements perform better than highly distorted hexahedral elements. Since reduced integration is applied to all finite elements, a more dense mesh is needed at locations with stress concentrations, in order to reduce errors in the numerical analysis.

A summary of the characteristics of the finite element type is given in Table 4.2 and the finite element mesh of the numerical model is shown in Figure 4.8.

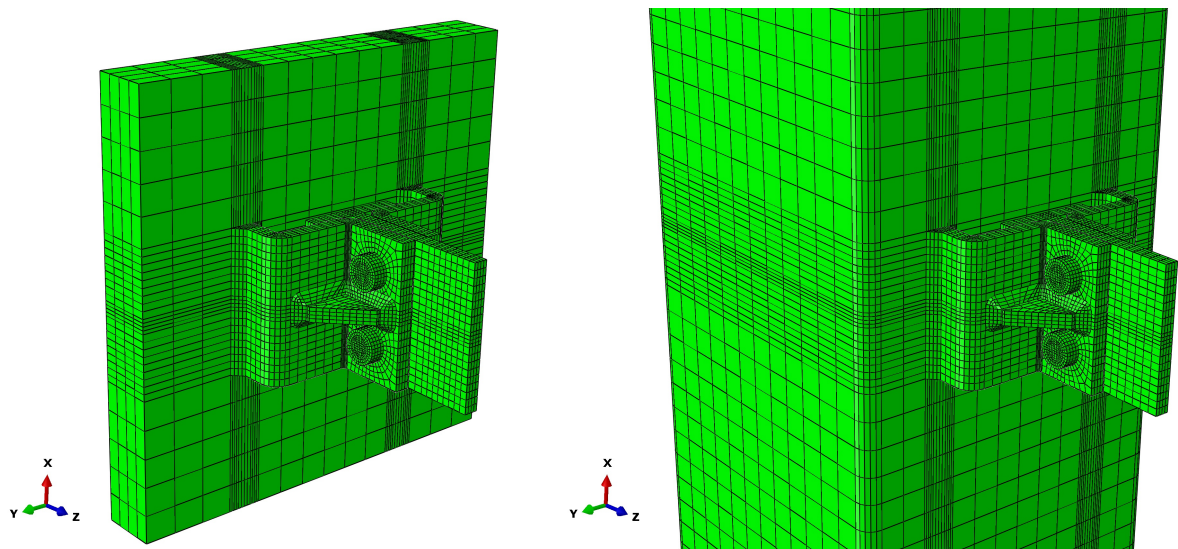


Figure 4.8: Finite element mesh of the numerical model

Table 4.2: Characteristics summary of the finite element type

	Hexahedral "C3D8R" element
Family	Continuum (solid)
Degrees of freedom	3 translations
Interpolation	Linear 8-node
Formulation	Lagrangian
Integration	1 integration point (reduced)

#### 4.1.4. Assembly conditions

The numerical model is built up from a number of independent modelled parts; rigid plate, reverse channel, T-plug, stiffeners and support plate. For an accurate computational analysis, all the different parts have to be assembled by either constraint, contact or boundary conditions, assigned to the specific surface of the parts. In this paragraphs the properties of these three conditions are elaborated.

##### Constraint conditions

In the numerical model two types of constraint conditions are used, namely multi-point constraints (MPC) and tie constraints. MPC conditions are used to assign boundary conditions to a selection of surfaces through a single point. In the numerical model reference points (RP) are used to assign boundary conditions. Secondly, the assembly of the joint in the experiment is achieved by welding, where tie constraints are used for the assembly of parts in the numerical model. In order to accurately reproduce reality, welds are modelled separately as an isosceles triangular cross-section, see Paragraph 4.1.1, and the tie constraint is applied between the weld surface and adjacent faces of the reverse channel, tubular section, rigid plate, T-plug or stiffener. Although the constraint condition increases the complexity of the model/mesh and the computational time, it also significantly influences the accuracy of results, since reverse channel and T-plug experience considerable deformations. The stress distribution in parts under large deformations is more accurately distributed using welds, generating a smooth transition compared to hard surface contact.

##### Contact conditions

For the contact definition of the numerical model the general contact algorithm with the default settings is used. However, by default, ABAQUS assumes that contact between surfaces is frictionless. Therefore a friction model is defined, describing the contact properties in both tangential and normal direction. The normal behaviour is defined as a "hard" contact between surfaces and for the tangential behaviour, a penalty friction formulation is set with an isotropic friction coefficient ( $\mu$ ) of 0.2. The general contact condition with the defined friction model is applied on the surface domain "all with self" automatically including all contact interactions, which includes bolt/reverse channel, shank/hole and T-plug/reverse channel. General contact always uses finite-sliding, surface-to-surface contact formulation, as shown in Figure 4.9. The benefits of surface-to-surface contact discretization compared to node-to-surface discretization are a generally better stress performance and accuracy, reduced likelihood of major localized penetrations, reduced sensitivity of roles (master and slave) and better convergence (smoothing).

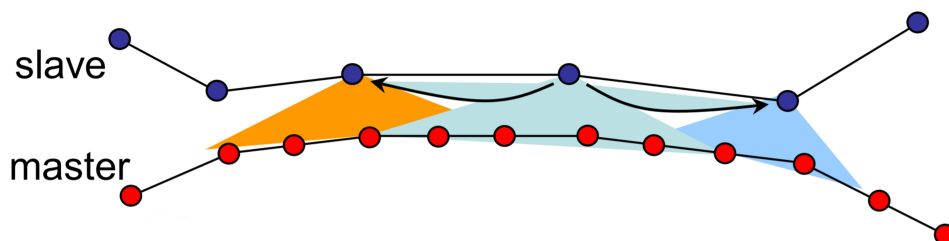


Figure 4.9: Surface-to-surface discretization

### Boundary conditions

Based on the preliminary numerical study on the loading condition, performed in Appendix B.1, a distinction is made between a pure bending and a shear boundary condition. In reality, the rotational degree of freedom is restrained by the floor providing diaphragm action. In both the experimental and numerical study the reality is approximated by using the shear boundary condition. All three situations; pure bending boundary conditions, shear boundary condition and actual structural behaviour, are schematized in Figure 4.10.

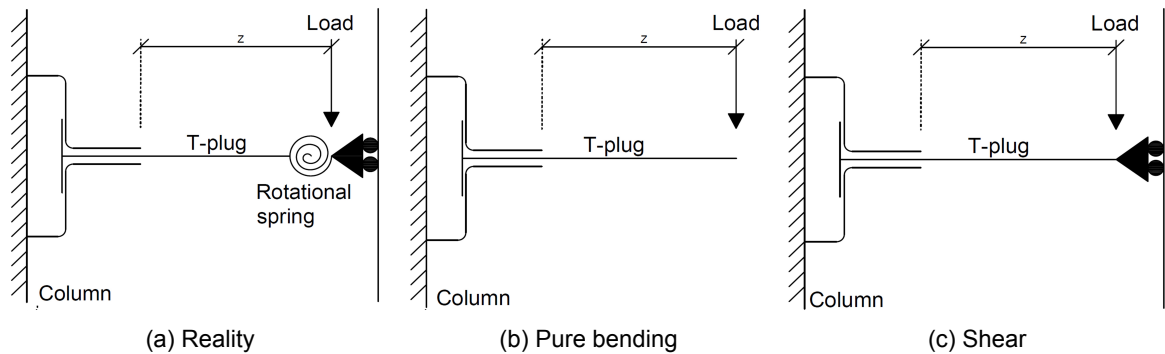


Figure 4.10: Boundary condition schematization

In the laboratory set-up the load is applied in a displacement-controlled manner by a hydraulic jack through a load beam on the specimens, see Figure 3.11. Based on the preliminary numerical study, performed in Appendix B.2, a modelling simplification is introduced in the numerical study, in which the load beam is replaced by directly applying the boundary conditions on the support plate surface. As both models give similar results and the simplified model reduces the computational time enormously, the simplified model is used in both experimental and numerical study.

Following this simplification and schematization above, a summary of the boundary conditions is given in Table 4.3. In the numerical model, the boundary conditions are assigned to a specific reference point (RP), see Figure 4.11, which degrees of freedom are coupled to the nodes of the element surface by a multi-point constraint (MPC). The benefit of using this tool is not only simple control of the boundary conditions but also quick extraction of support reactions. In the end, the boundary condition for the vertical translation is set at an upper-limit displacement of 40 mm. ABAQUS (2014)

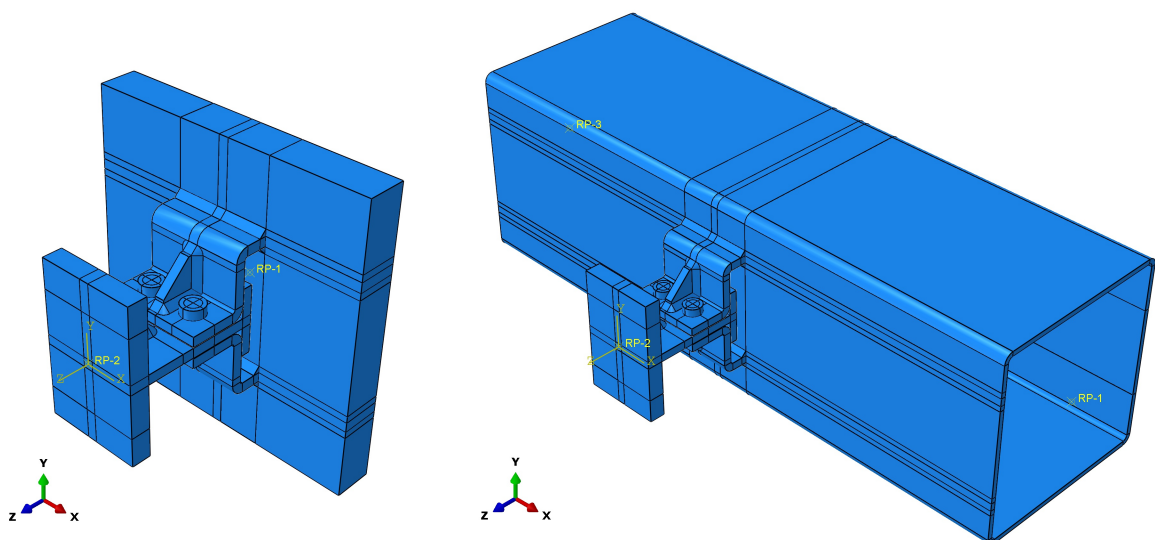


Figure 4.11: Reference point location in the numerical model

Table 4.3: Summary of the boundary conditions

Time function	Displacement-controlled
Initial BC	Displacement/rotation at RP1/RP3: $U1=U2=U3=UR1=UR2=UR3=0$
	Displacement/rotation at RP2: $U1=U2=U3=UR1=UR2=UR3=0$
Step 1 BC	Displacement/rotation at RP1/RP3: $U1=U2=U3=UR1=UR2=UR3=0$
	Displacement/rotation at RP2: $U1=U2=U3=UR1=UR2=UR3=0$
Step 2 BC	Displacement/rotation at RP1/RP3: $U1=U2=U3=UR1=UR2=UR3=0$
	Displacement/rotation at RP2: $U1=U3=UR1=UR2=UR3=0, U2=40\text{mm}$

\*Note 1: RP3 only applicable to numerical models containing a tubular section.

\*Note 2: Step 1 is skipped in the Dynamic, Explicit analysis.

#### 4.1.5. Computational solver

For the validity of the numerical results, two computational solvers are used; Static, General (Implicit) and Dynamic, Explicit. As some major differences exist between the solving procedures, understanding the advantage and disadvantages of these algorithms is key is choosing the right algorithm for the problem.

Dealing with a slow contact problem in this numerical study the Static, General (Implicit) solver is chosen with the Dynamic, Explicit solver as a back-up check since the explicit solver is only conditionally stable with respect to the time and increment size. This is a major drawback in comparison with the implicit solver, being unconditionally stable. Besides, the explicit solver does not allow the application of bolt loads, which are needed to accurately model the initial stiffness. On the other hand, the implicit solver does encounter earlier problems with a complex three-dimensional model. This causes a reduction in time increments, drastically increasing the computational time and possibly leading to divergence. Besides, local instabilities can cause force equilibrium difficult to be achieved. For this reason, the explicit solver can help with finding the ultimate resistance and failure mode. In this paragraph, the computational settings for each solver are elaborated in detail. (Sun et al., 2000)

##### Static, General (Implicit)

As mentioned above, the implicit solver is preferred when dealing with a slow contact problem. Moreover, the Static, General (Implicit) solver allows for the use of bolt loads. Besides, being a more realistic representation of the experiment, bolt loads are required in order to converge due to the hole clearances in the model. Therefore two steps are required, one for the adjustment of the length (clearance) of 2 mm and one for the fixation at the current length.

The Static, General (Implicit) solver neglects inertia and time-dependent material effects (creep, swelling, viscoelasticity). The assigned time period is 1 and is not cross-referenced to any amplitude options, due to the load setting; ramp linearly over step. Even though dealing with small displacements, the geometrical non-linearity and local instabilities are considered in the model by the settings; NLGeom and Automatic stabilization.

Based on the computational efficiency, the incrementation is set to automatic with the increment size restrictions per step as shown in Table 4.4. The Static, General (Implicit) solver

uses Full Newton technique with direct integration, due to its beneficial convergence rate compared to alternative methods. A complete summary of the computational settings for the Static, General (Implicit) solver is given in Table 4.4.

Table 4.4: Computational settings: Static, General (Implicit)

	<b>Static, General (Implicit)</b>
Bolt loads	Step 1: Adjust length (2 mm) Step 2: Fixed at current length
Time period	1
NLGeom	On
Automatic stabilization	Dissipated energy fraction: 0.0002
Incrementation	Automatic
Increment size step 1	Initial: 0.02 mm Minimum: $2 \times 10^{-10}$ mm Maximum: 0.2 mm
Increment size step 2	Initial: 0.04 mm Minimum: $4 \times 10^{-10}$ mm Maximum: 0.4 mm
Equation solver	Direct integration
Solution technique	Full Newton
Load	Ramp linearly over step

### **Dynamic, Explicit**

For the validity of the numerical results obtained by the Static, General (Implicit) solver, a second computational solver is used for verification, namely the Dynamic, Explicit solver. Although it has a couple of major drawbacks; as being only conditionally stable and not able to perform bolt loads, it supplies a sufficient check on the implicit solver. Due to the exclusion of bolt loads, the Dynamic, Explicit solver has only one step, as step 1 is skipped. A summary of the setting is given in Table 4.5.

The Dynamic, Explicit solver has a time period of 200, cross-referenced to an amplitude curve for an uniformly increasing load application. Similar to the Static, General (Implicit) solver the NLGeom setting is switched on, accounting for geometrical non-linearity. Also the incrementation is set to automatic again, due to the computational efficiency. The Dynamic, Explicit solver uses mass scaling on the whole model as its solving technique. The mass is scaled at the beginning of the step at a target time increment of 0.0001, to prevent extremely small or poorly shaped elements to consequently control the stable time increment. Since it is a quasi-static load, the scaling of the element mass is set to "nonuniformly to equal target". (ABAQUS, 2014)

Table 4.5: Computational settings: Dynamic, Explicit

	<b>Dynamic, Explicit</b>
Bolt loads	-
Time period	200
NLGeom	On
Incrementation	Automatic
Solving technique	Mass scaling
Region	Whole model
Type	Target time increment
Frequency/interval	At beginning of step
Target time increment	0.0001
Scale element mass	Nonuniformly to equal target



## 4.2. Numerical results

The numerical results form the basis of both the experiment and the extending parametric study on the component derivations. Therefore a good understanding of these results is of major importance. As explained in Section 4.1, the numerical model is solved by two different methods to verify the obtained numerical results in the absence of experimental results. Besides, the numerical model is validated for a different loading condition on three experimental configurations; A-RP, B-RP and B-U-RP. The component test; T-plug in tension, performed by the University of Coimbra (UC), considers identical joint configurations and is used to verify the numerical model. For a detailed elaboration of this verification is referred to Appendix A. In the upcoming paragraphs, a prediction of the experiment results is discussed in detail. This includes an analysis of the force-displacement curves, computational solver, and its behaviour in terms of, initial stiffness, yield strength, ultimate strength and failure mode.

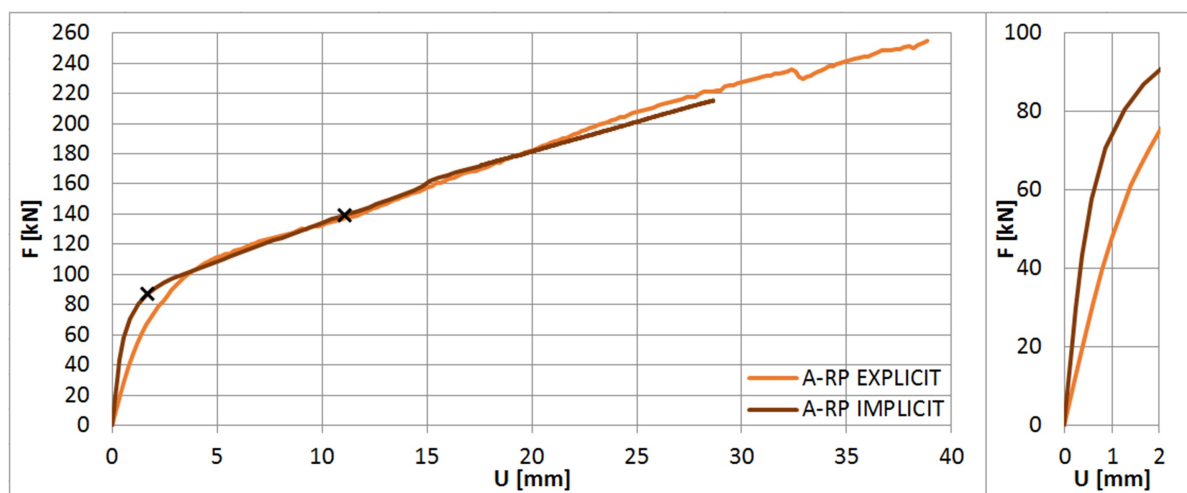


Figure 4.12: Force-displacement curves of specimen model: A-RP (X at 5% and 25% PEEQ limit)

Comparing the computational solvers for specimen model A-RP, approximately similar results in joint behaviour are found, as is shown in Figure 4.12. However, there are some key differences to be mentioned. In general, a clear underestimation of the initial stiffness is noticed for the explicit solver, caused by its limitation not being able to apply bolt loads. Therefore the first step of pre-loading the bolt, closing the initial gap by tolerances between T-plug and reverse channel, can not be modelled accurately. By excluding the tolerances in the initial geometry, the same underestimation is found, as the initial stress distribution still differs from the pre-loaded situation and a second reason is a slightly reduced lever arm in the reverse channel. To conclude, the implicit solver is preferred to determine the initial stiffness.

Secondly, the implicit curve stops converging, unlike the explicit curve, before the upper-limit displacement of 40 mm, as is determined in Paragraph 4.1.4, is reached. Generally, this is explained by the implicit solver being unconditionally stable, which complicates the convergence especially regarding tolerances between shank and bolt hole. By equalizing the diameter of shank and bolt hole, it helps to overcome the converge problem on one hand, but leads to an inaccurate bolt stiffness on the other hand, which is not desired as well. For this reason, the explicit solver can be used to find the ultimate strength of the joint. Although beyond 25% plastic strain (second cross on the curve) an accurate prediction of the ultimate resistance can not be guaranteed. Since the elasto-plastic material model is used in the component derivation, checking the stress does not verify the resistance of the joint, as the stress never exceeds the yield strength. Therefore the resistance is determined using the 5% plastic equivalent strain (PEEQ), recommended by the EC3-1-5 clause [C.8(1)] (EN 1993-1-5, 2005). This limit is based on the necking of the base material, as the use of a damage model is required after this point, which removes elements with fracture strains. Given the yield

strength derived at 5% PEEQ, both explicit and implicit solvers are applicable.

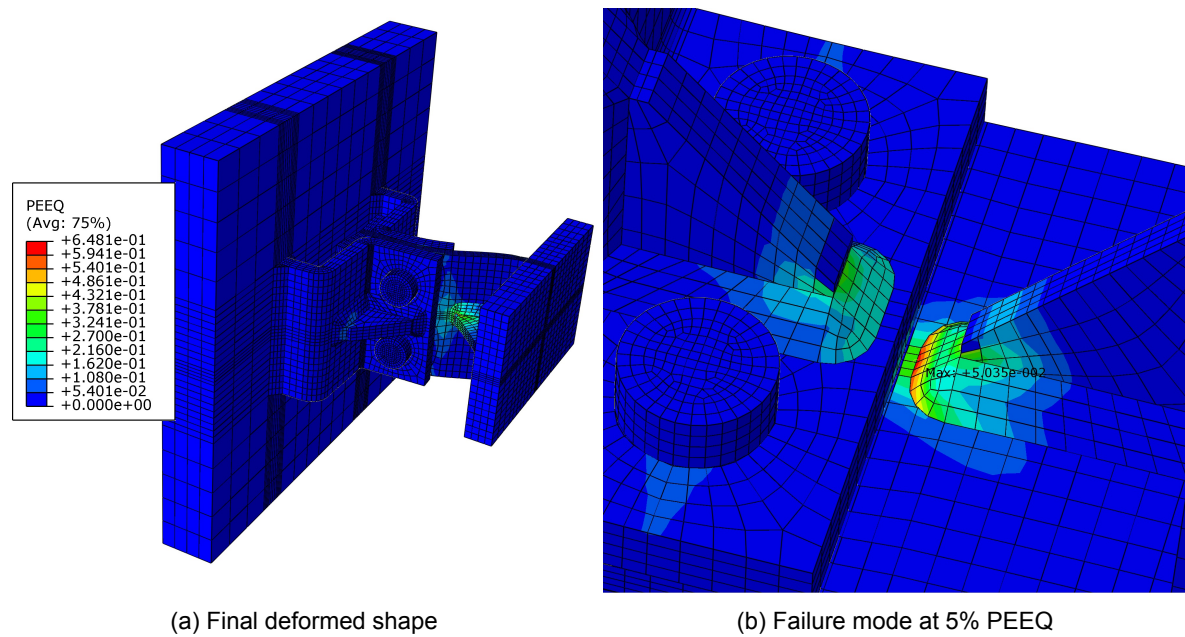


Figure 4.13: Numerical results of specimen model: A-RP

As mentioned in the previous paragraph, before the 25% PEEQ limit the ultimate resistance for specimen model A-RP has not been reached yet. Therefore no explicit failure mode can be determined, but since this displacement is undesired in practice, the failure mode can be characterized due to excessive deformations. For practical purposes, the EC3-1-8 component method is followed, in which the 5% PEEQ limit is governing for the failure mode. As Figure 4.13b present the location where 5% PEEQ limit is reached first, the failure mode is determined as yielding of the T-plug in bending, corresponding to a yield strength of 88.2 kN. Other characteristic values for specimen model A-RP are an initial stiffness of 34.0 kN/mm and ultimate strength of 254.6 kN, see Table 4.6.

Table 4.6: Joint model characteristics

Model	Initial stiffness [kN/mm]	Yield strength [kN]	Ultimate strength [kN]
A-RP	134.0	88.2	254.6
B-RP	60.4	127.8	232.5
B-U-RP	47.3	100.3	215.5
B-UU-RP	25.2	76.7	157.9
C-RP	172.1	158.8	358.8
C-SHS200	132.1	157.9	364.4
C-SHS260	64.2	119.7	323.0

Note: ultimate strength is measured at the maximum applied displacement, before the ultimate resistance is reached.

In Figure 4.14 the force-displacement curves for specimen models B-RP, B-U-RP and B-UU-RP are shown. From these curves can be concluded that the use of stiffeners has a considerable influence on both resistance and stiffness, which is also reflected by the values in Table 4.6. As the B-RP model is double stiffened on reverse channel and T-plug, this model gives the highest stiffness/resistance and by removing the reverse channel stiffener (B-U-RP) and then the T-plug stiffener (B-UU-RP) these values significantly drop. For a more detailed analysis of the use of stiffeners is referred to Paragraph 4.3.2. Breaking down these curves in more detail, on each curve, approximately between 4 mm and 9 mm, a sudden increase in



stiffness is recognised. By further analysis can be concluded that this is caused by the fillet weld of the T-plug stiffener making contact with the reverse channel.

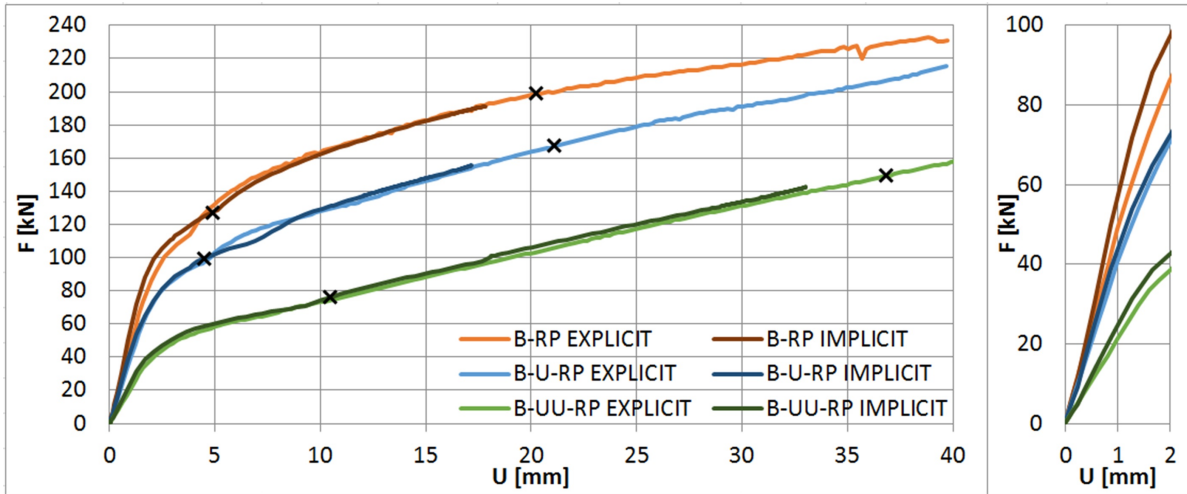


Figure 4.14: Force-displacement curves of specimen models: B-RP, B-U-RP and B-UU-RP (X at 5% and 25% PEEQ limit)

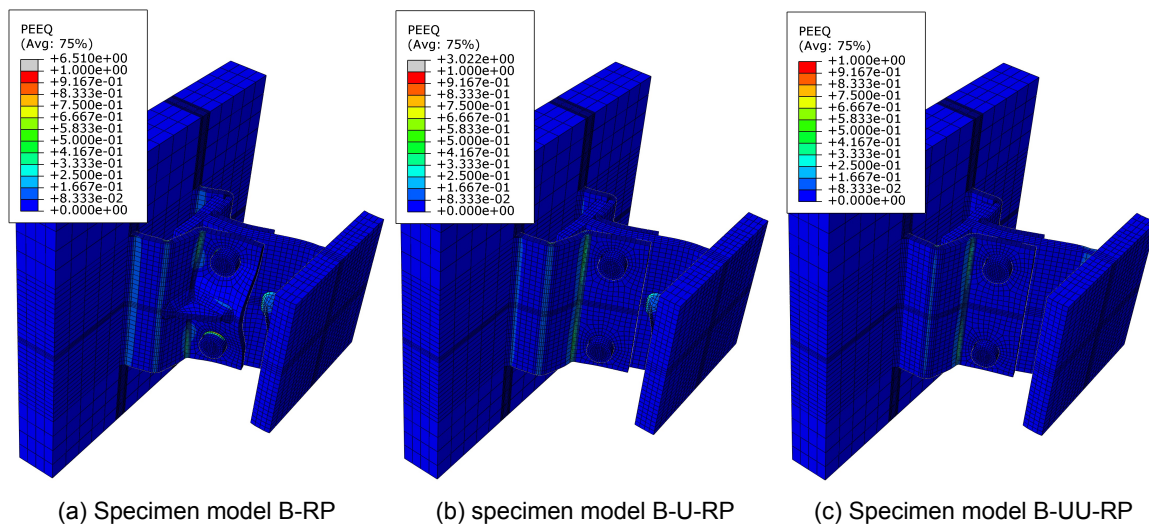


Figure 4.15: Final deformed shape of specimen models B

In Figure 4.15 the final deformed shape of specimen models: B-RP, B-U-RP and B-UU-RP, are shown. Similar to specimen model A-RP, no explicit failure mode is found before the maximum applied displacement and the 25% PEEQ limit. In all three specimen B models, failure occurs due to excessive deformations in the ultimate state. However, in the component model, the 5% PEEQ limit is first reached in the reverse channel, see Paragraph 4.3.2. This is explained by the use of different material models in the experiment and component model. Where the true stress-strain curve with isotropic hardening is used in the experiment model to predict the actual behaviour in the experiment, the component model uses an elasto-plastic relation for practical use in design codes. In addition, special attention should be given to the corner regions of the reverse channel, where the highest PEEQ values are found in the component model. As mentioned in Paragraph 4.1.2, these regions are assigned to plastic material properties, which results in lower PEEQ values even with higher stresses compared to surrounding elements. In conclusion, following the component model with unified material properties, the governing failure mode for the models B-RP, B-U-RP and B-UU-RP is the yielding of the reverse channel in bending.

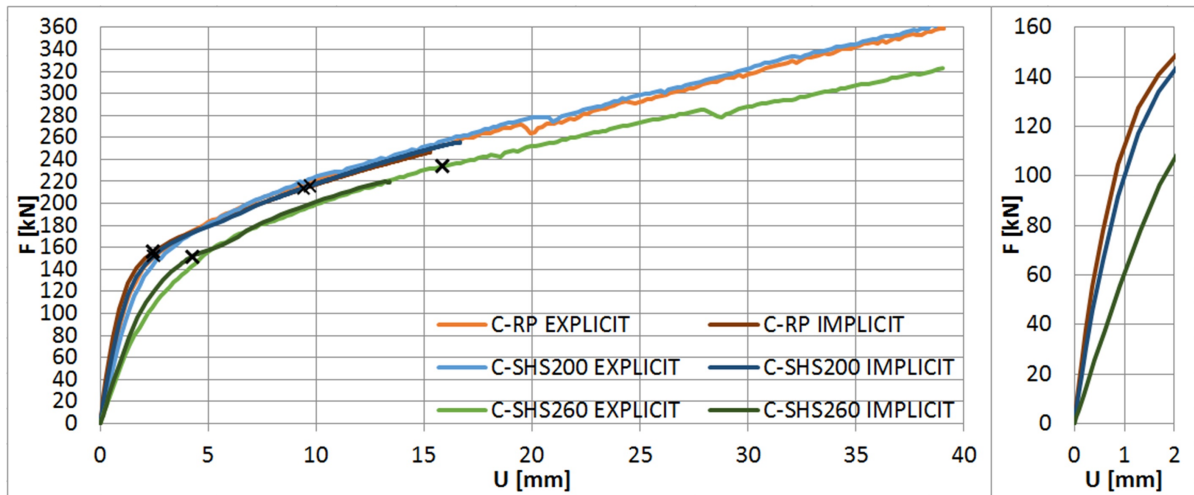


Figure 4.16: Force-displacement curves of specimen models: C-RP, C-SHS200 and C-SHS260 (X at 5% and 25% PEEQ limit)

At last, the remaining specimen models: C-RP, C-SHS200 and C-SHS260, are analysed and all similar characteristics in joint behaviour are found as specimen model A-RP. From Figure 4.16 can be concluded that the rigid plate simplification is an accurate equivalent to a "stiff" tubular hollow column section with a wall thickness of  $12.5\text{ mm}$  and a rather small distance between the legs of the reverse channel and the chord side wall, indicated as specimen model C-SHS200. Comparing it to the "flexible" specimen model C-SHS260,  $260\times 260\times 6\text{ mm}$ , this simplification considerably overestimates both strength and stiffness.

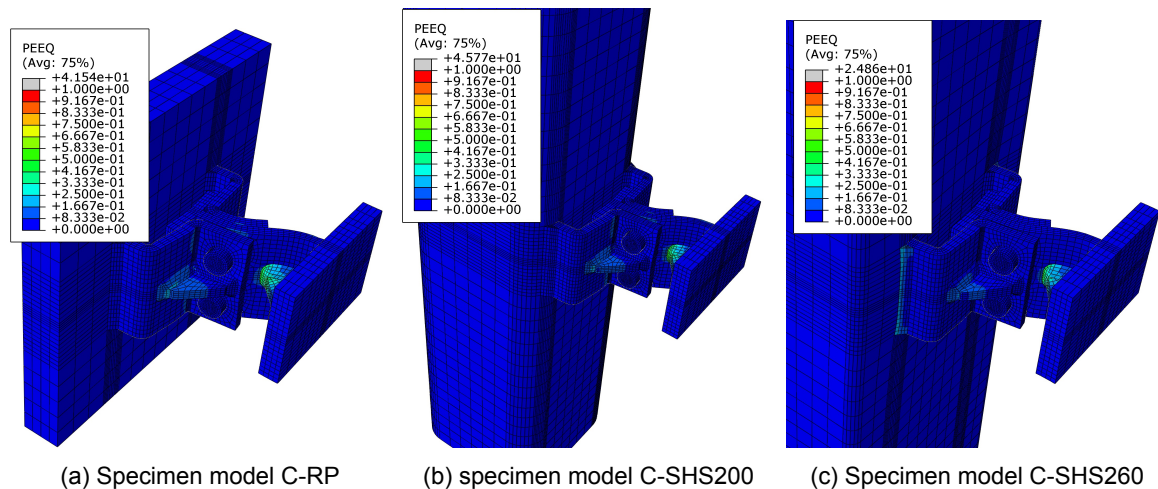


Figure 4.17: Final deformed shape of specimen models C

In Figure 4.17, the final deformed shapes for the specimen models C are shown. From these figures can be concluded that the failure mode, excessive deformation in combination with yielding of the T-plug in bending is found. The influence of the use of tubular sections of the final deformed shape is negligible when comparing C-SHS200 to C-RP. However, with an increased distance between the legs of the reverse channel and the chord side wall increases deformation in the chord along with a higher PEEQ value in the weld between the reverse channel and tubular column section is found.

In conclusion, based on these findings can be concluded that both computational solvers have their benefits and limitations compared to one another. However, to this specific application, considering initial stiffness and yield strength at 5% PEEQ, the use of the implicit solver is preferred. Furthermore, this numerical study gives an upper-boundary, as rigid

constraints and perfect nominal dimensions are assumed in the numerical model. In practice, deviations are likely to occur and therefore the prediction of the experimental results is slighting overestimating the actual behaviour during testing.

### 4.3. Parametric study

An extending parametric study is performed for a couple of reasons. Firstly, the parametric study is used in the derivation of the design resistance and stiffness coefficient of new components, elaborated in Section 5.1. Secondly, specific parameters are studied to provide an answer to the numerous sub-questions stated in Section 1.3. In the upcoming paragraphs, the influence of the following parameters is studied: thickness ratio (reverse channel vs. T-plug web), use of stiffeners, use of tubular sections, length of T-plug web and width. As mentioned in Paragraph 4.1.2, an elasto-plastic material model is used in the parametric study of the component models.

#### 4.3.1. Thickness ratio (reverse channel vs. T-plug web)

The goal of this parametric study is to describe the general influence of the thickness ratio (reverse channel vs. T-plug web) on the joint level and include this parameter as a variable ( $\omega$ ) in the derivations of the design resistance and stiffness coefficient on the component level. Therefore parametric study on thickness ratio is devoted to the derivation of both new components; RC in bending and T-plug in bending.

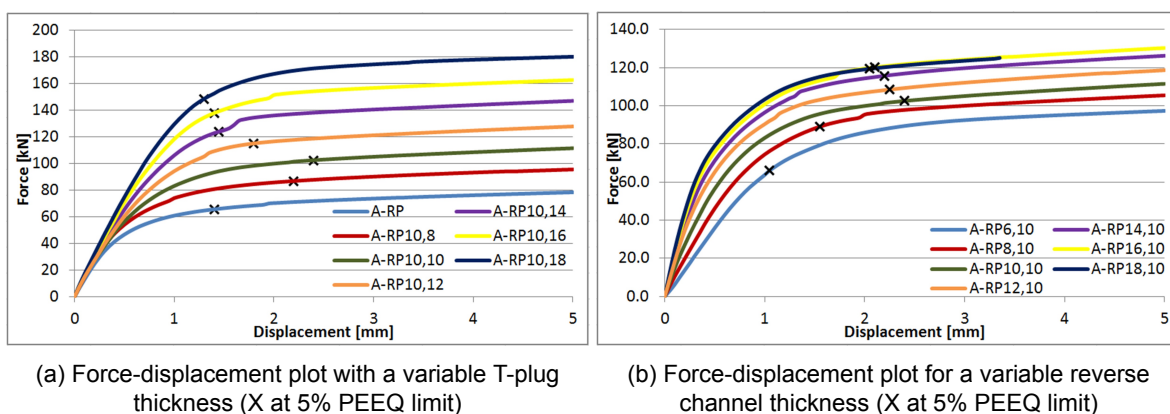


Figure 4.18: Results of the parametric study: thickness ratio

In Figure 4.18a the influence of the thickness ratio is studied for a variable T-plug thickness ( $t_p$ ) and a constant reverse channel thickness ( $t_{rc}$ ). From this figure can be concluded that a variable  $t_p$  has a significant influence on the design resistance and a much lesser influence on the initial stiffness. This is confirmed by the values given in Table 4.7. When analysing the design resistance at 5% PEEQ a clear shift can be seen for a thickness ratio  $\omega = 1.0$ . This leads to the definition of the governing failure mode, either the component; RC in bending or the component; T-plug in bending.

Table 4.7: Joint characteristics: thickness ratio (1)

Model	$t_{rc}$ [mm]	$t_p$ [mm]	$\omega$ [-]	Initial stiffness [kN/mm]	Design resistance [kN]
A-RP	10	6	1.67	123.3	65.7
A-RP10,8	10	8	1.33	138.6	86.9
A-RP10,10	10	10	1.00	135.6	102.6
A-RP10,12	10	12	0.83	136.6	115.2
A-RP10,14	10	14	0.71	144.5	124.1
A-RP10,16	10	16	0.63	153.1	138.0
A-RP10,18	10	18	0.56	161.6	148.8

In Figure 4.18b the influence of the thickness ratio is studied for a variable ( $t_{rc}$ ) and a constant ( $t_p$ ). From this figure can be concluded that a variable  $t_{rc}$  has a significant influence on the initial stiffness and a much lesser influence on the design resistance. This is confirmed by the values given in Table 4.8. When analysing the design resistance at 5% PEEQ the same shift at  $\omega = 1.0$  is identified.

Table 4.8: Joint characteristics: thickness ratio (2)

Model	$t_{rc}$ [mm]	$t_p$ [mm]	$\omega$ [-]	Initial stiffness [kN/mm]	Design resistance [kN]
A-RP6,10	6	10	0.60	71.9	30.1
A-RP8,10	8	10	0.80	99.4	91.8
A-RP10,10	10	10	1.00	135.6	102.6
A-RP12,10	12	10	1.20	173.0	108.6
A-RP14,10	14	10	1.40	187.2	115.8
A-RP16,10	16	10	1.60	208.4	120.2
A-RP18,10	18	10	1.80	221.8	119.4

Therefore, on the component level, the influence of the thickness ratio is expressed by the condition determining the governing failure mode. Moreover, in both component derivations, the design resistance and stiffness coefficient include factors accounting for the thickness ratio. Therefore can be concluded the thickness ratio has a huge influence on both joint and component level.

### 4.3.2. Use of stiffeners

The goal of this parametric study is to describe the general influence of the use of stiffeners on the joint level and include this parameter as a variable in the derivations of the design resistance and stiffness coefficient on the component level. Therefore parametric study on the use of stiffeners devoted to the derivation of both new components; RC in bending and T-plug in bending. Based on the conclusion on the influence of the thickness ratio above, the specimen models; B-RP, B-U-RP (B-U1-RP) and B-UU-RP, form the basis of this parametric study on the derivation of the component; RC in bending. Besides, a configuration with an unstiffened T-plug in combination with a stiffened reverse channel (B-U2-RP) is studied. For the same reason, these stiffener configurations are studied on the "base" model A-RP for the derivation of the component; T-plug in bending. Since experimental model A-RP has a width of 100 mm and B-RP of 150 mm, also the width of the joint is studied for a range  $100 \leq b \leq 150$  mm. Given the trend of an increased design resistance and stiffness for an increased width, in general the B-models higher values compared to A.

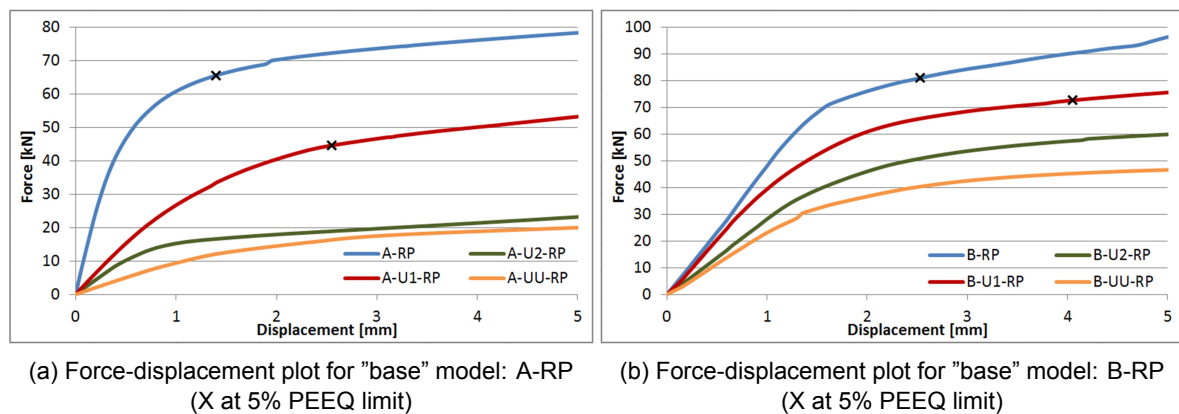


Figure 4.19: Results of the parametric study: use of stiffeners

Based on Figure 4.19a can be concluded that the presence of the T-plug stiffener results in significant higher resistance and initial stiffness (-RP and -U1-RP). To a much lesser extent

the same conclusion holds for the presence of the reverse channel stiffener, comparing A-U1-RP to A-RP and A-UU-RP to A-U2-RP. In Figure 4.19b, the same general trend is found, with the double stiffened (-RP) configuration being the strongest and double unstiffened (-UU-RP) configuration is weakest. This is also expressed in numbers in Table 4.9. However, on a different reverse channel design, B compared to A configuration, the individual influence of the stiffeners is also different. Therefore an additional study on the effect of the reverse channel design is recommended since it is outside the scope of this research. Although both resistance and stiffness decrease from double stiffened (-RP) to double unstiffened (-UU-RP) configurations, the ductility increases. This is indicated by the 5% PEEQ limit shifting to the right, which even results in values for (-U2-RP) and (-UU-RP) outside the plotted range.

Table 4.9: Joint characteristics: use of stiffeners

Model	Initial stiffness [kN/mm]	Design resistance [kN]
A-RP	123.3	65.7
A-U1-RP	32.3	44.7
A-U2-RP	22.1	28.3
A-UU-RP	10.5	25.1
B-RP	48.3	81.1
B-U1-RP	41.5	72.8
B-U2-RP	28.2	62.4
B-UU-RP	23.3	47.9

On the component level, the influence of the use of stiffeners is moreover expressed by the four categorized groups: 1. Double stiffened (-RP), 2. Stiffened T-plug/unstiffened RC (-U1-RP), 3. Unstiffened T-plug/stiffened RC (-U2-RP) and 4. Double unstiffened (-UU-RP). In both component derivations, the design resistance and stiffness coefficient include factors defined upon these categorized groups and has a direct influence of every single configuration. In addition, the influence of the stiffener thickness is included in the derivation of both design resistance and stiffness coefficient. Therefore can be concluded the use of stiffeners is the most contributing parameter on the behaviour on both joint and component level.

### 4.3.3. Use of tubular sections

In Figure 4.16 a flexible (SHS260x6) and a stiff (SHS200x12.5) tubular column section are studied for a rigid plate "benchmark" model (C-RP). These configurations are chosen as the boundaries of the range of interest. Based on these results can be concluded that the rigid plate simplification quite accurately approximates the stiff tubular configuration. In specific, the design resistance can be accurately approximated, but the initial stiffness is slightly overestimated by the rigid plate simplification, see Table 4.10. This is explained by the legs of the reverse channel have a small eccentricity to the chord side wall, as with an increased eccentricity the initial stiffness is reduced. Although there are some differences between the flexible and stiff configuration in design resistance and initial stiffness, there is decided to perform no further parametric study on the use of tubular sections as no failure mode in the column section is found for any configuration in the parametric study. Given these two findings can be concluded that the use of tubular section has a minor influence on both component and joint level.

Table 4.10: Joint characteristics: use of tubular sections

Model	Initial stiffness [kN/mm]	Design resistance [kN]
C-RP	148.7	119.6
C-SHS200	117.7	119.4
C-SHS260	61.0	88.3



#### 4.3.4. Length T-plug web

The goal of this parametric study is to describe the general influence of the length of the T-plug web on the joint level and include this parameter as a variable in the derivations of the design resistance and stiffness coefficient on the component level. The length of the T-plug is studied for the range  $51 \leq l_x \leq 93 \text{ mm}$ , where  $l_x = 51 \text{ mm}$  corresponds to the "base" model A-RP. On the component level, an increased length of the T-plug web causes always the component; T-plug in bending to be governing. Therefore in this paragraph only results on a "base" model A-RP with  $\omega \geq 1.0$  are presented.

Table 4.11: Joint characteristics: length T-plug web

Model	$l_x$ [mm]	Initial stiffness [kN/mm]	Design resistance [kN]
A-RP	51	123.3	56.2
A-RP16	58	87.9	51.8
A-RP23	65	59.9	39.9
A-RP30	72	43.2	34.4
A-RP37	79	30.9	28.5
A-RP44	86	22.1	24.8
A-RP51	93	16.7	23.6

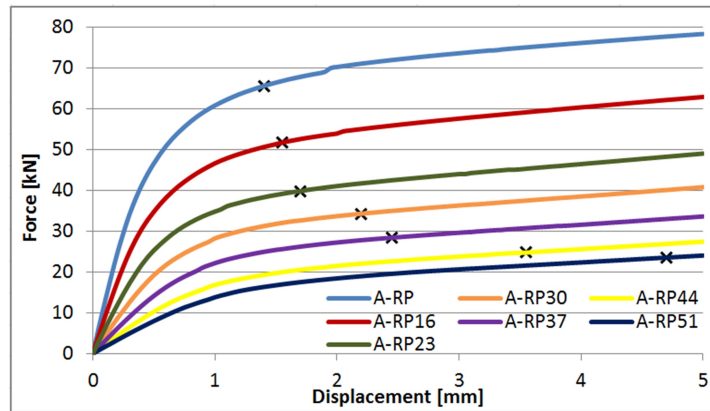


Figure 4.20: Results of the parametric study: length T-plug web (X at 5% PEEQ limit)

Based on Figure 4.20 can be concluded that with an increased length of the T-plug web both design resistance and initial stiffness considerable reduce. In addition, an increased length of the T-plug web also leads to larger deformation before reaching its 5% plastic limit, indicated by the cross signs in the figure. In Table 4.11 the values of the initial stiffness and design resistance are given. As mentioned above, on the component level, for every length of the T-plug web larger than the absolute minimum, the free length is equal to the length of the T-plug stiffener ( $l_x = l_{st}$ ), the component; T-plug in bending is governing. Therefore only for the derivation of the design resistance and stiffness coefficient of this component the contribution of the length of the T-plug web is included as a dimension factor. Given these findings can be concluded the length of the T-plug web has an influence on the joint level, but regarding the component level only contributes to the component; T-plug in bending.

# 5

## Component method application

As introduced in Section 2.4, the component method application consists of three steps; identification, evaluation and assembly. This chapter elaborates the application of these steps on the plug-and-play joint studied. Based on the parametric study, Section 5.1 provides a list of active components for the specific plug-and-play joint. Next, in Section 5.2 design resistance and stiffness coefficient are individually evaluated on the component level. Finally, in Section 5.3 the individual components are assembled to derive the design resistance, rotational stiffness and rotation capacity on the joint level.

### 5.1. Active components

Following the EC3-1-8 component method approach, the structural properties of joints are determined for a joint considered as a set of individual components. In the first step, all active components of the specific plug-and-play joint are identified. The EC3-1-8 makes a distinction between structural joints connecting H or I sections and hollow section joints, of which the current component method approach is only applicable to the structural joints connecting H or I sections. As the plug-and-play joint studied includes features from both type of joints, a unified approach for steel joints independent of the type of connected sections is desired. This is realized by extending the field of application of the component method approach to tubular joints, as is studied by Weynand et al. in the CIDECT report 16F: *Components for tubular joints*. (Weynand et al., 2015)

Based on the results of the parametric study, performed in Section 4.3, a list of active components is composed for the plug-and-play joint. The list of active components contains components from the list of basic components in the current EC3-1-8, the CIDECT report 16F: *Components for tubular joints* (Weynand et al., 2015) and new components to be derived. For the studied plug-and-play joint the following active components are identified and shown in Figure 5.1:

1. Chord side wall in transverse compression;
2. Chord side wall in transverse tension;
3. Chord face in bending;
4. Welds
5. Reverse channel in bending;
6. Bolts in tension;
7. T-plug web in bending.

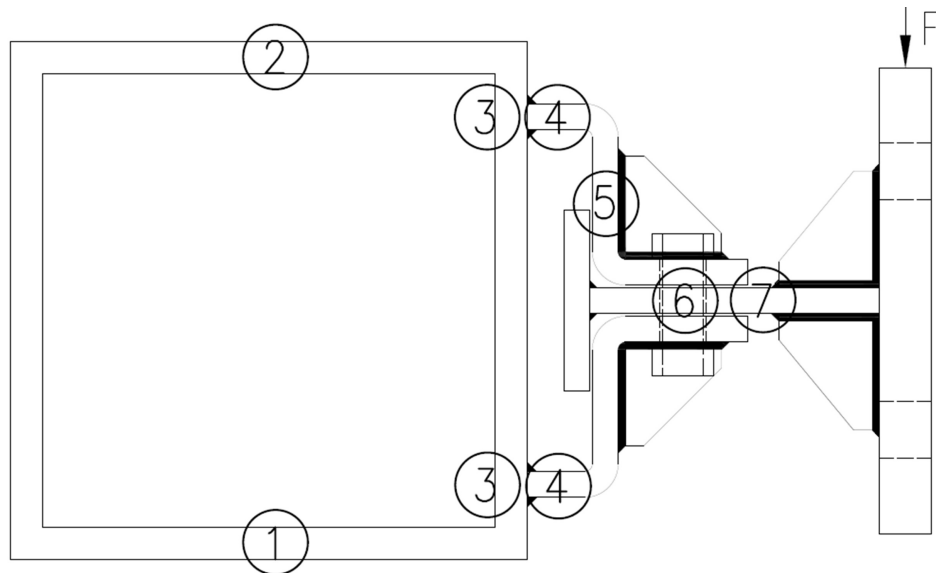


Figure 5.1: Active components for the plug-and-play joint to tubular column section

From the list of active components, only two components are identified with the list of basic components in the EC3-1-8, namely component 4: welds, and component 6: bolts in tension. Besides, components 1-3 are adopted and converted for the application on tubular joints in the CIDECT report 16F. In the end, for two components; reverse channel in bending and T-plug in bending, new analytical expressions are derived. The derivations of the design resistance and stiffness coefficient are elaborated in Paragraphs 5.2.5 and 5.2.7.

## 5.2. Evaluation

The second step in the application of the component method is the evaluation of the resistance and stiffness characteristics for each of the seven individual components selected in Section 5.1. In the next paragraphs, analytical expressions for these characteristics are derived and/or discussed.

### 5.2.1. Chord side wall in transverse compression

The component; chord side wall in transverse compression, is currently not covered in the EC3-1-8, as no component method approach yet exists for tubular joints. However, the CIDECT research group has proposed implementation of the component method for tubular joints, which includes the derivation of the component; chord side wall in transverse compression, as an extension to the component; column web in transverse compression, covered in the EC3-1-8, as shown in Figure 5.2.

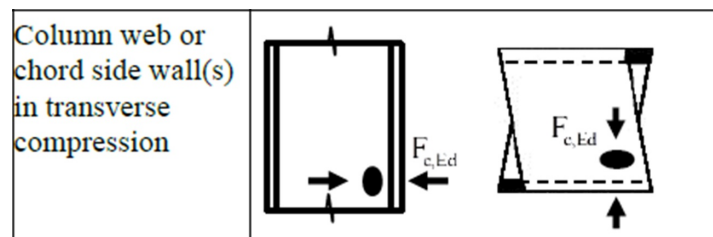


Figure 5.2: Chord side wall in transverse compression (Weynand et al., 2015)

For the component method application of the plug-and-play joint, the design resistance defined in the CIDECT report 16F is adopted, where an improved equation for the stiffness coefficient by Garifullin is used. The component; chord side wall in transverse compression, only has a significant impact for  $0.85 < \beta \leq 1.0$  and therefore only for this range both design



resistance and stiffness coefficient have to be determined (Weynand et al., 2015). In this paragraph a summary is presented on both design resistance and stiffness coefficient of the component; chord side wall in transverse compression.

### Design resistance

Following the CIDECT report 16F, the design resistance of chord side wall subject to transverse compression should be determined from Equation 5.1.

$$F_{c,wc,Rd} = 1.43k_{wc}\kappa_{\theta,wc}b_{eff,c,wc}tf_{y,wc}/\gamma_{M0} \text{ but } F_{c,wc,Rd} \leq 1.43k_{wc}\kappa_{\theta,wc}\rho b_{eff,c,wc}tf_{y,wc}/\gamma_{M1} \quad (\text{Eq. 5.1})$$

Where,

- $b_{eff,c,wc} = 0.025 \left( h_1(9\beta - 1) + \frac{2.4b_0}{1.2-\beta} \right)$ , the effective width of chord side wall in transverse compression (Garifullin et al., 2019);
- $k_{wc}$  is the reduction factor for chord;
- $\kappa_{\theta,wc}$  is the reduction factor to account for the layout of the joint configuration;
- $\rho$  is the reduction factor for plate buckling;
- $t = t_0$ , the reference thickness for hollow chords;
- $f_{y,wc}$  is the yield strength of the chord.

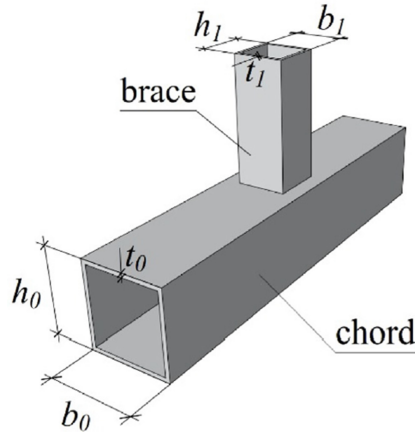


Figure 5.3:  $\beta = b_1/b_0$  ratio, where  $b_1$  is the leg between both legs of the reverse channel (Garifullin et al., 2019)

An improved equation by Garifullin is adopted for  $b_{eff,c,wc}$ , considering various  $\beta = b_1/b_0$  ratios, where the CIDECT report only considers the case  $\beta = 1.0$ . Therefore the use of the improved Garifullin equation is preferred, as it provides a more complete definition to the whole spectrum of chord-to-brace ratios. However, the effective width by Garifullin is derived based on a stiffness study and therefore a conversion factor:  $1/0.7 = 1.43$ , is added to the equation of the design resistance. Furthermore, for the application on the plug-and-play joint of interest, the following values are defined;  $k_{wc} = 1.0$ ,  $\kappa_{\theta,wc} = 1.3 - 0.4n/\beta$ , with  $n = (\sigma_{0,Ed}/f_{y0})/\gamma_{M5}$ , and  $\rho$  obtained from EC3-1-1 using the relevant buckling curve for flexural buckling and normalized slenderness;  $\lambda_p = 3.46(h_0/t - 2)\sqrt{1/\sin\theta_i}/(\pi\sqrt{E/f_{y,wc}})$ .

### Stiffness coefficient

For tubular joints the stiffness coefficient, derived in the CIDECT report 16F, remains questionable for a couple of reasons. First, the stiffness coefficient has been developed for specific X joint applications but lacks reliability for T joints. Second, the CIDECT report 16F does not include  $\beta$  as a variable, providing only a general solution, and therefore the application

for  $\beta < 1.0$  remains unclear as well. For these reasons, as mentioned in the introducing paragraph, an improved equation by Garifullin for the stiffness coefficient is adopted. As the equation by Garifullin is derived based on axial loading, a slight adaptation is made to be applicable for the out-of-plane bending, assuming perfect symmetry, of the plug-and-play joint. The equation for the stiffness coefficient is given below. (Garifullin et al., 2019)

$$k_1 = \frac{b_{eff,c,wc}t_0}{h_0 - t_0} \quad (\text{Eq. 5.2})$$

The equation looks very similar to the stiffness coefficient for the component; column web in transverse compression, presented in the EC3-1-8. However, this equation does not consider the coefficient 0.7, but as  $b_{eff}$  is determined by numerical analysis, this correction factor is by default considered. The same effective width is used as in the derivation of the design resistance;  $b_{eff} = b_{eff,c,wc}$ .

### 5.2.2. Chord side wall in transverse tension

Similar to the component; chord side wall in transverse compression, this component is not covered in the current EC3-1-8, but an extension to the component; column web in transverse tension, is proposed in the CIDECT report 16F, see Figure 5.4. The same approach as the component; chord side wall in transverse compression, is applied, which includes the adoption of the design resistance defined in the CIDECT report 16F and an improved equation for the stiffness coefficient by Garifullin. Similar to the component in compression, this component only has to be determined for the range  $0.85 < \beta \leq 1.0$  (Weynand et al., 2015). In this paragraph a summary is presented for both design resistance and stiffness coefficient of the component; chord side wall in transverse tension.

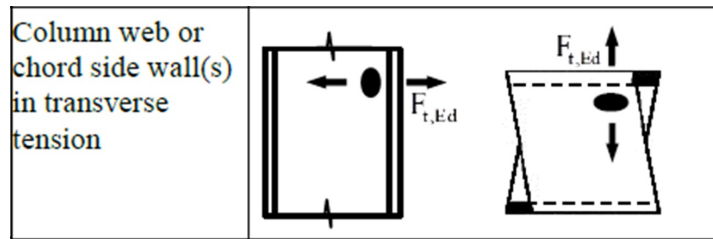


Figure 5.4: Chord side wall in transverse tension (Weynand et al., 2015)

#### Design resistance

Following the CIDECT report 16F, the design resistance of chord side wall subject to transverse tension is determined by Equation 5.3.

$$F_{t,wc,Rd} = 1.43k_{wc}\kappa_{\theta,wc}\rho b_{eff,t,wc}t f_{y,wc}/\gamma_{M0} \quad (\text{Eq. 5.3})$$

According to the CIDECT report 16F, the effective width of the chord side wall in tension and compression are similar. Since an improved equation by Garifullin is adopted for the component; chord side wall in transverse compression, the same is applied for this component. This gives the following effective width;  $b_{eff,t,wc} = 0.025(h_1(9\beta - 1) + \frac{2.4b_0}{1.2-\beta})$ , and the inclusion of the conversion factor ( $1/0.7 = 1.43$ ) for the design resistance. Besides, the factors  $\rho$ ,  $k_{wc}$  and  $\kappa_{\theta,wc}$  are all equal to 1.0 for the component; chord side wall in transverse tension.

#### Stiffness coefficient

According to the CIDECT report 16F, the stiffness of the chord side wall is assumed to be the same in tension and compression. For similar reasons as the component; chord side wall in transverse compression, an improved equation for the stiffness coefficient by Garifullin is slightly adapted and given below. (Garifullin et al., 2019)

$$k_2 = \frac{b_{eff,t,wc}t_0}{h_0 - t_0} \quad (\text{Eq. 5.4})$$

The equation looks very similar to the stiffness coefficient of the component; column web in transverse tension, presented in the EC3-1-8. However, this equation does not consider the coefficient 0.7, but as  $b_{eff}$  is determined by numerical analysis, this correction factor is by default considered. The same effective width is used as in the derivation of the design resistance;  $b_{eff} = b_{eff,t,wc}$ .

### 5.2.3. Chord face in bending

The component; chord face in bending, is currently not covered in the EC3-1-8, as no component method approach yet exists for tubular joints. However, the CIDECT research group has proposed implementation of the component method for tubular joints, which includes the derivation of the component; chord face in bending, as an extension to the component; column flange in bending, covered in the current EC3-1-8, as shown in Figure 5.5. The design resistance defined in the CIDECT report 16F is adopted, where an improved equation for the stiffness coefficient by Garifullin is used. Besides, the component; chord face in bending, only has a significant impact for  $\beta \leq 0.85$  and therefore only for this range both design resistance and stiffness coefficient have to be determined (Weynand et al., 2015). In this paragraph a brief summary is presented for both design resistance and stiffness coefficient of the component; chord face in bending.

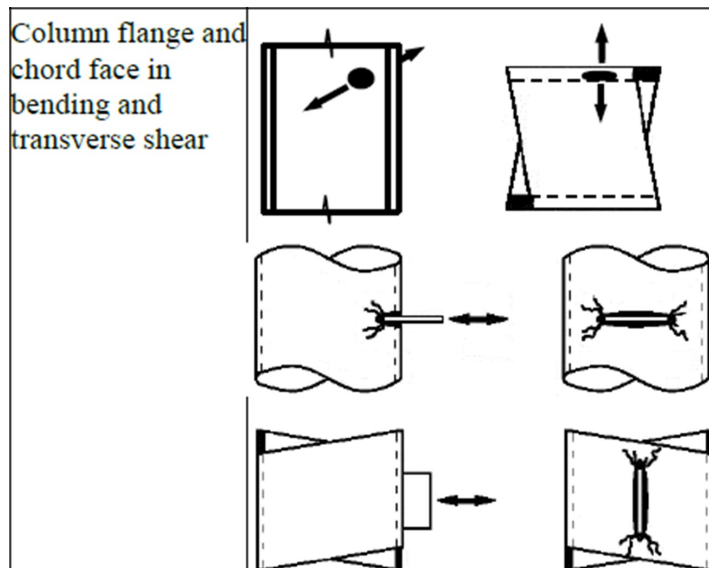


Figure 5.5: Chord face in bending (Weynand et al., 2015)

#### Design resistance

Following the CIDECT report 16F, the design resistance of the component; chord face in bending, is determined from Equation 5.5. The resistance is determined for an equivalent T joint connection between SHS (chord) and longitudinal plate (brace). Perfect symmetry is assumed and therefore the lowest resistance of to the longitudinal plate loaded in tension/compression is multiplied by two to determine the overall resistance of the component.

$$F_{fc,Rd} = k_{fc} (0.5l_{eff,1} + l_{eff,2}) m_{pl,Rd} \quad (\text{Eq. 5.5})$$

Where,

- $k_{fc}$  is a reduction factor for longitudinal stresses in the chord, given in Equation 5.6;
- $l_{eff,1} = 4\eta$ , non-dimensional effective length ( $\eta = \frac{h_1}{b_0}$ );
- $l_{eff,2} = 4\sqrt{1-\beta}$ , non-dimensional effective length;
- $m_{pl,Rd} = 0.25t_0^2 f_{y0} / \gamma_{M5}$ .

$$k_{fc} = \begin{cases} 1.3(1-n) \leq 1.0 & \text{in compression } (n > 0) \\ 1.0 & \text{in tension } (n \leq 0) \end{cases} \quad (\text{Eq. 5.6})$$

For an equivalent T joint with two longitudinal plates  $\beta = t_1/(0.5b_0)$  in  $l_{eff,2}$ .

#### Stiffness coefficient

For similar reasons as previously derived components, an improved equation for the stiffness coefficient by Garifullin is adopted, which is given below. (Garifullin et al., 2019)

$$k_3 = \frac{4l_{eff}t_0^3}{((b_0 - b_1)/2 - t_0)^3} \quad (\text{Eq. 5.7})$$

Considering a longitudinal plate instead of a hollow brace section, the original equation, derived by Garifullin, is slightly adjusted. Given the presence of a longitudinal plate in compression and another in tension, assuming both plates are equally opposite axially loaded, both effective length ( $l_{eff}$ ) and width ( $b_0 - b_1 - 2t_0$ ) are divided by 2, which is for the latter visible in the denominator. The slightly adjusted derivation of the effective length, following the numerical analysis by Garifullin, results in the following length:  $l_{eff} = 0.5h_1(2 - \beta) + 0.625b_0(1 - \beta)$ .

#### 5.2.4. Welds

This component is fully adopted from EC3-1-8 for both design resistance and stiffness coefficient of which a summary is given below.

##### Design resistance

At all times rupture of the welds should be avoided as the failure mode behaves in a brittle way. Therefore the welds are designed as "full strength", so the rupture strength of the "full strength" welds is greater than its connecting components. In the case of overloading, failure appears in the connecting component before the welds. The "full-strength" of welds is achieved by expressing the design resistance of the weld as equal to or higher than the design resistance of the weakest component in the joint. (Jaspart and Weynand, 2016)

The evaluation of the design resistance of welds is presented in Paragraph 4.1.1. Therefore no additional information is given here.

##### Stiffness coefficient

According to EC3-1-8 [Table 6.11: Note 4], the stiffness coefficient for welds should be taken equal to infinity:

$$k_4 = \infty \quad (\text{Eq. 5.8})$$

Therefore this component does not need to be accounted for when calculating the rotational stiffness ( $S_{j,ini}$ ) and is not included in the spring model of Figure 5.8. (EN 1993-1-8, 2005)

#### 5.2.5. Reverse channel in bending

The component; reverse channel in bending, is currently not covered in EC3-1-8 on both design resistance and stiffness coefficient. Therefore it is analytically derived in the format of the component method based on the results of the parametric study. The derivation is categorized into four groups, based on the stiffener configuration on two locations; reverse channel (RC) and T-plug. This leads to the following four groups: 1. Double stiffened (-RP), 2. Stiffened T-plug/unstiffened RC (-U1-RP), 3. Unstiffened T-plug/stiffened RC (-U2-RP) and 4. Double unstiffened (-UU-RP). The complete elaboration is given in Appendix C and briefly summarized below.

##### Design resistance

The design resistance of the component; reverse channel in bending, is derived based on the EC3-1-1 bending moment theory for cross-sections under elastic deformation. Considering

the bending moment at the rigid plate/tubular section caused by the load transferred in the net-section, the relation  $F_{rc,Rd} = M_{Rd}/l$  is applied, which results in the following equation for the design resistance:

$$F_{rc,Rd} = \frac{b_{eff} t_{rc}^2 f_y}{6l\gamma_{M0}} \quad (\text{Eq. 5.9})$$

Where,

- $l = l_1 + l_2$  = the length between the rigid plate/tubular section to the net-section;
- $b_{eff} = ab$ , the effective width of the T-plug;
- $t_{rc}$  = thickness reverse channel;
- $f_y$  = yield strength of the reverse channel;
- $\gamma_{M0} = 1.0$ , partial safety factor.

The effective width is derived by the factor  $\alpha$ , which is constructed by a total of four factors, each accounting for an individual variable dimension. These factors include the influence of the width, thickness stiffener, thickness ratio and thickness T-plug, respectively given in the order of the equation below.

$$\alpha = \alpha_b \alpha_{st} \alpha_\omega \alpha_t \quad (\text{Eq. 5.10})$$

The values of each factor are presented by Equations 5.11-5.12 and Tables 5.1-5.2. For a detailed derivation of each individual multiplication factor is referred to Appendix C.1.

$$\alpha_b = \begin{cases} 2.1 \left(\frac{b}{b_0}\right)^2 + 4.3 \left(\frac{b}{b_0}\right) + 3.2 & \text{for stiffened RC} \\ -0.1 \left(\frac{b}{b_0}\right) + 1.1 & \text{for unstiffened RC} \end{cases} \quad (\text{Eq. 5.11})$$

$$\alpha_{st} = \begin{cases} -0.33 \left(\frac{t_{stiff}}{t_0}\right) + 1.55 & \text{for stiffened RC} \\ 1 & \text{for unstiffened RC} \end{cases} \quad (\text{Eq. 5.12})$$

Table 5.1: Values of  $\alpha_\omega$

	Group	$\alpha_\omega$ [-]	Condition
1	Double stiffened (A-RP)	$-0.63\omega^2 + 1.07\omega + 0.6$	$\omega < 1.0$
	Double stiffened (B-RP)	$-2.51\omega + 17.47$	$\omega < 1.0$
2	Stiffened T-plug / unstiffened RC (A-U1-RP)	$26\omega - 48.7\omega + 31$	$\omega < 1.0$
3	Unstiffened T-plug / stiffened RC (A-U2-RP)	1	$\omega < 1.0$
4	Double unstiffened (A-UU-RP)	$19.2\omega^2 - 39.7\omega + 24.85$	$\omega < 1.25$

Table 5.2: Values of  $\alpha_t$

	Group	$\alpha_t$ [-]	Condition
1	Double stiffened (A-RP)	$17.4 \left(\frac{t_p}{t_0}\right) - 9.6$	$\omega < 1.0$
	Double stiffened (B-RP)	1	$\omega < 1.0$
2	Stiffened T-plug / unstiffened RC (A-U1-RP)	1	$\omega < 1.0$
3	Unstiffened T-plug / stiffened RC (A-U2-RP)	$16.7 \left(\frac{t_p}{t_0}\right) - 9.1$	$\omega < 1.0$
4	Double unstiffened (A-UU-RP)	1	$\omega < 1.25$

### Stiffness coefficient

The stiffness coefficient of the component; reverse channel in bending, is derived based on the simplified mechanical model shown in Figure 5.6.

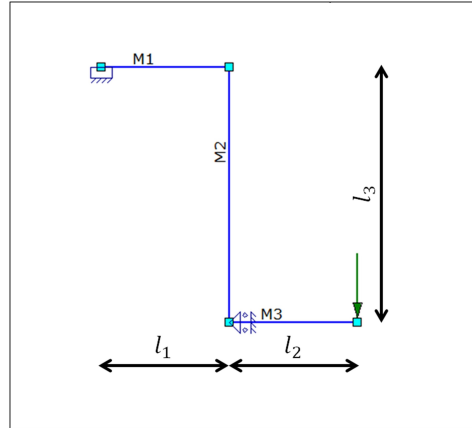


Figure 5.6: Simplified reverse channel model

Applying the Euler-Bernoulli beam theory on the simplified mechanical model, this results in the following equation for the stiffness coefficient:

$$k_5 = \frac{b_{eff} t_{rc}^3}{l_{eff}^3} \quad (\text{Eq. 5.13})$$

Where,

- $b_{eff} = ab$ , effective width;
- $l_{eff}^3 = 4l_2^3 + 3l_2^2 l_3 + 4l_1^3 - 3l_2 l_1^2$  = the effective length of the simplified mechanical model in Figure 5.6.

As the stiffness coefficient and design resistance follow a different trend, the effective width of the design resistance multiplied with a dimension factor can not be used here. Therefore  $b_{eff}$  is derived separately for the stiffness coefficient, but using the same dimension factor  $\alpha$  and individual contributions of the width, thickness stiffener, thickness ratio and thickness T-plug. Besides, a factor accounting for the design of the reverse channel is added, resulting in the equation below.

$$\alpha = \alpha_b \alpha_{st} \alpha_{rc} \alpha_\omega \alpha_t \quad (\text{Eq. 5.14})$$

The values of each factor are presented by Equations 5.15-5.17 and Tables 5.3-5.4. For a detailed derivation of each individual multiplication factor is referred to Appendix C.2.

$$\alpha_b = \begin{cases} -0.3 \left( \frac{b}{b_0} \right) + 1.3 & \text{for stiffened T-plug} \\ -0.25 \left( \frac{b}{b_0} \right) + 1.25 & \text{for unstiffened T-plug} \end{cases} \quad (\text{Eq. 5.15})$$

$$\alpha_{st} = \begin{cases} 0.12 \left( \frac{t_{stiff}}{t_0} \right) + 0.88 & \text{for stiffened T-plug} \\ 1 & \text{for unstiffened T-plug} \end{cases} \quad (\text{Eq. 5.16})$$

$$\alpha_{rc} = -0.99 \left( \frac{l_2}{l_3} \right) + 1.65 \quad (\text{Eq. 5.17})$$

Table 5.3: Values of  $\alpha_\omega$ 

	Group	$\alpha_\omega$ [-]	Condition
1	Double stiffened (-RP)	$-0.22\omega + 1.13$	$\omega < 1.25$
2	Stiffened T-plug / unstiffened RC (A-U1-RP)	$3.02\omega^2 - 5.54\omega + 3.43$	$\omega < 1.0$
3	Unstiffened T-plug / stiffened RC (A-U2-RP)	1	$\omega < 1.0$
4	Double unstiffened (A-UU-RP)	$4.82\omega^2 - 9.84\omega + 6.04$	$\omega < 1.25$

Table 5.4: Values of  $\alpha_t$ 

	Group	$\alpha_t$ [-]	Condition
1	Double stiffened (A-RP)	$-2.88\left(\frac{t_p}{t_0}\right) - 5.84$	$\omega < 1.0$
	Double stiffened (B-RP)	1	$\omega < 1.0$
2	Stiffened T-plug / unstiffened RC (A-U1-RP)	1	$\omega < 1.0$
3	Unstiffened T-plug / stiffened RC (A-U2-RP)	$-4.19\left(\frac{t_p}{t_0}\right) + 8.11$	$\omega < 1.0$
4	Double unstiffened (A-UU-RP)	$0.05\left(\frac{t_p}{t_0}\right)^2 - 0.2\left(\frac{t_p}{t_0}\right) + 0.735$	$\omega < 1.25$

### 5.2.6. Bolts in tension

This component is fully adopted from EC3-1-8 for both design resistance and stiffness coefficient, of which a short summary is given below.

#### Design resistance

Following EC3-1-8 the tension resistance of an individual bolt, preloaded or non-preloaded, is determined using Equation 5.18. For the overall resistance of the component, the determined resistance has to be multiplied by the number of bolts present.

$$F_{t,Rd} = \frac{0.9f_{ub}A_s}{\gamma_{M2}} \quad (\text{Eq. 5.18})$$

Where  $f_{ub}$  is the ultimate tensile strength and  $A_s$  is the tensile stress area of the bolt.

#### Stiffness coefficient

The stiffness coefficient of the component; bolts in tension, preloaded or non-preloaded, for a single bolt-row is for this configuration assumed to be infinite:

$$k_6 = \infty \quad (\text{Eq. 5.19})$$

Since the bolts in the plug-and-play joint are not loaded in pure tension, its contribution to the stiffness is neglected.

### 5.2.7. T-plug in bending

The component; T-plug in bending, is currently not covered in EC3-1-8 on both design resistance and stiffness coefficient. Therefore it is analytically derived in the format of the component method based on the results of the parametric study. The derivation is categorized into four groups, based on the stiffener configuration on two locations; reverse channel (RC) and T-plug. This leads to the following four groups: 1. Double stiffened (-RP), 2. Stiffened T-plug/unstiffened RC (-U1-RP), 3. Unstiffened T-plug/stiffened RC (-U2-RP) and 4. Double unstiffened (-UU-RP). The complete elaboration of the component; T-plug in bending, is given in Appendix D and briefly summarized below.

### Design resistance

The design resistance of the component; T-plug in bending, is derived using a partial T-stub model analogy, where the yielding of the T-plug web is identified with the yielding of the flange (failure mode 1) of the T-stub model. This results in the relation  $F_{tp,Rd} = 0.5F_{T,1,Rd}$ , accounting for the presence of only one equivalent flange in the component. The following equation for the design resistance is derived:

$$F_{tp,Rd} = \frac{0.5b_{eff}t_p^2f_y}{m\gamma_{M0}} \quad (\text{Eq. 5.20})$$

Where,

- $m$  = distance between two equivalent yield lines, given in Table D.4;
- $b_{eff} = \alpha_b b - \alpha_l(l_x - l_{st})$ , the effective width of the T-plug;
- $t_p$  = thickness T-plug;
- $f_y$  = yield strength of the T-plug;
- $\gamma_{M0} = 1.0$ , partial safety factor.

For the derivation of parameter "m", the distance between two equivalent yield lines is approximated by the equations given in Table 5.5. Also, a condition regarding the thickness ratio ( $\omega$ ) is added, to assure the failure mode appears in the T-plug. The factor  $\alpha_m$  and its sub-factors are given below. For a detailed derivation is referred to Appendix D.1.2.

$$\alpha_m = \alpha_t \alpha_\omega \alpha_{bm} \quad (\text{Eq. 5.21})$$

With,

$$\alpha_t = \left( -0.3195 \left( \frac{t_p}{t_0} \right)^2 + 1.2255 \left( \frac{t_p}{t_0} \right) - 0.1575 \right) \quad (\text{Eq. 5.22})$$

$$\alpha_\omega = \begin{cases} \left( \frac{-0.37}{\omega} \right) + 1.17 & \text{for } A_p \leq 800 \text{ mm}^2 \\ 1 & \text{for } A_p > 800 \text{ mm}^2 \end{cases} \quad (\text{Eq. 5.23})$$

$$\alpha_{bm} = \left( -0.0006 \left( \frac{b}{t_{stiff}} \right)^2 + 0.035 \left( \frac{b}{t_{stiff}} \right) + 0.385 \right) \quad (\text{Eq. 5.24})$$

Table 5.5: Values of m

	Group	m [mm]	Condition
1	Double stiffened (-RP)	$\alpha_m l_{st} + (l_x - l_{st}) + l_{rc}$	$1.0 \leq \omega < 1.5$
		$\alpha_m l_{st} + (l_x - l_{st})$	$\omega \geq 1.5$
2	Stiffened T-plug / unstiffened RC (-U1-RP)	$\alpha_m l_{st} + (l_x - l_{st}) + l_{rc}$	$\omega \geq 1.0$
3	Unstiffened T-plug / stiffened RC (-U2-RP)	$l_x$	$\omega \geq 1.0$
4	Double unstiffened (-UU-RP)	$l_x$	$\omega > 1.25$

The parameter  $b_{eff}$  is partly composed by the factor  $\alpha_b$ , which is the multiplication of factors each accounting for an individual variable parameter. A total of four factors are derived based on the influence of the width, thickness stiffener, thickness ratio and thickness T-plug, respectively given in the order of the equation below. For a detailed derivation of the individual multiplication factors is referred to Appendix D.1.

$$\alpha = \alpha_b \alpha_\omega \alpha_{st} \alpha_t \quad (\text{Eq. 5.25})$$



The values of each factor are given by Equation 5.26 - 5.27 and in Tables 5.7 - 5.6.

$$\alpha_b = -0.27 \left( \frac{b}{b_0} \right) + 1.27 \quad (\text{Eq. 5.26})$$

Table 5.6: Values of  $\alpha_\omega$

	Group	$\alpha_\omega$ [-]	Condition
1	Double stiffened (-RP)	$0.362\omega + 0.64$	$1.0 \leq \omega < 1.5$
		$0.085\omega + 0.867$	$\omega \geq 1.5$
2	Stiffened T-plug / unstiffened RC (-U1-RP)	$0.96\omega + 0.04$	$1.0 \leq \omega < 1.5$
		$0.53\omega + 0.17$	$\omega \geq 1.5$
3	Unstiffened T-plug / stiffened RC (-U2-RP)	1	$\omega \geq 1.0$
4	Double unstiffened (-UU-RP)	1	$\omega > 1.25$

$$\alpha_{st} = \begin{cases} -0.104 \left( \frac{t_{stiff}}{t_0} \right) + 1.105 & \text{for stiffened T-plug} \\ 1 & \text{for unstiffened T-plug} \end{cases} \quad (\text{Eq. 5.27})$$

Table 5.7: Values of  $\alpha_t$

	Group	$\alpha_t$ [-]	Condition
1	Double stiffened (-RP)	$-1.01 \left( \frac{t_p}{t_0} \right) + 5.46$	$1.0 \leq \omega < 1.5$
		$-0.48 \left( \frac{t_p}{t_0} \right)^2 + 0.86 \left( \frac{t_p}{t_0} \right) + 2.66$	$\omega \geq 1.5$
2	Stiffened T-plug / unstiffened RC (-U1-RP)	$-0.227 \left( \frac{t_p}{t_0} \right) + 2$	$1.0 \leq \omega < 1.5$
		$-0.28 \left( \frac{t_p}{t_0} \right) + 4.08$	$\omega \geq 1.5$
3	Unstiffened T-plug / stiffened RC (-U2-RP)	$1.33 \left( \frac{t_p}{t_0} \right)^2 - 4.52 \left( \frac{t_p}{t_0} \right) + 4.21$	$\omega \geq 1.0$
4	Double unstiffened (-UU-RP)	$1.51 \left( \frac{t_p}{t_0} \right)^2 - 4.7 \left( \frac{t_p}{t_0} \right) + 4$	$\omega > 1.25$

Besides,  $b_{eff}$  includes the factor  $\alpha_l$ , which accounts for the influence of a varying T-plug length and is described by the Equation 5.28. For the complete derivation of  $b_{eff}$  is referred to Appendix D.1.3.

$$\alpha_l = 11.58 \left( \frac{l_{st}}{l_x} \right) - 2.41 \quad (\text{Eq. 5.28})$$

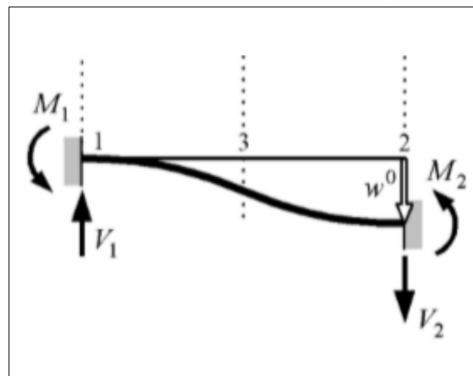


Figure 5.7: Simplified mechanical model

### Stiffness coefficient

The stiffness coefficient of the component; T-plug in bending, is derived applying the Timoshenko beam theory on the simplified mechanical model of Figure 5.7. Given the results in Table D.15, is concluded that bending is dominant in the derivation of the stiffness coefficient, which results in the following equation for the stiffness coefficient:

$$k_7 = Ck_b \quad (\text{Eq. 5.29})$$

Where,

- $C = c_b c_\omega c_{st} c_l c_t$ , dimension factor;
- $k_b = \frac{12I}{l^3} = \frac{b_{eff} t_p^3}{m^3}$ , bending stiffness coefficient.

The factor C is composed by the influences of the T-plug width, thickness ratio, stiffener, length and thickness. The values of the individual factors are given by Equations 5.30 - 5.32 and in Tables 5.8 - 5.9. For a detailed derivation of the individual multiplication factors is referred to Appendix D.2.

$$c_b = \begin{cases} -0.1 \left( \frac{b}{b_0} \right) + 1.1 & \text{for } 1.0 \leq \omega < 1.5 \\ 0.29 \left( \frac{b}{b_0} \right) + 0.71 & \text{for } \omega \geq 1.5 \end{cases} \quad (\text{Eq. 5.30})$$

Table 5.8: Values of  $c_\omega$

	Group	$c_\omega$ [-]	Condition
1	Double stiffened (-RP)	$0.66\omega + 0.073$	$1.0 \leq \omega < 1.5$ *
		$0.37\omega + 0.344$	$\omega \geq 1.5$ *
2	Stiffened T-plug / unstiffened RC (-U1-RP)	$-0.13\omega^2 + 1.28\omega - 0.16$	$\omega \geq 1.0$
3	Unstiffened T-plug / stiffened RC (-U2-RP)	1	$\omega \geq 1.0$
4	Double unstiffened (-UU-RP)	$-0.145\omega^2 + 0.592\omega - 0.367$	$\omega \geq 1.25$

\*Note 1: this conditions only holds if  $A_p \leq 800 \text{ mm}^2$ , see Equation D.6, if not  $c_\omega = 1$ .

$$\begin{cases} c_{st} = \begin{cases} -0.11 \left( \frac{t_{stiff}}{t_0} \right) + 1.11 & 1.0 \leq \omega < 1.5 \\ -0.36 \left( \frac{t_{stiff}}{t_0} \right) + 1.36 & \omega \geq 1.5 \end{cases} & \text{for stiffened T - plug} \\ c_{st} = 1 & \text{for unstiffened T - plug} \end{cases} \quad (\text{Eq. 5.31})$$

Table 5.9: Values of  $c_t$

	Group	$c_t$ [-]	Condition
1	Double stiffened (-RP)	$-0.35 \left( \frac{t_p}{t_0} \right) + 1.333$	$1.0 \leq \omega < 1.5$
		0.3	$\omega \geq 1.5$
2	Stiffened T-plug / unstiffened RC (-U1-RP)	$-0.174 \left( \frac{t_p}{t_0} \right)^2 + 0.47 \left( \frac{t_p}{t_0} \right) + 0.034$	$\omega \geq 1.0$
3	Unstiffened T-plug / Stiffened RC (-U2-RP)	$0.064 \left( \frac{t_p}{t_0} \right) + 0.16$	$\omega = 1.0$
		$-0.145 \left( \frac{t_p}{t_0} \right)^2 + 0.37 \left( \frac{t_p}{t_0} \right) + 0.06$	$\omega > 1.0$
4	Double stiffened (-UU-RP)	1	$\omega \geq 1.25$

$$c_l = \begin{cases} -0.8 \left(\frac{l_{st}}{l_x}\right)^2 + 2.15 \left(\frac{l_{st}}{l_x}\right) - 0.35 & \text{for stiffened T-plug} \\ 1 & \text{for unstiffened T-plug} \end{cases} \quad (\text{Eq. 5.32})$$

### 5.3. Joint assembly

The final step in the component method approach is the assembly of all the individual components, as parallel and/or series springs, to describe the behaviour on the joint level. In the following paragraphs, the design resistance (Paragraph 5.3.1), rotational stiffness (Paragraph 5.3.2) and rotation capacity (Paragraph 5.3.3) of the plug-and-play joint are elaborated in detail.

#### 5.3.1. Design resistance

Following the EC3-1-8 component method, the design resistance of a joint is expressed by the design moment resistance ( $M_{j,Rd}$ ). The design moment resistance is equal to the maximum moment given by the minimum design resistance of the active basic components, determined in Section 5.2. Regarding the plug-and-play joint, the design resistance is checked on the component level for the governing components; RC in bending and T-plug in bending. As explained in Paragraph 4.1.4, the rotational degree of freedom is restrained at the point of load application, due to the diaphragm action provided by the floor. Therefore the design resistance is checked in terms of force ( $F_{j,Rd}$ ) instead of the bending moment ( $M_{j,Rd}$ ).

#### 5.3.2. Rotational stiffness

Following the component method, the rotational response of a joint is based on the mechanical properties of its different constitutive components. Table 5.10 lists the active components, determined in Section 5.2, considered in the assembly of the spring model.

Table 5.10: Overview of stiffness coefficients part of the assembly

Component	Stiffness coefficient $k_i$
1 Chord side wall in transverse compression	$k_1 = \frac{b_{eff,c} w_c t_0}{h_0 - t_0}$
2 Chord side wall in transverse tension	$k_2 = \frac{b_{eff,t} w_c t_0}{h_0 - t_0}$
3 Chord face in bending	$k_3 = \frac{4 I_{eff} t_0^3}{((b_0 - b_1)/2 - t_0)^3}$
5 Reverse channel in bending	$k_5 = \frac{b_{eff} t_{rc}^3}{I_{eff}^3}$
7 T-plug in bending	$k_7 = \frac{C b_{eff} t_p^3}{I^3}$

The initial stiffness ( $S_{j,ini}$ ) is derived from the elastic stiffness of the individual components from Table 5.10. The elastic stiffness of each component is represented by an extensional spring, given by the following force-deformation relation:

$$F_i = k_i E \Delta_i \quad (\text{Eq. 5.33})$$

with,

- $F_i$  = the equivalent force in spring  $i$ ;
- $k_i$  = the stiffness coefficient of component  $i$ ;
- $E$  = the Young's modulus;
- $\Delta_i$  = the deformation of spring  $i$ .

The equivalent spring of each component of the joint is assembled in a spring model. Figure 5.8a presents the physical spring model for the plug-and-play joint to a hollow column section under the circumstances prescribed in the INNO3DJOINTS project. In this assembly model,

the rotation at the point of load application is restrained due to the diaphragm action of the floor. In the remainder of this report, the physical spring model is worked out for application in the INNO3DJOINTS project. However, for the component method application following the EC3-1-8 approach a free rotation is considered, resulting in a pure bending situation, see Figure 5.8b. This Eurocode aligned component model is recommended for practical use in design standards and is established using the following two transformations:

$$k_{5,h} * z_1 = k_5 * z_2 \quad (\text{Eq. 5.34})$$

$$k_{7,h} * z_1 = k_7 * z_3 \quad (\text{Eq. 5.35})$$

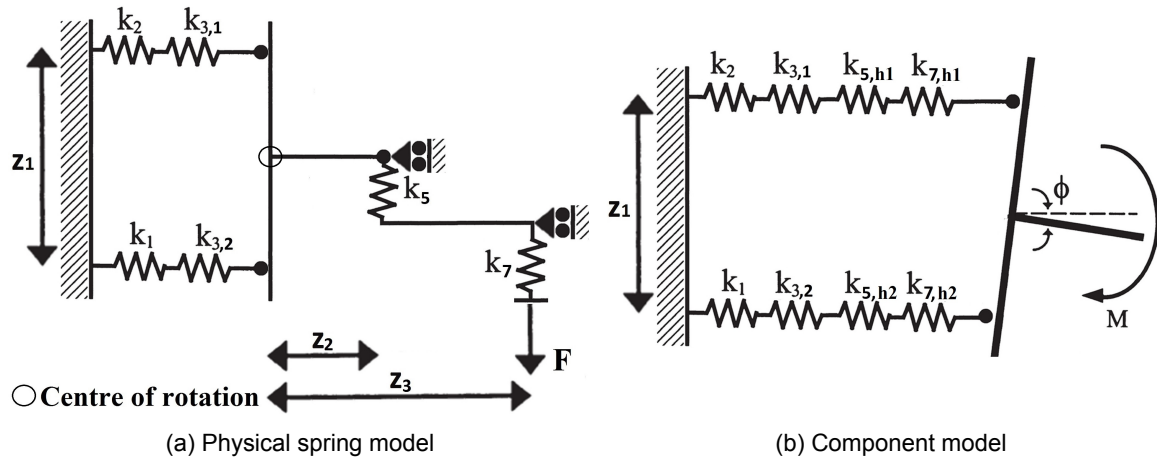


Figure 5.8: Comparison between the physical (INNO3DJOINTS) vs. component (Eurocode) model

Since the rotational degree of freedom is restrained at the point of load application, the stiffness is checked on the joint level instead of the rotational stiffness. Given Equation 5.33, the following equation for the stiffness of the physical spring model in Figure 5.8 is derived:

$$S_{j,ini} = \frac{F_{j,Rd}}{\sum_i \Delta_i} = \frac{F_{j,Rd}}{\Delta_1 + \Delta_2 + \Delta_3} = \frac{F_{j,Rd}}{\frac{F_{j,Rd} z_3^2}{k_{eq} E} + \frac{F_{j,Rd}}{k_5 E} + \frac{F_{j,Rd}}{k_7 E}} = \frac{E}{\frac{z_3^2}{k_{eq}} + \frac{1}{k_5} + \frac{1}{k_7}} \quad (\text{Eq. 5.36})$$

The total deflection of the joint ( $\Delta$ ) is described by the contribution of three parts. The first part ( $\Delta_1$ ) is defined by the springs representing the tubular components ( $k_1$ - $k_3$ ). Since the elastic forces in each spring are dependent on the stiffness of the components, the deformations of components 2 and 3,1 are replaced by an effective spring with an effective stiffness coefficient  $k_{eff,1}$ , and components 1 and 3,2 by  $k_{eff,2}$ .

$$k_{eff,1} = \frac{1}{\frac{1}{k_2} + \frac{1}{k_{3,1}}} \quad (\text{Eq. 5.37})$$

$$k_{eff,2} = \frac{1}{\frac{1}{k_1} + \frac{1}{k_{3,2}}} \quad (\text{Eq. 5.38})$$

Equation 5.39 gives the replacement of the first part of the spring model by a simple equivalent spring acting at a lever arm  $z_1$ .  $z_1 = b_1 - t_{rc}$  for  $\beta \leq 0.85$  as stiffness is governed by bending ( $k_3$ ) and compression/tension ( $k_1/k_2$ ) can be neglected and for  $0.85 < \beta \leq 1.0$  vice versa and  $z_1 = b_0 - t_0$ . Furthermore, perfect symmetry is assumed, which results in equal values for stiffness coefficients of the component; chord face in bending,  $k_{3,1} = k_{3,2}$ , on the compression and tension side. With Equation 5.39 and  $z_3 = l_1 + l_2 + l_{rc} + l_x$  the first part on the deflection is derived in Equation 5.40, which is directly implemented in Equation 5.36. (Jaspart and Weynand, 2016)

$$k_{eq} = \frac{z_1^2}{\frac{1}{k_{eff,1}} + \frac{1}{k_{eff,2}}} \quad (\text{Eq. 5.39})$$

$$\Delta_1 = \frac{F_{j,Rd} z_3^2}{k_{eq} E} \quad (\text{Eq. 5.40})$$

The derivation of the second part of deflection ( $\Delta_2$ ) of the physical spring model only includes a vertical spring, representing the component; reverse channel in bending ( $k_5$ ).  $\Delta_2$  is derived by Equation 5.41 is directly implemented in Equation 5.36.

$$\Delta_2 = \frac{F_{j,Rd}}{k_5 E} \quad (\text{Eq. 5.41})$$

At last, the third part of deflection ( $\Delta_3$ ) includes a vertical spring, representing the stiffness coefficient of the component; T-plug in bending ( $k_7$ ).  $\Delta_3$  is derived by Equation 5.42 is directly implemented in Equation 5.36.

$$\Delta_3 = \frac{F_{j,Rd}}{k_7 E} \quad (\text{Eq. 5.42})$$

### 5.3.3. Rotation capacity

Presently Eurocode 3 has no consistent "component approach for ductility" in which the ductility of the individual components is first evaluated before an assembly procedure is used to derive the rotational capacity of the joint (Jaspart and Weynand, 2016).

As mentioned in Paragraph 2.4.3, EC3-1-8 Clause [6.4.1.3] states that the rotation capacity of a joint does not need to be checked and is assumed sufficient if the design moment resistance ( $M_{j,Rd}$ ) of the joint is at least 1.2 times the design plastic moment resistance ( $M_{pl,Rd}$ ) of the cross-section of the connected member. Alternatively, EC3-1-8 contains specific provisions for the rotation capacity of bolted and welded joints on two conditions. The design axial force ( $N_{Ed}$ ) in the connected members does not exceed 5% of the design plastic resistance ( $N_{pl,Rd}$ ) of its cross-section and the steel grade is either S235, S275 or S355.

The plug-and-play joint, subject of this research, fits in the group of bolted joints. Since the components; reverse channel and T-plug in bending, are not part of the Eurocode 3, the assumption is made that these component have the same behaviour as the components in EC3-1-8 Clause [6.4.2.2]. This clause states the connection has sufficient rotation capacity, provided both of the following conditions are satisfied:

1. The design moment resistance of the joint is governed by the design resistance of either the reverse channel in bending or the T-plug in bending.
2. The thickness of either the reverse channel or T-plug satisfies  $t \leq 0.36d\sqrt{f_{ub}/f_y}$ . (EN 1993-1-8, 2005)

## 5.4. Component results

Given the list of active components in Section 5.1 and the assembly model in Section 5.3, a verification on both component and joint level is performed.

### 5.4.1. Component level

Based on the results of the parametric study, performed in Section 4.3, two components are governing for the failure of the plug-and-play joint, namely the reverse channel in bending and the T-plug in bending. On the component level, the reverse channel in bending is verified for the experimental configuration B-RP and the T-plug in bending is for the experimental configuration A-RP, in terms of design resistance and stiffness.

### Design resistance

In Figure 5.9a, the design resistance is checked for the B-RP configuration with governing failure mode: yielding of the top corner reverse channel, at the 5% PEEQ limit. When analysing the FE results, a significantly lower design resistance for the component (elasto-plastic) model is found compared to the experiment (isotropic hardening) model, due to the use of a different material model. The analytical equation of the component method is derived from the component model. As the curves of the component method and component (elasto-plastic) model approximately intersect at the 5% limit, can be concluded that the design resistance is sufficiently accurate derived. The average unity check on the design resistance of the component; T-plug in bending, is 1.001 with a standard deviation of 0.031 and a maximum deviation of 0.089, elaborated in Appendix C.1.

In Figure 5.9b, the design resistance is checked for the A-RP configuration with governing failure mode: yielding of the T-plug web, at the 5% PEEQ limit. As the curves of the component method and component (elasto-plastic) model intersect at the 5% limit, can be concluded that the design resistance is sufficiently accurate derived. Based on 76 studied configurations, the average unity check on the design resistance of the component; T-plug in bending, is 0.999 with a standard deviation of 0.025 and a maximum deviation of 0.069, elaborated in Appendix D.1.

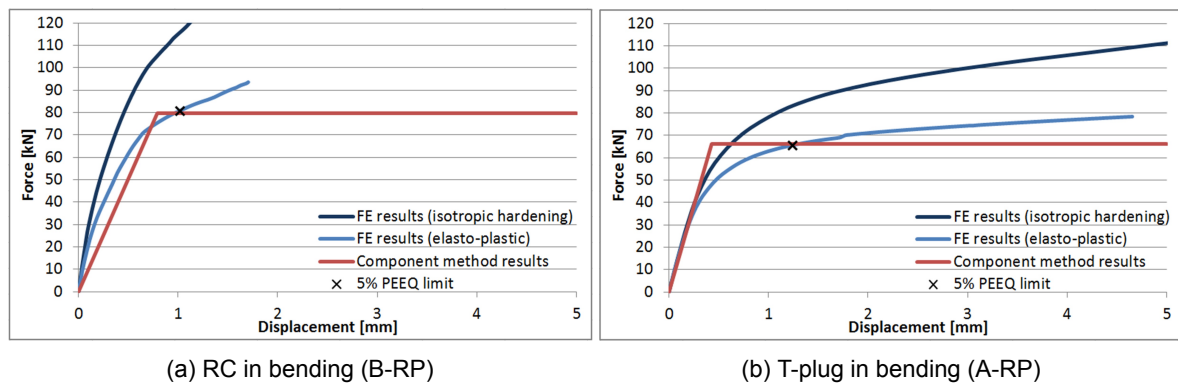


Figure 5.9: Force-displacement verification on component level

Table 5.11: Results on the component level

		A-RP		B-RP	
Stiffness (RC)	FE	323.3 kN/mm	-	170.0 kN/mm	-
	Component method	140.0 kN/mm	56.7%	100.9 kN/mm	40.6%
Stiffness (T-plug)	FE	153.6 kN/mm	-	121.2 kN/mm	-
	Component method	154.4 kN/mm	0.5%	72.4 kN/mm	40.3%
Design resistance	FE	65.7 kN	-	81.1 kN	-
	Component method	66.2 kN	0.8%	79.7 kN	1.7%

### Stiffness

In Figure 5.9, the verification of the stiffness coefficient for components; RC in bending and T-plug bending, is presented for the experimental configurations A-RP and B-RP. From Figure 5.9a can be concluded that the stiffness coefficient of the component; RC in bending, is slightly underestimated for experimental configuration B-RP. However, the average unity check on the stiffness of the component; RC in bending, derived in Appendix C.2 is 1.000 with a standard deviation of 0.029 and a maximum deviation of 0.064. This underestimation can be explained by the component derivation not taking into account the position of the bolt holes along the net-section. The component derivation in Appendix C.2, did consider a slightly adjusted configuration of B-RP with a general position of the bolt hole closer to each other. From these results can be concluded that although the stiffness is accurately derived

upon the 51 configurations in Appendix C.2, for the extrapolation to the experimental B-RP configuration, an additional parameter, defining the position of the bolt hole along the net-section, should be derived. Based Figure 5.9b can be concluded that the stiffness coefficient of the component; T-plug in bending, is accurately derived, as component method and FE (component) curves overlap on the elastic stage. Besides, the average unity check on the stiffness of the component; T-plug in bending, is 1.000 with a standard deviation of 0.029 and a maximum deviation of 0.116, elaborated in Appendix D.2.

Additionally, in Table 5.11 the stiffness is checked for the non-governing component of configurations A-RP and B-RP. From this table can be concluded that in particular the stiffness of a non-governing reverse channel in bending is hugely underestimated, assuming the same deviation of the B-RP configurations for both components. This underestimation eventually leads to an underestimation of the stiffness on the joint level, as explained in Paragraph 5.4.2.

### 5.4.2. Joint level

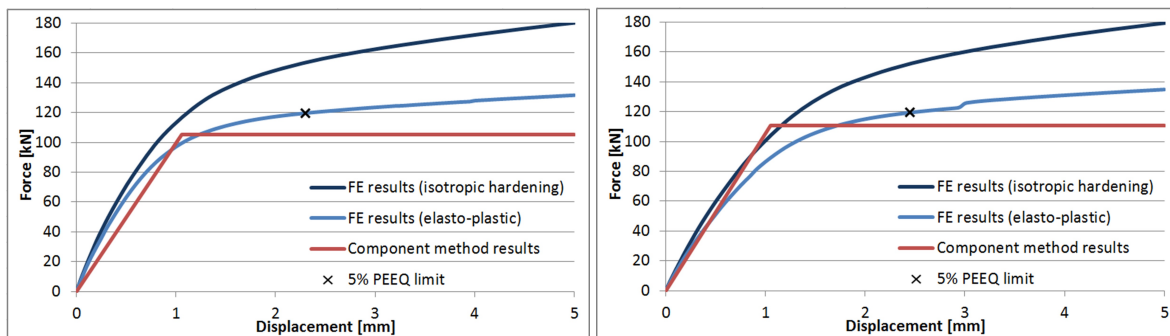
On the joint level, the experimental configurations C-RP and C-SHS200 are verified. Both configurations are identical but connected to different column sections. On the joint level, the verification is performed in terms of design resistance, stiffness and rotation capacity.

#### Design resistance

On the joint level the design resistance is verified for specimen models C-RP and C-SHS200. Based on the numerical study the governing failure is yielding in the T-plug web for an applied force of 119.6 kN for C-RP and 119.4 kN for C-SHS200, see Table 4.10. In Table 5.12 the design resistance of each individual component is derived. The welds are in such a way designed that its resistance is always higher than the connection parts and therefore not considered here. Given the results in Table 5.12, indeed the component; T-plug in bending, is governing and with a design resistance of 110.5 kN for both configurations. Although the numerical resistance is slightly underestimated, see Figure 5.10, it can be concluded that the design resistance can also be accurately predicted on the joint level.

Table 5.12: Overview of design resistance per component: model C-SHS200

Component	Design resistance $F_{i,Rd}$
1 Chord side wall in transverse compression	$F_{c,wc,Rd} = 334.0 \text{ kN}$
2 Chord side wall in transverse tension	$F_{t,wc,Rd} = 265.9 \text{ kN}$
3 Chord face in bending	$F_{fc,Rd} = 133.0 \text{ kN}$
4 Welds	-
5 Reverse channel in bending	$F_{rc,Rd} = 199.0 \text{ kN}$
6 Bolts in tension	$F_{t,Rd} = 226.1 \text{ kN}$
7 T-plug in bending	$F_{tp,Rd} = 110.5 \text{ kN}$



(a) Rigid plate column section (C-RP)

(b) Tubular column section (C-SHS200)

Figure 5.10: Force-displacement verification on joint level

Table 5.13: Results on the joint level

		C-RP		C-SHS200	
Stiffness	FE	148.7 kN/mm	-	131.8 kN/mm	-
	Component method	105.0 kN/mm	29.4%	104.8 kN/mm	20.5%
Design resistance	FE	119.6 kN	-	119.4 kN	-
	Component method	110.5 kN	7.6%	110.5 kN	7.5%

### Stiffness

In Figure 5.10, the verification of the joint stiffness for the experimental configurations C-RP and C-SHS200 is plotted. From Figure 5.9a can be concluded that the stiffness coefficient of C-RP is slightly underestimated. This underestimation follows from the incorrect value of the non-governing component; RC in bending, as explained in Paragraph 5.4.1. From Figure 5.10b, can be concluded that a slightly lesser underestimation is found for the tubular configuration. From this finding can be concluded that the influence of the use of tubular sections needs to be considered in the stiffness derivation.

### Rotation capacity

Regarding the rotation capacity of the plug-and-play studied, both conditions, defined in Paragraph 5.3.3, are satisfied for all seven experimental configurations. First, either failure of the T-plug in bending (A/C configurations) or failure of the RC in bending (B configurations) is governing and second in all experimental configurations either  $t_p \leq 10 \text{ mm}$  or  $t_{rc} \leq 10 \text{ mm}$ . Besides, the second condition is prescribed for sufficient ductility of a T-stub connection. As a partial T-stub model analogy is applied to the component; T-plug in bending, see Appendix D.1.1, this assumption is also supported with a theoretical background. Therefore is stated that the rotation capacity of the experimental configurations of the plug-and-play joint is considered as sufficient.



# 6

## Conclusion

*How does the component test; T-plug bending around weak axis, perform in terms of strength, stiffness and deformation capacity, and can its behaviour be characterized following the component method approach?*

To answer to the main research question, the following sub-questions are answered first:

*What is the influence of the thickness ratio (reverse channel vs. T-plug web), in terms of strength, stiffness and deformation capacity on the joint behaviour?*

The governing failure mode of the plug-and-play joints is determined by a condition depending on the thickness ratio. Yielding of the T-plug web is found for the case  $\omega \geq 1.0$  or  $\omega \geq 1.25$  for group 4 (-UU-RP) configurations. Furthermore, the thickness ratio is present as a dimension factor in the derivation of the design resistance and stiffness coefficient of both components; reverse channel in bending and T-plug in bending. Therefore can be concluded the thickness ratio has a major influence of the joint behaviour.

*What is the influence of the use of stiffeners on the reverse channel and/or T-plug in terms of strength, stiffness and deformation capacity on the joint behaviour?*

In the derivation of new components, configurations are categorized into four groups, based on the use of stiffeners on reverse channel/T-plug. The influence is moreover expressed in both component derivations, where the design resistance and the stiffness coefficient include various factors defined upon these categorized groups. Therefore can be concluded that the use of stiffeners has a large influence on both component derivation and joint behaviour.

*What is the influence of the use of tubular sections in terms of strength, stiffness and deformation capacity on the joint behaviour?*

On the first sight, the influence of the use of tubular sections is marginal, as in none of the models failure in the tubular section is found. Besides, comparing tubular specimen C-SHS200 with the rigid plate specimen C-RP, the same design resistance and only a slightly lower initial stiffness are found. However, in order to accurately predict the stiffness on the joint level, the influence of the use of tubular sections has to be included in particular in the derivation of the stiffness component; RC in bending.

*What is the influence of the length of the T-plug web in terms of strength, stiffness and deformation capacity on the joint behaviour?*

As failure in the reverse channel is only found for the minimum length of the length,  $l_x = l_{st}$ , it can be concluded that the influence of the length of the T-plug web is marginal on the component level. However, on the joint level, an increased length of the T-plug web significantly reduces both strength and stiffness of the joint and therefore has a considerable influence on the joint behaviour.

*Given the parametric study defined by the previous sub-questions, what new components have to be defined?*

Based on the parametric study performed on the geometrical properties mentioned above, a total of two new components are derived; reverse channel in bending and T-plug in bending. Besides, three tubular components are introduced as an extension to basic component currently present in the EC3-1-8.

By answering the sub-questions, an answer is given on the performance of the plug-and-play joint using the component test; T-plug bending around weak axis. The behaviour of the joint is characterized by its failure mode, either in the yielding in the reverse channel or the T-plug web. Therefore the design resistance of the joint is governed by the new derived components; RC in bending and T-plug in bending. The stiffness of the plug-and-play joint established by proposing a physical spring model and a component model suitable for Eurocode implementation. Thirdly, the rotation capacity is determined on the joint level, as the Eurocode 3 has no consistent component approach for ductility. This results in the characterization of the joint behaviour, as presented in figure 6.1. The experimental configuration C-SHS200 is characterized with a 7.5% deviation on the resistance and a 20.5% deviation on the stiffness compared to the numerical result.

The accuracy of the joint stiffness can be improved if the component stiffness derivation also includes non-governing configurations and a wider range of parameters is studied, such as the position of the bolt holes along the net-section and the use of tubular section. The results, derivations and the physical spring model contribute to the INNO3DJOINTS project and could be used for implementation in the software tool, to be developed by the French Institute CTICM. Besides, the Eurocode aligned component model is recommended for practical use in design standards, but further research should be performed on the verification of the rotational stiffness on the joint level.

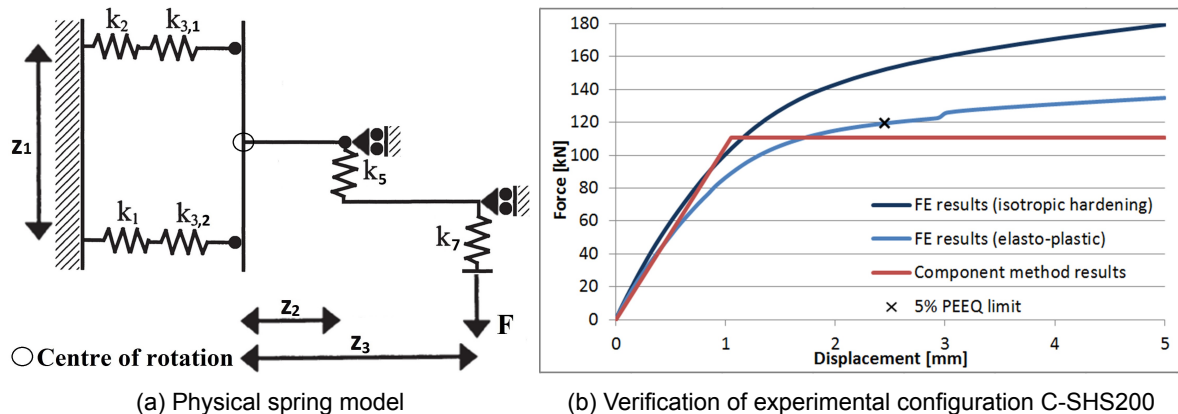


Figure 6.1: Characterization of the joint behaviour

# 7

## Recommendations

Due to circumstances, concerning a delay in delivery of the test specimens and the addition of the ongoing pandemic, COVID-19, the designed experiment is not included in this report. To put more value to the component derivations of reverse channel and T-plug in bending, the experiments should be performed and the obtained results should be used to validate the models of the numerical study. The validation of the numerical model should be performed in terms of geometrical dimensions, boundary conditions and to a lesser extend actual material properties, since the component model already uses a simplified elasto-plastic material relation for practical use in design codes.

The behaviour of the plug-and-play joint is described based on a parametric study on the geometry, including the thickness ratio (reverse channel vs. T-plug web), use of stiffeners, use of tubular sections, length of the T-plug web and the width of the reverse channel/T-plug. Although these parameters do not cover the complete range of the joint behaviour, at least a good prediction is provided. However, if a wider range of parameters is studied the stiffness for non-governing components and the joint stiffness can be improved. In order to gain a better insight in the behaviour of the plug-and-play joint the following additions and/or improvements are recommended:

- Perform a parametric study on the bolt position along the net-section to capture its influence on the design resistance and in particular the stiffness of experimental configurations B-RP, B-U-RP and B-UU-RP.
- Include the use of tubular sections as a variable in the component stiffness of the reverse channel in bending. Besides, rectangular hollow sections (RHS) and circular hollow sections (CHS) can be studied for a broader range of chord configurations.
- Extend the research on the design of the reverse channel, in order to derive a general expression including both A-RP and B-RP configurations for both resistance and stiffness.
- Vary the length and height of the stiffener on both reverse channel and T-plug in the study on the use of stiffeners.
- Review the design resistance and stiffness coefficient of the CIDECT tubular components for its applicability on plug-and-play joints, including the parametric study proposed in the previously mentioned.
- Update the various weld thicknesses, according to the EC3-1-8 directional method, for each model in the parametric study. As this includes a very time consuming iterative process, this effect neglected and the base model throat thickness is applied to all other configurations in this research.



# Bibliography

- ABAQUS. Analysis user's manual, version 6.14. *Dassault Systemes Simulia Corporation*, 2014.
- ABAQUS/CAE. Version 6.14. *Dassault Systemes Simulia Corporation*, 2014.
- Autodesk. Inventor 2018. *Autodesk, Inc*, 2018.
- Bijlaard, F. Eurocode 3, a basis for further development in joint design. *Journal of Constructional Steel Research*, 62(11):1060–1067, 2006.
- Bijlaard, F. S., Coelho, A. M. G., and Magalhães, V. J. Innovative joints in steel construction. *Steel Construction: Design and Research*, 2(4):243–247, 2009.
- Bijlaard, F. and Brekelmans, J. Plug and play type joints in steel and steel-concrete composite constructions. *ICASS 2007: Volume I*, 2007.
- Da Silva, L. S., Costa, R., Simões, R., Craveiro, H., Tankova, T., and Silva, L. Innovative 3d joints for robust and economic hybrid tubular construction. Technical report, Research Programme of the Research Fund for Coal and Steel, 2019.
- Da Silva, L. S. Towards a consistent design approach for steel joints under generalized loading. *Journal of Constructional Steel Research*, 64(9):1059–1075, 2008.
- Da Silva, L. S. and Coelho, A. G. A ductility model for steel connections. *Journal of Constructional Steel Research*, 57(1):45–70, 2001.
- Da Silva, L. S., Neves, L., Baniotopoulos, L., Perdikaris, P., Zygomalas, M., Bosiljkov, V., Bouchair, H., De Matteis, G., Dubina, D., Haller, P., et al. Evaluation of structural robustness of members and connections. In *Proceedings of the COST C12 seminar on improvement of structural building's quality by new technologies*, European Commission, Brussels, pages 155–174, 2003.
- Díaz, C., Martí, P., Victoria, M., and Querin, O. M. Review on the modelling of joint behaviour in steel frames. *Journal of constructional steel research*, 67(5):741–758, 2011.
- EN 10002-1. *Metallic materials–Tensile testing–Part 1: Method of test at ambient temperature*, 2001.
- EN 1993-1-1. *Eurocode 3: Design of steel structures - Part 1.1: General rules and rules for buildings*. European Committee for Standardization, Brussels, 2005.
- EN 1993-1-5. *Eurocode 3: Design of steel structures - Part 1.5: Plated structural elements*. European Committee for Standardization, Brussels, 2005.
- EN 1993-1-8. *Eurocode 3: Design of steel structures - Part 1.8: Design of joints*. European Committee for Standardization, Brussels, 2005.
- Garifullin, M., Bronzova, M., Pajunen, S., Mela, K., and Heinisuo, M. Initial axial stiffness of welded rhs t joints. *Journal of Constructional Steel Research*, 153:459–472, 2019.
- Gil, B. and Goñi, R. T-stub behaviour under out-of-plane bending. i: Experimental research and finite element modelling. *Engineering Structures*, 98:230–240, 2015.
- Gil, B., Bijlaard, F., and Bayo, E. T-stub behavior under out-of-plane bending. ii: Parametric study and analytical characterization. *Engineering Structures*, 98:241–250, 2015.

INNO3DJOINTS. Proposal description, September 2015.

Jaspart, J.-P. and Weynand, K. *Design of joints in steel and composite structures: Eurocode 3: Design of steel structure, Part 1-8-Design of joints; Eurocode 4: Design of composite steel and concrete structures, Part 1-1-general rules and rules for building*. Brussels: ECCS, 2016., 2016.

Kim, J., Yoon, J. C., and Kang, B. S. Finite element analysis and modeling of structure with bolted joints. *Applied mathematical modelling*, 31(5):895–911, 2007.

Liu, S., Tian, X., Cai, W., Chen, W., and Wang, Y. How the transitions in iron and steel and construction material industries impact china's co2 emissions: Comprehensive analysis from an inter-sector linked perspective. *Applied energy*, 211:64–75, 2018.

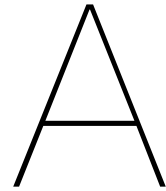
Lytle, A., Saidi, K., Stone, W., and Gross, J. Report of the nist workshop on automated steel construction. *NIST special publication SP*, pages 247–254, 2003.

Mavrodontis, N. Converting engineering stress-strain to true stress-strain in abaqus, Oct 2017. URL <https://info.simuleon.com/blog/converting-engineering-stress-strain-to-true-stress-strain-in-abaqus>.

Sun, J., Lee, K., and Lee, H. Comparison of implicit and explicit finite element methods for dynamic problems. *Journal of Materials Processing Technology*, 105(1-2):110–118, 2000.

Veljkovic, M., Simões Da Silva, L., Simões, R., Wald, F., Jaspart, J.-P., Weynand, K., Dubina, D., Landolfo, R., VITA REAL, P., and Gervásio, H. Eurocodes: Background & applications design of steel buildings worked examples. Technical report, Joint Research Center, 2015.

Weynand, K., Jaspart, J., Demonceau, J., and Zhang, L. Component method for tubular joints. In *CIDECT Report 16F-3/15*. [www.cidect.com](http://www.cidect.com), 2015.



# Validation numerical tension model

Three specimens of the component test; T-plug in tension, are used as a first validation of the numerical model, in terms of geometry and material properties. This numerical model is used for performing a preliminary numerical study on the component test; T-plug bending around weak axis, to predict the behaviour for the experiment to be performed. This validation is made possible due to the availability of the workshop drawings of the three specimens: A-RP, B-RP and B-U-RP, mentioned in Table 2.3, and the corresponding numerical models, provided by the University of Coimbra (UC) a partner in the research team of INNO3DJOINTS. Based on these workshop drawings, numerical models are built for the different specimens using the finite element software of ABAQUS, version 6.14.

In Section A.1 this general built-up of the numerical tension model is discussed in terms of geometry, material properties, finite element and mesh type, assembly conditions and computational solver. Next, the same component test; T-plug in tension, is performed on each numerical model and in Section A.2 these results are validated with the corresponding experimental and numerical results of the University of Coimbra. The analysis of results includes a force-displacement graph and a comparison on the failure modes of the experiment and numerical model. Finally, in Section A.3, results are compared in terms of ultimate resistance and a conclusion is drawn upon its applicability in the research on the behaviour of the component test; T-plug bending around weak axis.

## A.1. Numerical tension model

The particular plug-and-play joint taken into consideration, uses the same dimensions as the component test: T-plug in tension. Therefore a numerical model is built based on the workshop drawing for the component test; T-plug in tension, of the University of Coimbra. The numerical model is validated on the following subjects, namely the geometry, material properties and other computational settings, finite element and mesh type, assembly conditions and computational solver, elaborated in the upcoming paragraphs.

### A.1.1. Geometry

As mentioned above, the geometry of the numerical model is based on the workshop drawing of the corresponding test specimen, see Figures A.1, A.2 and A.3 for the drawings of respectively model A-RP, B-RP and B-U-RP. Independent of the configuration the connection between the T-plug and reverse channel is bolted by a pair of M16 bolts. Besides, the welded connection between the rigid plate and reverse channel is simplified with an isosceles triangular shape and apply tie constraints between the weld and other surfaces. For a detailed description of the geometry specifications, see Paragraph 4.1.1.





### A.1.2. Material properties

In the numerical model a total of three different materials are defined, named "Bolt 8.8", "Steel S355" and "Steel S355 hardened". The "Bolt 8.8" material is used for elements representing the bolts and nuts in the numerical model with the assumed strength class of 8.8. For all remaining elements, which includes the reserve channels, stiffeners, T-plug and the set-up supporting elements, the "Steel S355" is used. Special attention is given to the reverse channel element, which is defined by both "Steel S355" for the straight sections and "Steel S355 hardened" for the curved sections.

Both the elastic and plastic material properties for the validation of the numerical model are obtained from the numerical model of specimen B-U-RP shared by the University of Coimbra. The elastic material input parameters are similar for all three defined materials, with a specified density of  $7850 \text{ kg/m}^3$ , Young's modulus of  $210000 \text{ N/mm}^2$  and a Poisson's ratio of 0.3. The plastic material input parameters for "Bolt 8.8", "Steel S355" and "Steel S355 hardened" are shown in Table A.1. For the derivation of the plastic material properties see Paragraph 4.1.2.

Table A.1: Plastic material input parameters

<b>Bolt 8.8</b>		<b>Steel S355</b>		<b>Steel S355 hardened</b>	
Yield stress [N/mm <sup>2</sup> ]	Plastic strain [-]	Yield stress [N/mm <sup>2</sup> ]	Plastic strain [-]	Yield stress [N/mm <sup>2</sup> ]	Plastic strain [-]
641.95	0	460.59	0	716.447	0
655.803	0.021583	470.403	0.00851912	739.264	0.033549336
776.075	0.0439202	511.609	0.019115766	773.015	0.095404643
896	0.109081	546.569	0.034014879		
		580.075	0.044016885		
		615.22	0.059588791		
		641.974	0.075663904		
		670.547	0.097126711		
		716.447	0.143927169		
		739.264	0.177476505		
		773.015	0.239331812		

### A.1.3. Finite element and mesh type

In Table A.2 the characteristics regarding the finite element and mesh type are given. For a complete elaboration of the characteristics see Paragraph 4.1.3.

Table A.2: Finite element characteristics tension models

	Hexahedral "C3D8R" element
Family	Continuum (solid)
Degrees of freedom	3 translations
Interpolation	Linear 8-node
Formulation	Lagrangian
Integration	Reduced integration

### A.1.4. Assembly conditions

In Table A.3 all the assembly condition for the tension model are given. For a complete elaboration of the constraint, contact and boundary conditions see Paragraph 4.1.4.

Table A.3: Assembly conditions tension model

Constraints	Load/support: MPC beam Inter-element: Tie
Interface conditions	General contact
Time function	Displacement-controlled
Initial BC	Pinned at load: $U1=U2=UR1=UR2=UR3=0$ Pinned at support: $U1=U2=U3=0$
Step 1 BC	Pinned at load: $U1=U2=UR1=UR2=UR3=0$ Pinned at support: $U1=U2=U3=0$
Step 2 BC	Pinned at load: $U1=U2=UR1=UR2=UR3=0$ Pinned at support: $U1=U2=U3=0$
Step 3 BC	Pinned at load: $U3=20$ $U1=U2=UR1=UR2=UR3=0$ Pinned at support: $U1=U2=U3=0$

### A.1.5. Computational solver

In short, the remaining computational settings applied to all three numerical tension models are listed in Table A.4. All settings correspond with the numerical models of the University of Coimbra, for the completeness of the validation process. For a full elaborated description on each setting is referred to the Paragraph 4.1.5.

Table A.4: Computational settings tension model

	<b>Static, General (Implicit)</b>
Preload bolts	Step 1: 2 adjust length Step 2: 20000 apply force Step 3: fixed at current
Time period	1
NLGeom	On
Automatic stabilization	Dissipated energy fraction: 0.0002
Incrementation	Automatic
Increment size step 1	Initial: 0.01 Minimum: 1E-15 Maximum: 0.1
Increment size step 2	Initial: 0.01 Minimum: 1E-15 Maximum: 0.1
Increment size step 3	Initial: 0.001 Minimum: 1E-15 Maximum: 0.01
Equation solver	Direct integration
Solution technique	Full Newton
Load	Ramp linearly over step

## A.2. Analysis of results

In this section, the results for the numerical tension model are analysed and validated with the corresponding experimental and numerical results obtained by the University of Coimbra. The analysis of results includes a force-displacement graph and a comparison on the failure modes of both experiment and numerical model.

### A.2.1. Specimen: A-RP

In Figure A.5 the final deformed shapes of the experiment (left) and numerical model (right) are shown. As can be seen in the figure, in both situations the same failure mode occurs, namely the failure in the net-section of the T-plug. This is highlighted by the highest plastic equivalent strains (PEEQ) occurring in the net-section. The plastic equivalent strain is a dimensionless quantity, which divides the actual strain by the plastic strain of element. Since the same behaviour is shown in both situations, this forms a good basis of validation.

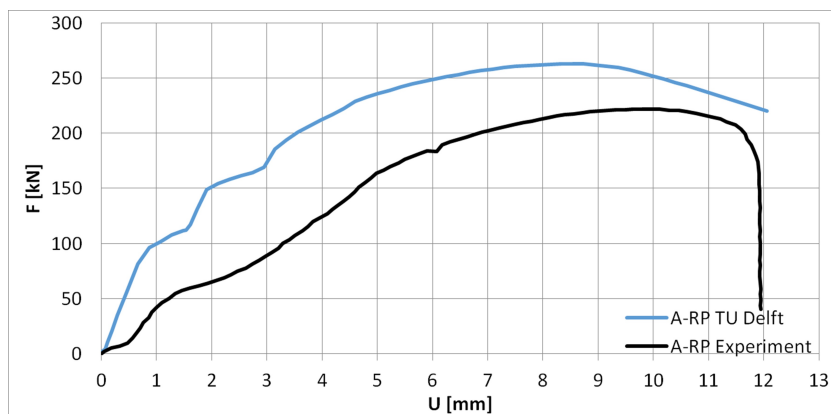
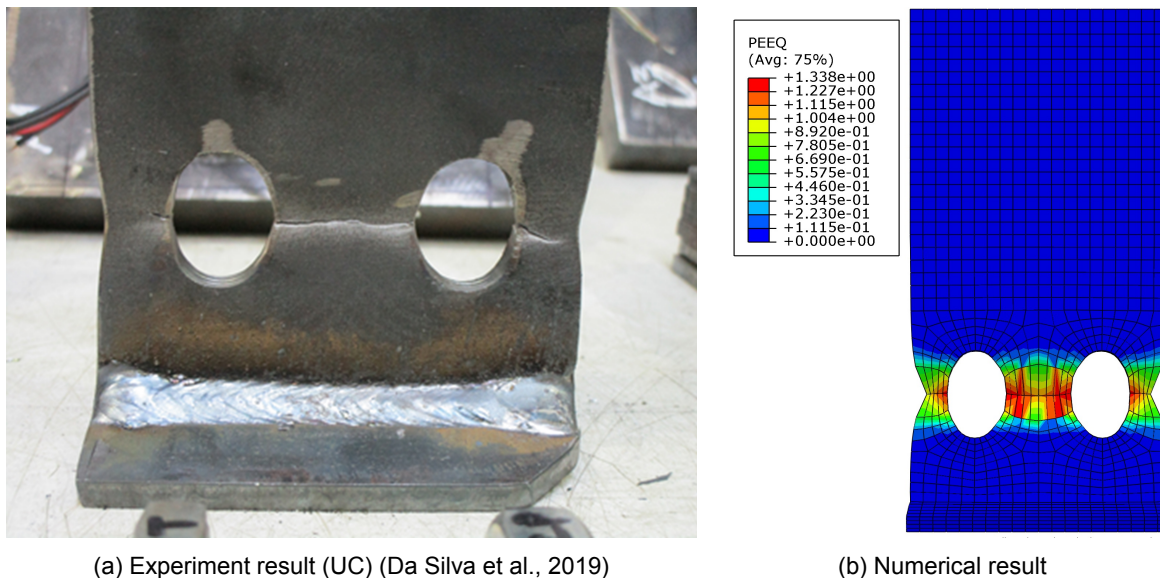


Figure A.4: Force-displacement tension validation of test specimen: A-RP



(a) Experiment result (UC) (Da Silva et al., 2019)

(b) Numerical result

Figure A.5: Final deformed shape tension validation for test specimen: A-RP

One of the differences is the ultimate strength, which is 217 kN in the experiment and 262.1 kN for the numerical model. This difference can be caused by the application of higher material properties for the stress-strain relation in the experiment. Secondly, the drop of strength is not recorded in the numerical model, which can be caused by the limitations of the numerical model in combination with the mesh. However, both curves show similar behaviour in order

of displacement. Small deviations between experiment and model can be explained by the way the displacement is recorded in the experiment. As is shown in the legend, there is made use of strokes, which generally record a larger deformation compared to the numerical model. Furthermore, the exact locations of LVD's are unknown, so a similar measurement can not be reproduced in the numerical model.

### A.2.2. Specimen: B-RP

In Figure A.7, the force-displacement graph is shown for the specimen B-RP. When comparing the ultimate strength of the numerical model (378.4 kN) with the experiment (414 kN), again a considerable difference is noticed. Partly, this can be explained by the use of a different stress-strain relation in the numerical model. However, the curve shows in both instances similar behaviour, which is a valuable asset in the validation as well.

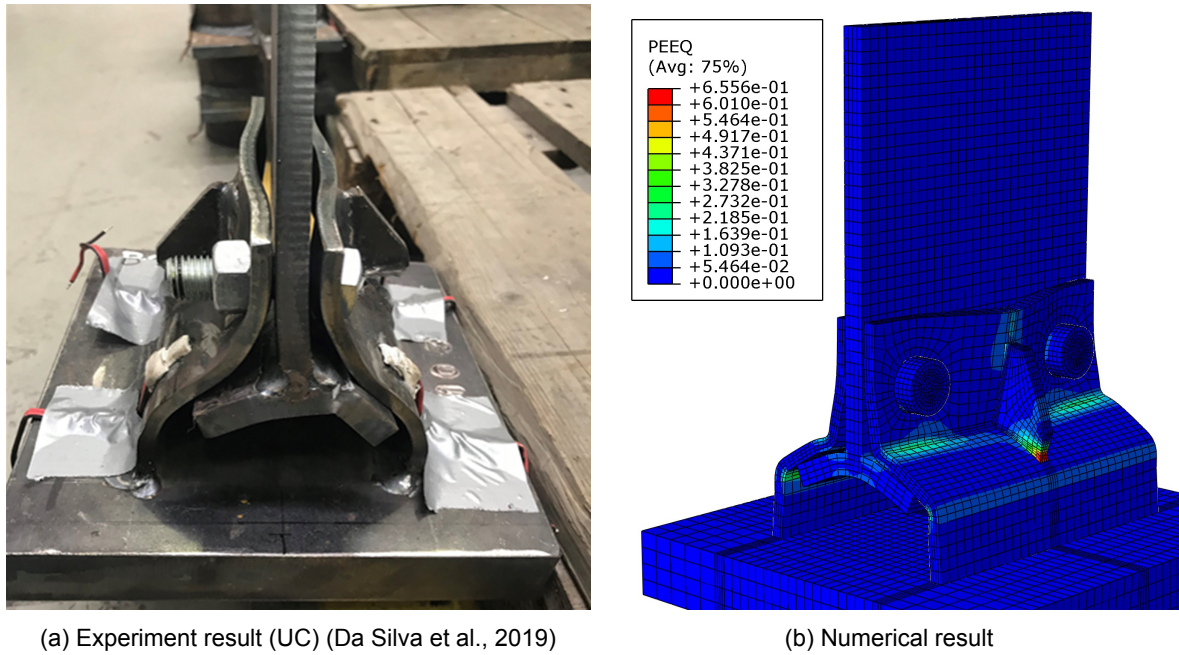


Figure A.6: Final deformed shape tension validation for test specimen: B-RP

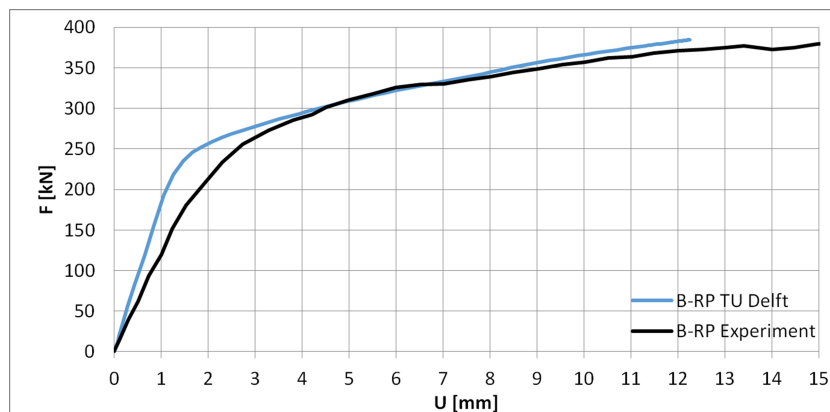


Figure A.7: Force-displacement tension validation of test specimen: B-RP

Since the results in the force-displacement behaviour can be doubted, the comparison of failure mode can be more valuable. In Figure A.6 the final deformed shapes of the experiment (left) and numerical model (right) are shown. In the numerical model of the specimen, the first rupture between the stiffener and the reverse channel is noticed, followed by a yield line in

the reverse channel. When closely analysing Figure A.6a, both phenomena are identified and it is assumed they occur in the same order. Therefore, the failure modes are identical, which is a good indication for the validation of the model, although force-displacement behaviour somehow differs between model and experiment.

### A.2.3. Specimen: B-U-RP

As can be seen in Figure A.9, the ultimate strength of the numerical model is 394.1 kN and 400 kN in the experiment. When comparing the relation of the ultimate strength with the B-RP specimen, similar behaviour is shown. When comparing the results with the numerical model of the University of Coimbra, an almost perfect fit is found. Given the ultimate strength of the UC model of 403.1 kN, this shows good validation with the experiment.

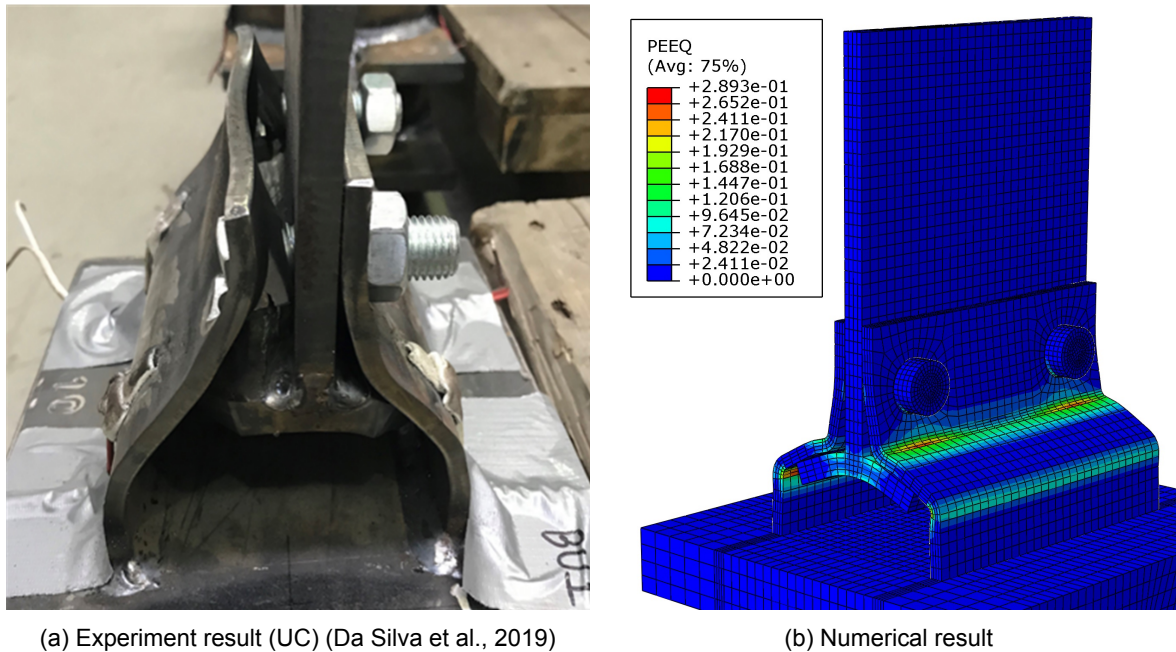


Figure A.8: Final deformed shape tension validation for test specimen: B-RP

As shown in Figure A.8 the governing failure mode is the yield pattern in the reverse channel for both numerical model and experiment. When closely analysing the deformed shape of the experiment, also a shear out failure of the bolts can be seen. The assumption is made that this failure mode only happens after the yield pattern in the reverse channel since it is not covered in the numerical analysis.

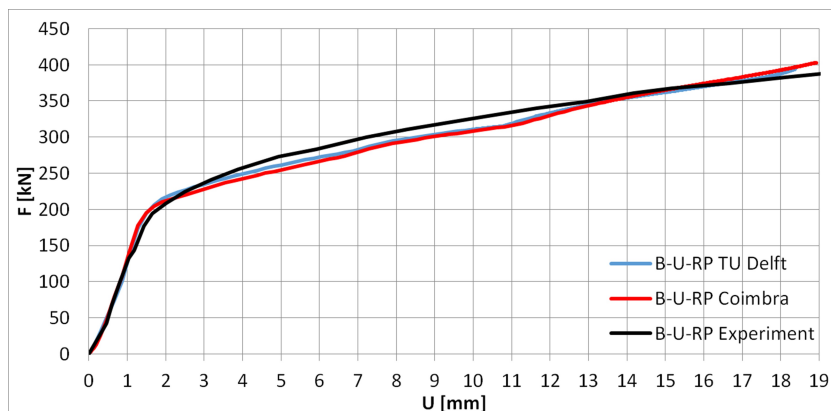


Figure A.9: Force-displacement tension validation of test specimen: B-U-RP

### A.3. Conclusion

In conclusion, after comparing these three numerical models, having identical dimensions as the workshop drawings component test: T-plug in tension, with the corresponding experimental test results, some interesting findings on the behaviour are found. All three numerical models show good similarities in the general behaviour of the corresponding specimens, as similar failure modes can be recognised. However, the force-displacement relation differs still up to 20.8% compared to the experiment.

In Table A.5 the deviation in the force-displacement relation is expressed in a percentage of the experiment. From this table can be concluded that similar behaviour is found without reaching the same ultimate strength yet. To a large extent this can be devoted to the fact that the true stress-strain relation is missing in the numerical model. Besides, since both numerical model of specimen B-U-RP, show a comparable force-displacement relation this excludes errors in the solvers.

Table A.5: Ultimate strength comparison

	<b>A-RP</b>		<b>B-RP</b>		<b>B-U-RP</b>	
Experiment (UC)	217.0 kN	-	413.6 kN	-	400.6 kN	-
Numerical model (UC)	-	-	-	-	403.1 kN	0.6%
Numerical model (TUD)	262.1 kN	20.8%	384.6 kN	7.0%	394.1 kN	1.6%

Based on these findings, the decision is made to approve the numerical model for applicability of the preliminary numerical study of the research on the component; T-plug bending around weak axis, as it can be considered as sufficiently accurate to predict the actual behaviour of the joint under a certain applied load. However, after the experimental study has been performed, the actual stress-strain relation has to be implemented for better accuracy. Hereafter, a second validation of the numerical model has to be performed in order to gather useful information from the extending parametric study.



# B

## Preliminary numerical study

To obtain a first impression of the behaviour in the component test; T-plug bending around weak axis, and to determine the set of specimens for the experimental study, a preliminary numerical study is performed in ABAQUS. The configurations validated in Appendix A form the starting point of the preliminary numerical study. The first part of the preliminary numerical study consists of an analysis of the loading conditions, discussed in Section B.1. Hereafter, the possibilities of modelling simplifications are analysed in Section B.2, regarding the proposed experimental set-up and the computational efficiency of the numerical model. Finally, a preliminary numerical study is performed on the geometry, based on the sub-questions defined in Section 1.3, which is used to define the set of specimens for the experimental study.

The results in this appendix are analysed in terms of the dimensionless quantity plastic equivalent strain (PEEQ), which is the recorded strain divided by the predefined plastic strain of the material. The PEEQ gives the best presentation of the critical sections when multiple materials with different stress-strain relations are used within the same model. Where the highest Von Mises stresses occur in the bolts, suggesting the bolt is the critical cross-section, the predefined stress-strain relation also indicates the bolt material has the highest yield stress. Therefore comparing Von Mises stresses would lead to misleading results, unlike the comparison of the PEEQ.

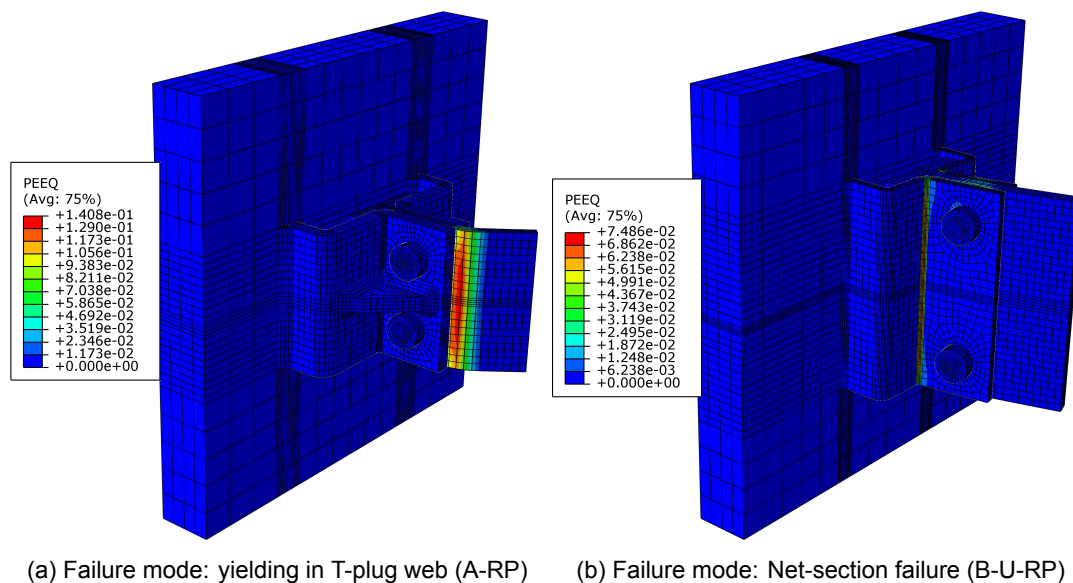


Figure B.1: Pure bending loading conditions

## B.1. Loading conditions

Given the definition of the component test; T-plug bending around weak axis, a pure bending moment around the T-plug web in the lateral direction is defined as the first applied load condition. A numerical analysis is performed on this conditions, resulting regardless the configuration in the failure mode; yielding of the T-plug web, either in the web (Figure B.1a) or the net-section (Figure B.1b). Besides, the trivial appearance of the failure mode, the joint also has a marginal yield resistance, due to the weak stiffness of the T-plug web in the load direction. In addition, this yield resistance can be rather easily estimated with basic hand calculations from the current EC3-1-1. In conclusion, the load condition pure bending around the T-plug web in lateral direction leads to an undesired and unrealistic representation of the actual behaviour in the structure. Besides, due to the trivial appearance of failure mode and the simplicity of the determination, this load condition is of little interest to further analysis in an experimental study.

For the next step of the analysis a deeper look is taken into the actual behaviour of the joint within the structure, as the plug-and-play joint provides a connection between a lightweight steel frame and tubular cold-formed steel columns. Given this, the joint is part of a series of portal frames within the structure with a continuous floor providing diaphragm action. Given the diaphragm action, the rotational degree of freedom is more likely to be constrained, instead of the free rotation in the pure bending load condition. Therefore a new load condition is analysed, where a shear load is applied in the weak axis of the T-plug web. Please note, that the actual behaviour of the joint lays somewhere in between both conditions, but the shear load simplification can be considered as an accurate approximation. In the shear load condition, only the translation in the load direction is allowed, where all other degrees of freedom are restrained, including the translations in the horizontal plane (the vertical plane in the structure, as the experiment is performed under a 90° rotation). Under this load condition, both shear and bending deformations are considered.

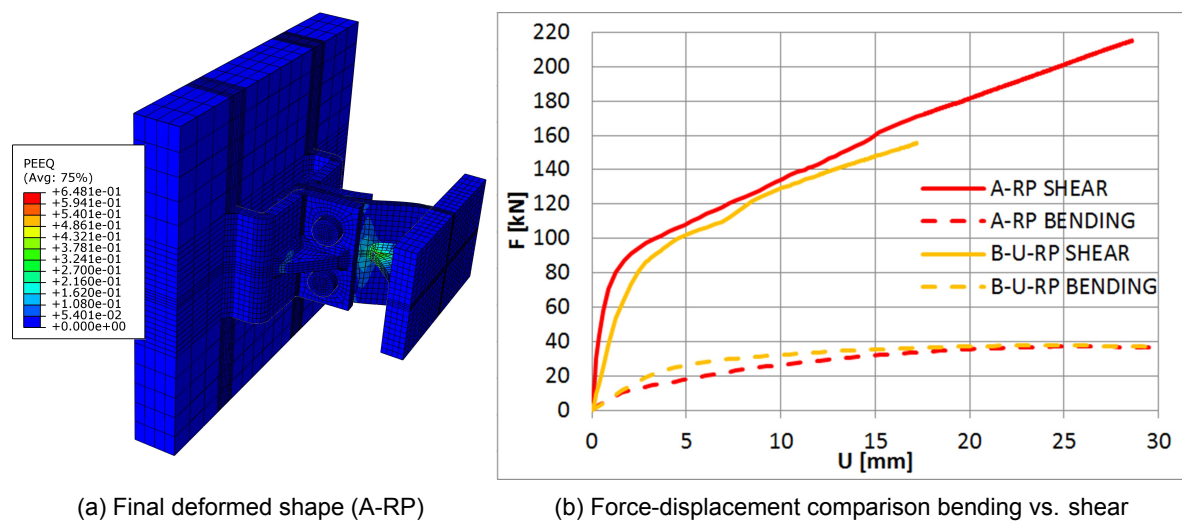


Figure B.2: Results of the shear load condition

In Figure B.2a, the final deformed shape of the specimen model A-RP is shown for the shear load condition. The load is applied on a stiffened supporting plate, which welded onto the T-plug web. In terms of the failure mode, still yielding of the T-plug web in bending is governing. However, the plug-and-play joint acts much stronger compared to the pure bending load conditions, in terms of strength and stiffness, presented in Figure B.2b. Given the significant increase in mechanical properties of the joint and the more realistic approximation of the load conditions, the shear load condition is chosen for use in the experiment and further numerical analyses.



## B.2. Modelling simplification

After determining the load condition for the experimental study, the laboratory set-up is designed, see Section 3.4. Part of the laboratory set-up is the addition of the "so-called" load beam, to transfer the applied load from the hydraulic to the specimen, see Figure 3.11. Regarding the numerical model, this load beam results in a much more complex mesh, see Figure B.4a, and ultimately also in a longer computational time. Therefore a simplified model is designed in which the load beam is removed and the load is directly applied on the supporting plate, see Figure B.4b.

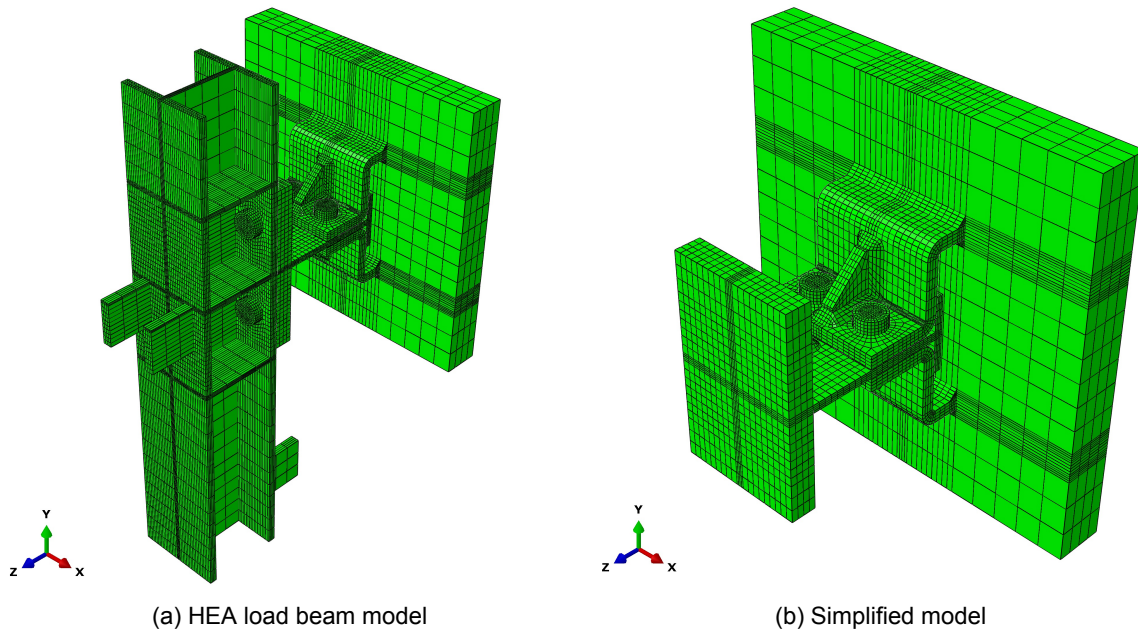


Figure B.3: Load beam model vs. simplified model comparison

A numerical analysis is performed on both models under the identical load and loading conditions. In Figure B.4 the force-displacement curves for both models are presented and, as these curves are almost perfectly overlapping, it can be concluded that the simplified model and load beam model give similar results in both strength and stiffness. Therefore is chosen to perform the parametric study on the simplified model, given its main advantages of a strongly reduced computational time.

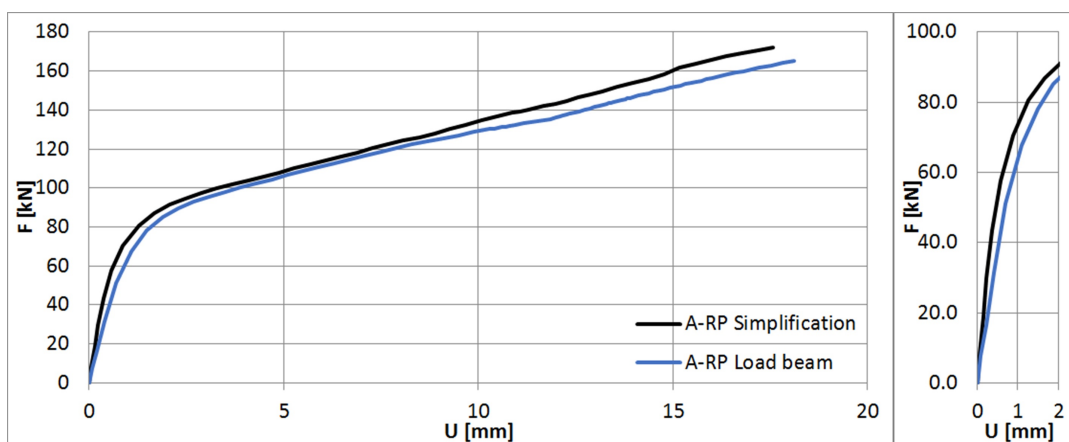


Figure B.4: Load beam model vs. simplified model force-displacement comparison

### B.3. Prediction of experimental results

The purpose of the preliminary parametric study is to provide several configurations for the experiment, where special focus is given on the variation of the following parameters: thickness ratio (reverse channel vs. T-plug web), the use of stiffeners and the use of tubular sections. The numerical configurations discussed in the preliminary numerical study correspond with the test specimens mentioned in Section 3.2.

#### B.3.1. Thickness ratio (reverse channel vs. T-plug web)

The first subject of investigation is the influence of the thickness ratio (reverse channel vs. T-plug web) on the overall behaviour of the plug-and-play joint. For this subject two cases are distinguished; ratio  $<1$  with expected failure in the reverse channel and ratio  $>1$  with expected failure in the T-plug. Given the configurations A-RP and B-RP used in previous research, see Appendix A, with respectively thickness ratios  $>1$  and  $<1$ , already the first two configurations are in place. The configuration A-RP has a 10 mm reverse channel and a 6 mm T-plug, where for the configuration B-RP the thickness is vice versa. Besides, a third configuration C-RP is also adopted in this subject, although its main purpose is to act as a rigid plate benchmark configuration in the investigation on the influence of tubular section. The configuration C-RP has a thickness ratio equal to 1, with a reverse channel and T-plug of 10 mm. For the motivation of this ratio is referred to Paragraph B.3.3.

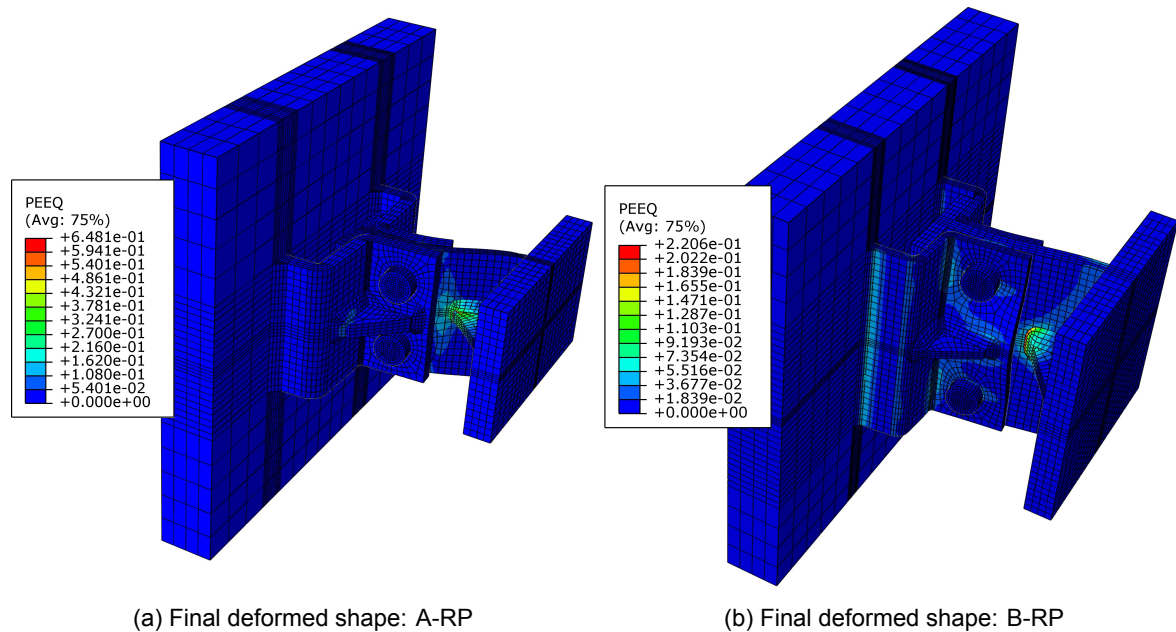


Figure B.5: Comparison of final deformed shapes

In Figure B.5 the corresponding final deformed shapes of configurations A-RP (left) and B-RP (right) are expressed in PEEQ values. On first sight, no significant difference can be distinguished from these figures, as both configurations have peak PEEQ values in the T-plug web at the height of the stiffener weld. However, when comparing the deformation in the reverse channel, configuration B-RP has on various locations above average PEEQ values, which suggest a different type of failure mode. Performing a more detailed analysis on the reverse channel, yielding in the corner of the reverse channel seems to be the governing failure mode for configuration B-RP. Although this is not visible at the PEEQ level, as only plastic material properties are assigned to the corners of the reverse channel due to residual stresses by the cold-forming process, this suggestion is confirmed at the Von Mises level in Figure B.6. Since in design standards uniform elasto-plastic material properties are used, the yielding in the corner of the reverse channel is governing.

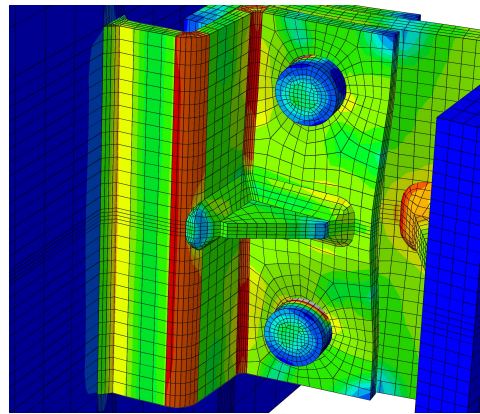


Figure B.6: Failure mode: B-RP (Von Mises)

In Figure B.7 the force-displacement relation is given for the configurations regarding the thickness ratio. For this figure can be concluded that there is a small difference in initial stiffness for configuration B-RP compared to the others, due to the slight difference in design of the reverse channel. Beside, the strength increases with an increasing thickness ratio and with the use of reverse channel design B compared to A. Based on the findings of this preliminary numerical study the aim of the experimental study is to investigate the influence on the thickness ratio on the following specimens: A-RP (ratio of 10:6), B-RP (6:10) and C-RP (10:10).

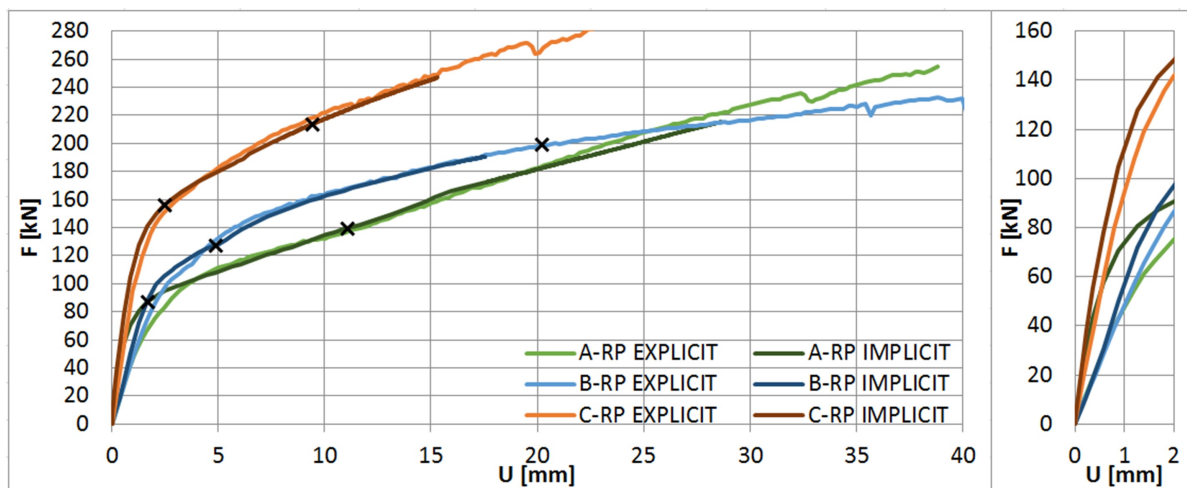


Figure B.7: Force-displacement graph on varying thickness ratio (X at 5% and 25% PEEQ limit)

### B.3.2. Use of stiffeners

The second subject of investigation is the influence of the use of stiffener for reverse channel and T-plug on the overall behaviour of the plug-and-play joint. Based on the findings in Paragraph B.3.1, the use of stiffeners is expected to have the most influence on the B-RP configuration, as it compared to the A-RP configuration already has significant more deformation in the reverse channel. At the same time configuration B-RP acts as a benchmark model to combine the influences of thickness ratio and use of stiffeners. For this subject three cases are distinguished; double stiffened reverse channel/T-plug (B-RP), unstiffened reverse channel/stiffened T-plug (B-U-RP) and double unstiffened reverse channel/T-plug (B-UU-RP).

In Figure B.8 the final deformed shapes of configurations B-RP, B-U-RP and B-UU-RP are compared. The influence of the reverse channel stiffener is best visible when comparing configurations B-RP with B-U-RP. In B-RP the presence of the stiffener causes big deformation in

the net-section of the reverse channel, where in B-U-RP peak PEEQ values are found in both corners of the reverse channel. The influence of the T-plug stiffener is best visible when comparing configurations B-U-RP and B-UU-RP. The presence of the T-plug stiffener in B-U-RP causes for the T-plug peak PEEQ values at the stiffener weld, where in B-UU-RP a straight yield line is present close to the support plate.

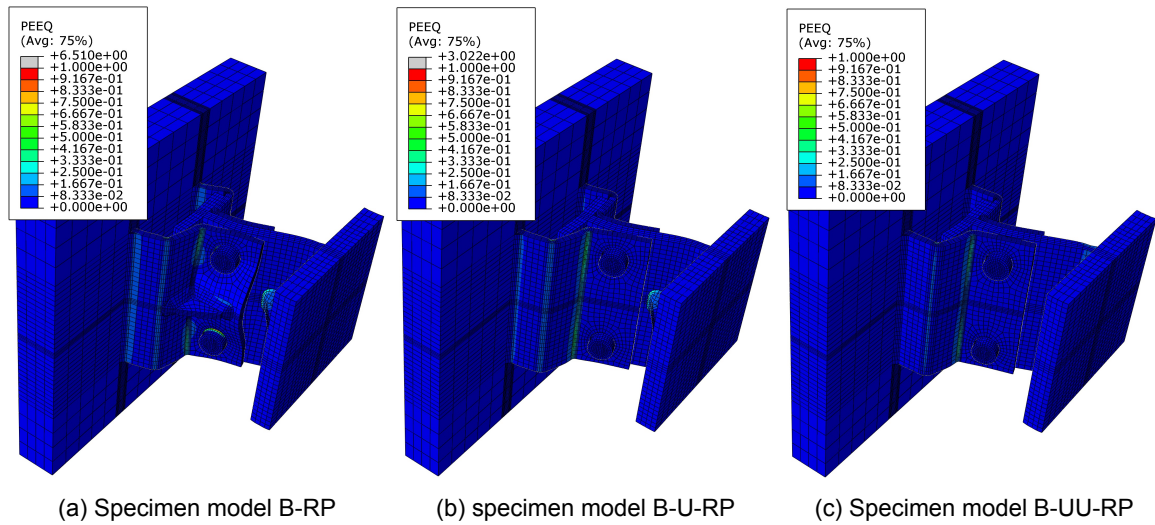


Figure B.8: Final deformed shape of specimen models B

As can be seen in Figure B.9, the influence of the use of stiffeners has a big influence on both strength and stiffness of the plug-and-play joint. The double stiffened configuration (B-RP) has the highest strength and stiffness, which decreases considerably when first the reverse channel is unstiffened (B-U-RP) and second both reverse channel and T-plug are unstiffened (B-UU-RP). Given these significant differences in deformation, stiffness and strength, these three configurations are also used to investigate the influence of the use of stiffeners in the experimental study.

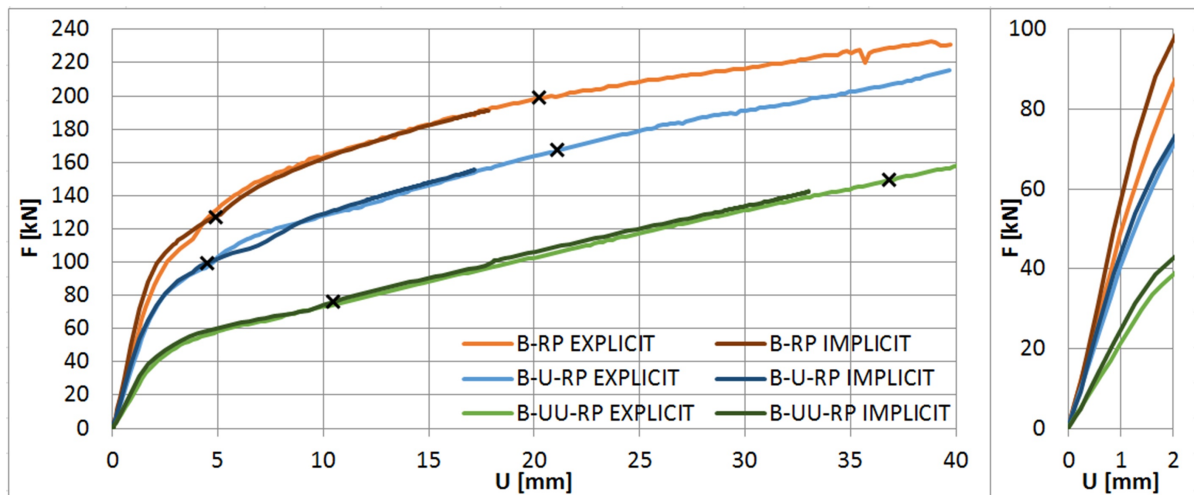


Figure B.9: Force-displacement graph on the use of stiffener (X at 5% and 25% PEEQ limit)

### B.3.3. Use of tubular sections

The last subject of the preliminary numerical study is the influence of the use of tubular sections on the overall behaviour of the plug-and-play joint. Based on the findings in Paragraph B.3.1, the use of tubular sections is expected to have the most influence on the strongest configuration. Therefore the new configuration C-RP is also introduced to the investigation



on the thickness ratio, with an increased T-plug thickness compared to the A-RP configuration. The configuration C-RP acts as a benchmark model to combine the influences of thickness ratio and use of tubular sections. For this subject three cases are distinguished; a rigid plate benchmark connection (C-RP), a stiff tubular connection of 200x200x12.5 mm (C-SHS200) and flexible tubular connection of 260x260x6 mm (C-SHS260).

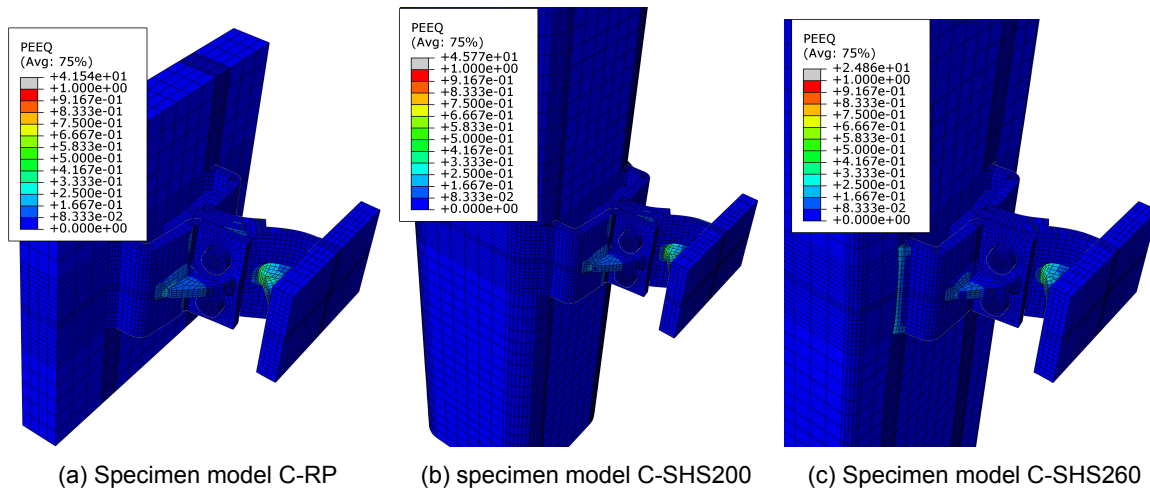


Figure B.10: Final deformed shape of specimen models C

In Figure B.10 the corresponding final deformed shapes and details of the specific failure modes are shown. From this preliminary numerical study on the use of tubular sections can be concluded that the rigid plate simplification (C-RP) and the stiff tubular connection (C-SHS200) has very matching results in both strength and stiffness, see Figure B.11. For the flexible tubular connection (C-SHS260) both strength and stiffness are reduced, although the failure mode has not been changed. Based on the findings of this preliminary numerical study, the influence of the tubular sections is studied in the experiment on the following configurations: rigid plate benchmark connection (C-RP), stiff tubular connection (C-SHS200) of 200x200x12.5 mm and a flexible tubular connection (C-SH260) of 260x260x6 mm.

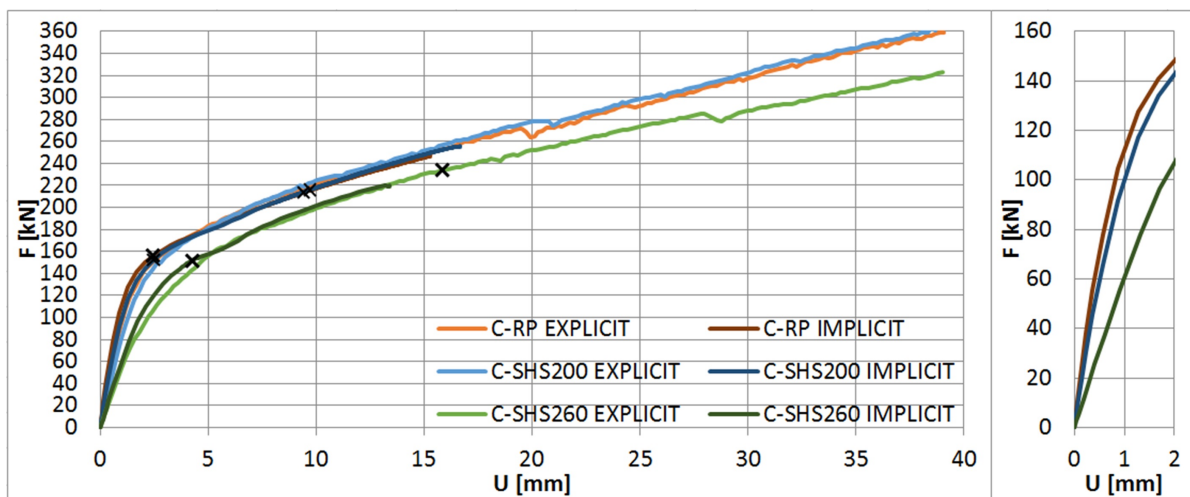
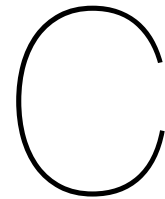


Figure B.11: Force-displacement graph on the use of tubular sections (X at 5% and 25% PEEQ limit)





# Component derivation: reverse channel in bending

This appendix elaborates the derivation of the component; RC in bending, in terms of design resistance, Section C.1, and stiffness coefficient, Section C.2. The component is part of the component method application, see Chapter 5, on the plug-and-play joint. The component derivation is based on a parametric study performed in Section 4.3. For the component; RC in bending, only models with a failure mode in the reverse channel are considered. From these models, the ultimate resistance is determined at the 5% plastic strain limit (PEEQ).

At first, the physical problem of the component; RC in bending, is identified with the simplified mechanical model in Figure C.1b. The simplified mechanical model includes the assumption of a rigid constraint at the column section, represented by the left boundary in Figure C.1. The right boundary represents the net-section on which the load is transferred during the experiment. However, the simplified mechanical model does not take into account the presence of stiffeners. These contributions are accurately incorporated in the derivation of effective width for the design resistance and the stiffness coefficient.

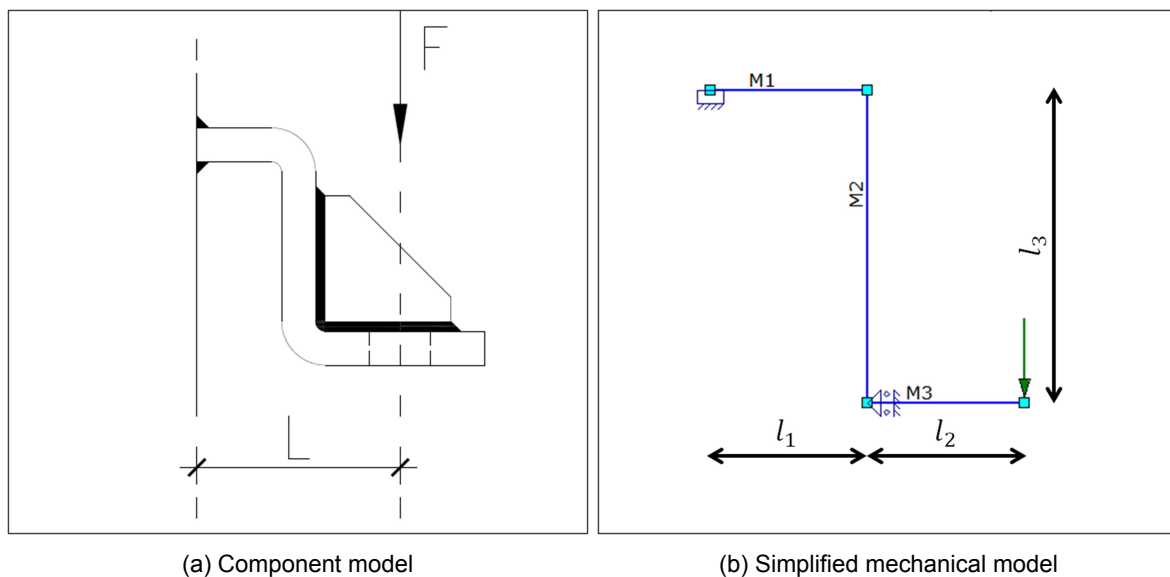


Figure C.1: Component simplification: RC in bending

## C.1. Design resistance

Given the simplified mechanical model of Figure C.1, the design resistance is determined using the EC3-1-1 bending moment theory applied around the column connection (left boundary). Since the design resistance is determined at the 5% plastic strain limit, the elastic section modulus is used. This results in Equation C.1, which is adapted for the application on the design resistance of the component; RC in bending, described by Equation C.2, in which  $l = l_1 + l_2$  see Figure C.1.

$$M_{Rd} = F_{rc,Rd}l = \frac{W_{el}f_y}{\gamma_{M0}} \quad (\text{Eq. C.1})$$

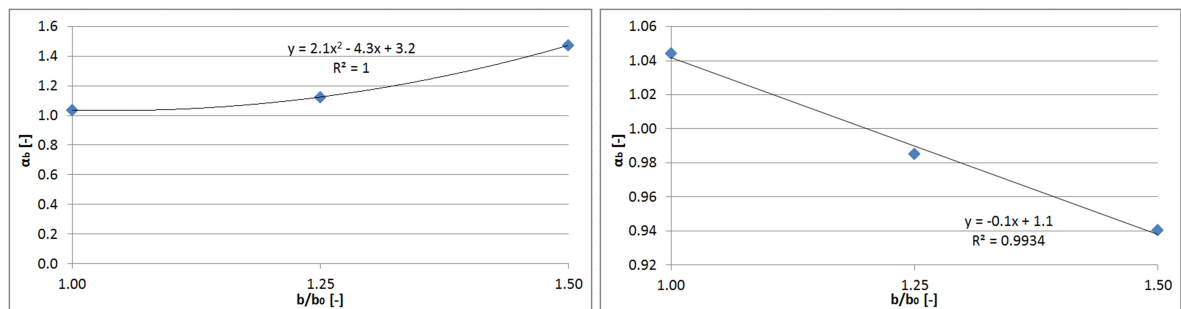
$$F_{rc,Rd} = \frac{b_{eff}t_{rc}^2f_y}{6l\gamma_{M0}} \quad (\text{Eq. C.2})$$

Given the numerical resistance, derived at the 5% plastic strain limit, Equation C.2 is used reversed to predict a numerical value for the only undefined parameter  $b_{eff}$ . Hereafter, an analytical expression is derived to accurately approximate the numerical value of  $b_{eff}$  for the four categorized groups, based on the stiffener configuration on two locations, reverse channel (RC) and T-plug: 1. Double stiffened (-RP), 2. Stiffened T-plug/unstiffened RC (-U1-RP), 3. Unstiffened T-plug/stiffened RC (-U2-RP) and 4. Double unstiffened (-UU-RP). The contributions of the following parameters are used in the derivation of  $b_{eff}$ :

- Width:  $b$ ;
- Thickness stiffener:  $t_{stiff}$ ;
- Thickness ratio:  $\omega$ ;
- Thickness T-plug:  $t_p$ .

A parametric study is performed on two "base" models; A-RP6,8 and A-U1-RP10,12, to study the contribution of  $b$  for the range  $100 \text{ mm} \leq b \leq 150 \text{ mm}$  on both stiffened and unstiffened configurations. By dividing the numerical  $b_{eff}$  by  $b$ , a dimensionless factor  $\alpha_b$  is found, whose behaviour is described by the dimensionless ratio  $b/b_0$ . In Figure C.2,  $\alpha_b$  is plotted, scaled to the value for  $b = 100 \text{ mm}$ , against  $b/b_0$  for the models from Table C.1. This results in the derivation of the following equation:

$$\alpha_b = \begin{cases} 2.1 \left(\frac{b}{b_0}\right)^2 + 4.3 \left(\frac{b}{b_0}\right) + 3.2 & \text{for stiffened RC} \\ -0.1 \left(\frac{b}{b_0}\right) + 1.1 & \text{for unstiffened RC} \end{cases} \quad (\text{Eq. C.3})$$



(a) Group 1 (A-RP) configurations

(b) Group 2 (A-U1-RP) configurations

Figure C.2: Regression plots for the derivation of  $\alpha_b$

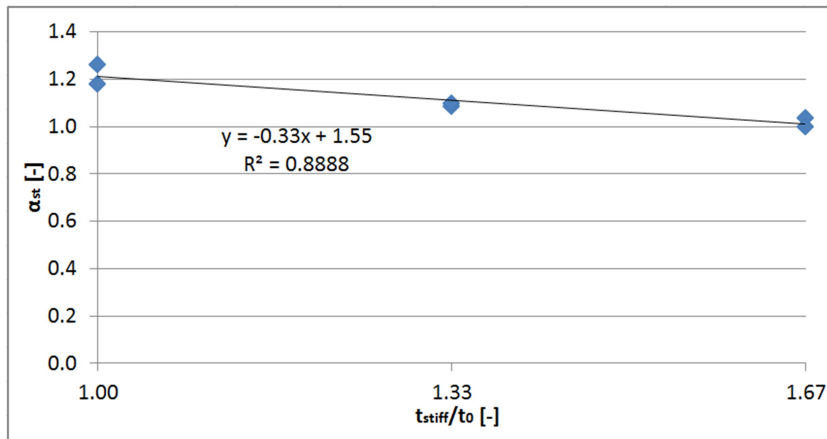


Table C.1: Results  $F_{rc,Rd}$ :  $\alpha_b$  contribution

Model	b [mm]	b/b <sub>0</sub>	numerical $F_{rc,Rd}$ [kN]	analytical $F_{rc,Rd}$ [kN]	UC
A-RP6,8	100	1.0	32.2	31.1	0.96
	125	1.25	43.7	43.0	0.98
	150	1.5	68.7	68.8	1.00
A-U1-RP10,12	100	1.0	87.3	83.5	0.96
	125	1.25	102.9	101.8	0.99
	150	1.5	117.9	119.1	1.01

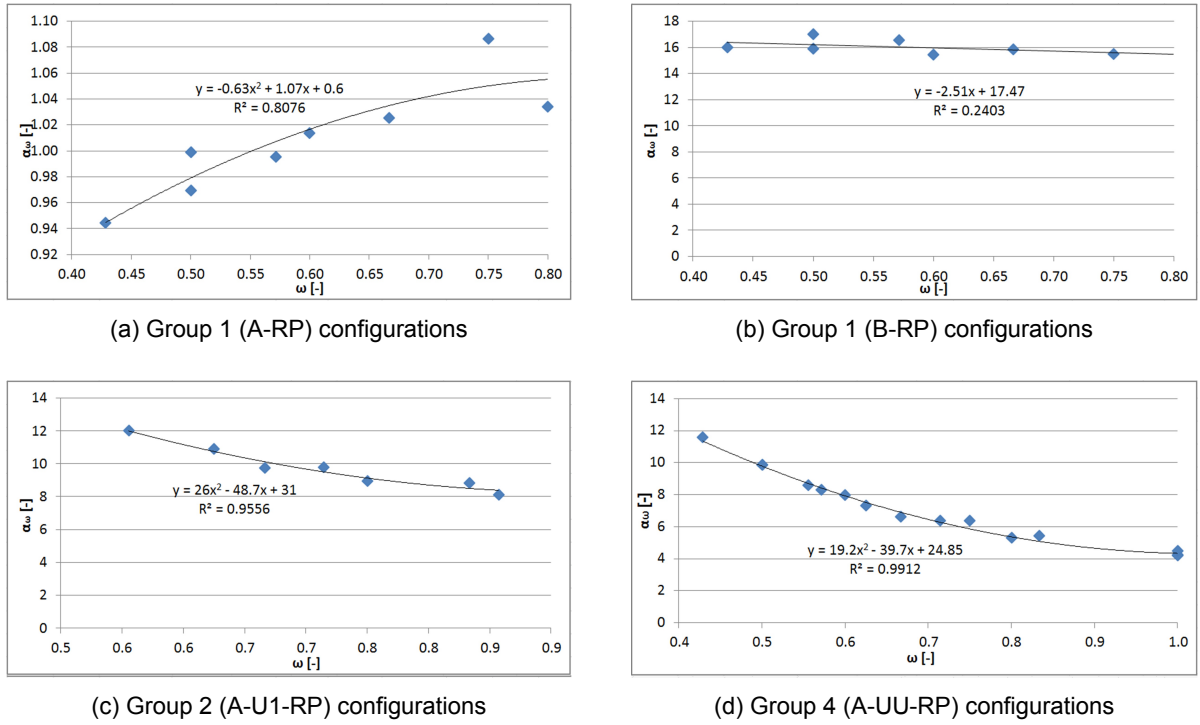
Secondly, the contribution of  $t_{stiff}$ , expressed by the factor  $\alpha_{st}$ , is studied. As  $\alpha_{st}$  is dependent on the presence of the T-plug stiffener, its value for groups 3 and 4 is automatically equal to 1 and are not considered in the parametric study.  $\alpha_{st}$  is derived by dimensionless ratio  $t_{stiff}/t_0$ , where  $t_0 = 6$  mm again. In Figure C.3,  $\alpha_{st}$  is plotted against  $t_{stiff}/t_0$  for the two "base" models A-RP6,8 and A-RP10,12 within the range  $6 \leq t_{stiff} \leq 10$ , see Table C.2. This results in the following general equation for  $\alpha_{st}$ :

$$\alpha_{st} = \begin{cases} -0.33 \left( \frac{t_{stiff}}{t_0} \right) + 1.55 & \text{for stiffened RC} \\ 1 & \text{for unstiffened RC} \end{cases} \quad (\text{Eq. C.4})$$

Figure C.3: Regression plot for the derivation of  $\alpha_{st}$ Table C.2: Results  $F_{rc,Rd}$ :  $\alpha_{st}$  contribution

Model	$t_{stiff}$ [mm]	$t_{stiff}/t_0$	numerical $F_{rc,Rd}$ [kN]	analytical $F_{rc,Rd}$ [kN]	UC
A-RP6,8	6	1.00	36.7	37.9	1.03
	8	1.33	33.7	34.5	1.02
	10	1.67	32.2	31.1	0.96
A-RP6,14	6	1.00	35.3	34.1	0.97
	8	1.33	30.8	31.1	1.01
	10	1.67	28.0	28.0	1.00

Next, the contribution of  $\omega$  is studied, expressed by the factor  $\alpha_\omega$ . In Figure C.4a-d,  $\alpha_\omega$  is plotted against  $\omega$  for group 1 (A-RP) / (B-RP), group 2 (A-U1-RP) and group 4 (A-UU-RP) configurations from Tables C.5-C.9. The results are summarized in Table C.3. From each group, except group 1 (A-RP), this factor is determined at last and is depended on all previously derived factors. Therefore the contribution is not scaled to a "base" model, but to the numerical value, indicated by the larger scale on the y-axis. Note for group 3 (A-U2-RP) configurations the value of  $b_{eff}$  is independent of  $\omega$  and therefore  $\alpha_\omega = 1$ .

Figure C.4: Regression plots for the derivation of  $\alpha_\omega$ Table C.3: Values of  $\alpha_\omega$ 

	Group	$\alpha_\omega$ [-]	Condition
1	Double stiffened (A-RP)	$-0.63\omega^2 + 1.07\omega + 0.6$	$\omega < 1.0$
	Double stiffened (B-RP)	$-2.51\omega + 17.47$	$\omega < 1.0$
2	Stiffened T-plug / unstiffened RC (A-U1-RP)	$26\omega - 48.7\omega + 31$	$\omega < 1.0$
3	Unstiffened T-plug / stiffened RC (A-U2-RP)	1	$\omega < 1.0$
4	Double unstiffened (A-UU-RP)	$19.2\omega^2 - 39.7\omega + 24.85$	$\omega < 1.25$

Similar to  $\omega$ ,  $t_p$  is dependent on all previously derived factors and scaled to the numerical value for the two remaining groups. The contribution of  $t_p$  is expressed by the factor  $\alpha_t$  and derived by the dimensionless ratio  $t_p/t_0$  with  $t_0 = 6 \text{ mm}$ . In Figure C.5, the average  $\alpha_t$  is plotted against  $t_p/t_0$  for group 1 (A-RP) and group 3 (A-U2-RP) configurations of Tables C.5 and C.8. A summary of the results of  $\alpha_t$  is given in Table D.8 for the range  $6 \leq t_p \leq 8$ .

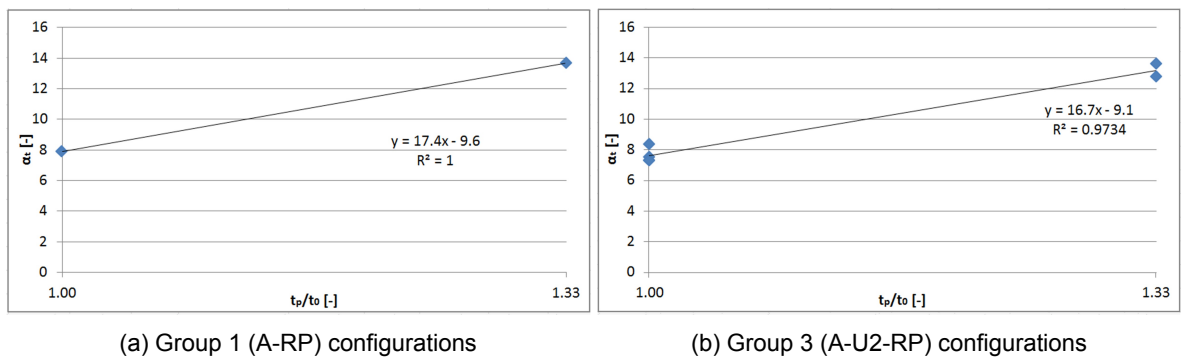
Figure C.5: Regression plots for the derivation of  $\alpha_t$

Table C.4: Values of  $\alpha_t$ 

	Group	$\alpha_t$ [-]	Condition
1	Double stiffened (A-RP)	$17.4 \left( \frac{t_p}{t_0} \right) - 9.6$	$\omega < 1.0$
	Double stiffened (B-RP)	1	$\omega < 1.0$
2	Stiffened T-plug / unstiffened RC (A-U1-RP)	1	$\omega < 1.0$
3	Unstiffened T-plug / stiffened RC (A-U2-RP)	$16.7 \left( \frac{t_p}{t_0} \right) - 9.1$	$\omega < 1.0$
4	Double unstiffened (A-UU-RP)	1	$\omega < 1.25$

Since  $\alpha_b$ ,  $\alpha_{st}$ ,  $\alpha_\omega$  and  $\alpha_t$  are all multiplication factors of  $b$ , these contributions can be even further simplified with the introduction of the following factor  $\alpha$ :

$$\alpha = \alpha_b \alpha_{st} \alpha_\omega \alpha_t \quad (\text{Eq. C.5})$$

Unlike the component; T-plug in bending, the length of the T-plug web has no contribution. For every case of  $l_x > l_{st}$ , the failure mode is always in the T-plug. Given this and all contributions elaborated in the previous paragraphs, a general equation for  $b_{eff}$  is defined as follows:

$$b_{eff} = \alpha b \quad (\text{Eq. C.6})$$

For the first group (-RP) only double stiffened configurations are considered, whereby a distinction is made between two reverse channel designs; A-RP and B-RP. Both cases are defined by the general Equation C.6 but have different values for  $\alpha_t$  and  $\alpha_\omega$ . In Table C.5, the unity check on the design resistance is given for group 1 (A-RP) configurations and in Table C.6 for group 1 (B-RP). The average unity check on the design resistance for those two tables is 1.000 with a standard deviation of 0.023. In addition, the unity checks for group 1 (A-RP) configurations with a varying width, Table C.1, and thickness stiffener, Table C.2, have an average of 1.002 with a standard deviation of 0.022.

Table C.5: Results definition  $F_{rc,Rd}$ : 1. Double stiffened (A-RP)

Model	Numerical $F_{rc,Rd}$ [kN]	Analytical $F_{rc,Rd}$ [kN]	UC
A-RP6,8	32.2	31.1	0.96
A-RP6,10	30.1	30.1	1.00
A-RP6,12	29.6	29.0	0.98
A-RP6,14	28.0	28.0	1.00
A-RP8,10	91.8	93.5	1.02
A-RP8,12	91.0	91.8	1.01
A-RP8,14	88.4	89.3	1.01
A-RP8,16	86.1	86.8	1.01

Table C.6: Results definition  $b_{eff}$ : 1. Double stiffened (B-RP)

Model	Numerical $F_{rc,Rd}$ [kN]	Analytical $F_{rc,Rd}$ [kN]	UC
B-RP6,8	51.6	51.9	1.01
B-RP6,10	51.4	53.1	1.03
B-RP6,12	52.9	54.0	1.02
B-RP6,14	53.2	54.6	1.03
B-RP8,12	90.9	90.6	1.00
B-RP8,14	94.9	92.0	0.97
B-RP8,16	97.5	93.0	0.95

Group 2 (A-U1-RP) considers all configurations with a stiffened T-plug in combination with an unstiffened reverse channel. The general equation of  $b_{eff}$  is also applicable to this group,

but with different values for  $\alpha_t$  and  $\alpha_\omega$ , which are defined in respectively Table C.3 and C.4. In addition, Equation C.3 has a different value for the unstiffened RC. In Table C.7, the unity check on the design resistance is given for group 2 (A-U1-RP) configurations, with an average of 0.998 and a standard deviation of 0.020.

Table C.7: Results definition  $F_{rc,Rd}$ : 2. Stiffened T-plug / unstiffened RC (A-U1-RP)

Model	Numerical $F_{rc,Rd}$ [kN]	Analytical $F_{rc,Rd}$ [kN]	UC
A-U1-RP10,12	87.3	83.5	0.96
A-U1-RP10,14	96.7	93.5	0.97
A-U1-RP10,16	107.5	105.7	0.98
A-U1-RP10,18	118.4	118.0	1.00
A-U1-RP12,14	111.7	114.9	1.03
A-U1-RP12,16	122.9	125.1	1.02
A-U1-RP12,18	134.0	138.6	1.03

Unlike previous groups, group 3 (A-U2-RP) show only one effective width per thickness. This finding is explained by comparing the strength of the reverse channel to the T-plug. The stiffened RC behaves extremely strong and therefore dominates the resistance, which on the other hand results in a negligible influence of the T-plug thickness. This is also confirmed by same stiffener configurations in the derivation of the component; T-plug in bending. The unity check on design resistance for group 3 (A-U2-RP) configurations has an average of 1.002 and a standard deviation of 0.053, see Figure C.8.

Table C.8: Results definition  $F_{rc,Rd}$ : 3. Unstiffened T-plug / stiffened RC (A-U2-RP)

Model	Numerical $F_{rc,Rd}$ [kN]	Analytical $F_{rc,Rd}$ [kN]	UC
A-U2-RP6,8	31.7	28.9	0.91
A-U2-RP6,10	28.5	28.9	1.01
A-U2-RP6,12	27.7	28.9	1.04
A-U2-RP6,14	27.7	28.9	1.04
A-U2-RP8,14	83.2	86.0	1.03
A-U2-RP8,16	88.8	86.0	0.97

As explained in Paragraph D.1.2, group 4 (-UU-RP) configurations have a different upper bound value of  $\omega = 1.25$  for the failure mode in the reverse channel. In Table C.9 the unity check on design resistance is given for group 4 (A-UU-RP) configurations. The average of the unity check is 1.003 with a standard deviation of 0.034.

Table C.9: Results definition  $F_{rc,Rd}$ : 4. Double unstiffened (A-UU-RP)

Model	Numerical $F_{rc,Rd}$ [kN]	Analytical $F_{rc,Rd}$ [kN]	UC
A-UU-RP6,6	16.0	16.5	1.03
A-UU-RP6,8	24.1	22.3	0.93
A-UU-RP6,10	30.2	30.2	1.00
A-UU-RP6,12	37.5	37.3	1.00
A-UU-RP6,14	43.9	43.2	0.98
A-UU-RP8,8	27.1	28.4	1.05
A-UU-RP8,10	34.5	35.1	1.02
A-UU-RP8,12	43.1	45.2	1.05
A-UU-RP8,14	53.9	55.1	1.02
A-UU-RP8,16	64.2	64.0	1.00
A-UU-RP10,10	43.9	42.9	0.98
A-UU-RP10,12	53.1	50.3	0.95
A-UU-RP10,14	62.4	62.0	0.99
A-UU-RP10,16	71.9	74.3	1.03
A-UU-RP10,18	84.3	86.0	1.02

In conclusion, on a basis of 51 unique configurations accounting for the contribution various geometrical dimensions, an average unity check on design resistance of 1.001 with a standard deviation of 0.031 and a maximum deviation of 0.089 is determined. In general, the range of validity for the component; RC in bending, is defined for  $\omega < 1.0$ , with the exception for group 4 (A-UU-RP) configurations being  $\omega < 1.25$ . However, within this condition failure in the T-plug is still possible. Therefore it is recommended to perform further research on this condition definition. Based on the configuration with failure in the RC, can be concluded that the definition of the component derivation is sufficiently accurate, being well within the accepted 5% margin of error.

## C.2. Stiffness coefficient

Following the simplified mechanical model of Figure C.1, the Euler-Bernoulli beam theory is applied to determine the initial stiffness by splitting up the design in three parts with lengths  $l_1$ ,  $l_2$  and  $l_3$ . The following differential equation is solved to determine the stiffness coefficient of the component: RC in bending, given the absence of a distributed load:

$$EI \frac{d^4 w}{dx^4} = 0 \quad (\text{Eq. C.7})$$

Given the relation  $k_i = \frac{S_{j,ini}}{E}$  and  $I_{eff}^3 = 4l_2^3 + 3l_2^2 l_3 + 4l_1^3 - 3l_2 l_1^2$  following the EC3-1-8 component method, the stiffness coefficient is defined as follows:

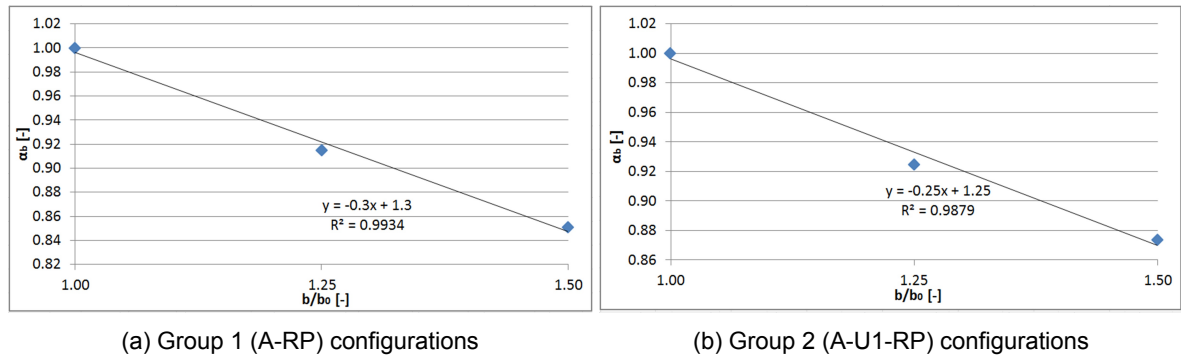
$$k_5 = \frac{b_{eff} t_{rc}^3}{I_{eff}^3} \quad (\text{Eq. C.8})$$

By using linear line regression on elastic stage of the force-displacement curve  $k_5 = \frac{S_{j,ini}}{E}$  is numerically predicted. The displacement is the relative displacement between the column connection and the net-section, defined in Figure C.1. For the stiffness coefficient, a different effective width is required compared to the design resistance. Since the trends in stiffness coefficient and design resistance differ, a separate effective width is derived instead of deriving a dimension factor for the same effective width. Therefore similar to the design resistance, the term  $b_{eff}$  is derived to accurately approximate the numerical value of  $k_5$  for the four categorized groups: 1. Double stiffened (-RP), 2. Stiffened T-plug / unstiffened RC (-U1-RP), 3. Unstiffened T-plug / stiffened RC (-U2-RP) and 4. Double unstiffened (-UU-RP). To derive  $b_{eff}$  the contributions of the following geometrical dimensions are considered:

- Width:  $b$ ;
- Thickness stiffener:  $t_{stiff}$ ;
- Thickness ratio:  $\omega$ ;
- Reverse channel profile  $l_2/l_3$ ;
- Thickness T-plug:  $t_p$ .

First, a parametric study is performed on two "base" models; A-RP6,8 and A-U1-RP10,12, to study the contribution of  $b$  for the range  $100 \text{ mm} \leq b \leq 150 \text{ mm}$  on both stiffened and unstiffened RC configurations. By dividing the numerical  $b_{eff}$  by  $b$ , a dimensionless factor  $\alpha_b$  is found, whose behaviour is described by the dimensionless ratio  $b/b_0$ . In Figure C.6,  $\alpha_b$  is plotted, scaled to the value for  $b = 100 \text{ mm}$ , against  $b/b_0$  for the models from Table C.10. This results in the derivation of the following equation:

$$\alpha_b = \begin{cases} -0.3 \left( \frac{b}{b_0} \right) + 1.3 & \text{for stiffened T-plug} \\ -0.25 \left( \frac{b}{b_0} \right) + 1.25 & \text{for unstiffened T-plug} \end{cases} \quad (\text{Eq. C.9})$$

Figure C.6: Regression plots for the derivation of  $\alpha_b$ Table C.10: Results  $k_5$ :  $\alpha_b$  contribution

Model	b [mm]	$b/b_0$	numerical $k_5$ [mm]	analytical $k_5$ [mm]	UC
A-RP6,8	100	1.0	0.656	0.637	0.97
	125	1.25	0.750	0.737	0.98
	150	1.5	0.837	0.813	0.97
A-U1-RP10,12	100	1.0	0.610	0.617	1.01
	125	1.25	0.706	0.723	1.02
	150	1.5	0.800	0.809	1.01

Secondly, the contribution of  $t_{stiff}$ , expressed by the factor  $\alpha_{st}$ , is studied. As  $\alpha_{st}$  is dependent on the presence of the T-plug stiffener, its value for groups 3 and 4 is automatically equal to 1 and are not considered in the parametric study.  $\alpha_{st}$  is derived by dimensionless ratio  $t_{stiff}/t_0$ , where  $t_0 = 6 \text{ mm}$  again. In Figure C.7,  $\alpha_{st}$  is plotted against  $t_{stiff}/t_0$  for the two "base" models A-RP6,8 and A-RP10,12 within the range  $6 \leq t_{stiff} \leq 10$ , see Table C.11. The configurations are scaled to the "base" stiffener thickness  $t_{stiff} = 6 \text{ mm}$ , which results in the following general equation for  $\alpha_{st}$ :

$$\alpha_{st} = \begin{cases} 0.12 \left( \frac{t_{stiff}}{t_0} \right) + 0.88 & \text{for stiffened T - plug} \\ 1 & \text{for unstiffened T - plug} \end{cases} \quad (\text{Eq. C.10})$$

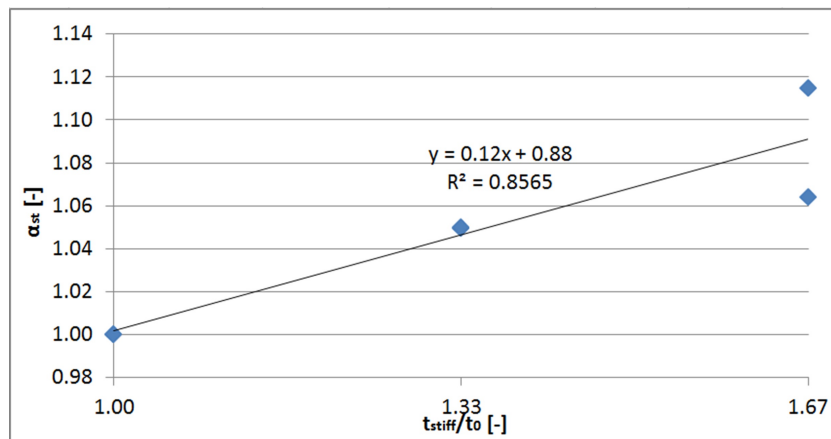
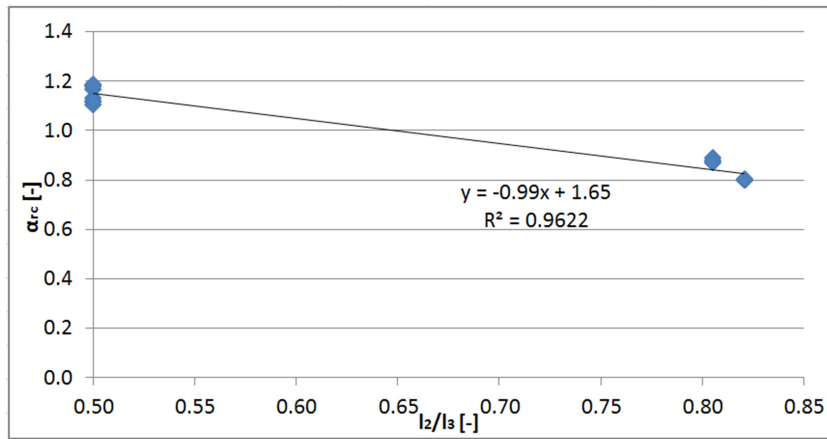
Figure C.7: Regression plot for the derivation of  $\alpha_{st}$

Table C.11: Results  $k_5$ :  $\alpha_{st}$  contribution

Model	$t_{stiff}$ [mm]	$t_{stiff}/t_0$	numerical $k_5$ [mm]	analytical $k_5$ [mm]	UC
A-RP6,8	6	1.00	0.590	0.616	0.96
	8	1.33	0.614	0.647	0.95
	10	1.67	0.656	0.637	0.97
A-RP6,14	6	1.00	0.627	0.633	1.01
	8	1.33	0.659	0.659	1.00
	10	1.67	0.699	0.684	0.98

Thirdly, the contribution of the design of the reverse channel, expressed by the dimensionless ratio  $l_2/l_3$ , is studied. Given this ratio, the relation between the A-RP and B-RP configurations is described, unlike the design resistance derivation. In Figure C.8,  $\alpha_{rc}$  is plotted against  $l_2/l_3$  for the A-RP and B-RP models within the range  $0.50 \leq l_2/l_3 \leq 0.82$ , see Tables C.14 and C.15. This results in the following general equation for  $\alpha_{rc}$ :

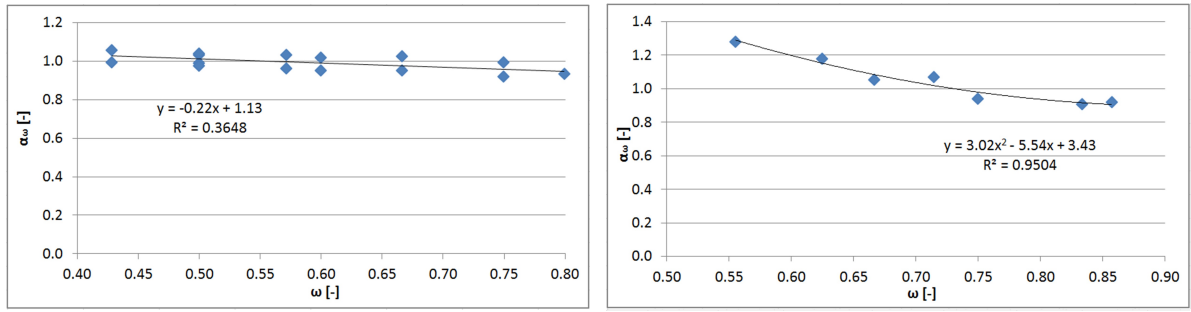
$$\alpha_{rc} = -0.99 \left( \frac{l_2}{l_3} \right) + 1.65 \quad (\text{Eq. C.11})$$

Figure C.8: Regression plot for the derivation of  $\alpha_{rc}$ 

Next, the contribution of  $\omega$ , expressed by the factor  $\alpha_\omega$ , is studied. In Figure C.9a-c,  $\alpha_\omega$  is plotted against  $\omega$  for group 1 (-RP), group 2 (A-U1-RP) and group 4 (A-UU-RP) configurations. The results are summarized in Table C.12. For all groups, this factor is depended on all previously derived factors and therefore the contribution is not scaled to a "base" model but scaled to the numerical value of  $b_{eff}$ . Note for group 3 (A-U2-RP) configurations the value of  $b_{eff}$  is independent of  $\omega$  and therefore  $\alpha_\omega = 1$ .

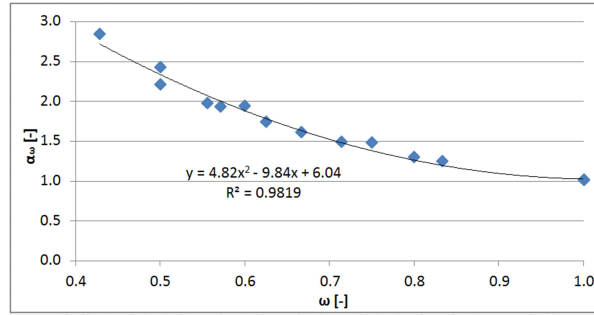
Table C.12: Values of  $\alpha_\omega$ 

	Group	$\alpha_\omega$ [-]	Condition
1	Double stiffened (-RP)	$-0.22\omega + 1.13$	$\omega < 1.25$
2	Stiffened T-plug / unstiffened RC (A-U1-RP)	$3.02\omega^2 - 5.54\omega + 3.43$	$\omega < 1.0$
3	Unstiffened T-plug / stiffened RC (A-U2-RP)	1	$\omega < 1.0$
4	Double unstiffened (A-UU-RP)	$4.82\omega^2 - 9.84\omega + 6.04$	$\omega < 1.25$



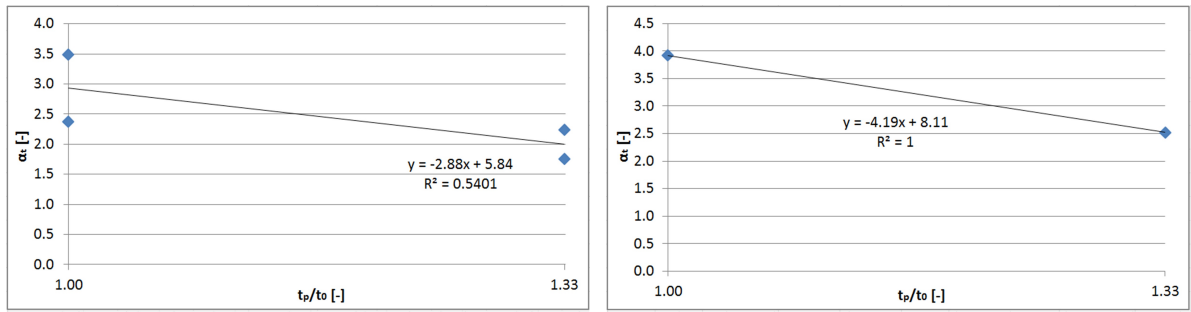
(a) Group 1 (-RP) configurations

(b) Group 2 (A-U1-RP) configurations



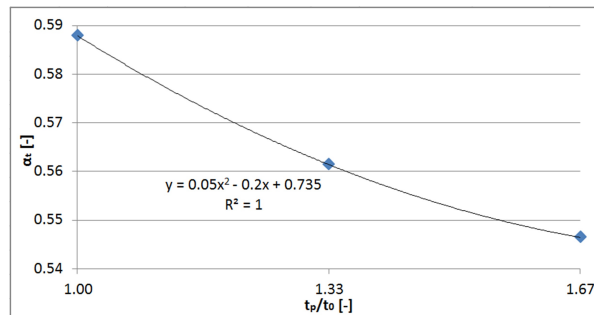
(c) Group 4 (A-UU-RP) configurations

Figure C.9: Regression plots for the derivation of  $\alpha_\omega$



(a) Group 1 (A-RP) configurations

(b) Group 3 (A-U2-RP) configurations



(c) Group 4 (A-UU-RP) configurations

Figure C.10: Regression plots for the derivation of  $\alpha_t$

Similar to  $\omega$ ,  $t_p$  can not be scaled to a "base" model and is dependent on all previously derived contribution equations. Therefore this contribution is derived at last. The contribution of  $t_p$  is expressed by the factor  $\alpha_t$  and derived by the dimensionless ratio  $t_p/t_0$  with  $t_0 = 6 \text{ mm}$ . In Figure C.10a-c,  $\alpha_t$  is plotted against  $t_p/t_0$  for group 1 (-RP), group 3 (A-U2-RP) and group



4 (A-UU-RP) configurations. The results are summarized in Table C.13. Note for group 2 (A-U2-RP) configurations the value of  $b_{eff}$  is independent of  $t_p$  and therefore  $\alpha_t = 1$ .

Table C.13: Values of  $\alpha_t$ 

	Group	$\alpha_t$ [-]	Condition
1	Double stiffened (A-RP)	$-2.88 \left( \frac{t_p}{t_0} \right) - 5.84$	$\omega < 1.0$
	Double stiffened (B-RP)	1	$\omega < 1.0$
2	Stiffened T-plug / unstiffened RC (A-U1-RP)	1	$\omega < 1.0$
3	Unstiffened T-plug / stiffened RC (A-U2-RP)	$-4.19 \left( \frac{t_p}{t_0} \right) + 8.11$	$\omega < 1.0$
4	Double unstiffened (A-UU-RP)	$0.05 \left( \frac{t_p}{t_0} \right)^2 - 0.2 \left( \frac{t_p}{t_0} \right) + 0.735$	$\omega < 1.25$

Since  $\alpha_b$ ,  $\alpha_{st}$ ,  $\alpha_{rc}$ ,  $\alpha_\omega$  and  $\alpha_t$  are all multiplication factors of  $b$ , these contributions can be even further simplified with the introduction of the following factor  $\alpha$ :

$$\alpha = \alpha_b \alpha_{st} \alpha_{rc} \alpha_\omega \alpha_t \quad (\text{Eq. C.12})$$

Unlike the component; T-plug in bending, the length of the T-plug web has no contribution, but the contribution of design of the reverse channel is included. Furthermore, due to a different trend, a new effective width is derived instead of a dimension scaling factor. This leads to the following general equation for  $b_{eff}$ :

$$b_{eff} = \alpha b \quad (\text{Eq. C.13})$$

For the first group (-RP) only double stiffened configurations are considered for two reverse channel designs; A-RP and B-RP. Both designs are defined by the general Equation C.13 with the same individual contributions. In Table C.14, the unity check on the design resistance is given for group 1 (A-RP) configurations and in Table C.15 for group 1 (B-RP). The average unity check for those two tables is 1.010 with a standard deviation of 0.034. In addition, the unity checks for group 1 (-RP) configurations with a varying width, Table C.10, and thickness stiffener, Table C.11, have an average of 0.988 with a standard deviation of 0.027.

Table C.14: Results  $k_5$ : 1. Double stiffened (A-RP)

Model	Numerical $k_5$ [mm]	Analytical $k_5$ [mm]	UC
A-RP6,8	0.656	0.637	0.97
A-RP6,10	0.672	0.659	0.98
A-RP6,12	0.682	0.674	0.99
A-RP6,14	0.699	0.684	0.98
A-RP8,10	0.890	0.908	1.02
A-RP8,12	0.906	0.936	1.03
A-RP8,14	0.916	0.956	1.04
A-RP8,16	0.942	0.971	1.03

Table C.15: Results  $k_5$ : 1. Double stiffened (B-RP)

Model	Numerical $k_5$ [mm]	Analytical $k_5$ [mm]	UC
B-RP6,8	0.375	0.394	1.05
B-RP6,10	0.388	0.407	1.05
B-RP6,12	0.398	0.416	1.05
B-RP6,14	0.405	0.422	1.04
B-RP8,12	0.617	0.592	0.96
B-RP8,14	0.622	0.604	0.97
B-RP8,16	0.625	0.614	0.98

Group 2 (A-U1-RP) considers all configurations with a stiffened T-plug in combination with an unstiffened reverse channel. The general equation of  $b_{eff}$  is also applicable to this group, but with a different value for  $\alpha_\omega$ , which are defined in respectively Table C.12 and C.13. In addition, Equation C.9 has a different value for the unstiffened RC. In Table C.16, the unity check on the design resistance is given for group 2 (A-U1-RP) configurations, with an average of 1.000 and a standard deviation of 0.030.

Table C.16: Results  $k_5$ : 2. Stiffened T-plug / unstiffened RC (A-U1-RP)

Model	Numerical $k_5$ [mm]	Analytical $k_5$ [mm]	UC
A-U1-RP10,12	0.610	0.617	1.01
A-U1-RP10,14	0.720	0.686	0.95
A-U1-RP10,16	0.793	0.776	0.98
A-U1-RP10,18	0.863	0.868	1.01
A-U1-RP12,14	0.969	0.955	0.98
A-U1-RP12,16	0.993	1.032	1.04
A-U1-RP12,18	1.109	1.143	1.03

Unlike previous groups, group 3 (A-U2-RP) show only one effective width per thickness. This finding is explained by comparing the strength of the reverse channel to the T-plug. The stiffened RC behaves extremely strong and therefore dominates the resistance, which on the other hand results in a negligible influence of the T-plug thickness. This is also confirmed by same stiffener configurations in the derivation of the component; T-plug in bending. The unity check for group 3 (A-U2-RP) configurations has an average of 1.000 and a standard deviation of 0.010, see Figure C.17.

Table C.17: Results  $k_5$ : 3. Unstiffened T-plug / stiffened RC (A-U2-RP)

Model	Numerical $k_5$ [mm]	Analytical $k_5$ [mm]	UC
A-U2-RP6,8	0.701	0.701	1.00
A-U2-RP6,10	0.698	0.701	1.00
A-U2-RP6,12	0.702	0.701	1.00
A-U2-RP6,14	0.704	0.701	1.00
A-U2-RP8,14	0.969	0.963	0.99
A-U2-RP8,16	0.957	0.963	1.01

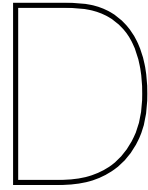
Table C.18: Results  $k_5$ : 4. Double unstiffened (A-UU-RP)

Model	Numerical $k_5$ [mm]	Analytical $k_5$ [mm]	UC
A-UU-RP6,6	0.105	0.107	1.01
A-UU-RP6,8	0.155	0.144	0.93
A-UU-RP6,10	0.203	0.196	0.97
A-UU-RP6,12	0.254	0.243	0.96
A-UU-RP6,14	0.297	0.283	0.95
A-UU-RP8,8	0.214	0.217	1.01
A-UU-RP8,10	0.276	0.266	0.96
A-UU-RP8,12	0.343	0.345	1.01
A-UU-RP8,14	0.411	0.423	1.03
A-UU-RP8,16	0.468	0.494	1.06
A-UU-RP10,10	0.368	0.371	1.01
A-UU-RP10,12	0.451	0.432	0.96
A-UU-RP10,14	0.540	0.535	0.99
A-UU-RP10,16	0.631	0.645	1.02
A-UU-RP10,18	0.717	0.750	1.05

As explained in Paragraph D.1.2, group 4 (-UU-RP) configurations have a different upper bound value of  $\omega = 1.25$  for the failure mode in the reverse channel. In Table C.18 the unity check on design resistance is given for group 4 (A-UU-RP) configurations. The average of the unity check is 0.994 with a standard deviation of 0.038.

In conclusion, on a basis of 51 unique configurations accounting for the contribution of various geometrical dimensions, an average unity check of 0.999 with a standard deviation of 0.032 and a maximum deviation of 0.064 is determined. In general, the range of validity for the component; RC in bending, is defined for  $\omega < 1.0$ , with the exception for group 4 (A-UU-RP) configurations being  $\omega < 1.25$ . However, within this condition failure in the T-plug is still possible. Therefore it is recommended to perform further research on this condition definition. Based on the configuration with failure in the RC, can be concluded that the definition of the component derivation is sufficiently accurate, being well within the accepted 5% margin of error.





# Component derivation: T-plug in bending

This appendix elaborates the derivation of the component; T-plug in bending, in terms of design resistance, Section D.1, and stiffness coefficient, Section D.2. The component is part of the component method application, see Chapter 5, on the plug-and-play joint. The component derivation is based on a parametric study performed in Section 4.3. For the component; T-plug in bending, only models with a failure mode in the T-plug are considered. From these models, the ultimate resistance is determined at the 5% plastic strain limit (PEEQ).

At first, the physical problem of the component; T-plug in bending, is identified with the simplified mechanical model in Figure D.1b. The simplified mechanical model includes the assumption of a rigid constraint in the net-section, represented by the left boundary in Figure D.1. The right boundary represents the support plate on which the load/displacement is introduced during the experiment. However, the simplified mechanical model does not take into account the presence of stiffeners and the overlapping length of the reverse channel. These contributions are accurately incorporated in the derivation of effective width for the design resistance and a dimension factor for the stiffness coefficient.

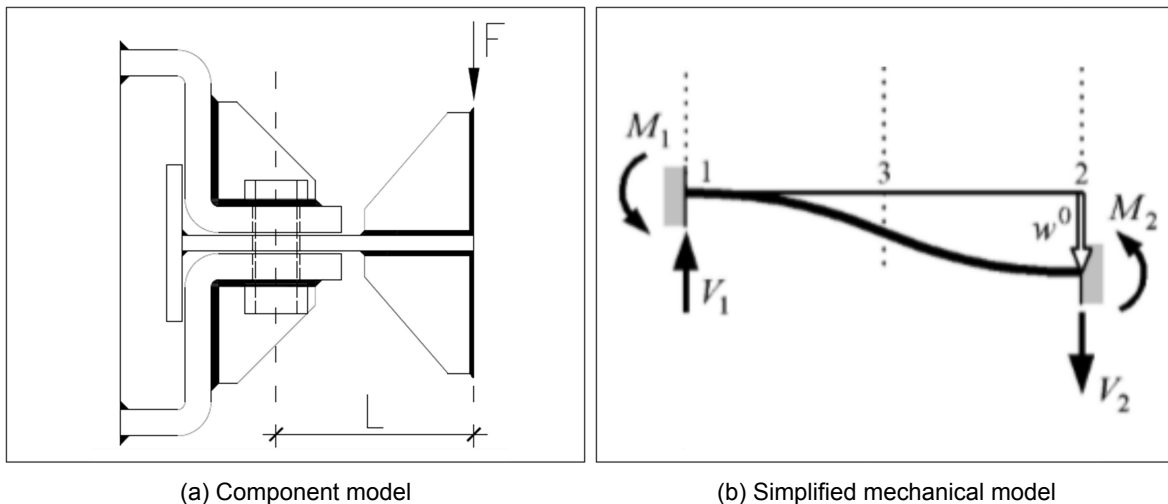


Figure D.1: Component simplification: T-plug in bending

## D.1. Design resistance

Based on the axial stress (S33) distribution in the T-plug web, it is concluded that the contribution due to bending is dominant over shear for the design resistance. As shown in Figure D.2a, along the equivalent yield line, constructed by the element with the highest stress per

element row, the characteristic bending stress distribution is found, highlighted by equal maximum tensile (red) and compressive (blue) stress in opposite utmost fibres.

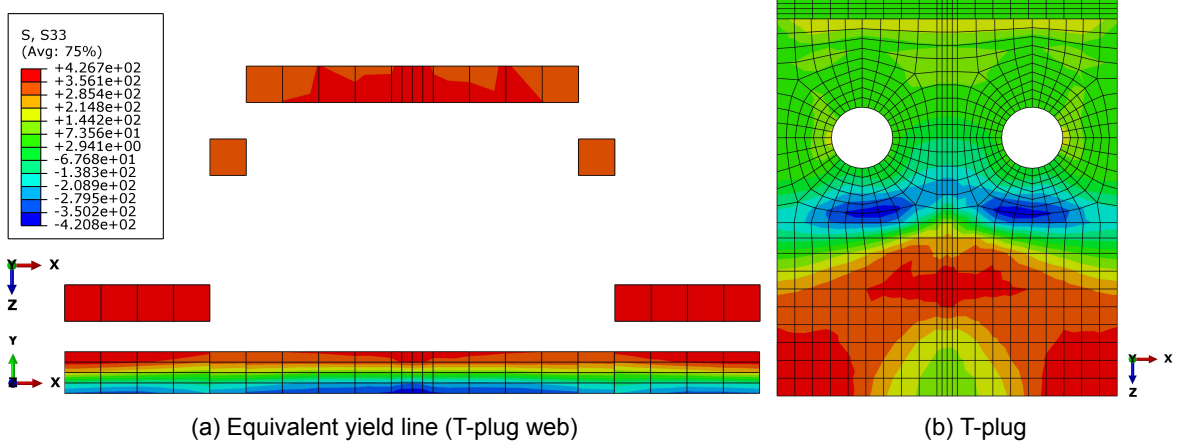


Figure D.2: Axial stress (S33) distribution in the T-plug of numerical model: A-RP

### D.1.1. Partial T-stub model analogy

Following the findings on the bending distribution, a partial T-stub model analogy is made, in which the same bending distribution is present, see Figure D.3 circled in red. Therefore the yielding of the T-plug web is identified with the yielding of the flange (failure mode 1) of the T-stub model.

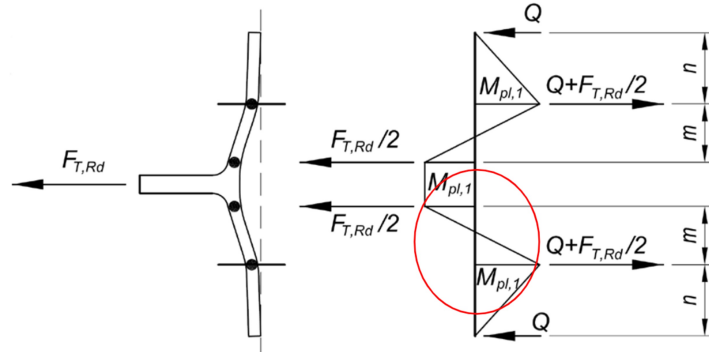


Figure D.3: T-stub model: yielding of the flange (failure mode 1)

$$F_{T,1,Rd} = \frac{4M_{pl,1,Rd}}{m} \quad (\text{Eq. D.1})$$

$$M_{pl,1,Rd} = \frac{0.25\Sigma l_{eff,1} t_p^2 f_y}{\gamma_{M0}} \quad (\text{Eq. D.2})$$

This results in the derivation of the design resistance, using the relation:  $F_{tp,Rd} = 0.5F_{T,1,Rd}$ , where the factor 0.5 accounts for the presence of only one equivalent flange, circled in red in Figure D.3. In this analogy, it is assumed that prying forces develop, caused by the T-plug flange making contact with the reverse channel. Given the Equations D.1, D.2 and  $b_{eff} = l_{eff}$ , the derivation for the equation for the design resistance is as follows:

$$F_{tp,Rd} = \frac{0.5b_{eff} t_p^2 f_y}{m\gamma_{M0}} \quad (\text{Eq. D.3})$$

In this equation there are two undefined parameters, namely "m", the distance between two equivalent yield lines, and " $b_{eff}$ ", the effective width of the T-plug. In the upcoming paragraphs a definition for each of these two parameters is derived.

### D.1.2. Derivation parameter: "m"

The first parameter to be defined is "m", the distance between two equivalent yield lines, as illustrated in Figure D.3. With the presence of a T-plug stiffener, a curved equivalent yield line is observed in the T-plug. The numerical value of "m" is determined by approximating the curved yield line by a straight yield line, using its weighted average. The curved yield line is constructed by the element with the highest axial stress per element row, obtained by a numerical analysis, with a distance  $m_n$  to the other equivalent yield line on the reverse channel side. For each element row,  $m_n$  is multiplied by its bending moment  $M_n$ , resulting in the following equation to derive the numerical value of "m":

$$m = \frac{m_1 M_1 + m_2 M_2 + \dots + m_n M_n}{\sum_n M_n} \quad (\text{Eq. D.4})$$

In Figure D.4, some specific dimensions, used in the derivation, are defined for reverse channel (blue) and T-plug (green). The free length of the T-plug, between the reverse channel and the support plate, is defined by  $l_x$ , the T-plug length between net-section to the edge of the reverse channel is defined by  $l_{rc}$  and at last the total length of T-plug stiffener and weld combined is defined by  $l_{st}$ .

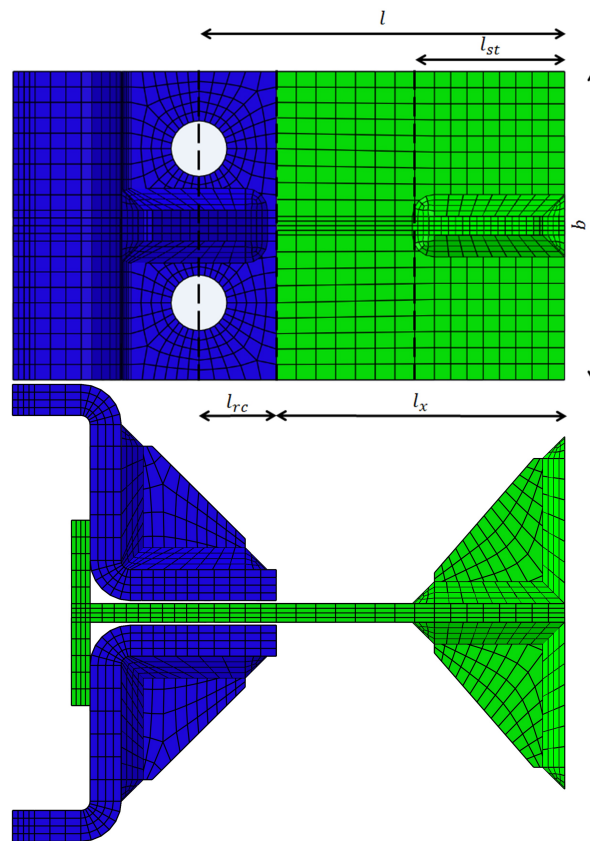


Figure D.4: definition of various lengths of the T-plug

In the analysis the numerical models are categorized in four groups, based on the stiffener configuration on two locations, reverse channel (RC) and T-plug: 1. Double stiffened (-RP), 2. Stiffened T-plug/unstiffened RC (-U1-RP), 3. Unstiffened T-plug/stiffened RC (-U2-RP) and 4. Double unstiffened (-UU-RP). Based on the parametric study, lower bound values for the failure mode in the T-plug are found at a thickness ratio ( $\omega = t_{rc}/t_p$ ) of 1.0 for groups 1-3 and  $\omega = 1.25$  for group 4. For the remaining models, an analysis on the axial stresses (S33) in the T-plug at the 5% plastic strain limit (PEEQ) is performed, from which a total of three unique yield patterns are identified, see Figures D.8 to D.10. These yield patterns are described by the contributions of the following parameters:

- Yield line location on RC side:  $l_{rc}$ ;
- Length T-plug:  $(l_x - l_{st})$ ;
- Length T-plug stiffener:  $l_{st}$ ;
- Thickness T-plug:  $t_p$ ;
- Thickness ratio ( $A_p \leq 800 \text{ mm}^2$ ):  $\omega$ ;
- Width T-plug/thickness T-plug stiffener:  $b/t_{stiff}$ .

The first parameter in the derivation is the contribution of the yield line location on the RC side. Based on the parametric study, a limit values of  $\omega = 1.5$  is found for group 1 (-RP) configurations, which distinguish whether the yield line occurs in the net-section or at the edge of the reverse channel. The contribution of this parameter is expressed by the length  $l_{rc}$ , see Figure D.4. For all models in the parametric study holds  $l_{rc} = 25 \text{ mm}$ .

Secondly, the contribution of  $(l_x - l_{st})$  is studied on the "base" model A-RP. For this configuration the length of the stiffener is equal to the free length;  $l_{st} = l_x$ . A parametric study is performed in which the free length is increased linearly, while the length of the stiffener is kept constant. A relative shift of the equivalent yield line compared to the T-plug stiffener is observed, which is expressed by the relation  $0.25(l_x - l_{st})$ . For the sake of simplicity, for all remaining models in the parametric study holds  $l_{st} = l_x = 51 \text{ mm}$ .

Based on the analysis of the axial stress distribution, the presence of the T-plug stiffener plays a complex role is the shape of the yield line. When varying  $t_p$ ,  $\omega$  or  $b$  on a stiffened T-plug configuration an unique yield line is found, where a trivial yield is found for all unstiffened T-plug configurations. Therefore is decided to account for the influence of these parameters as a multiplication factor of the T-plug stiffener ( $l_{st}$ ). This leads to an iterative derivation process to find the optimal solution of the remaining three parameters combined.

The first iteration is performed on  $t_p$ , expressed by the multiplication factor  $\alpha_t$ . As  $\alpha_t$  is multiplied with  $l_{st}$ , the dimensionless ratio  $t_p/t_0$  is studied, where  $t_0 = 6 \text{ mm}$  is the base thickness of the T-plug. In Figure D.5, the average  $\alpha_t$  per T-plug thickness, obtained from Tables D.2-D.3, is plotted against  $t_p/t_0$ . An average value is chosen to eliminate the contribution of  $\omega$ , which is elaborated in the next paragraph. In the end, after an iterative process the following equation for  $\alpha_t$  is derived for the range  $6 \leq t_p \leq 10$ :

$$\alpha_t = \left( -0.3195 \left( \frac{t_p}{t_0} \right)^2 + 1.2255 \left( \frac{t_p}{t_0} \right) - 0.1575 \right) \quad (\text{Eq. D.5})$$

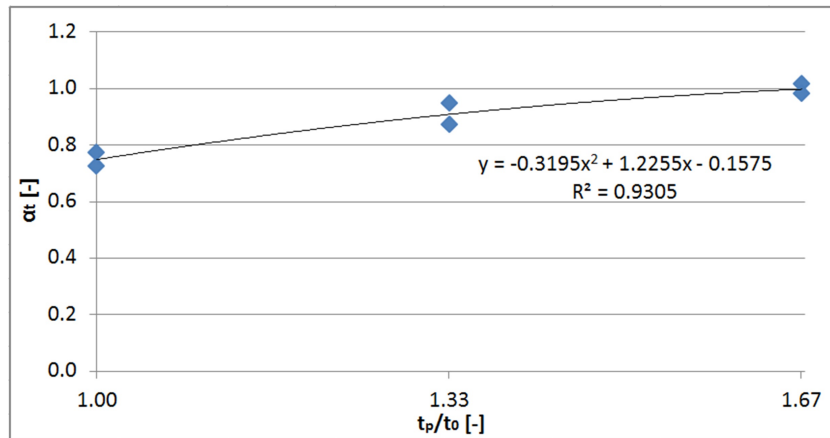


Figure D.5: Regression plot for the derivation of factor  $\alpha_t$



Next, the contribution of  $\omega$ , expressed by the factor  $\alpha_\omega$ , is incorporated in the equation. Based on the numerical values of  $m$ , it is concluded that  $\omega$  only plays a significant role for a T-plug thickness 6 and 8 mm in combination with a 100 mm width. Therefore the limit value is determined at a T-plug area of  $A_p = 800 \text{ mm}^2$ . In Figure D.6,  $\alpha_\omega$  is plotted against  $1/\omega$  for the condition  $A_p \leq 800 \text{ mm}^2$ . This results in the following conditional equation for  $\alpha_\omega$ :

$$\alpha_\omega = \begin{cases} \left(\frac{-0.37}{\omega}\right) + 1.17 & \text{for } A_p \leq 800 \text{ mm}^2 \\ 1 & \text{for } A_p > 800 \text{ mm}^2 \end{cases} \quad (\text{Eq. D.6})$$

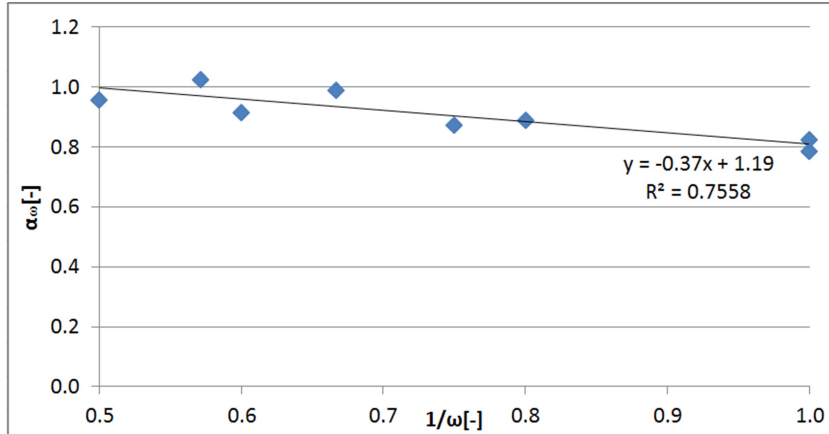


Figure D.6: Regression plot for the derivation of factor  $\alpha_\omega$

At last, a parametric study is performed on the ratio  $b/t_{stiff}$  for two new "base" models; A-RP10,10 and A-RP16,10, see Table D.1. The contribution is expressed by  $\alpha_{bm}$  derived by using the dimensionless ratio  $b/t_{stiff}$ . In Figure D.7,  $\alpha_{bm}$  is plotted against  $b/t_{stiff}$ . Finally, after an iterative process, this results in the following equation for  $\alpha_{bm}$  for the range  $10 \leq b/t_{stiff} \leq 25$ :

$$\alpha_{bm} = \left(-0.0006 \left(\frac{b}{t_{stiff}}\right)^2 + 0.035 \left(\frac{b}{t_{stiff}}\right) + 0.385\right) \quad (\text{Eq. D.7})$$

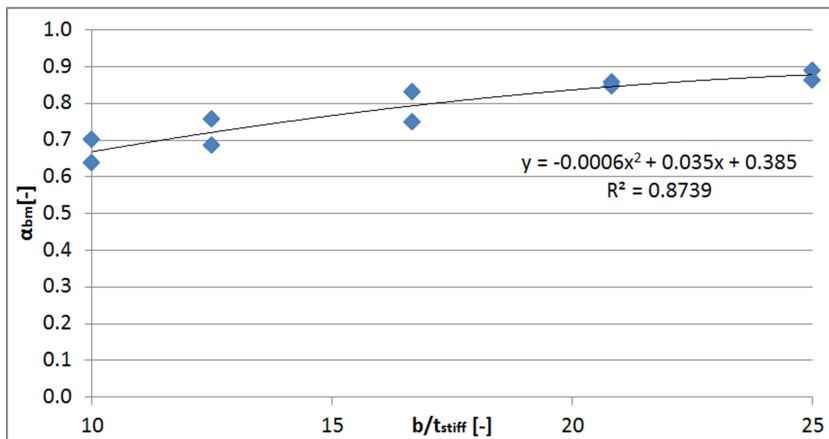


Figure D.7: Regression plot for the derivation of factor  $\alpha_{bm}$

Since  $\alpha_t$ ,  $\alpha_\omega$  and  $\alpha_{bm}$  are all multiplication factors of  $l_{st}$ , these contributions can be even further simplified with the introduction of a general dimension factor  $\alpha_m$ :

$$\alpha_m = \alpha_t \alpha_\omega \alpha_{bm} \quad (\text{Eq. D.8})$$

Table D.1: Results  $m$ :  $\alpha_{bm}$  contribution

Model	$t_{stiff}$ [mm]	b [mm]	$b/t_{stiff}$	numerical m [mm]	analytical m [mm]	UC
A-RP10,10	6	100	16.67	63.1	65.8	1.04
	8	100	12.5	59.9	62.1	1.04
	10	100	10	57.5	59.3	1.03
A-RP16,10	6	125	20.83	68.7	68.4	1.00
	6	150	25	69.0	70.0	1.01
	6	100	16.67	42.3	40.8	0.96
	8	100	12.5	38.6	37.1	0.96
	10	100	10	35.8	34.3	0.96
	6	125	20.83	43.2	43.4	1.01
	6	150	25	45.3	45.0	0.99

Table D.2: Results  $m$ :  $b = 100$  mm

Model	$t_p$ [mm]	$t_{rc}$ [mm]	$\omega$	$t_p/t_0$	numerical m [mm]	analytical m [mm]	UC
A-RP6,6	6	6	1.00	1.00	49.0	50.1	1.02
A-RP8,6	6	8	1.33	1.00	51.8	52.9	1.02
A-RP	6	10	1.67	1.00	28.1	29.6	1.06
A-RP12,6	6	12	2.00	1.00	29.3	30.8	1.05
A-RP8,8	8	8	1.00	1.33	55.7	55.5	1.00
A-RP10,8	8	10	1.25	1.33	58.1	58.2	1.00
A-RP12,8	8	12	1.50	1.33	36.8	35.0	0.95
A-RP14,8	8	14	1.75	1.33	38.2	36.3	0.95
A-RP10,10	10	10	1.00	1.67	63.1	65.8	1.04
A-RP12,10	10	12	1.20	1.67	67.9	65.8	0.97
A-RP14,10	10	14	1.40	1.67	67.3	65.8	0.98
A-RP16,10	10	16	1.60	1.67	42.3	40.8	0.96
A-RP18,10	10	18	1.80	1.67	42.3	40.8	0.96

Table D.3: Results  $m$ :  $b = 150$  mm

Model	$t_p$ [mm]	$t_{rc}$ [mm]	$\omega$	$t_p/t_0$	numerical m [mm]	analytical m [mm]	UC
A-RP6,6	6	6	1.00	1.00	58.0	58.8	1.01
A-RP8,6	6	8	1.33	1.00	60.6	58.8	0.97
A-RP	6	10	1.67	1.00	35.4	33.8	0.96
A-RP12,6	6	12	2.00	1.00	35.6	33.8	0.95
A-RP8,8	8	8	1.00	1.33	64.1	66.0	1.03
A-RP10,8	8	10	1.25	1.33	64.2	66.0	1.03
A-RP12,8	8	12	1.50	1.33	39.5	41.0	1.04
A-RP14,8	8	14	1.75	1.33	39.5	41.0	1.04
A-RP10,10	10	10	1.00	1.67	69.0	70.0	1.01
A-RP12,10	10	12	1.20	1.67	69.4	70.0	1.01
A-RP14,10	10	14	1.40	1.67	69.6	70.0	1.01
A-RP16,10	10	16	1.60	1.67	45.3	45.0	0.99
A-RP18,10	10	18	1.80	1.67	45.3	45.0	0.99

Figure D.8 presents yield pattern 1, containing a straight yield line in the net-section and a curved yield line caused by the presence of the T-plug stiffener. This yield pattern is defined by Equation D.9, where the average "m" to the curved yield line is determined based on its weighted average. In conclusion, yield pattern 1 is applicable for all group 2 (-U1-RP) configurations with  $\omega \geq 1.0$  and group 1 configurations under the conditions  $1.0 \leq \omega < 1.5$ .

#### Yield pattern 1:

$$m = \alpha_m l_{st} + (l_x - l_{st}) + l_{rc} \quad (\text{Eq. D.9})$$

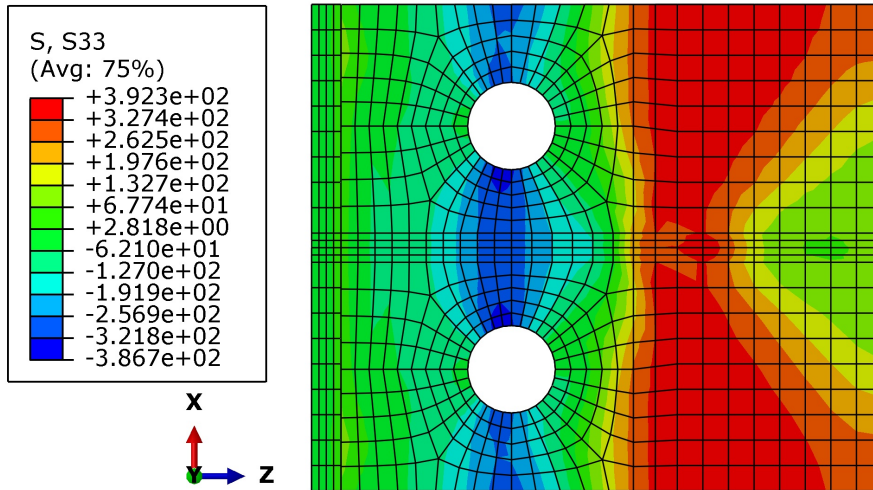


Figure D.8: Yield pattern 1: (A-U1-RP)

Next, Figure D.9 presents yield pattern 2, containing a straight yield line at the edge of the reverse channel and a similar curved yield line as in yield pattern 1. Based on a large range of numerical models, can be concluded that the shift in yield line, from the net-section to the edge of the reverse channel, occurs at a limit value of  $\omega = 1.5$  for group 1 (-RP) configurations. This length is expressed by the factor  $l_{rc}$ , which is, for this reason, the only difference in Equation D.10 compared to yield pattern 1. In conclusion, yield pattern 2 is only applicable for group 1 (-RP) under the specific condition  $\omega \geq 1.5$ .

**Yield pattern 2:**

$$m = \alpha_m l_{st} + (l_x - l_{st}) \tag{Eq. D.10}$$

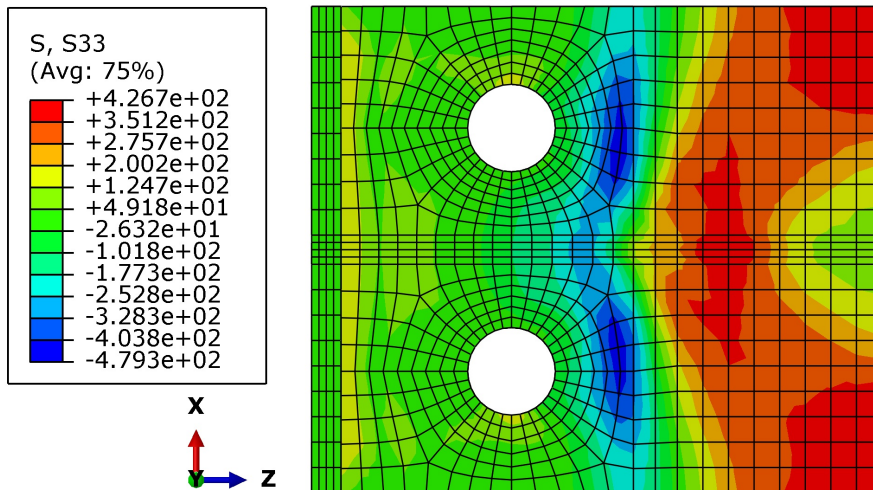


Figure D.9: Yield pattern 2: (A-RP)

At last, Figure D.10 presents yield pattern 3, consisting of a straight yield at the edge of the reverse channel and the at the edge of the support plate. This second straight yield is characteristic for the unstiffened T-plug configuration. This yield pattern is described by Equation D.11 and is applicable for all configurations of group 3 (-U2-RP) under the condition  $\omega \geq 1.0$  and group 4 (-UU-RP) for  $\omega \geq 1.25$ .

**Yield pattern 3:**

$$m = l_x \tag{Eq. D.11}$$

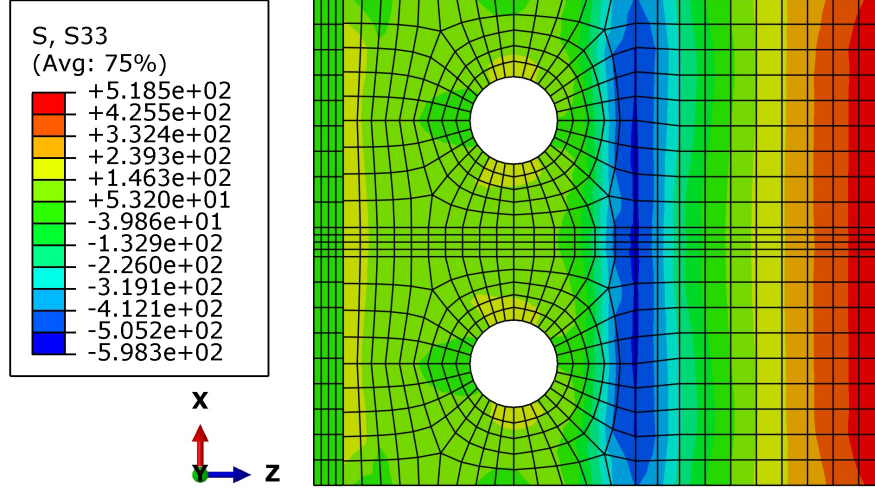


Figure D.10: Yield pattern 3: (A-U2-RP)

In Table D.4, the definition of  $m$  is summarized based on the derivations elaborated above. As mentioned before, there are a total of four groups: 1. Double stiffened (-RP), 2. Stiffened T-plug/unstiffened RC (-U1-RP), 3. Unstiffened T-plug/stiffened RC (-U2-RP) and 4. Double unstiffened (-UU-RP). Furthermore, the equations of  $m$  are only valid under certain conditions depending on  $\omega$ . The lower bound for  $\omega$  distinguishes whether the failure is located in the T-plug and the limit value of  $\omega = 1.5$  for group 1 make a distinction between the applicability of yield pattern 1 and 2.

Table D.4: Values of  $m$ 

	Group	$m$ [mm]	Condition
1	Double stiffened (-RP)	$\alpha_m l_{st} + (l_x - l_{st}) + l_{rc}$	$1.0 \leq \omega < 1.5$
		$\alpha_m l_{st} + (l_x - l_{st})$	$\omega \geq 1.5$
2	Stiffened T-plug / unstiffened RC (-U1-RP)	$\alpha_m l_{st} + (l_x - l_{st}) + l_{rc}$	$\omega \geq 1.0$
3	Unstiffened T-plug / stiffened RC (-U2-RP)	$l_x$	$\omega \geq 1.0$
4	Double unstiffened (-UU-RP)	$l_x$	$\omega \geq 1.25$

### D.1.3. Derivation parameter: " $b_{eff}$ "

Given the definition of  $m$  and the numerical resistance, derived at the 5% plastic strain limit, Equation D.3 is used reversed to predict a numerical value for  $b_{eff}$ . Hereafter, an analytical expression is derived to accurately approximate the numerical value of  $b_{eff}$  for the four categorized groups, defined in Paragraph D.1.2. The contributions of the following parameters are used in the derivation of  $b_{eff}$ :

- Width:  $b$ ;
- Thickness ratio:  $\omega$ ;
- Thickness stiffener:  $t_{stiff}$ ;
- Thickness T-plug:  $t_p$ ;
- Length T-plug/stiffener:  $l_{st}/l_x$ .

A parametric study is performed on two "base" models; A-RP10,10 and A-RP16,10, to study the contribution of  $b$  for the range  $100 \text{ mm} \leq b \leq 150 \text{ mm}$ . By dividing the numerical  $b_{eff}$  by  $b$ , a dimensionless factor  $\alpha_b$  is found, whose behaviour is described by the dimensionless

ratio  $b/b_0$ . In Figure D.11,  $\alpha_b$  is plotted, scaled to the value for  $b = 100 \text{ mm}$ , against  $b/b_0$  for the models from Table D.5. This trend is confirmed by all group 1 (-RP) configurations of the parametric study, which leads to the derivation of the following equation:

$$\alpha_b = -0.27 \left( \frac{b}{b_0} \right) + 1.27 \tag{Eq. D.12}$$

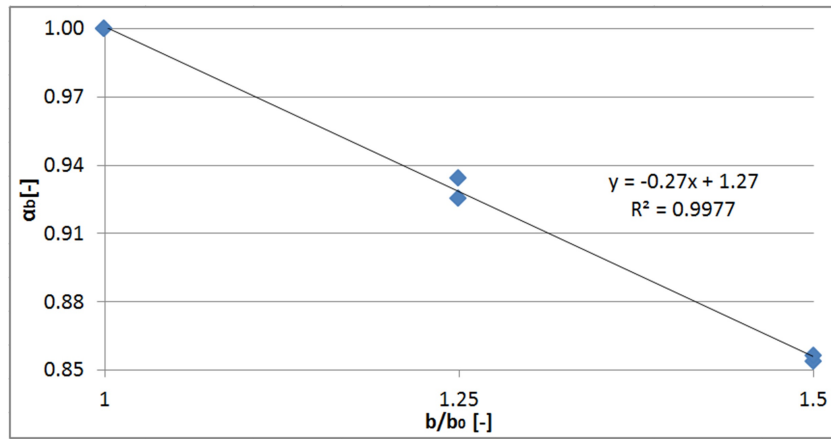
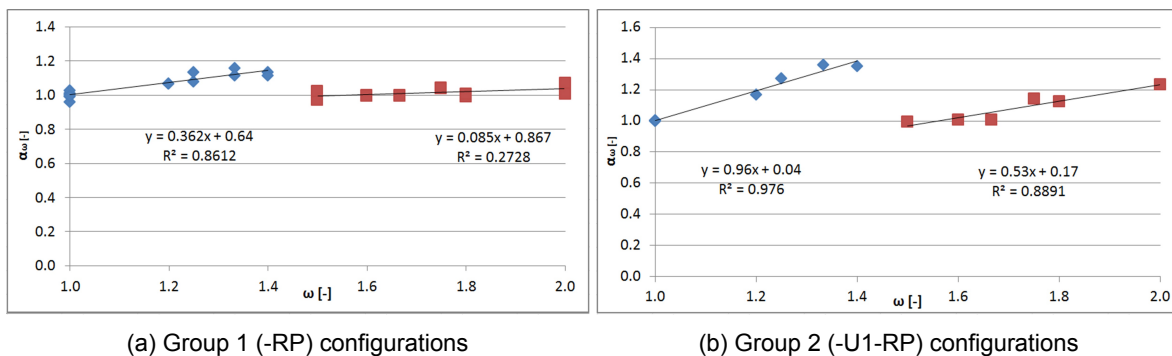


Figure D.11: Regression plot for the derivation of  $\alpha_b$

Table D.5: Results  $F_{tp,Rd}$ :  $\alpha_b$  contribution

Model	b [mm]	b/b <sub>0</sub> [-]	numerical $F_{tp,Rd}$ [kN]	analytical $F_{tp,Rd}$ [kN]	UC
A-RP10,10	100	1.0	102.6	102.2	1.00
	125	1.25	114.1	114.5	1.00
	150	1.5	123.5	124.6	1.01
A-RP16,10	100	1.0	120.2	120.6	1.00
	125	1.25	131.9	132.0	1.00
	150	1.5	139.9	141.8	1.01

Secondly, the contribution of  $\omega$  is studied, expressed by the factor  $\alpha_\omega$ . In Figure D.12a,  $\alpha_\omega$  is plotted against  $\omega$  for group 1 (-RP) configurations and in Figure D.12b for group 2 (-RP) configurations from Tables D.10 and D.11. A distinction is made between the conditions of  $1.0 \leq \omega < 1.5$  and  $\omega \geq 1.5$ , as previously explained in Paragraph D.1.2. The results are summarized in Table D.6. Note for the other groups the value of  $b_{eff}$  is independent of  $\omega$  and therefore  $\alpha_\omega = 1$ .



(a) Group 1 (-RP) configurations

(b) Group 2 (-U1-RP) configurations

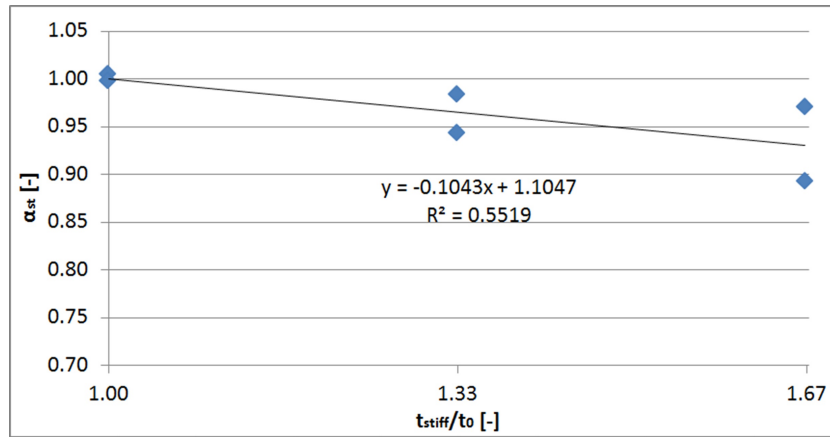
Figure D.12: Regression plots for the derivation of  $\alpha_\omega$

Table D.6: Values of  $\alpha_\omega$ 

	Group	$\alpha_\omega$ [-]	Condition
1	Double stiffened (-RP)	$0.362\omega + 0.64$	$1.0 \leq \omega < 1.5$
		$0.085\omega + 0.867$	$\omega \geq 1.5$
2	Stiffened T-plug / unstiffened RC (-U1-RP)	$0.96\omega + 0.04$	$1.0 \leq \omega < 1.5$
		$0.53\omega + 0.17$	$\omega \geq 1.5$
3	Unstiffened T-plug / stiffened RC (-U2-RP)	1	$\omega \geq 1.0$
4	Double unstiffened (-UU-RP)	1	$\omega \geq 1.25$

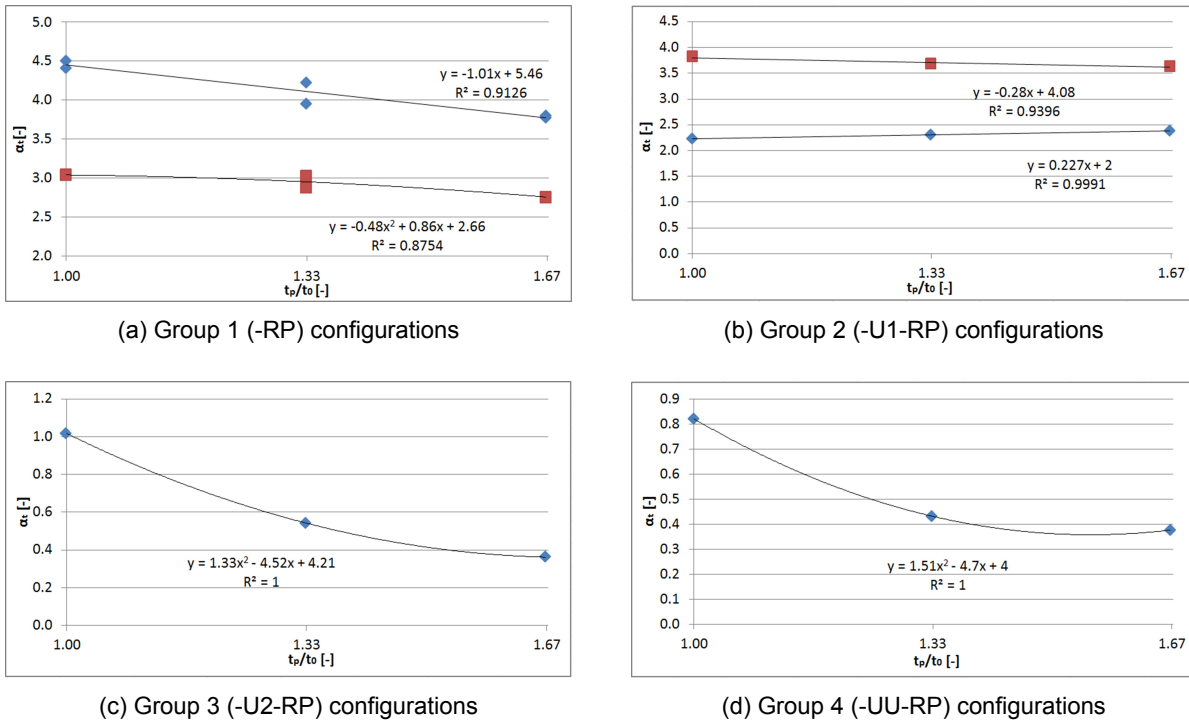
Next, the contribution of  $t_{stiff}$ , expressed by the factor  $\alpha_{st}$ , is studied. As  $\alpha_{st}$  is dependent on the presence of the T-plug stiffener, its value for groups 3 and 4 is automatically equal to 1 and are not considered in the parametric study.  $\alpha_{st}$  is derived by dimensionless ratio  $t_{stiff}/t_0$ , where  $t_0 = 6 \text{ mm}$  again. In Figure D.13,  $\alpha_{st}$  is plotted against  $t_{stiff}/t_0$  for the two "base" models A-RP10,10 and A-RP16,10 within the range  $6 \leq t_{stiff} \leq 10$ , see Table D.7. This results in the following general equation for  $\alpha_{st}$ :

$$\alpha_{st} = \begin{cases} -0.104 \left( \frac{t_{stiff}}{t_0} \right) + 1.105 & \text{for stiffened T-plug} \\ 1 & \text{for unstiffened T-plug} \end{cases} \quad (\text{Eq. D.13})$$

Figure D.13: Regression plot for the derivation of  $\alpha_{st}$ Table D.7: Results  $F_{tp,Rd}$ :  $\alpha_{st}$  contribution

Model	$t_{stiff}$ [mm]	$t_{stiff}/t_0$ [-]	numerical $F_{tp,Rd}$ [kN]	analytical $F_{tp,Rd}$ [kN]	UC
A-RP10,10	6	1.00	102.6	102.2	1.00
	8	1.33	106.4	104.6	0.98
	10	1.67	109.9	105.5	0.96
A-RP16,10	6	1.00	120.2	120.6	1.00
	8	1.33	125.0	133.3	1.02
	10	1.67	127.8	132.0	1.04

Unlike all other contributions elaborated above, the contribution of  $t_p$  can not be scaled to a "base" model. Instead, it is dependent on all the previously derived contribution equations and therefore derived at last. Similar to the derivation of  $m$ ,  $t_p$  is expressed by the factor  $\alpha_t$ , derived by the dimensionless ratio  $t_p/t_0$  with  $t_0 = 6 \text{ mm}$ . In Figure D.14a,  $\alpha_t$  is plotted against the ratio  $t_p/t_0$  for group 1 (-RP) configurations  $1.0 \leq \omega < 1.5$  (blue) and  $\omega \geq 1.5$  (red).  $\alpha_t$  represents the model with the smallest  $\omega$  per thickness of Tables D.10 and D.11. In the end, this derivation method is applied to each group, resulting in the equations for  $\alpha_t$  in Table D.8 for the range  $6 \leq t_p \leq 10$ .

Figure D.14: Regression plots for the derivation of  $\alpha_t$ Table D.8: Values of  $\alpha_t$ 

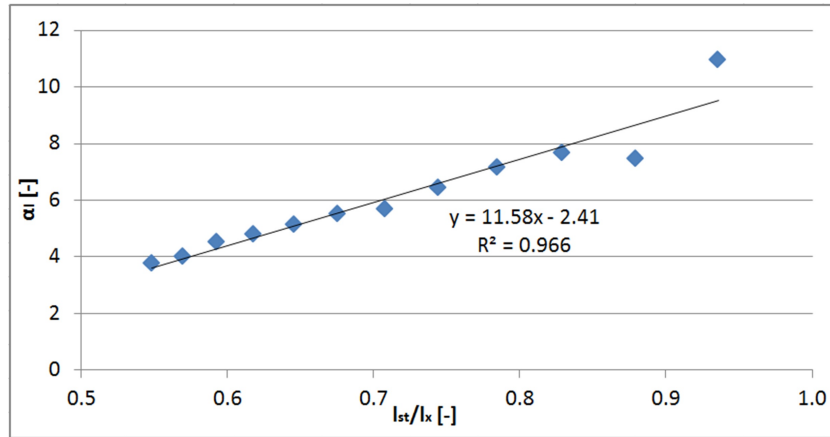
	Group	$\alpha_t$ [-]	Condition
1	Double stiffened (-RP)	$-1.01 \left(\frac{t_p}{t_0}\right) + 5.46$	$1.0 \leq \omega < 1.5$
		$-0.48 \left(\frac{t_p}{t_0}\right)^2 + 0.86 \left(\frac{t_p}{t_0}\right) + 2.66$	$\omega \geq 1.5$
2	Stiffened T-plug / unstiffened RC (-U1-RP)	$-0.227 \left(\frac{t_p}{t_0}\right) + 2$	$1.0 \leq \omega < 1.5$
		$-0.28 \left(\frac{t_p}{t_0}\right) + 4.08$	$\omega \geq 1.5$
3	Unstiffened T-plug / stiffened RC (-U2-RP)	$1.33 \left(\frac{t_p}{t_0}\right)^2 - 4.52 \left(\frac{t_p}{t_0}\right) + 4.21$	$\omega \geq 1.0$
4	Double unstiffened (-UU-RP)	$1.51 \left(\frac{t_p}{t_0}\right)^2 - 4.7 \left(\frac{t_p}{t_0}\right) + 4$	$\omega \geq 1.25$

Since  $\alpha_b$ ,  $\alpha_\omega$ ,  $\alpha_{st}$  and  $\alpha_t$  are all multiplication factors of  $b$ , these contributions can be even further simplified with the introduction of the following factor  $\alpha_b$ :

$$\alpha = \alpha_b \alpha_\omega \alpha_{st} \alpha_t \quad (\text{Eq. D.14})$$

The contribution of  $l_{st}/l_x$ , expressed by the factor  $\alpha_l$  and is studied by the relation  $(b_{eff} - \alpha b)/(l_x - l_{st})$  for "base" model A-RP. As can be observed in Table D.9,  $b_{eff}$  is significantly reduced when increasing  $l_x$ . Since  $l_{st} = 0$  for unstiffened T-plug configurations, the contribution has to be subtracted from the "base" model to avoid a negative effective width. In Figure D.15,  $\alpha_l$  is plotted against  $l_{st}/l_x$  for the range  $51 \leq l_x \leq 93$ , resulting in the generally applicable equation for  $\alpha_l$ :

$$\alpha_l = 11.58 \left(\frac{l_{st}}{l_x}\right) - 2.41 \quad (\text{Eq. D.15})$$

Figure D.15: Regression plot for the derivation of  $\alpha_l$ Table D.9: Results  $F_{tp,Rd}$ :  $\alpha_l$  contribution

Model	$l_x$ [mm]	$l_x/l_{st}$ [-]	Numerical $F_{tp,Rd}$ [kN]	Analytical $F_{tp,Rd}$ [kN]	UC
A-RP12.5	54.5	0.94	56.2	58.1	1.03
A-RP16	58	0.88	51.8	51.4	0.99
A-RP19.5	61.5	0.83	44.8	45.8	1.02
A-RP23	65	0.78	39.9	41.1	1.03
A-RP26.5	68.5	0.74	36.4	37.2	1.02
A-RP30	72	0.71	34.4	33.9	0.99
A-RP33.5	75.5	0.68	30.6	31.1	1.02
A-RP37	79	0.65	28.5	28.8	1.01
A-RP40.5	82.5	0.62	26.5	26.8	1.01
A-RP44	86	0.59	24.8	25.1	1.01
A-RP47.5	89.5	0.57	24.8	23.7	0.95
A-RP51	93	0.55	23.6	22.5	0.95

Given all contributions elaborated in the previous paragraphs, a general equation for  $b_{eff}$  is defined as follows:

$$b_{eff} = ab - \alpha_l(l_x - l_{st}) \quad (\text{Eq. D.16})$$

Table D.10: Results  $F_{tp,Rd}$ : 1. Double stiffened (-RP) ( $b = 100$  mm)

Model	Numerical $F_{tp,Rd}$ [kN]	Analytical $F_{tp,Rd}$ [kN]	UC
A-RP6,6	57.6	56.9	0.99
A-RP8,6	62.4	60.4	0.97
A-RP	65.7	66.2	1.01
A-RP12,6	67.7	65.6	0.97
A-RP8,8	81.1	84.5	1.04
A-RP10,8	86.9	87.8	1.01
A-RP12,8	93.2	95.3	1.02
A-RP14,8	96.4	93.8	0.97
A-RP10,10	102.6	102.2	1.00
A-RP12,10	108.9	109.6	1.01
A-RP14,10	115.8	117.0	1.01
A-RP16,10	120.2	120.6	1.00
A-RP18,10	119.4	122.6	1.03



For the first group (-RP) only double stiffened configurations are considered, whereby a distinction is made between the cases  $1.0 \leq \omega < 1.5$  and  $\omega \geq 1.5$ . Both cases are defined by the general Equation D.16, but have different values for  $\alpha_t$  and  $\alpha_\omega$ . In Table D.10, the unity check on the design resistance is given for group 1 (-RP) configurations with  $b = 100 \text{ mm}$  and in Table D.11 for  $b = 150 \text{ mm}$ . The average unity check for those two tables is 1.002 with a standard deviation of 0.022. Besides, the unity checks for group 1 (-RP) configurations with a varying width, Table D.5, thickness stiffener, Table D.7, and length, Table D.9, have an average of 1.003 with a standard deviation of 0.027.

Table D.11: Results  $F_{tp,Rd}$ : 1. Double stiffened (-RP) ( $b = 150 \text{ mm}$ )

Model	Numerical $F_{tp,Rd}$ [kN]	Analytical $F_{tp,Rd}$ [kN]	UC
A-RP6,6	63.2	63.0	1.00
A-RP8,6	70.4	70.5	1.00
A-RP	73.5	75.3	1.03
A-RP12,6	74.9	77.4	1.03
A-RP8,8	95.7	92.1	0.96
A-RP10,8	102.2	100.5	0.98
A-RP12,8	108.7	105.7	0.97
A-RP14,8	110.9	107.9	0.97
A-RP10,10	123.5	124.6	1.01
A-RP12,10	130.9	133.6	1.02
A-RP14,10	139.1	142.6	1.02
A-RP16,10	139.9	141.8	1.01
A-RP18,10	143.1	144.2	1.01

Similar to the first group, for the group 2 (-U1-RP) configurations a distinction is made between the cases  $1.0 \leq \omega < 1.5$  and  $\omega \geq 1.5$ . Group 2 (-U1-RP) considers all configurations with a stiffened T-plug in combination with an unstiffened reverse channel. The general equation of  $b_{eff}$  is also applicable to this group, but with different values for  $\alpha_t$  and  $\alpha_\omega$ , which are defined in respectively Table D.6 and D.8. In Table D.12, the unity check on the design resistance is given for group 2 (-U1-RP) configurations, with an average of 1.000 and a standard deviation of 0.025.

Table D.12: Results  $F_{tp,Rd}$ : 2. Stiffened T-plug / unstiffened RC (-U1-RP)

Model	Numerical $F_{tp,Rd}$ [kN]	Analytical $F_{tp,Rd}$ [kN]	UC
A-U1-RP6,6	28.4	28.4	1.00
A-U1-RP8,6	36.5	35.5	0.97
A-U1-RP	44.7	46.9	1.05
A-U1-RP12,6	53.8	53.6	1.00
A-U1-RP8,8	47.1	47.2	1.00
A-U1-RP10,8	57.1	55.8	0.98
A-U1-RP12,8	69.7	67.7	0.97
A-U1-RP14,8	78.4	75.4	0.96
A-U1-RP10,10	72.3	72.3	1.00
A-U1-RP12,10	80.9	82.6	1.02
A-U1-RP14,10	90.9	93.3	1.03
A-U1-RP16,10	100.5	102.0	1.01
A-U1-RP18,10	110.4	110.8	1.00

Unlike previous groups, group 3 (-U2-RP) show only one effective width per thickness. This finding is explained by comparing the strength of the reverse channel to the T-plug. The unstiffened T-plug behaves extremely weak and therefore dominates the resistance, which on the other hand results in a negligible influence of the reverse channel thickness. This is also confirmed by the value  $\alpha_\omega = 1$  in Table D.6. The unity check for group 3 (-U2-RP) configurations has an average of 0.992 and a standard deviation of 0.029, see Figure D.13.

This table includes one configuration with a different failure mode outside the T-plug, which is denoted with "N.A."

Table D.13: Results  $F_{tp,Rd}$ : 3. Unstiffened T-plug / stiffened RC (-U2-RP)

Model	Numerical $F_{tp,Rd}$ [kN]	Analytical $F_{tp,Rd}$ [kN]	UC
A-U2-RP6,6	25.9	28.2	N.A.
A-U2-RP8,6	28.0	28.2	1.01
A-U2-RP	28.3	28.2	1.00
A-U2-RP12,6	28.2	28.2	1.00
A-U2-RP8,8	39.0	39.6	1.01
A-U2-RP10,8	42.4	39.6	0.93
A-U2-RP12,8	39.7	39.6	1.00
A-U2-RP14,8	39.7	39.6	1.00
A-U2-RP10,10	55.2	55.7	1.01
A-U2-RP12,10	56.1	55.7	0.99
A-U2-RP14,10	59.8	55.7	0.93
A-U2-RP16,10	55.3	55.7	1.01
A-U2-RP18,10	54.9	55.7	1.01

As mentioned in Paragraph D.1.2, for the group 4 (-UU-RP) configurations a different lower bound value is retained of  $\omega = 1.25$ , since only group 4 (-UU-RP) configurations with  $\omega \geq 1.25$  have a failure mode in the T-plug. In general, group 4 configurations have similar behaviour as group 3 configurations, in terms of having only one effective width per thickness. Again this is confirmed by the value  $\alpha_\omega = 1$  in Table D.6. In Table D.14 the unity check on design resistance is given for group 4 (-UU-RP) configurations. The average of the unity check is 0.992 with a standard deviation of 0.027.

Table D.14: Results  $F_{tp,Rd}$ : 4. Double unstiffened (-UU-RP)

Model	Numerical $F_{tp,Rd}$ [kN]	Analytical $F_{tp,Rd}$ [kN]	UC
A-UU-RP	25.1	25.5	1.02
A-UU-RP12,6	26.3	25.5	0.97
A-UU-RP10,8	35.0	36.7	1.05
A-UU-RP12,8	37.3	36.7	0.98
A-UU-RP14,8	38.4	36.7	0.96
A-UU-RP14,10	56.5	55.3	0.98
A-UU-RP16,10	55.2	55.3	1.00
A-UU-RP18,10	56.1	55.3	0.99

In conclusion, on a basis of 76 unique configurations accounting for the contribution of various geometrical dimensions, an average unity check of 0.999 with a standard deviation of 0.025 and a maximum deviation of 0.069 is determined. In general, the range of validity for the component; T-plug in bending, is defined for  $1.0 \leq \omega \leq 2.0$ , with the exception for group 4 (-UU-RP) configurations being  $1.25 \leq \omega \leq 2.0$ . From this complete derivation can be concluded that the definition is sufficiently accurate, being well within the accepted 5% margin of error.

## D.2. Stiffness coefficient

Following the simplified mechanical model of Figure D.1, the Timoshenko beam theory is applied to double-check the dominance of the bending contribution. The following system of differential equations is solved to determine the stiffness coefficient of the component: T-plug in bending, given the absence of a distributed load:

$$EI \frac{d^2 \phi}{dx^2} - GA_s \left( \frac{dw}{dx^2} + \phi \right) = 0 \quad (\text{Eq. D.17})$$

$$GA_s \left( \frac{d^2 w}{dx^2} + \frac{d\phi}{dx} \right) = 0 \quad (\text{Eq. D.18})$$

Solving this system of differential equations gives the following equation, including four unknowns:

$$w = \frac{1}{6}C_1x^3 + \frac{1}{2}C_2x^2 + C_3x + C_4 \quad (\text{Eq. D.19})$$

To solve the unknowns a total of four boundary conditions are defined, two at  $x = 0$  (support plate boundary) and two at  $x = l$  (net-section boundary). At  $x = 0$  a known displacement/force is applied at a rigid boundary, resulting in the boundary conditions  $\phi = 0$  and  $V = -F$ . At  $x = l$  the simplified mechanical model is assumed to be rigid with zero vertical displacement, leading to the boundary conditions  $\phi = 0$  and  $w = 0$ . Implementing these four boundary conditions in Equation D.19 with corresponding standard relations for rotation, shear deformation, curvature and sectional forces, this gives the following solution:

$$w = \frac{Fx^3}{6EI} - \frac{Flx^2}{4EI} - \frac{Fx}{GA_s} + \frac{Fl(GA_sl^2 + 12EI)}{12EIGA_s} \quad (\text{Eq. D.20})$$

Given this general solution to the system of differential equations, the last term is split up to separately distinguish the bending (Equation D.21) and shear (Equation D.22) contribution to the stiffness coefficient. Given the relation  $k_i = \frac{S_j^{,ini}}{E}$  and  $l = m$  following the EC3-1-8 component method, the individual stiffness coefficients for bending and shear are defined:

$$k_b = \frac{12I}{l^3} = \frac{b_{eff}t_p^3}{m^3} \quad (\text{Eq. D.21})$$

$$k_s = \frac{A_s}{2l(1+\nu)} = \frac{A}{2\eta l(1+\nu)} = \frac{b_{eff}t_p}{2\eta m(1+\nu)} \quad (\text{Eq. D.22})$$

To determine the stiffness coefficient of the component; T-plug in bending, the combined serial spring theory is applied, given by Equation D.23. The individual bending and shear contributions to the stiffness coefficient are shown in Table D.15.

$$\frac{1}{k_7} = \frac{1}{k_b} + \frac{1}{k_s} \quad (\text{Eq. D.23})$$

Table D.15: Individual bending and shear contributions

Model	$k_i$ [mm]	$k_b$ [mm]	%	$k_s$ [mm]	%
A-RP6,6	1.36	1.30	95.7	0.06	4.3
A-RP8,6	1.43	1.37	96.1	0.06	3.9
A-RP	0.44	0.39	88.7	0.05	11.3
A-RP12,6	0.48	0.43	89.4	0.05	10.6
A-RP8,8	0.86	0.81	93.9	0.05	6.1
A-RP10,8	0.91	0.86	94.4	0.05	5.6
A-RP12,8	0.33	0.29	86.0	0.05	14.0
A-RP14,8	0.36	0.31	86.9	0.05	13.1
A-RP10,10	0.81	0.75	93.3	0.05	6.7
A-RP12,10	0.75	0.70	93.3	0.05	6.7
A-RP14,10	0.70	0.66	93.3	0.05	6.7
A-RP16,10	0.29	0.24	84.2	0.05	15.8
A-RP18,10	0.29	0.24	84.2	0.05	15.8

Based on the findings in Table D.15 is chosen to derive the equation for the stiffness coefficient by only accounting for the bending contribution and neglecting the shear contribution.

This is in line with the findings of the bending contribution on the design resistance, see Section D.1. Therefore the following equation for the stiffness coefficient is proposed:

$$k_7 = Ck_b \quad (\text{Eq. D.24})$$

Given the Equations D.21 and D.24, the dimension factor  $C$  is still undefined.  $k_7 = \frac{S_{jini}}{E}$  is numerically predicted by using linear line regression on the elastic stage of the force-displacement curve. The displacement is the relative displacement between the net-section and the support plate, defined in Figure D.1. The term  $C$  is derived to accurately approximate the numerical value of  $k_7$  for the four categorized groups: 1. Double stiffened (-RP), 2. Stiffened T-plug / unstiffened RC (-U1-RP), 3. Unstiffened T-plug / stiffened RC (-U2-RP) and 4. Double unstiffened (-UU-RP). To derive  $C$  the contributions of the following geometrical dimensions are considered:

- Width:  $b$ ;
- Thickness ratio:  $\omega$ ;
- Thickness stiffener T-plug:  $t_{st}$ ;
- Length T-plug/stiffener T-plug:  $l_{st}/l_x$ ;
- Thickness T-plug:  $t_p$ .

The first parameter considered is the contribution of  $b$ , expressed by the multiplication factor  $c_b$ . Similar to the derivation of  $b_{eff}$ , a parametric study is performed on two "base" models; A-RP10,10 and A-RP16,10, to study the contribution for the range  $100 \text{ mm} \leq b \leq 150 \text{ mm}$ . The value of  $c_b$  is scaled to the selected "base" width  $b = 100 \text{ mm}$ , using the dimensionless ratio  $b/b_0$  with  $b_0 = 100 \text{ mm}$ . In Figure D.16, the average  $c_b$  of the models from Tables D.16, D.21 and D.22, is plotted against the ratio  $b/b_0$  for the case  $1.0 \leq \omega < 1.5$  (red) and  $\omega \geq 1.5$  (blue). In the end, the following general equation is derived for both cases:

$$c_b = \begin{cases} -0.1 \left( \frac{b}{b_0} \right) + 1.1 & \text{for } 1.0 \leq \omega < 1.5 \\ 0.29 \left( \frac{b}{b_0} \right) + 0.71 & \text{for } \omega \geq 1.5 \end{cases} \quad (\text{Eq. D.25})$$

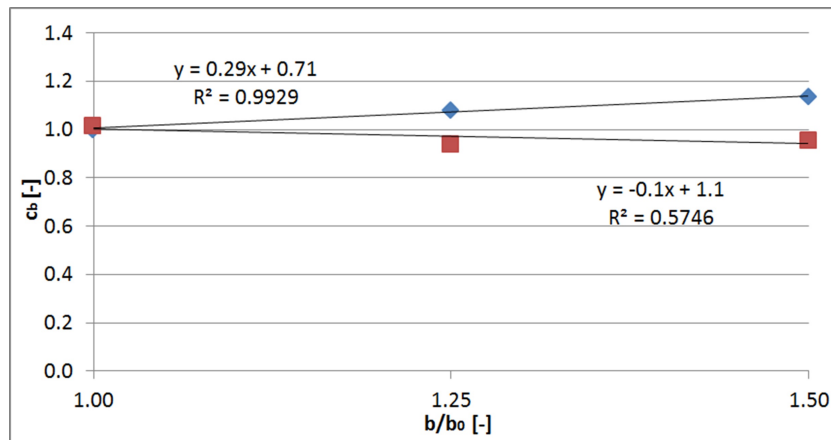


Figure D.16: Regression plot for the derivation of  $c_b$

Table D.16: Results  $k_7$ :  $c_b$  contribution

Model	b [mm]	b/b <sub>0</sub> [-]	numerical $k_7$ [mm]	analytical $k_7$ [mm]	UC
A-RP10,10	100	1.0	1.032	0.998	0.97
	125	1.25	0.971	1.007	1.04
	150	1.5	0.991	1.020	1.03
A-RP16,10	100	1.0	1.221	1.226	1.00
	125	1.25	1.275	1.268	0.99
	150	1.5	1.331	1.353	1.03

The contribution of  $\omega$ , expressed by the multiplication factor  $c_\omega$ , is derived independently of other contributing factors. In Figure D.17a and D.17b,  $c_\omega$  is plotted against  $\omega$  for the group 2 (-U1-RP) configurations and group 4 (-UU-RP) configurations. In general stiffened RC configurations are independent of  $c_\omega$ , although there is one conditional exception for  $A_p \leq 800 \text{ mm}$ , which follows from Equation D.6. These results for  $c_\omega$  are shown in Figure D.17c and a general summary is provided by Table D.17.

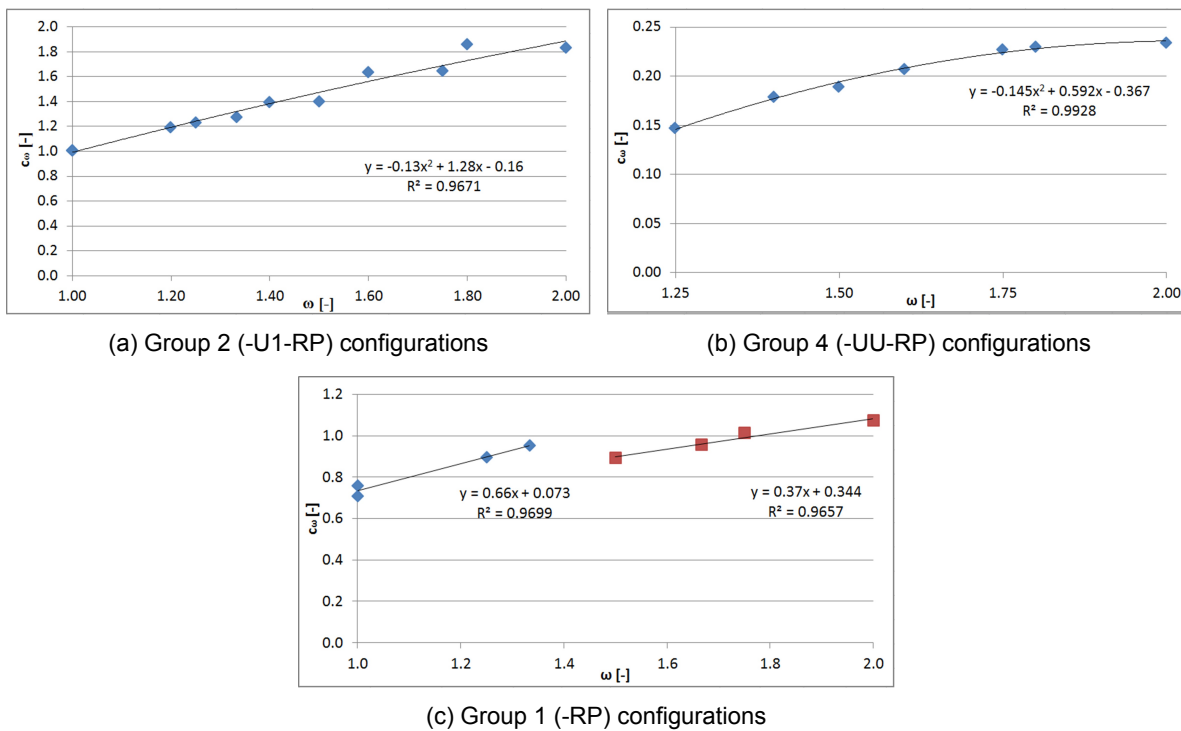


Figure D.17: Regression plots for the derivation of  $c_\omega$

Table D.17: Values of  $c_\omega$

Group	$c_\omega$ [-]	Condition
1	$0.66\omega + 0.073$	$1.0 \leq \omega < 1.5$ *
	$0.37\omega + 0.344$	$\omega \geq 1.5$ *
2	$-0.13\omega^2 + 1.28\omega - 0.16$	$\omega \geq 1.0$
3	1	$\omega \geq 1.0$
4	$-0.145\omega^2 + 0.592\omega - 0.367$	$\omega \geq 1.25$

\*Note 1: this conditions only holds if  $A_p \leq 800 \text{ mm}^2$ , see Equation D.6, if not  $c_\omega = 1$ .

Thirdly, the contribution of  $t_{stiff}$ , expressed by the multiplication factor  $c_{st}$ , is studied and scaled to the "base" T-plug stiffener thickness  $t_{stiff} = 6 \text{ mm}$ . The equation is derived using the dimensionless ratio  $t_{stiff}/t_0$  with  $t_0 = 6 \text{ mm}$  and is like previous factors independently derived. In Figure D.18,  $c_{st}$  is plotted against  $t_{stiff}/t_0$  for the two "base" models; A-RP10,10 and A-RP16,10, representing the cases  $1.0 \leq \omega < 1.5$  (red) and  $\omega \geq 1.5$  (blue). This results in the following conditional equation for  $c_{st}$  for the range  $6 \leq t_{stiff} \leq 10$ :

$$\left\{ \begin{array}{l} c_{st} = \begin{cases} -0.11 \left( \frac{t_{stiff}}{t_0} \right) + 1.11 & 1.0 \leq \omega < 1.5 \\ -0.36 \left( \frac{t_{stiff}}{t_0} \right) + 1.36 & \omega \geq 1.5 \end{cases} & \text{for stiffened } T\text{-plug} \\ c_{st} = 1 & \text{for unstiffened } T\text{-plug} \end{array} \right. \quad (\text{Eq. D.26})$$

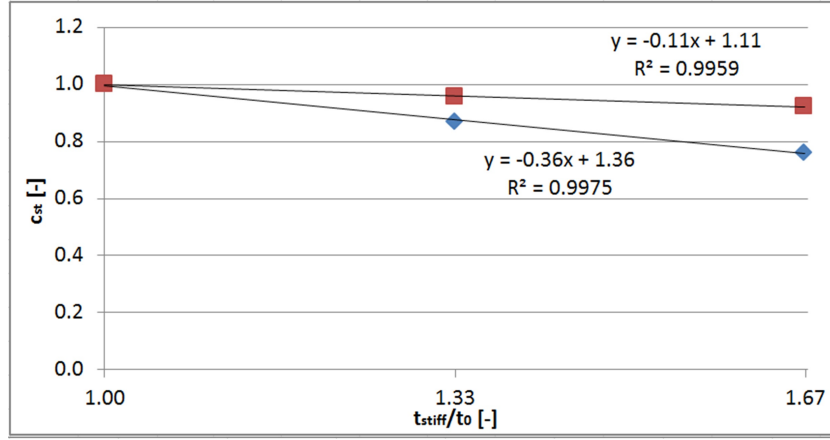


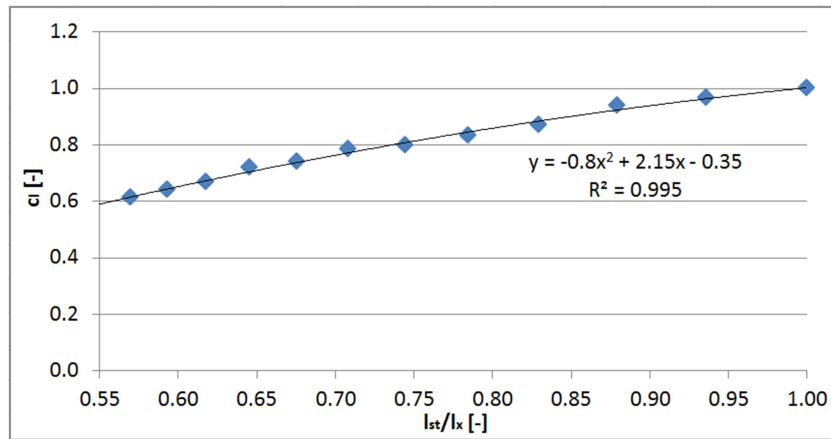
Figure D.18: Regression plot for the derivation of  $c_{st}$

Table D.18: Results  $k_7$ :  $c_{st}$  contribution

Model	$t_{stiff}$ [mm]	$t_{stiff}/t_0$ [-]	numerical $k_7$ [mm]	analytical $k_7$ [mm]	UC
A-RP10,10	6	1.00	1.032	0.998	0.97
	8	1.33	1.135	1.104	0.97
	10	1.67	1.208	1.172	0.97
A-RP16,10	6	1.00	1.221	1.226	1.00
	8	1.33	1.365	1.386	1.02
	10	1.67	1.448	1.452	1.00

Next, the contribution of  $l_{st}/l_x$  is considered, expressed by the multiplication factor  $c_l$ . A parametric study is performed on "base" models A-RP, for the range  $51 \text{ mm} \leq l_x \leq 93 \text{ mm}$ . Again, the multiplication factor  $c_l$  is independent of the other factors, as it is scaled to the ratio  $l_{st}/l_x = 1.0$  of the "base" model, using the same dimensionless ratio  $l_{st}/l_x$  in the function. In Figure D.19,  $c_l$  is plotted against  $l_{st}/l_x$  for the models of Table D.19. This results in the following conditional equation for  $c_l$ :

$$c_l = \begin{cases} -0.8 \left( \frac{l_{st}}{l_x} \right)^2 + 2.15 \left( \frac{l_{st}}{l_x} \right) - 0.35 & \text{for stiffened } T\text{-plug} \\ 1 & \text{for unstiffened } T\text{-plug} \end{cases} \quad (\text{Eq. D.27})$$

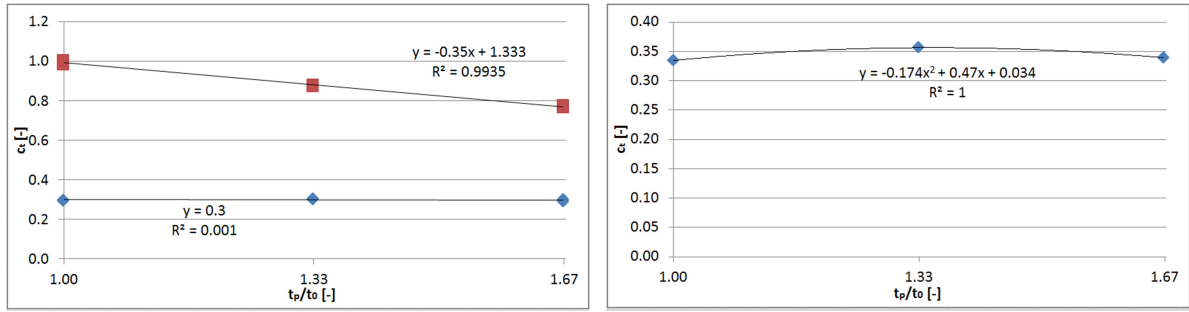
Figure D.19: Regression plot for the derivation of  $c_l$ Table D.19: Results  $k_7$ :  $c_l$  contribution

Model	$l_x$ [mm]	$l_x/l_{st}$ [-]	Numerical $k_7$ [mm]	Analytical $k_7$ [mm]	UC
A-RP	51	1.00	0.732	0.735	1.00
A-RP12.5	54.5	0.94	0.585	0.585	1.00
A-RP16	58	0.88	0.475	0.469	0.99
A-RP19.5	61.5	0.83	0.372	0.379	1.02
A-RP23	65	0.78	0.303	0.308	1.02
A-RP26.5	68.5	0.74	0.250	0.253	1.01
A-RP30	72	0.71	0.212	0.209	0.99
A-RP33.5	75.5	0.68	0.175	0.175	1.00
A-RP37	79	0.65	0.150	0.147	0.98
A-RP40.5	82.5	0.62	0.123	0.125	1.01
A-RP44	86	0.59	0.106	0.107	1.01
A-RP47.5	89.5	0.57	0.091	0.092	1.01
A-RP51	93	0.55	0.080	0.080	1.01

At last, the contribution of  $t_p$ , expressed by the multiplication factor  $c_t$  and derived by the dimensionless ratio  $t_p/t_0$  with  $t_0 = 6 \text{ mm}$ , is studied.  $t_p$  is not scaled to a "base" model and depends on all previously derived contributions. In Figure D.20a,  $c_t$  is plotted against the ratio  $t_p/t_0$  for group 1 (-RP) configurations  $1.0 \leq \omega < 1.5$  (red) and  $\omega \geq 1.5$  (blue).  $c_t$  represents the average value per T-plug thickness of the group 1 (-RP) models, Tables D.21 and D.22. This derivation method is repeated for the other groups and results are summarized in Table D.20. Note, group 4 (-UU-RP) models are completely independent of  $c_t$  and therefore equal to 1.

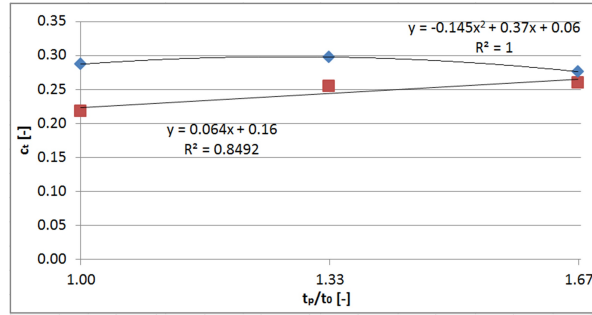
Table D.20: Values of  $c_t$ 

Group	$c_t$ [-]	Condition
1 Double stiffened (-RP)	$-0.35 \left(\frac{t_p}{t_0}\right) + 1.333$	$1.0 \leq \omega < 1.5$
	0.3	$\omega \geq 1.5$
2 Stiffened T-plug / unstiffened RC (-U1-RP)	$-0.174 \left(\frac{t_p}{t_0}\right)^2 + 0.47 \left(\frac{t_p}{t_0}\right) + 0.034$	$\omega \geq 1.0$
3 Unstiffened T-plug Stiffened RC (-U2-RP)	$0.064 \left(\frac{t_p}{t_0}\right) + 0.16$	$\omega = 1.0$
	$-0.145 \left(\frac{t_p}{t_0}\right)^2 + 0.37 \left(\frac{t_p}{t_0}\right) + 0.06$	$\omega > 1.0$
4 Double stiffened (-UU-RP)	1	$\omega \geq 1.25$



(a) Group 1 (-RP) configurations

(b) Group 2 (-U1-RP) configurations



(c) Group 3 (-U2-RP) configurations

Figure D.20: Regression plot for the derivation of  $c_t$ 

Given the derivation of each individual multiplication factor above, these factors can be combined in a general dimension factor  $C$ :

$$C = c_b c_\omega c_{st} c_l c_t \quad (\text{Eq. D.28})$$

Table D.21: Results  $k_7$ : 1. Double stiffened (-RP) ( $b = 100 \text{ mm}$ )

Model	Numerical $k_7$ [mm]	Analytical $k_7$ [mm]	UC
A-RP6,6	0.535	0.553	1.03
A-RP8,6	0.684	0.683	1.00
A-RP	0.732	0.735	1.00
A-RP12,6	0.756	0.762	1.01
A-RP8,8	0.813	0.786	0.97
A-RP10,8	0.907	0.909	1.00
A-RP12,8	0.936	0.944	1.01
A-RP14,8	0.974	0.952	0.98
A-RP10,10	1.032	0.998	0.97
A-RP12,10	1.115	1.070	0.96
A-RP14,10	1.179	1.142	0.97
A-RP16,10	1.221	1.226	1.00
A-RP18,10	1.260	1.246	0.99

The first group (-RP) includes only double stiffened configurations, divided into two cases of  $1.0 \leq \omega < 1.5$  and  $\omega \geq 1.5$ . Both cases are defined by the same general Equation D.24, but have an unique value for  $c_t$ . Besides, for the condition  $A_p \leq 800 \text{ mm}^2$  the value for  $c_\omega$  is determined in Table D.17, for each other condition  $c_\omega = 1$ . In Tables D.21 and D.22, the unity check on the stiffness coefficient with  $b = 100 \text{ mm}$  and  $b = 150 \text{ mm}$  are given, where in Tables D.18, D.19 and D.16 respectively the unity checks on a varying thickness T-plug stiffener, length and width are given. The average unity check of the group 1 is 0.999 with a standard deviation of 0.025.



Table D.22: Results  $k_7$ : 1. Double stiffened (-RP) ( $b = 150$  mm)

Model	Numerical $k_7$ [mm]	Analytical $k_7$ [mm]	UC
A-RP6,6	0.539	0.575	1.07
A-RP8,6	0.658	0.644	0.98
A-RP	0.753	0.766	1.02
A-RP12,6	0.773	0.788	1.02
A-RP8,8	0.764	0.784	1.03
A-RP10,8	0.890	0.855	0.96
A-RP12,8	0.985	0.973	0.99
A-RP14,8	1.028	0.994	0.97
A-RP10,10	0.991	1.020	1.03
A-RP12,10	1.141	1.093	0.96
A-RP14,10	1.224	1.167	0.95
A-RP16,10	1.311	1.353	1.03
A-RP18,10	1.334	1.376	1.03

Group 2 (-U1-RP) considers all configurations with a stiffened T-plug in combination with an unstiffened reverse channel. The same general equation of  $k_7$  is also applicable to this group, but with different values for  $c_t$  and  $c_\omega$ , which are defined in respectively Table D.20 and D.17. In Table D.12, the unity check on the stiffness coefficient is given for all group 1 (-RP) configurations, with an average of 1.006 and a standard deviation of 0.046.

Table D.23: Results  $k_7$ : 2. Stiffened T-plug / unstiffened RC (-U1-RP)

Model	Numerical $k_7$ [mm]	Analytical $k_7$ [mm]	UC
A-U1-RP6,6	0.127	0.125	0.99
A-U1-RP8,6	0.180	0.186	1.03
A-U1-RP	0.253	0.283	1.12
A-U1-RP12,6	0.352	0.362	1.03
A-U1-RP8,8	0.244	0.241	0.99
A-U1-RP10,8	0.321	0.322	1.01
A-U1-RP12,8	0.416	0.437	1.05
A-U1-RP14,8	0.522	0.534	1.02
A-U1-RP10,10	0.399	0.394	0.99
A-U1-RP12,10	0.498	0.497	1.00
A-U1-RP14,10	0.622	0.614	0.99
A-U1-RP16,10	0.763	0.726	0.95
A-U1-RP18,10	0.911	0.846	0.93

In group 3 (-U2-RP) configurations with an unstiffened T-plug / stiffened reverse channel are considered. For this group, a general the stiffness is found for all configuration with the same T-plug thickness, with the exception for a thickness ratio of  $\omega = 1.0$ . This is explained by a stiff reverse channel, due to the presence of the stiffener, resulting in the same boundary conditions to the T-plug, independent of the reverse channel thickness. However, this stiffness for  $\omega = 1.0$  configurations slightly deviates from this general stiffness and therefore Table D.17 makes a distinction for this case. Furthermore, due to the absence of a T-plug stiffener, the multiplication factors  $c_{st} = 1$  and  $c_l = 1$ . This results in an average unity check for group 3 (-U2-RP) configurations of 0.994 and a standard deviation of 0.027, see Figure D.24. This group includes one configuration, A-U2-RP6,6, with a different failure mode outside the T-plug, but unlike the design resistance, the stiffness coefficient can be determined and the unity check is included in Table D.24.

Table D.24: Results  $k_7$ : 3. Unstiffened T-plug / stiffened RC (-U2-RP)

Model	Numerical $k_7$ [mm]	Analytical $k_7$ [mm]	UC
A-U2-RP6,6	0.080	0.082	1.02
A-U2-RP8,6	0.100	0.104	1.05
A-U2-RP	0.106	0.104	0.98
A-U2-RP12,6	0.110	0.104	0.95
A-U2-RP8,8	0.175	0.168	0.96
A-U2-RP10,8	0.202	0.203	1.00
A-U2-RP12,8	0.209	0.203	0.97
A-U2-RP14,8	0.202	0.203	1.00
A-U2-RP10,10	0.315	0.321	1.02
A-U2-RP12,10	0.341	0.330	0.97
A-U2-RP14,10	0.328	0.330	1.01
A-U2-RP16,10	0.334	0.330	0.99
A-U2-RP18,10	0.330	0.330	1.00

As already explained in Paragraph D.1.2, group 4 (-UU-RP) double unstiffened configurations have a different lower bound value of  $\omega = 1.25$ . Similar to the group 3 configurations, due to the absence of a T-plug stiffener, the multiplication factors  $c_{st} = 1$  and  $c_l = 1$ . In Table D.14 the unity check on stiffness coefficient is given for group 4 (-UU-RP) configurations. The average of the unity check is 1.028 with a standard deviation of 0.070. Despite having a standard deviation exceeding the 5% margin of error, these results are sufficient. This is explained by the small batch of models in combination with a very small stiffness coefficient. Besides, this is solely caused by a single model having the slightest difference already leading to a big deviation, as with the exclusion of model A-UU-RP the average of the unity check is 1.004 with a standard deviation of 0.014.

Table D.25: Results  $k_7$ : 4. Double unstiffened (-UU-RP)

Model	Numerical $k_7$ [mm]	Analytical $k_7$ [mm]	UC
A-UU-RP	0.060	0.072	1.20
A-UU-RP12,6	0.078	0.079	1.01
A-UU-RP10,8	0.093	0.093	1.00
A-UU-RP12,8	0.120	0.124	1.03
A-UU-RP14,8	0.144	0.143	0.99
A-UU-RP14,10	0.214	0.213	0.99
A-UU-RP16,10	0.248	0.251	1.01
A-UU-RP18,10	0.276	0.274	1.00

In conclusion, on a basis of 76 unique configurations accounting for the contribution of various geometrical dimensions, an average unity check of 1.000 with a standard deviation of 0.029 and a maximum deviation of 0.116 is determined, with the exclusion of model A-UU-RP for above-given reasons. In general, the range of validity for the component; T-plug in bending, is defined for  $1.0 \leq \omega \leq 2.0$ , with the exception for group 4 (-UU-RP) configurations being  $1.25 \leq \omega \leq 2.0$ . From this complete derivation can be concluded that the definition is sufficiently accurate, being well within the 5% margin of error.